NOVEL ROLE OF LYMPHATIC AND BLOOD VASCULATURES IN BREAST CANCER GROWTH AND METASTASIS AND PEPTIDE AGENTS WITH ANTI-LYMPHANGIOGENIC AND ANTI-ANGIOGENIC ACTIVITY

by

Esak Lee

A dissertation submitted to Johns Hopkins University in conformity

with the requirements for the degree of Doctor of Philosophy

Baltimore, Maryland

March 2014

Abstract

Up to 90% of deaths from breast cancer are a result of metastasis. Metastasis is a very complex process that has been difficult to fully understand as it involves diverse parenchymal and stromal cells and their secreted factors in the tumor and organ microenvironment. Triple-negative breast cancer (TNBC) is one of the most aggressive subtypes of breast cancer for which current therapeutic options are very limited. This dissertation investigates molecular mechanisms of TNBC growth and metastasis by focusing on lymphatic and blood vasculatures in the tumor and organ microenvironment. Crosstalk between TNBC cells and lymphatic or blood endothelial cells reveals under-investigated roles of the microenvironment in pre-metastatic niche formation in distant organs as well as tumor progression in primary sites. The dissertation also focuses on development of novel anti-lymphangiogenic and anti-angiogenic peptides to treat TNBC.

For investigating cancer metastasis and testing anti-metastatic therapeutic agents, efficient and reproducible spontaneous metastasis models are needed. Conventional spontaneous breast cancer metastasis models require a long period of observation after establishment of primary tumors to see significant metastatic progression. The dissertation demonstrates that pre-treatment of animals with tumor-conditioned media (TCM) prepared from TNBC cells accelerates spontaneous metastasis in the corresponding TNBC animal models. The TCM contains all the factors secreted by TNBC cells; thus the injection of TCM conditions pre-metastatic niche. An inguinal breast tumor model facilitated by TCM showed robust thoracic metastasis in the lymph nodes (LN) and the lungs, compared to the serum-free media (SFM) treated control group. The TCM-induced metastasis model was further investigated by focusing on molecular crosstalk between lymphatic endothelial cells (LEC) and TNBC cells, as the pre-metastatic organs in TCM-treated animals showed highly enhanced lymphangiogenesis. The dissertation shows that

LEC within pre-metastatic niches are educated by TNBC cells to accelerate metastasis in the lungs and the LN. LEC within these organs, educated by tumor secretion secretes a chemokine, CCL5 that is not secreted by either physiological LEC or TNBC cells, directing CCR5-positive TNBC cell dissemination into the tissues. Moreover, tumor-educated LEC promote angiogenesis in these organs by secreting VEGFA, allowing tumor extravasation in the lungs and colonization in the LN. Mechanistically, interleukin-6 (IL6) secreted by the TNBC cells activates Stat3 phosphorylation, causing the formation of a pStat3-pc-Jun-pATF-2 ternary complex, inducing HIF-1α expression in LEC, and ultimately resulting in expression of CCL5 and VEGF. Additional crosstalk between TNBC cells and LEC shows that LEC promote TNBC cell proliferation and induce pericyte recruitment in primary tumor microenvironment by expressing EGF and PDGF-BB, thus promoting tumor growth. Surprisingly, microvascular endothelial cells (MEC) showed an opposite effect by suppressing tumor growth.

Motivated by the knowledge that angiogenesis supports tumor growth and metastasis and lymphangiogenesis actively conditions pre-metastatic niches and promotes breast tumor metastasis, novel anti-lymphangiogenic and anti-angiogenic peptides were developed to target tumor growth and metastasis in TNBC. Endogenous peptides derived from proteins containing a conserved somatotropin domain were screened for inhibition of angiogenesis and lymphangiogenesis using in vitro proliferation, migration, adhesion and tube formation assays with blood and lymphatic endothelial cells. A short 14-mer peptide derived from transmembrane protein 45A human shows the most potent multimodal inhibition of angiogenesis and lymphangiogenesis in breast tumor xenografts and tumor-conditioned lymph nodes. Mechanistically, the peptide blocks vascular endothelial growth factor receptors 2 and 3 (VEGFR2/3) and downstream proteins by binding to neuropilin 1/2 (NRP1/2) and inhibiting

VEGFR2/3 and NRP1/2 complex formation in the presence of VEGFA/C. A mimetic 20-mer peptide derived from Collagen IV shows synergy with the somatotropin-derived peptide as inhibitors of lymphangiogenesis in vitro and in vivo. The collagen-derived peptide was further optimized, and was evaluated in vitro in lymphangiogenesis and angiogenesis cell assays, and in animal experiments including TNBC breast tumor xenograft and TCM-induced distant metastasis models.

In summary, this dissertation investigates molecular mechanisms of breast cancer metastasis, proposing novel roles of lymphatic endothelial cells in pre-metastatic organs and primary tumor microenvironment; identifies key molecules regulating metastatic dissemination and colonization as well as tumor growth. The dissertation also explores several novel anti-angiogenic and anti-lymphangiogenic peptides to effectively treat TNBC tumor growth and metastasis.

Primary Advisor: Dr. Aleksander Popel

Committee: Dr. Aleksander Popel, Dr. Saraswati Sukumar, Dr. Sharon Gerecht,
Dr. Marc Ostermeier, Dr. Arvind Pathak

Acknowledgments

This study was supported by National Institute of Health and Safeway Foundation grants. Portions of this dissertation have previously been published and were reproduced with permission from the publishers of the journals: copies of permission were included in the Appendix. Published papers were cited in the rationale part in corresponding chapters. For protection of the unpublished contents in revision or in preparation (please see CV), I chose to embargo this dissertation for a period of four years. All the animal protocols described in this dissertation were approved by the Institutional Care and Use Committee at the Johns Hopkins Medical Institutions (JHMI).

I would like to thank all my collaborators and friends who supported me while earning my Ph.D. degree in Chemical and Biomolecular Engineering at Johns Hopkins University. I am grateful to have had such a knowledgeable and engaged thesis committee. Specifically, I would like to thank my thesis advisor Dr. Aleksander Popel, director of the Systems Biology Laboratory in the department of Biomedical Engineering at Johns Hopkins University School of Medicine. His trust and generosity, both personal and professional, provided the ideal working environment for my research. Dr. Popel has delivered a perfect balance of supervision and independence for me to make a progress efficiently. He is an example of a great scholar as well as an engaged educator to guide my progression in the field of angiogenesis and lymphangiogenesis. I also thank Dr. Saraswati Sukumar, co-director of the Breast Cancer Program in the Sidney Kimmel Comprehensive Cancer Center at Johns Hopkins University School of Medicine. She has given me a great chance to obtain relevant perspectives in breast cancer research. Her academic and professional support with insightful discussion has been invaluable for my research. Fruitful collaboration with Dr. Arvind Pathak's laboratory has

expanded my interests to MRI-based imaging of tumor vasculature. I gratefully thank Dr. Sharon Gerecht and Dr. Marc Ostermeier for their scientific guidance for the dissertation. I also need to thank all the members of the Popel laboratory. As a talented experimental biologist, Dr. Niranjan Pandey has been a kind advisor in my experiments. Research collaboration and interaction with Dr. Jacob Koskimaki, Dr. Elena Rosca, Dr. Princess Imoukhuede, Dr. Stacey Finley, Dr. Gang Liu, Dr. Kerri-Ann Norton, Dr. Spyros Stamatelos, and Lawrence Chu have given me valuable experiences in combination of experimental and computational biology. I have to thank my soul mate Jayoung Kim for her tremendous support, trust and encouragement in my pursuing of the doctoral degree. My scientific productivity and quality were greatly enhanced by Jayoung's sincere support and prayers. I also thank my beloved son, Elliott (Zion) Lee, my great joy and happiness. I must recognize my parents in South Korea. Because of their unconditional and empowering love, I have been able to live my life so far doing what I want to. Lastly, I worship and give thanks to my Lord who has led my life so far and will do in his perfect timing with his impeccable wisdom and unfailing love.

List of Abbreviations and Symbols

AMD, age-related macular degeneration

Ang-2, angiopoietin 2

APC, antigen presenting cells

Ax-LN, axillary lymph nodes

BEC, blood endothelial cells

bFGF, fibroblast growth factor basic

BMDC, bone marrow derived cells

Br-LN, brachial lymph nodes

BVD, blood vessel density

CC-3, cleaved caspase 3

CCL5, chemokine ligand 5 (also called RANTES)

CCR5, chemokine receptor 5

CCR7, chemokine receptor 7

CIM-plate, cell invasion and migration plates

Co-IP, coimmunoprecipitation

COX-2, cyclooxygenase 2

CM, conditioned media

c-Met, hepatocyte growth factor receptor

CK7, cytokeratin 7

d, days

Da, dalton unit

DAB, 3,3'-diaminobenzidine

DAPI, 4’,6-diamidino-2-phenylindole

DC, dendritic cells

DMSO, dimethyl sulfoxide

DTT, dithiothreitol

EBM-2, endothelial basal media

EGF, epidermal growth factor

EGFR, epidermal growth factor receptor

EGM-2, endothelial growth media

EGM-2MV, endothelial growth media for microvascular endothelial cells

ELISA, enzyme-linked immunosorbent assay

EMSA, electrophoretic mobility shift assay (also called gel shift assay)

EMT, epithelial-mesenchymal transition

ER, estrogen receptor

FAK, focal adhesion kinase

FBS, fetal bovine serum

FDA, food and drug administration

FITC, fluorescein isothiocyanate

GAPDH, glyceraldehyde 3-phosphate dehydrogenase

GF-dep-TCM, growth factor depleted tumor-conditioned media

GF/IL6-dep-TCM, growth factor/interleukin 6 depleted tumor-conditioned media

GM-CSF, granulocyte-macrophage colony-stimulating factor

Gp130, glycoprotein 130

h, hours

HB-EGF, heparin binding egf-like growth factor

H & E, hematoxylin and eosin

HIF1α, hypoxia-inducible factor 1 alpha

HEPES, (2-hydroxyethyl)-1-piperazineethanesulfonic acid

HER2, human epidermal growth factor receptor 2

HEV, high endothelial venules

HGF, hepatocyte growth factor

HPLC, high-performance liquid chromatography

HSP27, heat-shock protein 27

HUVEC, human umbilical vein endothelial cells

HUVEC-matrigel plug, human umbilical vein endothelial cell included matrigel plug

i.c., intracardiac

IC_{50}, the half maximal inhibitory concentration

IF, immunofluorescence

IGF1, insulin-like growth factor 1

IGF1R, insulin-like growth factor 1 receptor

IHC, immunohistochemistry

IL17, interleukin 17

IL6, interleukin 6

IL6-dep-TCM, interleukin 6 depleted tumor-conditioned media

Int α, integrin alpha

Int β, integrin beta

IP, immunoprecipitation

i.p., intraperitoneal

i.v., intravenous

IVIS, in vivo imaging systems

Jak2, janus kinase 2

JNK, c-jun amino-terminal kinase

LDH, lactate dehydrogenase

LEC, lymphatic endothelial cells

LEC-matrigel plug, lymphatic endothelial cell included matrigel plug

LN, lymph node

Luc, luciferase

LVD, lymphatic vessel density

LYVE-1, lymphatic vessel endothelial hyaluronan receptor 1

MAPK, mitogen-activated protein kinase

MB231-HUVEC, tumor-educated HUVEC

MB231-LEC, tumor-educated LEC

MB231-MEC, tumor-educated MEC

MCF-7, one of estrogen receptor positive (ER+) breast cancer cell lines

MDA-MB-231, one of mesenchymal-like triple negative breast cancer (TNBC) cell lines

MEC, microvascular endothelial cells

min, minutes

µl, microliter

µM, micromolar concentration

µm, micrometer

mm, millimeter

MMP-2/9, matrix metalloproteinase 2/9

m-TOR, mammalian target of rapamycin

MKK3/6, mitogen-activated protein kinase-kinase 3/6

MW, molecular weight

N, number of samples

NFkB, nuclear factor kappa-light-chain-enhancer of activated B cells

n-LEC, normal lymphatic endothelial cells

NRP-1/2, neuropilin-1/2

O.C.T. compound, optimal cutting temperature compound

P, p-value

PBST, phosphate buffered saline with triton

PCNA, proliferating cell nuclear antigen

PDGF-BB, platelet derived growth factor-BB

pI, isoelectric point

poly(dI-dC), poly(deoxyinosinic-deoxycytidylic) acid

Prox-1, prospero homeobox protein 1

PTTG, pituitary tumor transforming gene

PTX-3, pentraxin 3

pX, phosphorylated X protein

RANTES, regulated and normal t cell expressed and secreted (also called CCL5)

PR, progesterone receptor

PRL/GH, human prolactin/growth hormone

R, correlation coefficient

RTCA, real-time cell analysis

RTK, receptor tyrosine kinase

s.c., subcutaneous

SCID, severe combined immunodeficiency

SFM, serum-free media

SMA, smooth muscle actin

STAT3, signal transducer and activator of transcription 3

SUM-149, one of basal-like triple negative breast cancer (TNBC) cell lines

SP20XX, peptides derived from collagen IV domain-containing proteins

SP50XX, peptides derived from somatotropin domain-containing proteins

TBST, tris buffered saline with tween

TCGA, the cancer genome atlas

TCM, tumor-conditioned media

TIMP1, tissue inhibitor of metalloproteinases-1

TME, tumor microenvironment

TMEM45A, transmembrane protein 45A

TNBC, triple-negative breast cancer

TSP1, thrombospondin 1

VEGF, vascular endothelial growth factor

$mVEGF_{164}$, mouse vascular endothelial growth factor 164

$hVEGF_{165}$, human vascular endothelial growth factor 165

VEGFC, vascular endothelial growth factor C

VEGFR2, vascular endothelial growth factor receptor 2

VEGFR3, vascular endothelial growth factor receptor 3

ZO-1, tight junction protein-1

Table of Contents

List of Figures

List of Tables

Chapter 1: Introduction

1.1 MICROENVIRONMENT IN CANCER

Microenvironment in cancer has been an emerging target to efficiently inhibit tumor growth and metastasis. However, current understanding of the microenvironment is lacking and many roles of the microenvironment and their mechanisms and effects on tumor progression and metastasis are unknown. Tumor drug resistance and relapse are results of complex cell-to-cell communications between stromal and cancer cells in the microenvironment. Thus, understanding the roles of the microenvironment is essential to improve current cancer therapies. There are two different microenvironments in cancer: tumor microenvironment and organ microenvironment.

1.1.1 Tumor microenvironment (TME) in cancer

Tumor microenvironment (TME) consists of diverse types of cells, including cancer cells, cancer associated fibroblasts, pericytes, immune cells, adipocytes, bone-marrow derived cells, blood and lymphatic endothelial cells, smooth muscle cells, and non-defined other cell types (Catalano, Turdo et al. 2013). These cells communicate with cancer cells, extracellular matrix (ECM) and other stromal cells to promote tumor growth and metastasis. For example, cancer associated fibroblasts in the TME induce tumor growth and metastasis via upregulating tumor promoting gene expression; modifying host immunity; and conferring epithelial to mesenchymal transition (EMT) in cancer cells (Liao, Luo et al. 2009; Xing, Saidou et al. 2010; Yu, Chen et al. 2013). In addition, tumor macrophages, one of the immune cells in the TME express tumor promoting and proangiogenic factors to facilitate tumor growth (Stearman, Dwyer-Nield et al. 2008). Cell-to-cell communication among the TME residing cells employs direct cell-to-cell interactions via adhesion molecules and remote interactions via their secreted factors and surface receptors (Shekhar, Pauley et al. 2003; Calvo and Sahai 2011; Hale, Li et al. 2012; Schaaij-Visser, de Wit et al. 2013) to play a role in cancer growth and metastasis. This contributes to a

tremendous complexity of TME, conferring tumor heterogeneity in types of stromal cells, secreted factors, signals and resulting phenotypes. These also result in difficulties in identification of well-established druggable targets against tumor drug resistances and relapses (Shipitsin, Campbell et al. 2007; Marusyk and Polyak 2010; Mannello and Ligi 2013). For these reasons, understanding and targeting of stromal cells, cell-secreted factors and their signals are crucial to be combined with conventional cancer therapies (Loeffler, Kruger et al. 2006; Panni, Linehan et al. 2013).

1.1.2 Organ microenvironment in cancer

According to the "seed and soil hypothesis" by Stephen Paget (Paget 1989), metastatic cancer cells function as "seeds" and a particular organ microenvironment serves as the "soil". The "soil" should be prepared and pre-conditioned to function as a metastatic niche (Psaila and Lyden 2009). Several studies have provided a body of evidence supporting this hypothesis. For example, organs with low incidence of metastasis have been reported and these are associated with poor metastatic niche formation (Araki 1968). In contrast, some organs such as the lymph nodes and the lungs show high incidence of metastasis in many cancers (Hirasawa, Gotoda et al. 2009; Dos Santos, Garg et al. 2011; Nishida, Tsukushi et al. 2013; Lee, Fertig et al. 2014). It also has been reported that tumor metastases show organ-specific patterns (Nguyen, Bos et al. 2009; Lu, Yan et al. 2010; Lorusso and Ruegg 2012; Rigamonti and De Palma 2013). For example, breast cancer mostly shows metastasis in the lungs, brains, bones, and liver (Lorusso and Ruegg 2012). Leukemias do metastasize to the nervous system but rarely involve brain parenchyma and more involve the leptomeninges, two innermost layers of the membrane that envelops the brain and spinal cord (De Marco, Di Gioia et al. 2010). These studies suggest that conditions of organ microenvironment significantly influence tumor metastasis. Metastatic processes include initial

tumor cell intravasation, recruitment and survival, extravasation, seeding, angiogenesis and the resulting colonization (Stracke and Liotta 1992; Sahai 2007). Several mechanistic studies have demonstrated how the organ microenvironments are primed for cancer metastasis. It has been reported that TGF-beta primes breast tumors for lung metastasis seeding through the angiopoietin-like 4 induced tumor cell extravasation (Padua, Zhang et al. 2008). Other mediators of vascular remodeling in lung metastasis have also been discovered in breast cancer (Gupta, Nguyen et al. 2007). Selection of bone metastasis seeds by mesenchymal signals has been described focusing on CXCL12 and IGF1 in breast cancer bone metastasis and colonization (Zhang, Jin et al. 2013). Tumor conditioned media from breast cancer cells induced lymphangiogenesis and angiogenesis in regional lymph nodes (Lee, Pandey et al. 2014). Increased lymph node angiogenesis in draining lymph nodes were observed and correlated with lymph node metastasis and lower survival in breast cancer patients (Edel, Harvey et al. 2000; Guidi, Berry et al. 2000). Exosomes secreted from melanoma induced lymph node angiogenesis and blood vessel remodeling (Hood, San et al. 2011). Melanoma exosome mediated c-Met and its effects on bone marrow derived cells and organ niche formation has been reported (Peinado, Aleckovic et al. 2012). An exosome is a microvesicle derived from tumors, which is emerging in tumor and niche communication for metastatic progression. These examples suggest that targeting tumor secretomes, pre-metastatic organ-residing cells, cell-to-cell communication via tumor-secreted factors or exosomes, and the resulting signals can benefit current therapeutic strategies.

1.2 ANGIOGENESIS AND LYMPHANGIOGENESIS IN CANCER

Angiogenesis is the process of new blood vessel formation from pre-existing blood vasculature (Folkman and Klagsbrun 1987). Angiogenesis is an important process, occurring in both health and disease. Appropriate balance between angiogenic stimulators and inhibitors is fundamental for regulating and maintaining angiogenesis in health. Disturbed homeostasis in angiogenesis is associated with many diseases including cancer, age-related macular degeneration (AMD), diabetes, rheumatoid arthritis, psoriasis and cardiovascular diseases such as coronary and peripheral artery diseases and stroke (Carmeliet and Jain 2011). Lymphangiogenesis, the process of new lymphatic vessel formation from pre-existing lymphatic vessels, is important for functioning of the immune system, lymphoid organ formation, tissue fluid homeostasis, and absorption of dietary fats (Stacker, Achen et al. 2002). Dysregulated lymphangiogenesis can result in pathological conditions such as lymphedema, abnormal fat metabolism, hypertension, inflammatory diseases and lymph node mediated tumor metastasis (Tammela and Alitalo 2010).

Angiogenesis and lymphangiogenesis are closely involved in cancer progression. Tumor angiogenesis is an important target for inhibition of tumor growth (Carmeliet and Jain 2011; Potente, Gerhardt et al. 2011). Solid tumors with more than a certain size require intra-tumoral blood vessels providing tumor cells with oxygen and nutrients to support tumor growth. This can be explained by that the oxygen transfer to the cancer cells inside of the tumor mass would be inefficient without further extension of the blood vessels as the tumor becomes bigger (Vaupel, Kallinowski et al. 1988). Tumor angiogenesis is induced by tumor-secreted angiogenic factors such as the vascular endothelial growth factor (VEGF) (Plate, Breier et al. 1992). Thus, a monoclonal antibody for VEGF (bevacizumab) and others inhibitors of VEGF and its signaling

have been used as anti-angiogenic agents in several cancers (Ferrara, Hillan et al. 2004; Meadows and Hurwitz 2012).

In addition to angiogenic factors, tumor cells secrete lymphangiogenic factors (e.g., VEGF-C and VEGF-D) to promote tumor lymphangiogenesis (Karpanen, Egeblad et al. 2001; Von Marschall, Scholz et al. 2005), the formation of new lymphatic vessels in the tumor stroma. It has been known that stromal lymphatic vessels play a role as initial routes of tumor dissemination (Skobe, Hawighorst et al. 2001; Tammela and Alitalo 2010), thus the blockage of tumor lymphangiogenesis is regarded as one of anti-metastatic strategies (Jain and Padera 2002; Achen, Mann et al. 2006).

However, these blood and lymphatic vessels have been considered as passive conduits for the delivery of oxygen, nutrients, or metastatic cancer cells. Hence, conventional anti-angiogenic or anti-lymphangiogenic therapy has focused on the inhibition of the formation of the blood or lymphatic vasculatures to block the paths. However, recently, a number of studies have revisited blood and lymphatic endothelium, focusing on their mediated factor secretion and signals, suggesting inductive roles of blood and lymphatic vessels in cancer progression. This implies that the blood and lymphatic vessels are more than the conduits, even are active composites in the tumor microenvironment (Franses and Edelman 2011; Swartz, Iida et al. 2012). These recent advances add blood and lymphatic endothelial cells to other types of cells in the TME, including fibroblasts, immune cells, bone-marrow derived cells, etc. (Sugimoto, Mundel et al. 2006; Bergfeld and DeClerck 2010; Ruffell, Affara et al. 2012).

1.3 SECRETOMES OF BLOOD AND LYMPHATIC VASCULATURES

1.3.1 Blood vascular secretome in physiology and cancer

Blood vessels are distributed throughout the body to facilitate blood circulation. At the same time, blood endothelial cells residing in the vascular endothelium express and secrete diverse factors to communicate with other cells and maintaining homeostasis in physiology: these blood endothelial cell secreted factors are referred to as "angiocrine factors" (Butler, Kobayashi et al. 2010). The angiocrine factors play a role in human physiology. It has been reported that angiocrine factors are essential to balance self-renewal and differentiation of hematopoietic stem cells (Kobayashi, Butler et al. 2010). In addition, angiocrine factors are central for regeneration of tissues in the lungs and livers (Butler, Kobayashi et al. 2010; Ding, Nolan et al. 2010; Ding, Nolan et al. 2011; Tashiro, Nishida et al. 2012). The angiocrine factors also play a role as a director of thromboregulation (Stern, Kaiser et al. 1988). Blood endothelium also maintains blood fluidity and immunity by crosstalk with platelets (Ruggeri 2003).

Tumor angiogenesis has been a promising target for blocking oxygen supply and inhibiting tumor growth. According to this conventional understanding, blood endothelial cells and their crosstalk with other cells in tumor microenvironment result in tumor promotion (Witz 2006). The angiocrine factors modulate tumor cell proliferation and motility through Ephrin A2 repression of Slit2 tumor suppressor function (Brantley-Sieders, Dunaway et al. 2011). Endothelial cell-initiated signaling promotes the survival and self-renewal of cancer stem cells (Krishnamurthy, Dong et al. 2010). Microvascular endothelial cell secreted factors induce growth and migration of lymphoma cells (Hamada, Cavanaugh et al. 1992). Secreted factors from brain endothelial cells maintain glioblastoma stem-like cell expansion through the mTOR pathway (Galan-Moya, Le Guelte et al. 2011). Endothelium-dependent epithelial-mesenchymal transition (TME) of

cancer cells via transforming growth factor beta1 and beta2 (TGF-β1 and TGF-β2) has been reported (Kimura, Hayashi et al. 2013). Moreover, CD151 induces tumorigenesis by modulating communication between tumor cells and blood endothelium (Sadej, Romanska et al. 2009). Very interestingly, other studies reported the "opposite effects" of the angiocrine factors as suppressing tumor progression. Endothelial derived factors inhibit anoikis of head and neck cancer stem cells (Campos, Neiva et al. 2012). Stromal endothelial cells directly inhibit cancer progression via endothelium-derived perlecan, and the blockage of endothelial perlecan promotes tumor growth (Franses, Baker et al. 2011). Recently, it has been reported that stable perivascular niche constitutes tumor dormancy, whereas sprouting neovasculature sparks micrometastatic outgrowth (Ghajar, Peinado et al. 2013). These results suggest that roles of blood vascular secretome in TME are quite unpredictable and are not fully understood. Thus, there is unmet need to understand the role of blood vessel derived factors and their crosstalk with tumor cells to improve anti-angiogenic or other anti-cancer therapies.

1.3.2 Lymphatic vascular secretome in physiology and cancer

Lymphatic vessels are different from blood vessels. They do not have well-defined basement membrane, do not carry erythrocytes, and are composed of lymphatic endothelial cells that are distinct from blood endothelial cells (Hirakawa, Hong et al. 2003; Pepper and Skobe 2003). Generally physiological lymphatic vessels play a role as reservoirs for immune cells, antigens, lipids, macromolecules, and particulate matters that have leaked from the vascular system and transport lymph fluid back to the circulatory system (Weech, Goettsch et al. 1934; Olszewski 2003; Tammela and Alitalo 2010). Thus, in abnormal lymphatic vessels, lymph fluid cannot be efficiently drained and results in lymphedema. The lymphatic vessels also function in fat absorption and lipid transport. It has been reported that the consumption of fatty foods increase

lymph flow in human (Turner and Barrowman 1977). In addition, the lymphatic endothelium expresses several adhesion molecules and chemokine ligands that interact with immune cells, thus the lymphatic system facilitates maintenance of the host immunity (Dietrich, Bock et al. 2010; Steven, Bock et al. 2011). CC chemokine ligand 19 (CCL19) is expressed by LEC and attract CCR7 positive dendritic cells (DC) and antigen-presenting cells (APC) (Dieu, Vanbervliet et al. 1998; Bromley, Thomas et al. 2005; Forster, Davalos-Misslitz et al. 2008). These DC and APC are transported into lymph nodes (LN) and meet T-lymphocytes in the T-cell zone in the LN. Then, T lymphocytes and DC are activated and matured, departing from the LN through the efferent lymphatic vessels to modulate host immunity. In addition, T and B lymphocytes in the LN are important in regulation of lymphangiogenesis in the LN. T lymphocytes negatively regulate lymphangiogenesis via interferon gamma expression (Kataru, Kim et al. 2011). On the other hand, B lymphocytes promote lymphangiogenesis in the LN (Angeli, Ginhoux et al. 2006).

Compared to blood endothelial cells, lymphatic endothelial cells have not been studied as well in terms of their inductive signals and secreted factors (also called 'lymphangiocrine factors') in cancer (Tammela and Alitalo 2010). Recently, gene expressions and protein expression in LEC have been studied in several experimental conditions to identify LEC-induced signals and their distinct roles compared to the blood endothelial cells (Podgrabinska, Braun et al. 2002; Hirakawa, Hong et al. 2003; Mancardi, Vecile et al. 2003; Yong, Bridenbaugh et al. 2005; Irigoyen, Anso et al. 2007; Wick, Saharinen et al. 2007). One of well understood roles of lymphangiocrine factors is lymphatic endothelium induced CCL21 and CCL19 and the resulting recruitment of CCR7-positive tumor cells into the lymphatic system (Shields, Fleury et al. 2007). This has been a basis of understanding that the tumor lymphatic vessels serve as routes of tumor dissemination. Moreover, lymphatic vessels are manipulated by tumor cells to disrupt host

immunity and promote tumorigenesis (Lund and Swartz 2010; Shields 2011). However, this role of tumor escaping of host immunity via lymphatic vessels is still controversial (Dietrich, Bock et al. 2010; Mirsky, Miller et al. 2011; Kataru, Lee et al. 2014).

In this dissertation, we will investigate tumor and organ microenvironment in breast cancer focusing on the crosstalk between blood and lymphatic endothelial cells and tumor cells; then we will evaluate the signals that could serve as targets to efficiently inhibit breast tumor growth and metastasis.

Chapter 2: Tumor-Conditioned Media Induced Breast Cancer Metastasis Models

2.1 RATIONALE

Most of the deaths from breast cancer are the result of metastasis. Metastasis is a very complex process that has been difficult to investigate. Most cancer therapeutics have been developed and tested in preclinical animal models for inhibition of growth of primary tumors and not for inhibiting metastasis. This might be one of the reasons why most cancer drugs have not produced dramatic increases in overall survival of patients. The development of anti-metastatic agents has been hampered by the lack of spontaneous metastasis models for preclinical evaluation of therapeutic agents. Establishing spontaneous metastasis models has been difficult because of the dependence of spontaneous metastasis on diverse factors such as the degree of tumor growth (Maehara, Tomisaki et al. 1997), tumor angiogenesis (Mori, Arii et al. 1999), lymphatic networks (Ran, Volk et al. 2010), aggressiveness or invasiveness of cancer cells (Petrella 2009), and the condition of pre-metastatic niches (Carlini, De Lorenzo et al. 2011). Beyond these reasons, there are a number of unknown factors that affect metastatic rates. The effects of these factors are quite unpredictable in tumor-bearing animals thus causing inconsistent metastatic progression and inefficient metastasis.

Though experimental mouse models for metastasis such as the tail-vein injection model (Elkin and Vlodavsky 2001) and the intracardiac injection model (Scepansky, Goldstein et al. 2011) develop consistent metastases in a relatively short time, these models have drawbacks: they reflect only hematogenous (blood vessel-mediated) metastasis, and are triggered by artificially injected cancer cells into the blood stream. However, analyses of preclinical and clinical studies show that metastasis occurs through both the lymphatic vessels and the blood vessels (Alitalo and Carmeliet 2002; Ran, Volk et al. 2010; Tammela and Alitalo 2010). Thus,

there is an unmet need for spontaneous metastasis models in which lymphogenous and hematogenous metastasis occur rapidly and consistently.

A tumor-conditioned lymph node (LN) model has been developed by injecting tumor-conditioned media (TCM) subcutaneously into animals (Lee, Koskimaki et al. 2013). This model simulates the conditioning of tumor-draining LN by primary tumor-secreted factors which are transported through the lymphatic and blood vessels (Hirakawa, Kodama et al. 2005; Yamamoto, Kikuchi et al. 2008; Psaila and Lyden 2009; Wong, Zhang et al. 2012). In that study, LN in the TCM pre-treated animals had enhanced angiogenesis and lymphangiogenesis, compared to those in serum-free media (SFM) treated animals (Lee, Koskimaki et al. 2013). In this chapter, experiments are described such that the "TCM pre-treatment" step is added to general orthotopic tumor xenograft models to develop a more efficient spontaneous breast cancer metastasis model. This new model provides a valuable and relevant addition to the collection of mouse models for breast cancer metastasis (Kim and Baek 2010; Francia, Cruz-Munoz et al. 2011).

Portions of this chapter have previously been published (Lee, Pandey et al. 2014) and were reproduced with permission from the publishers of the journals: copies of permission were included in the Appendix.

2.2 MATERIALS & METHODS

2.2.1 Cell culture

Human triple-negative breast cancer (TNBC) cell lines, MDA-MB-231 (mesenchymal-like TNBC) and SUM-149 (basal-like TNBC) were provided by Dr. Zaver Bhujwalla (Radiology and Oncology, Johns Hopkins Medical Institutions). MDA-MB-231-luc-D3H2LN was purchased from Caliper (Hopkinton, MA). MDA-MB-231 and MDA-MB-231-luc-D3H2LN cells were propagated in RPMI-1640 media (Gibco, Carlsbad, CA) supplemented with 10% Fetal Bovine Serum (FBS, Sigma Aldrich, St. Louis, MO) and 1% penicillin streptomycin (Gibco). SUM-149 cells were cultured in F-12 media (Corning, Manassas, VA) supplemented with 5% FBS (Sigma Aldrich), 1 ng/ml hydrocortisone (Sigma Aldrich), 5 μg/ml insulin (Sigma Aldrich), 0.1mM 4-(2-Hydroxyethyl)-1-piperazineethanesulfonic acid (HEPES) (Gibco). Lymphatic endothelial cells (LEC) and microvascular endothelial cells (MEC) were purchased from Lonza (Walkersville, MD), and propagated in microvascular endothelial cell growth medium-2 (EGM-2MV, Lonza). Cells were maintained under standard conditions of 37°C and 5% CO_2. The passage numbers of the endothelial cells were between 3 and 6.

2.2.2 Preparation of tumor-conditioned media (TCM)

MDA-MB-231 cells or SUM-149 cells in complete media (RPMI-1640 or F-12 media with supplements) were plated on T175 tissue culture plates. When the cells formed a confluent monolayer, the complete media was removed and the cells were carefully rinsed with serum-free media (RPMI-1640 or F-12 without supplements). 8 ml of the same SFM was added to the cells. After 24 h incubation, the supernatant was collected, centrifuged, and filtered through 0.2 μm

syringe filters (Corning, Tewksbury, MA). The resulting tumor-conditioned media (TCM) was stored in aliquots at -80°C to avoid multiple freeze thaws.

2.2.3 Cell migration assay

Cancer cell migration was assessed by using the Oris^{TM} cell migration kit (Platypus, Madison, WI). MDA-MB-231 cells were pre-labeled with Cell Tracker Green (Invitrogen, Carlsbad, CA) according to the manufacturer's protocol. 50,000 labeled cancer cells in complete media (RPMI-1640) were added to each well of a 96-well plate containing stoppers to prevent the cells from settling in the center region of the wells. Cells were allowed to adhere for 4 h, after which the stoppers were carefully removed. TCM or serum-free media (SFM, 100 µl) was added, and the cells that migrated to the center of the well were quantified by measuring the fluorescence at 485/530 nm on a Victor V plate reader (PerkinElmer, Salem, MA). The migrated cells were visualized by imaging on the Eclipse T-100 fluorescence microscope (Nikon, Brighton, MI).

2.2.4 Tube formation assay

50 µl matrigel (growth factor reduced, BD Biosciences, Bedford, MA), thawed on ice at 4°C overnight, was loaded in each well of a pre-cooled 96-well plate, and the plate was incubated at 37°C for 30 min. Fifteen thousand lymphatic endothelial cells (LEC) and microvascular endothelial cells (MEC) in 100 µl MDA-MB-231 TCM or SUM-149 TCM were added on top of the matrix in the 96-well plate. For controls, LEC and MEC in endothelial cell growth media (EGM-2MV, Lonza) or serum-free media (EBM-2, endothelial basal media-2, Lonza) were also loaded. The plate was then incubated at 37°C, and the wells were imaged using a Nikon microscope at 14 h (Nikon Instruments Inc., Melville, NY).

2.2.5 Lymph node assay

Athymic nude mice were administered 50 µl MDA-MB-231 tumor-conditioned media (TCM) or serum-free media (SFM) subcutaneously on a daily basis. After 14 days of administration, mice were euthanized and the axillary and brachial lymph nodes (LN) were excised from each animal. The LN were rinsed in cold PBS and the LN were placed in 100 µl tissue lysis buffer containing 150 mM NaCl, 50 mM Tris HCl, 1 mM EDTA, 1% Triton-X, phosphatase inhibitors cocktail-2/3 and protease inhibitors (Sigma), homogenized using a tissue grinder (Pyrex Potter-Elvehjem Tissue Grinders with PTFE Pestle), and incubated at 4°C for 2 h. The lysed samples were spun to remove cell membranes and debris for 40 min at 14,000 rpm. LN lysate was separated with SDS-PAGE and transferred to nitrocellulose blots (Invitrogen, Carlsbad, CA). The membrane was blocked for 1 h with 5% non-fat milk in TBST (1X TBS with 0.1% Tween) and probed with antibodies of interest including MECA-79 (Santa Cruz Biotechnologies, Inc.), p-VEGFR-2 (Y1175), p-EGFR (Y1068), GAPDH (Cell Signaling Technologies, Inc.). GAPDH was used as a loading control. Secondary antibodies (GE Healthcare, UK) were added at 1:2000 dilution and protein bands detected with chemiluminescence detection reagent (GE Healthcare).

2.2.6 A tumor-conditioned media induced spontaneous metastasis model

Before orthotopic tumor inoculation, athymic nude mice (female, 5-6 weeks, 18-20 g) were pre-treated by injecting 50 µl tumor-conditioned media (TCM from Luc-MDA-MB-231 or SUM-149) or serum-free media (SFM) subcutaneously through the scruff for 2 weeks as described previously (Lee, Koskimaki et al. 2013). The body weight of the animals for the duration of the experiment was monitored to determine if there was TCM-induced toxicity in the animals. After 2 weeks of TCM pre-treatment, MDA-MB-231-luc-D3H2LN tumor xenografts were established

in the same animals. MDA-MB-231-luc-D3H2LN breast cancer cells (2 x 10^6) in 50 µl complete media (RPMI-1640 supplemented with 10% FBS) and 50 µl matrigel (high-concentrated, BD Biosciences) were well mixed and injected (total volume 100 µl/animal) into the upper inguinal mammary fat pad of the animals under anesthesia (50 mg/kg ketamine + 5 mg/kg acepromazine in PBS, intraperitoneally dosed). Surgical excision of the primary inguinal mammary tumors was not performed as the tumor injection site is sufficiently far from the anterior organs, metastasis to which investigators were interested in observing. The primary tumor size was measured by using a caliper, and the volume was calculated, using the formula: $V = 0.52 \times a \times b^2$, where 'a' is the long axis, and 'b' is the short axis of the tumor. Animals were imaged every week to track the development of anterior tumor metastases, using the IVIS Xenogen 200 optical imager (Xenogen, Alameda, CA) after intraperitoneal injection of D-luciferin (Caliper, 150 mg/kg). 100 µl D-luciferin (twice diluted) was intraperitoneally injected in both sides of the abdomen (total 200 µl/animals) to prevent i.p. injection failure (Jenkins, Hornig et al. 2005). After 4 weeks, the axillary and brachial LN, the lungs, and the brain were harvested and bathed in D-luciferin solution for 5-10 min and placed in the IVIS imager to detect metastases ex vivo. Luciferase-mediated photon flux was quantified by using Living Image® 3D Analysis (Xenogen), and the average photon flux was obtained from 8 lungs, 8 brains, and 14-16 lymph nodes as described before (Padua, Zhang et al. 2008). In case of animals showing intra-abdominal metastases, ex-vivo images of abdominal organs, including stomach, spleen, kidney, liver, and intestine, were obtained using the IVIS imager.

Another triple-negative breast cancer (TNBC) cell line, SUM-149, was tested by using the same metastasis model as above, to demonstrate the application of the model to other cell types of breast cancer. Because luciferase-transfected SUM-149 are not available, instead of using the

IVIS imager, 3,3' diaminobenzidine (DAB) mediated immunohistochemistry with cytokeratin 7 antibodies (anti-CK7) and human proliferating cell nuclear antigen (PCNA) antibodies was performed on the lungs and the LN. These organs were harvested after 6 weeks of tumor inoculation when the tumor size in both TCM and SFM-treated groups reaches approximately 1,000 mm^3, which is the same tumor size in the MDA-MB-231 model above (4 weeks). Ten lungs and 40 LN (2 axillary and 2 brachial LN, each mouse) were harvested from each group of animals (N=10). The organs were fixed, frozen and sectioned into 10 μm thick slices, yielding 3 slides from the top, the middle, and the bottom of the organs, resulting in a total of 30 slides for lungs and 120 slides for LN in each group.

2.2.7 Immunofluorescence and immunohistochemistry

For immunofluorescence, the tumors, LN, and lungs fixed in 4% formalin for 16 h were placed in 30% sucrose solution in PBS, incubated overnight at 4°C, and frozen in the Tissue-Tek Optimal Cutting Temperature (O.C.T.) compound (Sakura, Tokyo, Japan). Sections of 10-μm thickness were cut at -20°C. After blocking with 5% normal goat serum (Jackson ImmunoResearch, West Grove, PA) in PBST (1X PBS with 0.3% Triton) for 1 h at room temperature, the sections were treated with one or more of the following primary antibodies overnight at 4°C: rabbit anti-mouse LYVE-1 antibody (lymphatic vessel endothelial hyaluronan receptor-1, 1:200, AngioBio, Del Mar, CA), rat anti-mouse CD31 (1:100, BD Pharmingen, San Jose, CA), and rat anti-lectin FITC (fluorescein isothiocyanate) (1:100, Sigma Aldrich). After 3 rinses with PBST, sections were incubated for 1 h at room temperature with one or more of the secondary antibodies: fluorescein isothiocyanate (FITC)-conjugated goat anti-rat antibody, rhodamine-conjugated goat anti-rat antibody, Cy3-conjugated goat anti-rabbit antibody (all three from Jackson ImmunoResearch), Alexa Fluor 647 goat anti-rabbit antibody, and Alexa Fluor 488

goat anti-rabbit antibody (all two from Cell Signaling Technology, Danvers, MA). The samples were washed with PBST 3 times and DAPI (4',6-diamidino-2-phenylindole, 1:10,000, Roche, Indianapolis, IN) was used for nuclear staining for 5 min at room temperature. The samples were washed with PBST 1 time, and mounted with the ProLong Gold anti-fade reagent (Invitrogen, Carlsbad, CA). Fluorescent signals were visualized and digital images were obtained, using a LSM-510 confocal microscope equipped with argon and helium-neon lasers (Carl Zeiss, Baltimore, MD). The images were analyzed, averaging the pixel intensity of 12 images that are randomly selected (10x magnification) in each group by using ImageJ (National Institutes of Health, Bethesda, MD). For immunohistochemistry, LN and lungs from SUM-149 xenograft mice were fixed, frozen and sectioned as above. After blocking with 5% goat serum in PBST for 1 h at room temperature, the sections were treated with mouse anti-cytokeratin 7 antibodies (1:200, Sigma Aldrich) or mouse anti-human PCNA antibodies (1:2000, BD Pharmingen) overnight at 4°C. After 4 rinses with PBST, the sections were incubated for 30 min at room temperature with SignalStain® Boost IHC Detection Reagent (HRP-conjugated, for mouse antibody detection, Cell Signaling). The samples were washed with PBST 3 times, and treated with SignalStain® DAB Substrate (Cell Signaling) for 1 min. 0.1% Hematoxylin Solution (Sigma-Aldrich) was used for counterstaining. After washing with tap water, the slides were incubated in 0.1% Sodium bicarbonate (Sigma) for 1 min and rinsed with tap water. Dehydrated slides were mounted with glycerol, and covered with a glass slide. Slides were examined on the Olympus BX51TF with DP70 color camera (Olympus, Japan).

2.2.8 Statistical analysis

Error bars correspond to SEM. Differences between a control and treated groups are regarded as significant when p is less than 0.05 using the Student's t-test.

2.3 RESULTS

2.3.1 Accelerated metastasis to the LN and the lungs by pre-treatment of animals with TCM

Mice were separated into two groups: "TCM group", animals pre-treated with tumor-conditioned media (TCM); and "SFM group", animals pre-treated with serum-free media (SFM). After two weeks of TCM or SFM treatment, 2 x 10^6 MDA-MB-231-luc-D3H2LN or SUM-149 cells in 50% matrigel (high concentrated, BD Biosciences) were inoculated into the upper mammary fat pad in the inguinal region of the animals. In the MDA-MB-231-luc-D3H2LN model, anterior metastases were assessed every week using the IVIS imager: every animal in the "TCM group" had metastases in the anterior organs within 4 weeks, whereas the "SFM group" did not show significant distant metastasis (1 out of 8 mice at 4 weeks) (Figure 2.1.A). However, TCM pre-treatment did not influence the body weights of the animals (Figure 2.1.B) and the mean tumor volume (Figure 2.1.C). Four weeks of tumor inoculation, when the size of primary tumors was approximately 1,000 mm^3 (Figure 2.1.C), the animals were euthanized, and the axillary and brachial LN, the lungs, and the brains were excised. The luciferase-expressing tumor cells in these organs were detected ex vivo (Figure 2.1.D). Luciferase-mediated metastatic signals, the averaged photon flux from metastatic tumor cells in the organs (8 lungs, 8 brains, and 14-16 LN) were measured. LN and lungs showed significantly enhanced metastatic signals, however, brains showed no difference (Figure 2.1.E).

Similarly, SUM-149 xenograft models were pre-treated with TCM prepared from SUM-149 cells or serum-free media (SFM, F-12 media without supplements). In the SUM-149 model, metastases were assessed by performing immunohistochemistry with anti-cytokeratin 7 and anti-

human PCNA antibodies (Figure 2.2 and 2.3). Tumor growth data showed that primary tumor size was not influenced by TCM pre-treatment (Figure 2.2.A). SFM-treated animals had 4 axillary LN (ax-LN) and 7 brachial LN (br-LN) with metastases out of 40 LN (20 ax-LN + 20 br-LN). Notably, TCM pre-treated group showed increased LN metastasis with metastases in 13 ax-LN and 16 br-LN out of 40 LN (20 ax-LN + 20 br-LN) (Figure 2.2.B). We also observed that TCM-treated LN exhibited lymphadenopathy (swollen LN) with transparent fluid inside of the LN. LN from serum-free media (SFM) treated animals looked normal (Figure 2.2.C). Immunohistochemistry results showed that TCM-treated LN are highly metastasized and the area of lymphadenopathy is spatially associated with metastatic cancer cells (represented by black arrows) that are detected by anti-CK7 and anti-human PCNA (Figure 2.2.D, E). In the animals with SUM-149 tumors, the TCM pre-treated group showed profound lung metastases in the 9 lungs out of 10 lungs, but the SFM-treated control showed metastasis in 3 out of 10 lungs (Figure 2.3.A). Macroscopic images show metastatic tumor nodules on the lung surface in the TCM-treated group (Figure 2.3.B). Immunohistochemistry confirmed anti-cytokeratin 7 and anti-human PCNA positive metastatic cancer cells in the TCM-treated lung tissues (Figure 2.3.C, D).

2.3.2 TCM pre-treatment promotes lymphangiogenesis in primary tumors

Immunofluorescence was performed on MDA-MB-231 primary tumors from the "TCM group" or "SFM group". The primary tumors were excised 4 weeks after tumor inoculation on the inguinal mammary fat pads. Anti-mouse LYVE-1 and anti-mouse CD31 antibodies were used to detect mouse lymphatic and blood vessels in the tumors. TCM pre-treatment dramatically increased the number of lymphatic vessels in the tumor by 4.68 fold (**$P < 0.01$), compared to the SFM-treated group (Figure 2.4.A, C). However, blood vessel density in the tumors was not significantly influenced by TCM pre-treatment (Figure 2.4.B, C).

2.3.3 TCM-treatment induces lymphangiogenesis in the lungs and LN, angiogenesis was enhanced in the LN

The lungs and the LN from TCM or SFM pre-treated animals were analyzed (Figure 2.5). In this set of experiments, primary inguinal tumors were not established but just TCM pre-treated animals were used. This was done to investigate the change in blood vascular capillaries or lymphatics by TCM treatment and not by metastatic cancer cells or primary tumors. The lungs of the animals treated with TCM had 2.62 times more lymphatic vessels than the lungs of the SFM-treated animals (*$P < 0.05$); there were no significant differences in blood vessel density stained with anti-CD31 and anti-lectin (Figure 2.5.A, C). LN from TCM or SFM treated animals were analyzed (Figure. 2.5.B, D). The brachial LN of the TCM-treated animals had 3.20 times as many lymphatic vessels and 1.74 times as many blood vessels, compared to the brachial LN of the SFM-treated animals (**$P < 0.01$ in LV, *$P < 0.05$ in BV) (Figure 2.5.B, D). Enhanced angiogenesis in the LN was further analyzed by performing western blot assays with LN tissue lysates (Figure. 2.6.A, B). MECA-79 was used to measure LN-specific endothelium, high endothelial venules (Sadej, Romanska et al.). Phosphorylation of vascular endothelial growth factor receptor 2 (VEGFR-2) and epidermal growth factor receptor (EGFR) was additionally assessed to examine TCM-mediated proangiogenic signaling. The amount of MECA-79 and presumably the number of the LN-specific endothelial cells was changed by 4.1 fold in axillary LN and by 6.9 fold in brachial LN after TCM pre-treatment. Phosphorylation of VEGFR-2 was also increased 10.5 fold in axillary LN and 5.7 fold in brachial LN. Phosphorylation of EGFR was increased 3.3 fold in axillary LN and 3.0 fold in brachial LN (Figure. 2.6. A, B).

2.3.4 TCM exhibits lymphangiogenic and angiogenic potential in tube formation assays

The TCM effect was assessed in tube formation assays with lymphatic endothelial cells (LEC) and microvascular endothelial cells (MEC), evaluating the effect of TCM in functional lymphangiogenesis and angiogenesis (Figure 2.6.C). For controls, normal endothelial growth media for microvascular cells (EGM-2MV) and serum-free media (SFM) were employed. TCM prepared from MDA-MB-231 cells profoundly promoted MEC and LEC tube formation, compared to SFM in which the cells failed to form tubes. The tubes formed in TCM were comparable to the tubular network induced by normal growth media (EGM-2MV). SUM-149 had moderate angiogenic and lymphangiogenic activity, which was weaker than the induction by MDA-MB-231 TCM (Figure 2.6.C).

2.3.5 TCM enhances cancer cell motility and induces metastasis to the abdomen

MDA-MB-231 cell migration induced by TCM or by SFM was examined. TCM treatment enhanced cancer cell motility 3.13 fold at 9 h (*$P < 0.05$), and 5.26 fold at 18 h (**$P < 0.01$), compared to SFM treatment (Figure 2.7.A, B). TCM or SFM pre-treated animals were observed, comparing of intra-abdominal metastasis from the primary site, after 4 weeks of the primary tumor inoculation. Luc-MDA-MB-231 cancer cells from the primary tumors were disseminated to the abdominal site in five animals (out of 8 mice total) when the mice were pre-treated with TCM (Figure 2.7.C). Two animals showed intra-abdominal metastases when they were pre-treated with SFM. Internal organs placed in the abdominal area, including stomach, spleen, kidney, liver, and intestine were harvested and examined under the IVIS Xenogen imager. Metastases were mostly detected in the stomach, spleen, liver, jejunum and duodenum (Figure 2.7.C).

2.4 DISCUSSION

In this chapter, it was shown that TCM pre-treated animals had accelerated spontaneous metastasis to the LN and the lungs in two different triple-negative breast cancer (TNBC) models: MDA-MB-231 and SUM-149 mammary fat pad xenografts (Figure 2.1-3). These metastases spontaneously disseminated from the primary inguinal tumors within 4 weeks in the MDA-MB-231 model and 6 weeks in the SUM-149 model, which is significantly faster than serum-free media (SFM) treated animals as well as current spontaneous metastasis models that take more than 7 - 10 weeks (Jenkins, Hornig et al. 2005). TCM pre-treatment followed by tumor inoculation facilitated spontaneous metastasis by influencing lymphangiogenesis and angiogenesis in the primary tumors and pre-metastatic organs. Primary tumors in the animals that had been pre-treated with TCM showed more lymphatic vessels in their peripheral areas (Figure 2.4). The increased metastasis seen in animals that underwent TCM pre-treatment could be partly explained by the higher number of peritumoral lymphatic vessels which could facilitate the outflow of cancer cells from the primary tumor. These peritumoral lymphatic vessels also had lumens, which would be critical for the dissemination of cancer cells through these lymphatic vessels (Figure 2.4.A). It has been reported that the lymphatic vessels in the interior of the tumor do not function in lymphatic metastasis (Padera, Kadambi et al. 2002). This is thought to be the case because the lumens of the intratumoral lymphatic vessels tend to be compressed by the interstitial pressure of the tumor, making metastatic dissemination through these vessels impossible. Interestingly, tumor angiogenesis was not influenced by TCM pre-treatment (Figure 2.4.B, C). This is consistent with the result that primary tumor size is not changed by TCM pre-treatment (Figure 2.1.C).

Animals were just treated with TCM or SFM without subsequently establishing primary tumors in them to determine only the "TCM effects" (or "SFM effects") on pre-metastatic organs while avoiding the effects of the primary tumor and invaded cancer cells in the organs. Treatment with TCM induced lymphangiogenesis in the lungs and the LN (Figure 2.5) facilitating metastasis in these organs. The new lymphatic vessels in these organs might be connected to the rest of the lymphatic system and to the peritumoral lymphatic vessels. The result might be an increased number of cancer cells that travel from the primary tumor to these organs and more metastasis. It is generally thought that the LN are mostly metastasized through the lymphatic vessels as regional or sentinel LN are directly connected to the tumors through the lymphatic vessels (Ran, Volk et al. 2010). However, TCM-induced lymphangiogenesis in the lungs is unusual as it is known that lungs are metastasized via the hematogenous route (Hayashida, Takahashi et al. 2010; Wong, Zhang et al. 2012). Further studies are needed to investigate the role of increased lymphatic vessels within the LN and lungs to accelerate metastasis.

According to the "seed and soil hypothesis", metastatic cancer cells function as "seeds" and a particular organ microenvironment or niche serves as the "soil" (Paget 1989). The "soil" needs to be conditioned to function as a metastatic niche ahead of actual metastasis (Psaila and Lyden 2009). TCM pre-treatment induced neo-angiogenesis in LN and the enhanced angiogenesis is partly associated with phosphorylation of VEGFR-2 and EGFR (Figure 2.6.A, B). In recent reports tumor exosomes carrying tumor-derived cargo, including tumor-secreted factors have been shown to be released by tumors to condition sentinel LN to be more angiogenic for tumor metastasis (Hood, San et al. 2011; Alderton 2012). These results suggest that TCM in this study could function like tumor-secreted exosomes as a cocktail of several tumor-derived factors to

condition the LN. There needs to be further investigation into the key factors present in the TCM which are required for conditioning of the LN.

Surprisingly, TCM pre-treatment also facilitated tumor cell spreading in the abdominal sites (Figure 2.7.C). Intra-abdominal metastasis has not been observed in breast cancer patients in general. The intra-abdominal metastasis was determined by comparing of the luminescent image and the light image without luminescent signals. If the animal has luminescent signals beyond the boundary of the primary tumors that is found in the light image, we counted that the animal has the intra-abdominal metastases. Primary tumors with a statistically identical size within two groups suggest that the different intra-abdominal metastasis rate was independent of the progression of primary tumors. The results above and the TCM-induced cancer cell motility data (Figure 2.7.A, B) can suggest that TCM pre-treatment might create a gradient of factors that enhance the chemotaxis of cancer cells in vivo, inducing them to disperse from the primary site. This can also be explained by that the tumor inoculation was performed around the abdomen area, thus locally invading cancer cells could form intra-abdominal metastases, which is not usual in patients. The increase in the intra-abdominal metastases generally facilitated metastasis to other organs such as liver, spleen, stomach, jejunal and duodenal segment of the intestine as shown in Figure 2.7.C and is described in (Rouhanimanesh, Vanderstighelen et al. 2001; Shih, Hsu et al. 2012).

Pre-treatment with TCM to enhance metastasis has physiological relevance since a number of studies have employed conditioned media from solid tumors or cancer cells to understand mechanisms of tumor progression (Wason and Richkind 1992; Festuccia, Bologna et al. 1999; Burgess and Hall 2001; Kaplan, Riba et al. 2005; Mayorca-Guiliani, Yano et al. 2012; Michielsen, O'Sullivan et al. 2012). Primary tumors are probably always secreting factors, which

would be equivalent to the TCM used here, into circulation. As tumors get larger, the concentrations of factors in this physiological TCM will increase. Also, even when the tumors are small and the concentrations of factors in the physiological TCM are low, the pre-metastatic sites are continuously being induced and prepared for the arrival of metastasized tumor cells. The continuous and long-term exposure to the factors may make up for the low concentrations of the factors physiologically. The question of why only specific sites (e.g., lungs and lymph nodes) in particular organs eventually get colonized by the metastatic tumor cells when the whole body is exposed to the same tumor secreted factors remains unanswered. Moreover, adding a breast tumor excision step (lumpectomy), or complete removal of the gland (mastectomy) to the current models needs to be explored as it can provide more clinically relevant perspectives when evaluating the efficacy of anti-metastatic drugs after surgery as suggested in (Guerin, Man et al. 2013).

In summary, studies in this chapter demonstrate that TCM pre-treatment enhances breast tumor metastasis in the LN and the lungs, showing enhanced lymphangiogenesis and angiogenesis in these pre-metastatic organs. This model would allow the evaluation of anti-metastatic agents in a shorter time and with higher consistency.

2.5 FIGURES & TABLES

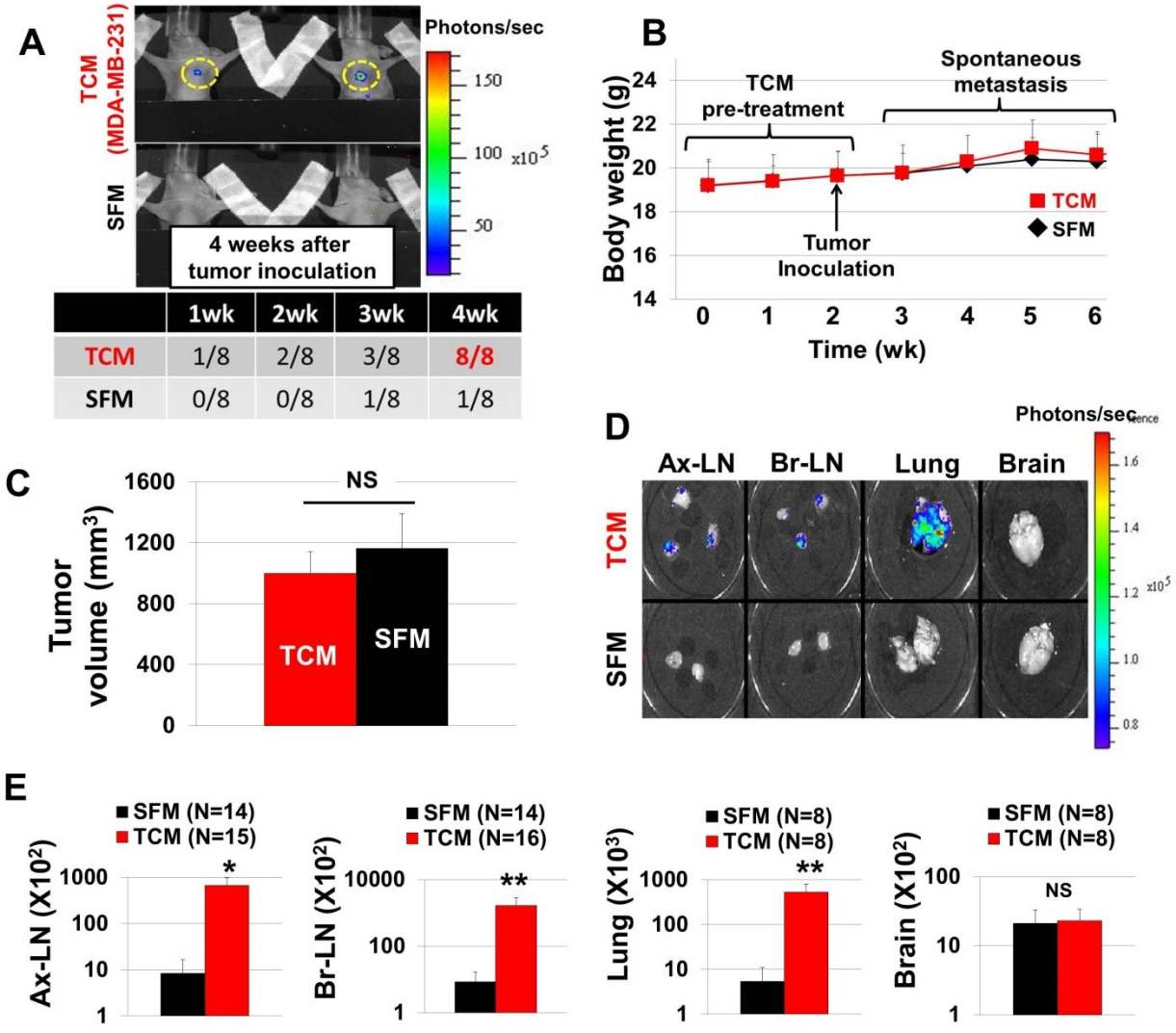

	1wk	2wk	3wk	4wk
TCM	1/8	2/8	3/8	8/8
SFM	0/8	0/8	1/8	1/8

Figure 2.1: TCM-induced spontaneous MDA-MB-231 breast tumor metastasis model. (A) Anterior metastases in 4 weeks. The table shows the number of animals that exhibit anterior metastases at the end of every week for 4 weeks. (B) Animal body weight. No significant body weight changes were observed during the experiment suggesting that the tumor-conditioned media (TCM) does not cause severe toxicity in the animals. (C) Primary tumor sizes were

determined after 4 weeks of tumor inoculation. There was no significant difference between TCM and serum-free media (SFM) treated groups. (D) Representative images of the organs (LN, lung, and brain) seen with the IVIS imager. (E) Metastatic flux in the LN, the lungs, and brains (**$P < 0.01$ and *$P < 0.05$).

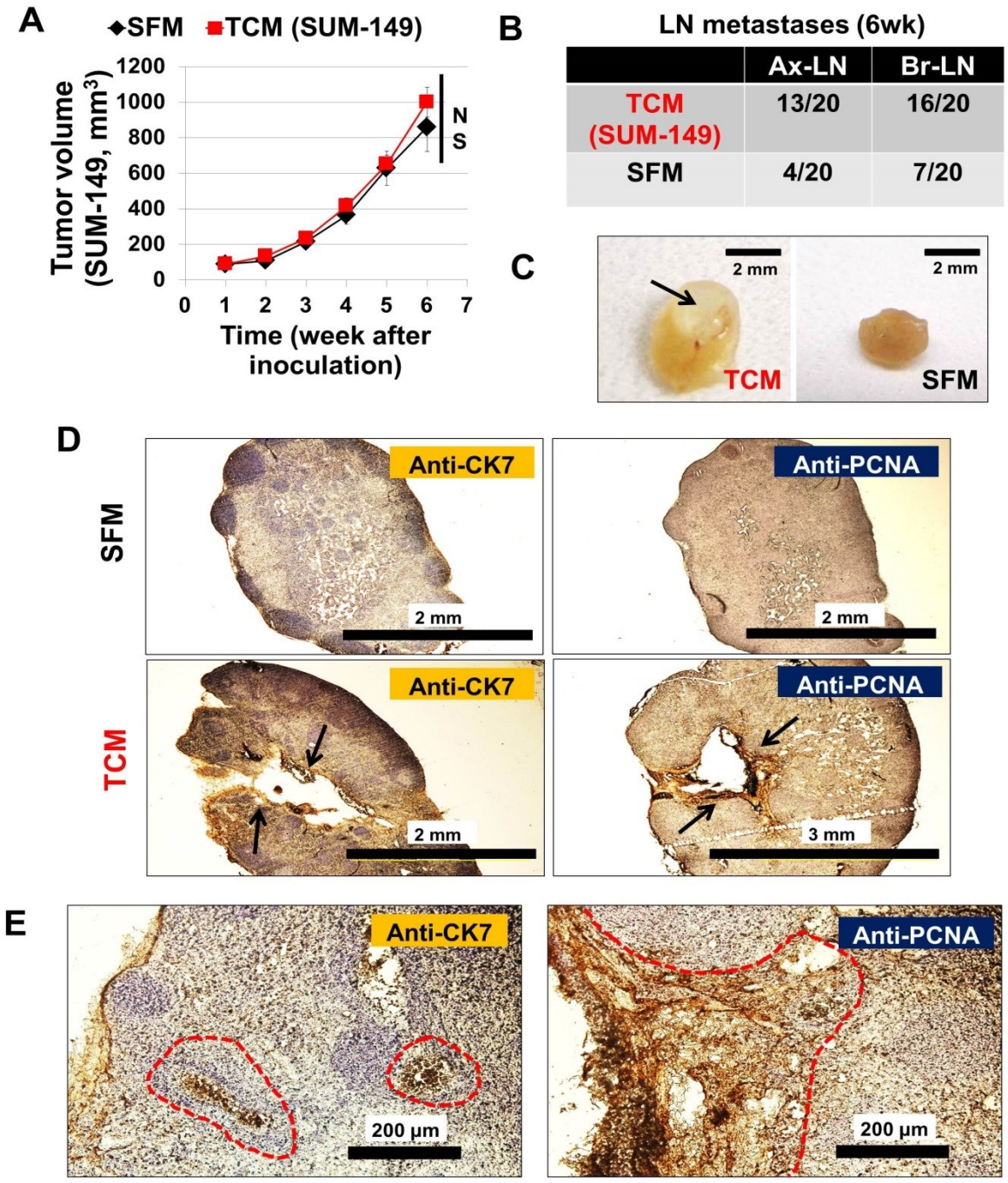

Figure 2.2: TCM-induced spontaneous SUM-149 breast tumor metastasis in LN. (A) SUM-149 primary tumor growth. SUM-149 tumor growth was slower than MDA-MB-231 tumor growth in Figure 2.1, showing 1,000 mm^3 primary tumors after 6 weeks of SUM-149 tumor

inoculation. There was no significant difference between TCM and SFM treated groups. (B) The number of the metastasized LN, which is determined by immunohistochemistry with anti-cytokeratin 7 (CK7) and anti-human PCNA. 2-3 times more metastatic LNs were observed in the TCM-treated group, compared to SFM-treated group. (C) Representative LN images. The black arrow represents lymphadenopathy (swollen LN with transparent fluid in the LN) in TCM-treated LN. (D) Representative images of DAB-mediated immunohistochemisty of LN sections with anti-CK7 and anti-PCNA. Hematoxylin was used for counterstaining. Black arrows represent metastatic tumor cells detected in TCM-treated LN. SFM-treated LN has less metastases and lymphadenopathy, showing intact LN structure. However TCM-treated LN has empty space where the fluid has placed before. Most tumor cells were detected around the area of lymphadenopathy. (E) Representative images of TCM-treated LN. CK7 and PCNA positive metastatic tumor cells were delineated by red-dotted curve.

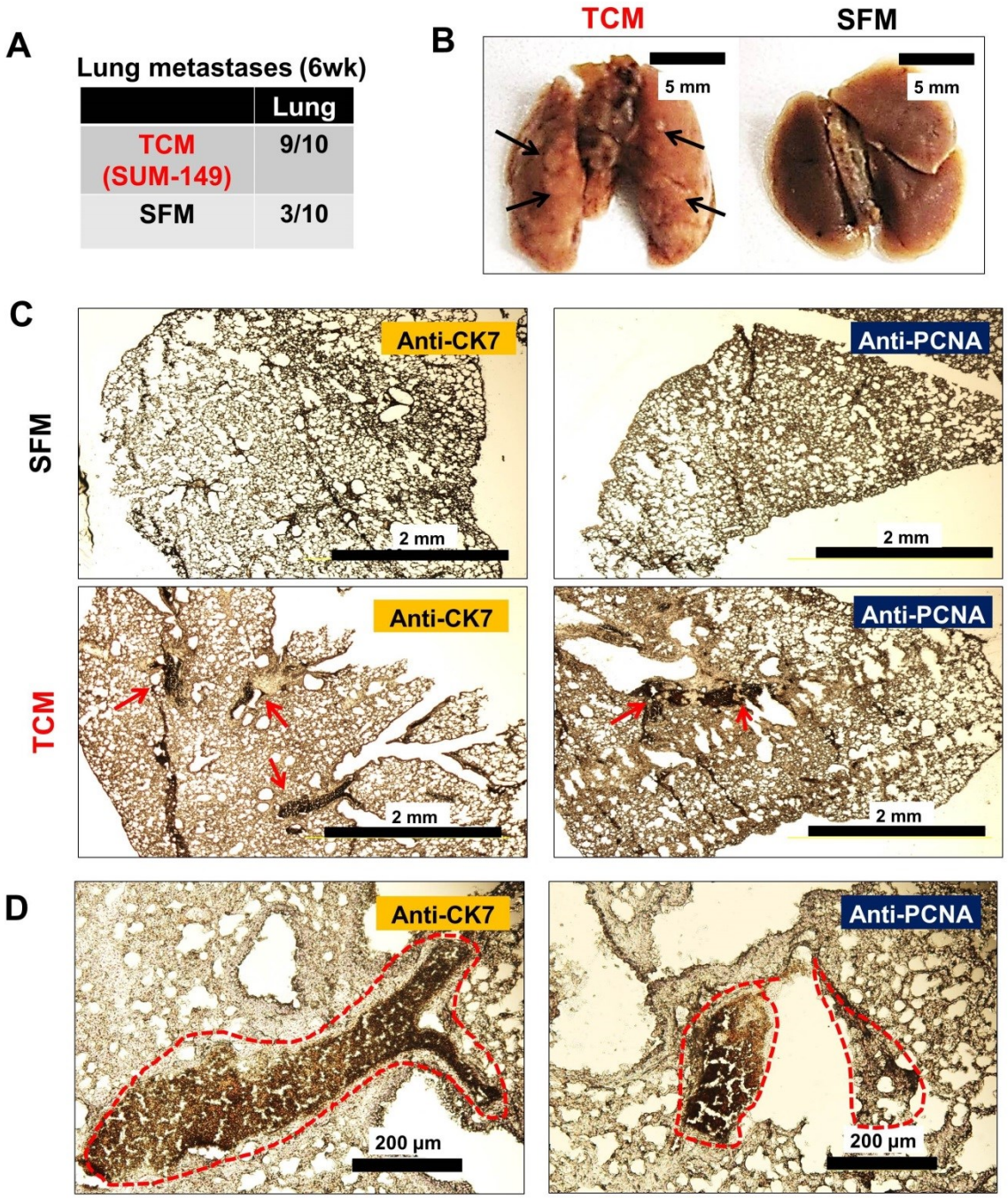

Figure 2.3: TCM-induced spontaneous SUM-149 breast tumor metastasis in the lungs. (A) The number of the metastasized lungs, which is determined by immunohistochemistry with anti-CK7 and anti-human PCNA. 3 times more lungs were metastasized in TCM-treated group,

compared to SFM-treated group. (B) Representative lung images. Black arrows represent metastatic tumor nodules on the surface of the TCM-treated lungs. (C) Representative images of lung immunohistochemisty with anti-CK7 and anti-PCNA. Red arrows represent metastatic tumor cells detected in TCM-treated lungs. (D) Representative immunohistochemistry images of TCM-treated lungs. CK7 and PCNA positive metastatic tumor cells were delineated by red-dotted curve.

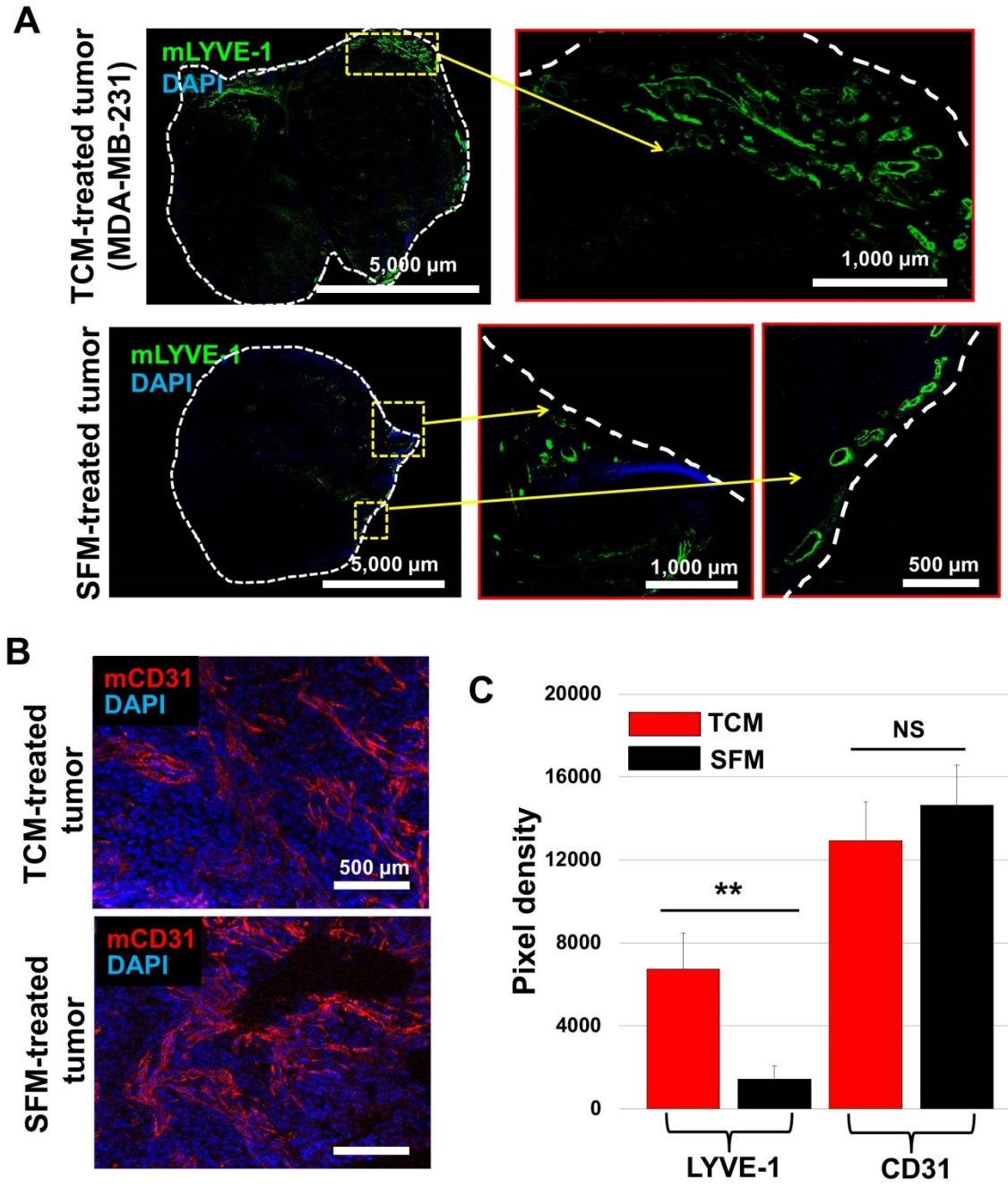

Figure 2.4: Changes in tumor microenvironment after TCM treatment. (A) The distribution of lymphatic vessels in tumors. TCM-treated animals showed enhanced peritumoral lymphangiogenesis compared to SFM-treated animals. Enlarged images show the presence of lumens in the lymphatic vessels. (B) Blood vessels in the tumor tissues. No significant change in

angiogenesis was seen after TCM treatment. (C) Quantification of (A) and (B). ImageJ was used to quantify lymphatic vessels and blood vessels in the tumors. The lymphatic vessel density was increased 4.68 times upon TCM treatment. **P < 0.01 versus SFM-treated control.

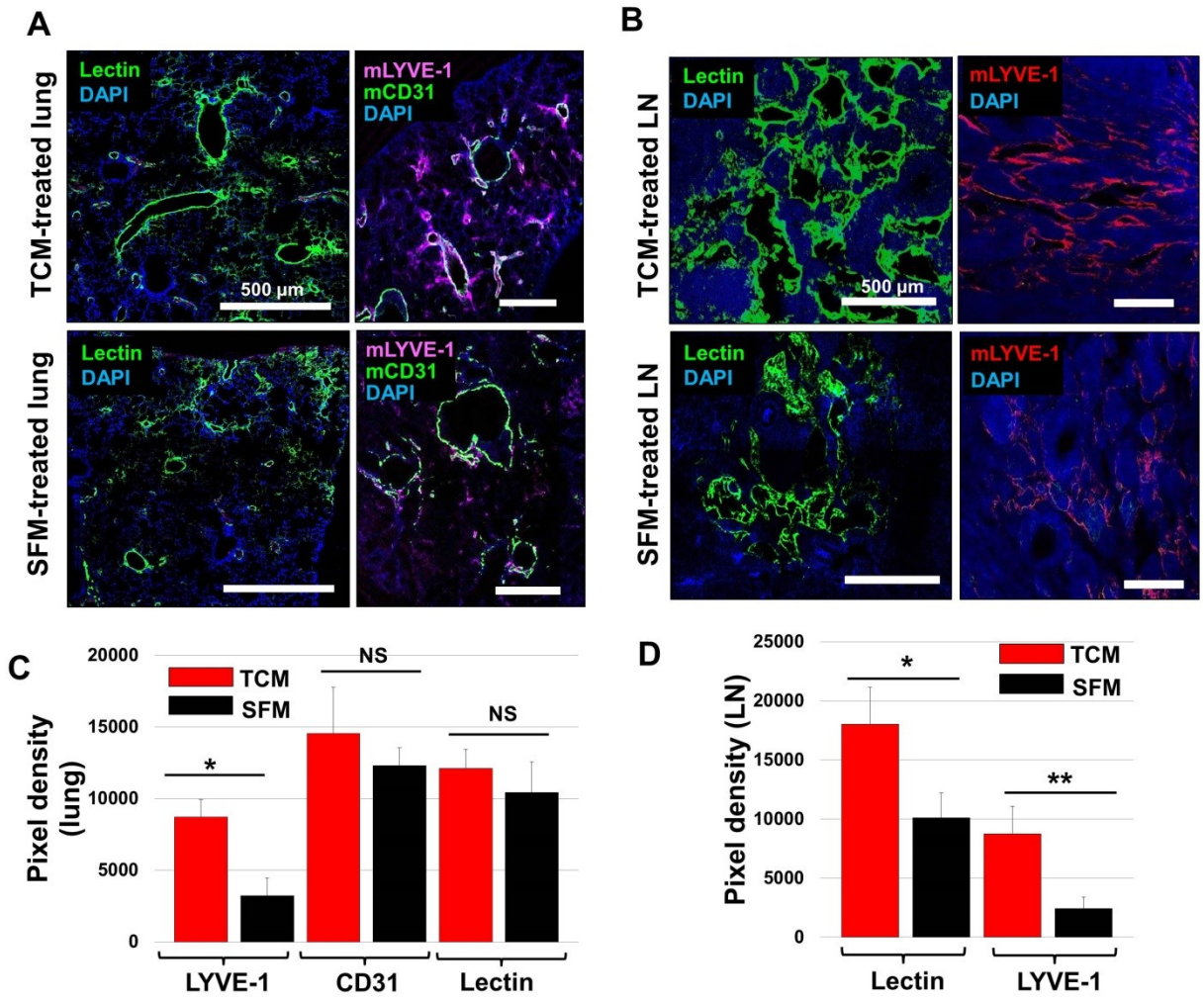

Figure 2.5: Changes in the lung and the LN microenvironment after TCM treatment. Lymphatic vessels (LYVE-1) and blood vessels (CD31 and lectin) were detected by immunofluorescence. (A) Representative images of the TCM or SFM-treated lungs. TCM-treated animals showed enhanced lymphangiogenesis in lungs compared to SFM-treated animals. However, angiogenesis was not influenced by TCM. (B) Lymphatic vessels and blood vessels within the LN. The TCM-treated animals showed enhanced lymphangiogenesis and angiogenesis in the LN compared to the SFM-treated animals. (C) Quantification of (A). The lymphatic vessel density was increased by TCM (*$P < 0.05$). The blood vessel density, determined by anti-CD31

and anti-lectin staining, was not influenced by the TCM treatment. (D) Quantification of (B). The lymphatic vessel density was increased 3.20 times, and blood vessel density (by anti-lectin) was increased 1.74 times. (**$P < 0.01$ and *$P < 0.05$).

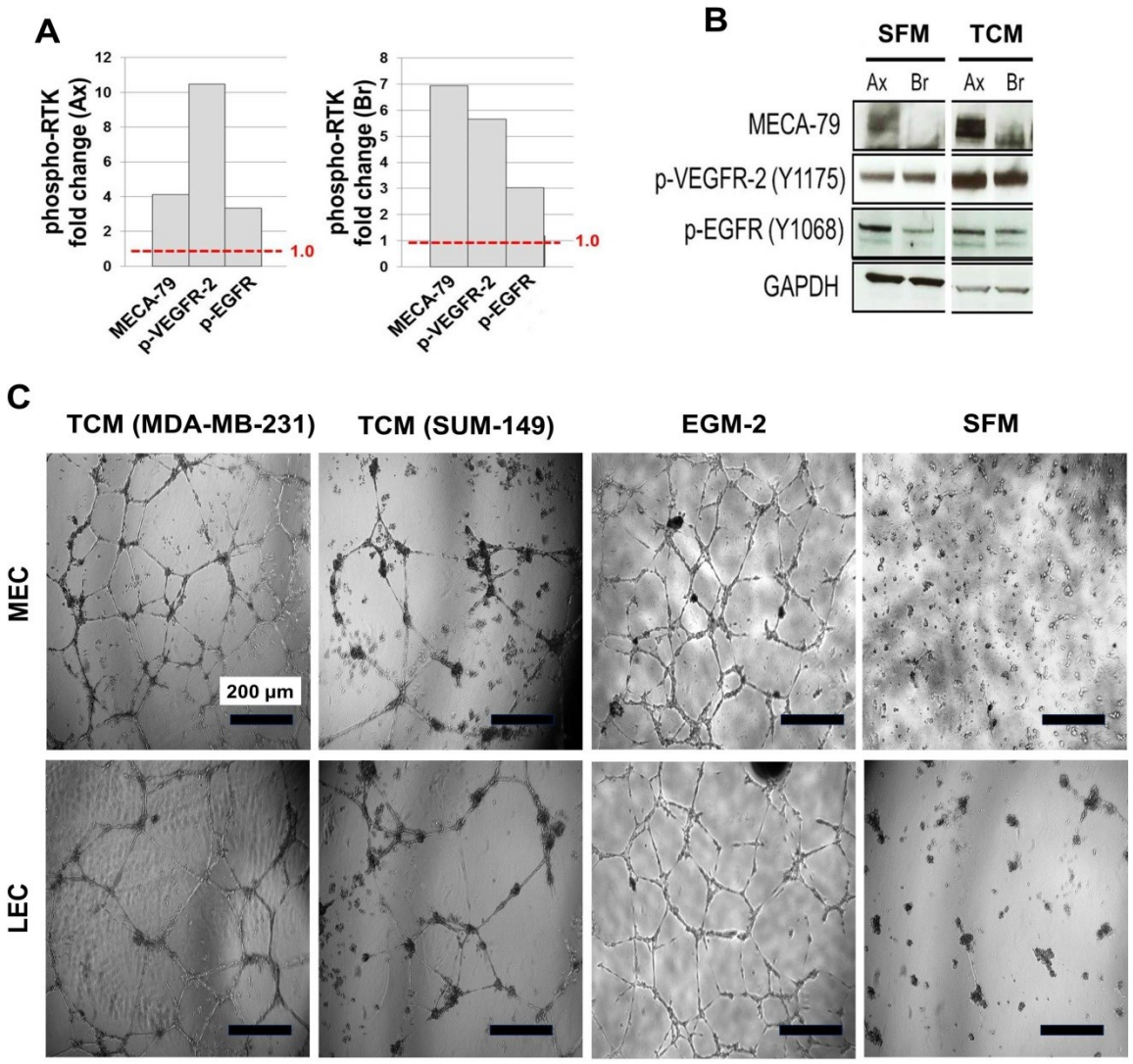

Figure 2.6: In vivo LN assays and in vitro tube formation. (A) Western blot assays were performed with tissue lysate prepared from TCM or SFM-treated axillary and brachial LN. Animals were dosed daily with 50 µl MDA-MB-231 tumor conditioned media (TCM) or serum-free media (SFM). After 14 days of administration, axillary and brachial lymph nodes (LN) were harvested, lysed, and probed with antibodies of interest including MECA-79, p-VEGFR-2 (Y1175), p-EGFR (Y1068), and GAPDH. Fold changes in these proteins after TCM treatment were obtained by normalized p-VEGFR-2, p-EGFR, and MECA-79 pixel density. Red dotted

line (1.0-fold change) was displayed as control (SFM-treated). (B) Western blot images. (C) Tumor-conditioned media (TCM) induced tube formation assays with microvascular and lymphatic endothelial cells (MEC and LEC). TCM prepared from MDA-MB-231 and SUM-149 cells promotes MEC/LEC tube formation. EGM-2 (normal endothelial media) and SFM were used as controls. Images were taken at 14 h after loading MEC and LEC.

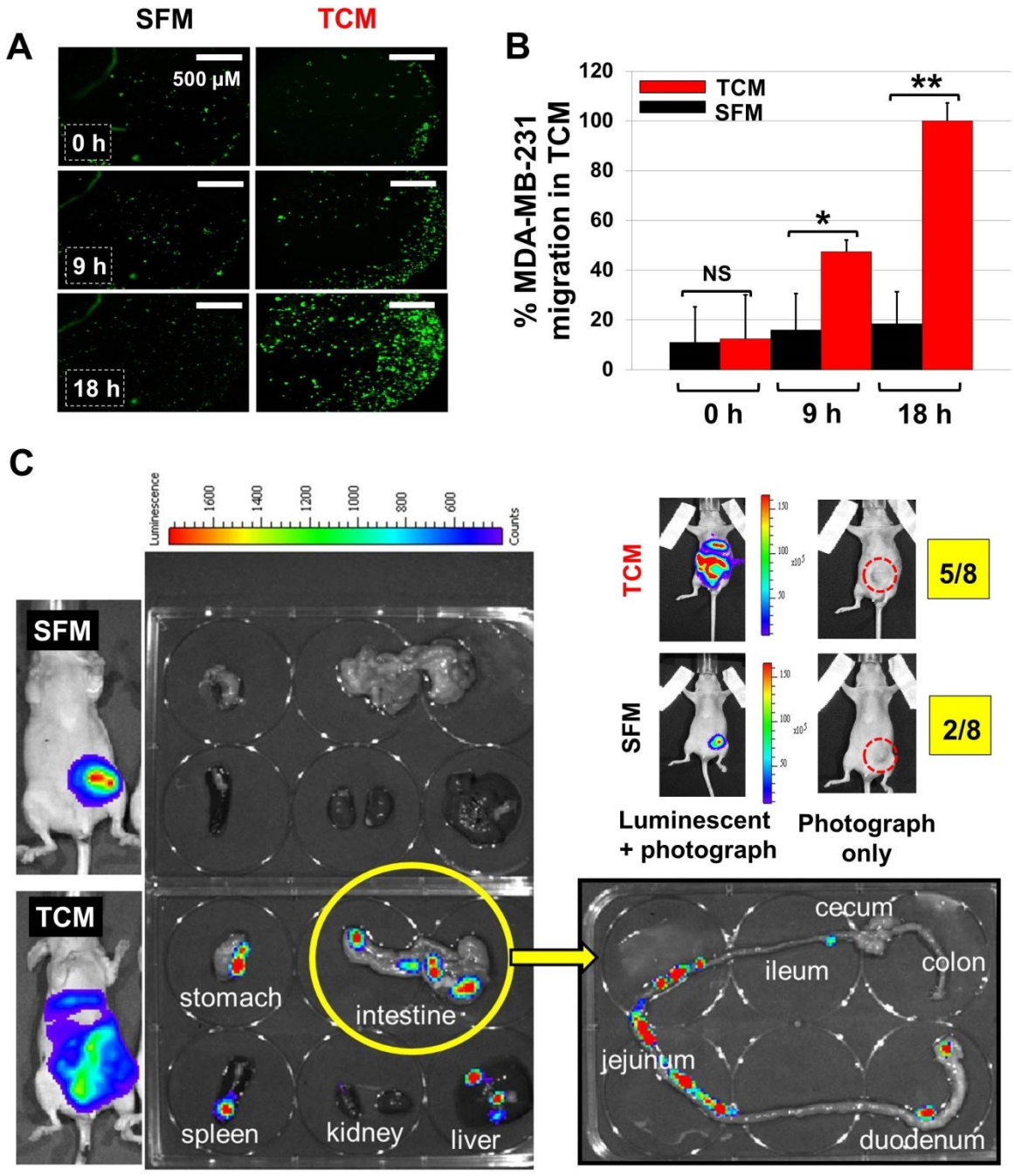

Figure 2.7: The effect of TCM on tumor cell motility and the intra-abdominal metastases. (A) Representative images of MDA-MB-231 tumor cell migration induced by MDA-MB-231 TCM or SFM at 0, 9, and 18 h. (B) Percent MDA-MB-231 migration in TCM. The extent of

migration in TCM at 18 h was set as 100% migration (*P < 0.05 and **P < 0.01). (C) Representative images of the luminescent scan of the whole animals after 4 weeks of tumor inoculation. Luminescent images showed that TCM-treated animals had more intra-abdominal dissemination of tumor cells compared to SFM-treated animals. The yellow rectangle represents the intra-abdominal metastasis rate (a/b) after 4 weeks of tumor inoculation: ‘a’ is the number of animals with intra-abdominal metastases, and ‘b’ is the total number of animals observed. Internal organs placed in the abdominal region were harvested and imaged by the IVIS imager, showing the stomach, the spleen, the liver, jejunal and duodenal parts of the intestine were metastasized.

Chapter 3: Crosstalk between Lymphatic Endothelial Cells and Cancer Cells for Breast Cancer Metastasis

3.1 RATIONALE

In chapter 2, pre-treatment of animals with tumor-conditioned media (TCM) prepared from triple-negative breast cancer (TNBC) cells (e.g., MDA-MB-231 and SUM-149) accelerated lung and lymph nodes (LN) metastasis (Lee, Pandey et al. 2014). Mechanistically, the lungs and the LN from TCM pre-treated animals had 2-4 times elevation in organ-residing lymphatic endothelial cells (LEC) implying increased lymphangiogenesis, compared to serum-free media (SFM) treated animals. Strikingly, the TCM pre-treated group also showed 3-10 times more metastases in those organs. This unexpected soaring of metastasis leads to a hypothesis that there are unknown pathways of metastatic promotion shared among the three partners: tumor-cell secretions (TCM), organ-residing LEC, and cancer cells.

In this chapter, we describe our studies investigating how TCM-treated organ-residing LEC influence metastasis. Specifically "tumor-educated LEC" models will be employed to simulate the effects of tumor-cell secretion on metastatic disease in patients. These models deal with TCM-treated LEC in vitro and in vivo. Gene expression in LEC is quite distinct from that in blood endothelial cells (BEC) (Hong and Detmar 2003; Wick, Saharinen et al. 2007). Hence, lymphatic vessel (LV)-mediated metastasis could be modulated by LEC-derived factors. For example, it is well known that stromal LEC attract tumor cells and immune cells into the LV by expressing CXCL12 and CCL21, chemokine ligands of CXCR4 and CCR7; CXCR4 and CCR7 are chemokine receptors expressed in several types of cancer cells and immune cells (Cabioglu, Yazici et al. 2005; Shields, Fleury et al. 2007). Therefore, what role LEC-derived factors, including chemokines, angiogenesis factors or cytokines, play in breast cancer metastasis will be investigated.

3.2 MATERIALS & METHODS

3.2.1 Cell culture

Human umbilical vein endothelial cells (HUVEC) and lymphatic endothelial cells (LEC) were purchased from Lonza, and grown in EGM-2 and EGM-2MV respectively. MDA-MB-231, SUM149, and MCF7 breast cancer cells were gifts from Dr. Zaver Bhujwalla (Radiology and Oncology, Johns Hopkins Medical Institutes). MDA-MB-231-luc-D3H2LN was purchased from Caliper. MDA-MB-231, MDA-MB-231-luc-D3H2LN, and MCF7 cells were propagated in RPMI-1640 medium supplemented with 10% FBS and 1% penicillin/streptomycin (Sigma). SUM149 cells were cultured in F-12 media supplemented with 5% FBS, 1 ng/ml hydrocortisone, 5 μg/ml insulin (Sigma), and 0.1mM HEPES (Gibco). Cells were maintained under standard conditions of 37°C and 5% CO_2. The passage numbers of all endothelial cells were between 3 and 6.

3.2.2 Conditioned media

When MDA-MB-231, MCF7 and SUM149 cells were confluent in T175 tissue culture flasks, the normal cancer cell growth media was replaced with 8 ml serum-free media (SFM). After 24 h incubation in a tissue culture incubator, the supernatant was centrifuged and filtered through 0.2 μm syringe filters (Corning). The resulting tumor-conditioned media (TCM) was stored in aliquots at -80°C. When LEC or HUVEC reached 30-40% confluence in T75 tissue culture flasks, EGM-2MV or EGM-2 was replaced with 30% TCM in EGM (TCM:EGM=3:7) to allow the TCM to educate the LEC and HUVEC. LEC or HUVEC were allowed to grow in the media for 3-4 days then the media was replaced with 3 ml SFM with 2% FBS (not supplemented with bullet kit). The EGM-2 bullet kit (for HUVEC) contains FBS 10.0 ml, VEGFA 0.5 ml, heparin

0.5 ml, bFGF 2.0 ml, IGF1 0.5 ml, EGF 0.5 ml, ascorbic acid 0.5 ml, hydrocortisone 0.2 ml for 500 ml EBM-2 (serum free media); the EGM-2MV bullet kit (for LEC) contains FBS 25.0 ml, VEGFA 0.5 ml, bFGF 2.0 ml, IGF1 0.5 ml, EGF 0.5 ml, ascorbic acid 0.5 ml, hydrocortisone 0.2 ml for 500 ml EBM-2 (serum free media). After 48 h, the supernatant was centrifuged and filtered. The resulting tumor-educated LEC/HUVEC (MB231-LEC or MB231-HUVEC) conditioned media was stored in aliquots at -80°C to avoid multiple freeze thaws.

3.2.3 Cell migration and adhesion assays

Cancer cell migration was assessed by using the Oris^{TM} cell migration kit (Platypus), as previously described (Lee, Pandey et al. 2014). MB231-LEC conditioned media (100 µl) with or without 20 µM of BX513 (Tocris), Maraviroc (R&D Systems), SB328437 (Tocris), or anti-CCR7 antibodies (R&D systems, 30 µg/ml) was added once the cancer cells had attached. HUVEC migration was assessed, using CIM-plates (Roche) and the RTCA system (ACEA Bioscience); adhesion was assessed using E-plate (Roche) in the RTCA system as previously described (Lee, Rosca et al. 2011). Details about the use of ACEA instruments are also described in the Materials and Methods in Chapter 2.

3.2.4 Cell proliferation and tube formation assays

HUVEC proliferation assays were performed using the WST-1 reagent (Roche) as described previously (Lee, Rosca et al. 2011) in HUVEC/LEC conditioned media, EGM, or TCM. HUVEC/LEC tube formation assays were performed as described previously (Lee, Rosca et al. 2011). These assays are also described in the Materials and Methods in Chapter 2.

3.2.5 TCM-induced spontaneous metastasis models

Before tumor inoculation, athymic nude mice (female, 5-6 weeks, 18-20 g) were pre-treated by injecting 50 µl tumor-conditioned media (TCM) or growth factor-depleted TCM (GF-dep-TCM), or serum-free media (SFM) subcutaneously for 2 weeks daily as described previously (Lee, Pandey et al. 2014). After 2 weeks of the induction, luc-MB231 cells ($2x10^6$/mouse in 100 µl of 50% matrigel solution) were injected into the upper inguinal mammary fat pad of the animals under anesthesia (50 mg/kg ketamine and 5 mg/kg acepromazine). The tumor size was measured by using a caliper, and the volume was calculated, using the formula: $V = 0.52 \times (\text{length}) \times (\text{width})^2$. Animals were imaged every week to track anterior tumor metastases, using the IVIS Xenogen 200 optical imager (Xenogen) after i.p. injection of D-luciferin (Caliper, 150 mg/kg). After 5 weeks, organs were harvested and bathed in D-luciferin solution for 5-10 min and placed in the IVIS imager to detect metastases ex vivo. Luciferase-mediated photon flux was quantified by using Living Image® 3D Analysis (Xenogen). Maraviroc (8 mg/kg, R&D systems) was administered orally daily; anti-$hVEGF_{165}$ or anti-$mVEGF_{164}$ (5 mg/kg, R&D systems) was administered intraperitoneally every 4 days. One hundred microliter of blood was collected from the tail-vein, and EDTA plasma was prepared to perform ELISA.

3.2.6 Conventional spontaneous metastasis models without TCM treatment

MB231 xenograft models were established as described above without TCM pre-treatment, after which the mice were systemically treated with a CCR5 inhibitor, 'maraviroc' (8 mg/kg, R&D systems). In 2007, Maraviroc has been approved by FDA as an anti-retroviral oral drug for HIV patients. The tumor size was measured as described above. We imaged animals every week to track anterior tumor metastases up to 7 weeks, using the IVIS Xenogen 200 optical imager

(Xenogen) after i.p. injection of D-luciferin (Caliper, 150 mg/kg). After 7 weeks, organs were harvested and bathed in D-luciferin solution for 3 min and placed in the IVIS imager to detect metastases ex vivo.

3.2.7 LEC-included matrigel plug assay

High-concentrated matrigel (500 μl, BD Biosciences) containing LEC or HUVEC (2×10^6/gel) and heparin (10 units/gel) was injected subcutaneously on the ventral side of both flanks of an athymic nude mouse. TCM or SFM (50 μl/injection) was subcutaneously dosed daily for 10 days, the mice were euthanized, and the gel plugs were excised and analyzed. For visualizing blood vessels, FITC-dextran (70 kDa, 80 mg/kg, Santa-Cruz) was injected through the tail-vein 1h before sacrifice.

3.2.8 Duration of TCM effect in vivo

Time-dependent changes in the concentrations of CCL5 in plasma were determined to understand the duration of the TCM effect in vivo. Athymic nude mice were treated with TCM or serum-free media (SFM) for 2 weeks. From week 0 (before the TCM induction), mouse blood samples were collected using the retro-orbital bleeding method, every week up to 7 weeks (4 animals/group). The collected blood samples were centrifuged for 20 min at 2000xg within 30 min of collection, after which the supernatant (EDTA plasma sample) was obtained and stored at -20°C avoiding repeated freeze-thaw cycles.

3.2.9 Immunofluorescence

Tumors, matrigel plugs, LN, and lungs fixed in 3.5% formalin were placed in 30% sucrose (Sigma) in PBS, incubated overnight at 4°C, and frozen in the O.C.T. compound (Sakura).

Sections of 10-µm thickness were cut at -20°C. After blocking with 5% normal goat or normal chicken serum (Jackson Immunoresearch) in PBST (0.3% Triton) for 1 h at room temperature (RT), the sections were treated with one or more of the following primary antibodies overnight at 4°C: rabbit anti-mouse LYVE-1 antibody (1:200, AngioBio), rat anti-mouse CCL5 (1:200, Abcam), rat anti-mouse CD31 (1:100, BD Pharmingen), goat anti-mouse $VEGF_{164}$, mouse anti-human $VEGF_{165}$ (1:300, R&D systems), rabbit anti-pVEGFR2 (1:400, Cell Signaling), mouse anti-smooth muscle actin Cy-3 (1:500, Sigma), goat anti-mouse F4/80 FITC (1:100, Serotec), goat anti-mouse lectin FITC (1:100, Sigma), rabbit anti-mouse CD33 antibody (1:50, Santa-Cruz), and goat anti-mouse Ly6g (1:200, Serotec). After 3 rinses with PBST, sections were incubated for 1 hour at RT with one or more of the following secondary antibodies (1:500): FITC-conjugated goat anti-rat, FITC-conjugated chicken anti-goat, rhodamine-conjugated goat anti-rat, Cy3-conjugated goat anti-rabbit, Alexa Fluor 647 goat anti-rabbit, Alexa Fluor 488 goat anti-rabbit, DyLight405 goat anti-rabbit, and DyLight405 goat anti-mouse antibodies (all from Jackson Immunoresearch). After 3 rinses with PBST, the samples were counterstained with DAPI (1:10,000, Roche) (5 min at RT). The samples were washed with PBST once and mounted with the ProLong Gold anti-fade reagent (Invitrogen) in dark. Fluorescent signals were visualized and digital images were obtained using the LSM-510 confocal microscope (Carl Zeiss).

3.2.10 Histology

The LN and lungs were fixed, frozen and sectioned as above. After blocking with 5% normal goat serum in PBST (0.3% Triton) for 1 hour at RT, the sections were treated with mouse anti-cytokeratin antibodies (1:500, Sigma) overnight at 4°C. The rest of the 3,3' diaminobenzidine

(DAB) procedure was performed as previously described (Lee, Pandey et al. 2014) and also documented in the Materials and Methods in Chapter 2.

3.2.11 Lung vascular permeability assay

After 2 weeks of TCM or SFM treatment with or without anti-VEGF antibodies, FITC-dextran was injected i.v. through the tail-vein (70 kDa, 80 mg/kg) 1h before sacrifice. Harvested lungs were stained with mCD31 and observed under the LSM-510 confocal microscope.

3.2.12 HUVEC monolayer integrity assay

HUVEC (10,000 cells) in complete media (EGM-2, 200 μl) were plated in fibronectin-coated 8-well Lab Tek chamber slides (Cole Palmer), and the slides were incubated for 4 h. After starving cells in 2% FBS based serum free media (no bullet kit) overnight, TCM or GF-dep-TCM or LEC CM with or without anti-hVEGF$_{165}$ (50 μg/ml, R&D systems) were added for 4 h. The cells were fixed for 10 min in 3.5% formalin in PBS, and incubated for 5 min on ice in 0.5% Triton X-100 in PBS. After blocking with 2% BSA or 5% normal goat serum for 1 h, the monolayers were processed for staining with anti-ZO-1 FITC (1:500, Cell Signaling), anti-Phalloidin Rhodamine (1:500, Molecular probe), rabbit anti-cleaved caspase 3 (1:500, Cell Signaling) and DAPI (1:10,000, Roche). Fluorescence images were obtained using a LSM-510 confocal microscope (Carl Zeiss).

3.2.13 Statistical Analysis

Error bars correspond to s.e.m, unless otherwise stated. Differences between two groups are regarded as significant when P is less than 0.05 using the Student's t-test.

3.3 RESULTS

3.3.1 Tumor-educated LEC express CCL5

Tumor-educated LEC (MB231-LEC) were prepared by growing normal LEC (n-LEC) in 30% TCM. Expression of CCL5 and CXCL7 was highly increased in MB231-LEC, compared to n-LEC (Figure 3.1.A). Since CXCL7 was also expressed in MB231 cells (Figure 3.2.A), CCL5 was further investigated. CCL5 expression in MB231-LEC plateaued at day 2, showing very high expression compared to n-LEC and MB231 cells (Figure 3.1.B, C). Another TNBC cell line, SUM149, and an estrogen receptor-positive (ER+) breast cancer cell line MCF7 were also tested: SUM149-TCM promoted CCL5 expression in LEC however MCF7-TCM did not (Figure 3.1.D).

TCM-induced CCL5 was observed in vivo, employing athymic nude mice to minimize T cell effects on CCL5 expression. CCL5 is also known as RANTES (Regulated And Normal T cell Expressed and Secreted), since T lymphocytes express and secrete CCL5 (Donlon, Krensky et al. 1990). 50 µl of SFM or TCM prepared from MB231, SUM149, or MCF7 cells were subcutaneously injected as previously described (Lee, Koskimaki et al. 2013). Mouse lymphatic vessels (mLV) in the lymph nodes (LN) and the lungs from the animals treated with MB231 or SUM149-TCM expressed mCCL5, whereas the mLV in animals treated with MCF7-TCM or SFM did not (Figure 3.1.E-G). Our data, although on a limited number of cell lines, suggests that TCM-induced CCL5 is TNBC specific. TNBC TCM-induced mCCL5 was not colocalized with smooth muscle actin (Schoppmann, Bayer et al.) which is a marker of pericytes and myofibroblasts (Figure 3.2.B). LN from lipopolysaccharide (LPS, 5 mg/kg, i.p.) treated animals showed infiltration of mF4/80-positive macrophages and mLy6g-positive neutrophils, but did not

show CCL5 expression (Figure 3.3). This demonstrates that TCM-mediated lymphatic expression of mCCL5 is not associated with LPS-mediated acute inflammation.

3.3.2 Tumor-educated LEC promote cancer cell migration through the CCL5-CCR5 axis

MB231-LEC (tumor-educated LEC) conditioned media induces MB231 cell migration, compared to normal LEC conditioned media or serum-free media, suggesting LEC have potential to induce cancer cell migration when they are educated with TCM (Figure 3.4.A). Combining with the results in Figure 3.1, LEC-expressed CCL5 was suspected as an inducer of cancer cell migration. Since CCL5 can interact with CCR1/3/5 (Mantovani, Bonecchi et al. 2006), CCR1, CCR3, and CCR5 were selectively blocked by BX513, SB328437, and maraviroc respectively to determine which of these receptors induces MDA-MB-231 cancer cell (MB231) migration. Only maraviroc blocked MB231 cell migration (Figure 3.5.A, B). LEC do not express CCR5 whereas MB231 cells do, suggesting that LEC-secreted CCL5 triggers chemotaxis of MB231 cells in a paracrine manner (Figure 3.5.C). Additionally the effect of CCR5 inhibitor was compared with that of anti-CCR7 neutralizing antibodies in MB231 cell migration assays, because CCL21, a chemokine ligand for CCR7, is another inducer of lymphatic metastasis (Shields, Fleury et al. 2007). Maraviroc blocked MB231 cell migration induced by MB231-LEC CM, whereas the anti-CCR7 antibody only blocked n-LEC CM induced migration, demonstrating that the CCL5-CCR5 axis is essential for MB231 cell migration toward tumor-conditioned LEC rather than toward physiological LEC (Figure 3.4.B, C).

3.3.3 Tumor-educated LEC promote tumor metastasis through the CCL5-CCR5 axis

Animals were pre-treated with TCM or SFM daily for 2 weeks, then MDA-MB-231-luc-D3H2LN breast cancer cells were inoculated into the upper inguinal mammary fat pads,

followed by treatment with maraviroc (8 mg/kg/day, p.o.) or vehicle. At week 5, in the TCM-treated group 9 out of 10 mice had metastases while only 2 out of 10 mice in the SFM-treated group had them. In the maraviroc-treated group only 4 mice had metastases (Figure 3.5.D). Primary tumor growth was not influenced by the treatment (Figure 3.5.E). Maraviroc treatment inhibited metastasis in the lungs and LN, as shown by the reduced photon flux in the organs (Figure 3.5.F, G). The hearts, brains, spleens, and livers did not show metastases with TCM induction (Figure 3.6). These data demonstrate that tumor-educated LEC within the lungs and the LN promote TNBC metastasis through the CCL5-CCR5 axis. The therapeutic effects of maraviroc were further evaluated in a conventional spontaneous metastasis model without TCM pre-treatment which may be more physiological (Figure 3.7). Since spontaneous metastasis develops slowly compared to the TCM-induced model, we assessed thoracic metastasis for 6 weeks after tumor inoculation. Maraviroc treatment did not influence tumor growth but potently inhibited tumor dissemination towards the lungs and LN, suggesting that the CCL5-CCR5 axis is also pivotal in general spontaneous metastasis models (Figure 3.7).

3.3.4 Tumor-educated LEC have dysregulated angiogenesis factor expression

Since subcutaneous matrigel (500 µl/ injection) mixed with LEC (2×10^6/gel plug) showed moderate intra-gel angiogenesis in vivo (Figure 3.8.A), LEC conditioned media (LEC CM) were screened for angiogenesis factors, using a panel of 55 angiogenesis-related factor antibodies. LEC secreted angiogenic factors, inflammatory factors, and antiangiogenic factors into the media (Figure 3.8.B-D). Though LEC CM moderately induced EC proliferation, the rate of proliferation was far smaller than in EC growth media (EGM-2), suggesting that LEC-secreted anti- and pro-angiogenic factors are in balance for angiogenic homeostasis (Figure 3.8.E, F).

We hypothesized that the angiogenic homeostasis in LEC can be perturbed by TCM treatment, since chemokine CCL5 was highly expressed by LEC after TCM treatment. Animals injected s.c. with matrigel mixed with LEC (LEC-Matrigel group) were systemically dosed with TCM or SFM for 2 weeks (Figure 3.9). For controls, 'HUVEC-Matrigel' and 'no cell' groups were used. Surprisingly, profound intra-gel angiogenesis was observed in the TCM-treated LEC-matrigel group (Figure 3.9.A-C). 'HUVEC group' or 'no cell group' showed no angiogenesis with either TCM or SFM treatment. Tail-vein injection of FITC-dextran (70 kDa) visualized angiogenesis in the plugs (Figure 3.9.B, C). Infiltration of the host blood vessels (BV) into the plugs was observed (Figure 3.9.D). Immunostaining (with anti-mCD31) showed that the recruitment of the host mouse BV was increased by TCM treatment (Figure 3.9.E, F).

Angiogenesis-related factors, expressed in LEC or HUVEC after TCM treatment were assessed (Figure 3.9.G). LEC-derived angiogenic factors that increased after TCM treatment were EGF, Endoglin, MMP-9, PDGF-AA, PDGF-BB, and VEGF. In contrast, five antiangiogenic factors (Endostatin, Pentraxin-3, TIMP1, Thrombospondin-1, and Angiopoietin-2) were decreased (Figure 3.9.G). The factors from HUVEC did not significantly change after TCM treatment. VEGF was dramatically increased in LEC as analyzed by ELISA; also immunostaining showed that $hVEGF_{165}$ is colocalized with human LEC in the LEC-matrigel plug (Figure 3.9.H). Phospho-VEGFR2 (Y1175) was detected around mouse BV in the LEC-matrigel, showing that the human LEC-secreted human $VEGF_{165}$ activated VEGFR2 signaling pathways in the host BV (Figure 3.9.I).

3.3.5 Tumor-educated LEC show angiogenic phenotypes

Vascular endothelial cell (EC) proliferation, migration, adhesion, and tube formation assays were performed (Figure 3.10.A, B). MB231-LEC CM promoted EC migration, adhesion, and proliferation, compared to n-LEC (normal LEC) CM. Though robust HUVEC tube formation was observed in MB231-LEC CM, LEC tube formation was relatively poor in the same CM. This suggests that MB231-LEC CM primarily promotes angiogenesis rather than lymphangiogenesis. Both $hVEGF_{165}$ and hEGF were depleted in TCM (the resulting growth factor depleted media is named 'GF-dep-TCM') by using anti-$hVEGF_{165}$ and anti-hEGF antibodies (Figure 3.11.A). In vitro angiogenesis assays confirmed that the immunodepletion was successful (Figure 3.11.B, C). The immunodepletion was performed because TCM containing $hVEGF_{165}$ and hEGF can also promote angiogenesis in vivo. The use of the GF-dep-TCM clarifies that "TCM-induced angiogenesis in vivo" is actually caused by host-derived $mVEGF_{164}$ rather than by $hVEGF_{165}$ or hEGF pre-existed in the TCM (Figure 3.12.A).

After treating animals with GF-dep-TCM or SFM, brachial lymph nodes (Br-LN) were harvested, sectioned and probed with anti-mCD31 antibodies. LN from GF-dep-TCM treated mice showed enhanced angiogenesis (Figure 3.10.C, D). Surprisingly, $mVEGF_{164}$ was detected around mLV in the GF-dep-TCM treated LN (Figure 3.10.E), but it was not found in the SMA (smooth muscle actin)-positive area (Figure 3.12.B). To measure lung vascular permeability, FITC-dextran (70 kDa) was intravenously injected after tumor education: extravasation of large molecular dextran into the lungs was facilitated by GF-dep-TCM treatment (Figure 3.10.F). Although TCM disrupted endothelial cell (EC) junctions of a HUVEC monolayer compared to SFM-treated controls, GF-dep-TCM did not cause junction disruption, consistent with $hVEGF_{165}$ depletion (Figure 3.10.G). Notably, conditioned media prepared from LEC treated with GF-dep-

TCM (GF-dep-TCM-LEC) caused EC junction disruption, and anti-hVEGF$_{165}$ treatment normalized it (Figure 3.10.H). It was confirmed that the junction disruption was not caused by EC apoptosis (Figure 3.11.C). All the HUVEC monolayer experiments in Figure 3.10 were carried out in 2% FBS condition to prevent undesired cell death. Cell death (apoptosis) could also disrupt endothelial cell junction; thus in Figure 3.11.C we wanted to clarify that the model in 2% FBS does not involve apoptosis. Comparing the 2% FBS condition with the serum-free media (SFM) condition, 2% FBS successfully supported HUVEC to survive without apoptosis, which was confirmed by negative signal with anti-cleaved caspase-3 (CC-3) antibody staining. But, obviously, in the SFM condition, severe apoptosis (red, CC-3) was observed, resulting in a smaller number of live cells (blue, DAPI).

3.3.6 Anti-mVEGF$_{164}$ antibody treatment inhibits lung and LN metastasis

Lungs from GF-dep-TCM or SFM-treated animals were stained with anti-hVEGF$_{165}$ and anti-mVEGF$_{164}$ antibodies (Figure 3.12.C). hVEGF$_{165}$ was not detected in either group, but mVEGF$_{164}$ was detected around the mLV in GF-dep-TCM treated lungs, demonstrating that TCM lacking hVEGF$_{165}$ influences the mLV to express mVEGF$_{164}$. For the functional confirmation, GF-dep-TCM treated animals were systemically dosed with anti-mVEGF$_{164}$ or anti-hVEGF$_{165}$ antibodies (5 mg/kg, i.p., every 4 days) during the GF-dep-TCM induction phase. Anti-mVEGF$_{164}$ normalized vascular permeability in GF-dep-TCM treated lungs whereas anti-hVEGF$_{165}$ did not (Figure 3.13.A). Based upon these results, anti-mVEGF$_{164}$ antibody was further tested in the GF-dep-TCM induced spontaneous metastasis model like the one discussed above induced by complete TCM (Figure 3.5.D-G). Two weeks GF-dep-TCM induction was done with or without anti-mVEGF$_{164}$ antibodies, after which Luc-MB231 cancer cells were orthotopically inoculated in the inguinal part of the animals. Five weeks after tumor inoculation,

the lungs and LN were harvested to assess metastases ex vivo. Anti-$VEGF_{164}$ antibody inhibited metastasis in the LN and lungs (Figure 3.13.B, C), demonstrating that lung vascular remodeling and LN angiogenesis (Lee, Koskimaki et al. 2013) initiated by GF-dep-TCM induced $mVEGF_{164}$ were blocked by anti-$mVEGF_{164}$, thus preventing metastatic colonization in the organs.

3.3.7 Dual inhibition of CCR5 and VEGF strongly inhibits metastasis

MB231 tumor xenografts were established and 100 µl of blood was collected at 2, 3, 4, and 5 week after tumor inoculation (N=10 at each time point) to estimate primary tumor induced mVEGF or mCCL5 in the plasma without TCM pre-treatment (Figure 3.13.D). Plasma samples from normal mice (N=8) with no xenografts were used for controls. Plasma concentration of mCCL5 and mVEGF increased as tumors grew: mCCL5 concentration in plasma was 259.2 ± 43.6 pg/ml, and mVEGF was 56.1 ± 4.9 pg/ml when the mean tumor volume was 1,232 ± 223 mm^3 (week 5). We hypothesized that dual inhibition of CCR5 and mVEGF would inhibit metastasis more effectively than single inhibition of each target, as CCL5 and VEGF function as the tumor recruitment factor and colonization factor, respectively (Figure 3.13.E). All the mice (100%) had thoracic metastasis in the no-treatment group. Sixty percent of the mice had metastases in the anti-$mVEGF_{164}$ group, 40% had metastases in the maraviroc group, and only 20% had metastases in the combination group (Figure 3.13.F). Conceptual summary of tumor education is described in Figure 3.16.

3.4 DISCUSSION

According to the "seed and soil hypothesis", metastatic cancer cells function as "seeds" and a particular organ microenvironment serves as the "soil" (Paget 1989). It is difficult for cancer cells ("seeds") to survive outside their site of origin, thus they have to find a suitable location ("soil") where they can settle and grow. They also manipulate the microenvironment to optimize these pre-metastatic locations (Valastyan and Weinberg 2011). This chapter documents that triple-negative breast cancer (TNBC) cell educates LEC in the pre-metastatic lungs and lymph nodes (LN) to prime them and promotes breast cancer metastasis.

In the study, TCM induced lymphatic expression of CCL5 in the pre-metastatic organs forming CCL5 chemotactic gradients to recruit CCR5-positive cancer cells into the organs (Figure 3.1-7). In order to better understand how TCM treatment accelerates metastasis, the concentration of mouse CCL5 (mCCL5) in plasma upon 2 week of TCM treatment was measured for 7 weeks (Figure 3.14). Tumor cells were not inoculated in these mice because we wanted to measure mCCL5 that was induced only by TCM. The concentration of mCCL5 increased with TCM treatment, and the increasing trend was sustained for an additional week after stopping the TCM treatment (maximum level = 470 pg/ml). Then the CCL5 concentration decreased although the level was higher than that of the negative group for up to 3 weeks from the end of TCM treatment. Based on the concentration of mCCL5 (250 pg/ml) in normal tumor xenograft models without TCM treatment (Figure 3.13.D), pre-treatment with TCM would create a dramatic mCCL5 gradient in the system to facilitate tumor dissemination, compared to the normal spontaneous metastasis models.

This study shows that tumor-educated LEC promote angiogenesis as well (Figure 3.9). While physiological LEC maintain angiogenic homeostasis (Figure 3.8), TCM-treated LEC show dysregulated secretion promoting angiogenesis (Figure 3.9). Breast cancer involves metastases in the lymph nodes (LN), thus the LN need to serve as metastatic niches (Kaplan, Rafii et al. 2006; Psaila and Lyden 2009). One way tumors prime LN is by enhancing LN angiogenesis ensuring sufficient oxygen and nutrients around metastatic tumors (Kaplan, Riba et al. 2005; Carlini, De Lorenzo et al. 2011; Lee, Koskimaki et al. 2013). LEC in the LN are educated by TCM and induce LN angiogenesis (Figure 3.10.C-E). Even upon treatment with growth factor depleted TCM (GF-dep-TCM), LEC-mediated angiogenic potential was significant, compared to non-induced animals. Additionally, CD33-positive myeloid cells in the LN were investigated (Figure 3.15). The myeloid cells are one type of bone marrow derived cells (BMDC), are known to promote angiogenesis in tumor microenvironment (Murdoch, Muthana et al. 2008). BMDC have been studied in metastasis (Kaplan, Psaila et al. 2007; Pawelek 2008; Pawelek and Chakraborty 2008; Gao and Mittal 2009; Peinado, Aleckovic et al. 2012). For example, mesenchymal stem cells, a class of BMDC, are recruited to the breast tumor stroma and promote metastasis (Karnoub, Dash et al. 2007); endothelial progenitor cells (EPC), another BMDC can turn on angiogenic switch in lung metastasis (Gao, Nolan et al. 2008; Ishida, Kimura et al. 2012). Local mouse $VEGF_{164}$ expression in myeloid cells and LEC was assessed, dissecting angiogenic potential of those cells in the LN. Both myeloid cells and LEC contribute to angiogenesis in the LN by locally expressing $VEGF_{164}$, but the distribution of myeloid cells in the LN was not as prevalent compared to LEC when the animals were treated with TCM. In addition to the LN angiogenesis, lung vascular permeability is important for metastatic extravasation as previously described (Padua, Zhang et al. 2008). Anti-VEGF therapy prevented lung metastasis,

normalizing the TCM effects, and very surprisingly, the anti-VEGF treatment showed synergy with maraviroc treatment in our metastasis models (Figure 3.13). This suggests that current FDA-approved anti-VEGF therapy could be combined with the FDA-approved anti-CCR5 therapies (i.e., HIV drugs) with possibilities for therapeutic intervention for metastatic breast cancer using repurposing of these drugs.

In summary, this chapter proposes a complex molecular crosstalk between tumor-conditioned media obtained from TNBC cells and LEC within distal organs for metastasis, and identifies the key players, CCL5-CCR5 and VEGF, which can be targeted in a singular or combinatorial manner and could be synergistic to treat breast cancer metastasis (Figure 3.16).

3.5 FIGURES & TABLES

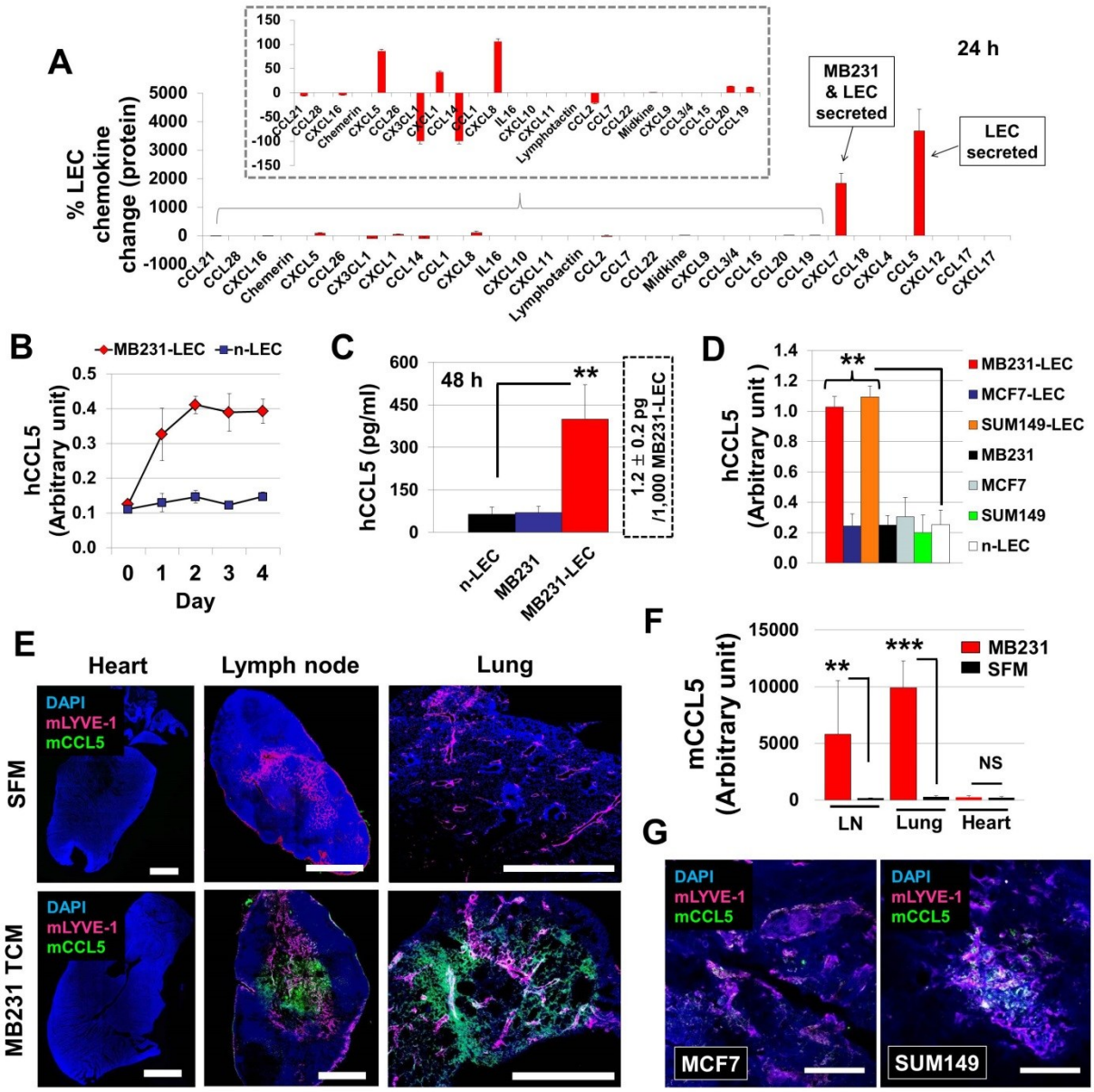

Figure 3.1: Tumor-educated LEC (MB231-LEC) express CCL5. Reverse western assays with human chemokine antibody arrays (R&D systems) simultaneously detected the relative changes of 31 chemokines. (A) Percent change in chemokine levels secreted by LEC after induction by

TCM. MB231-LEC overexpressed CXCL7 (1,850% increased) and CCL5 (3,690% increased), compared to n-LEC. (B) ELISA assays for human CCL5 were performed on MB231-LEC and n-LEC CM. MB231-LEC CM showed accumulation of CCL5 with time with the amounts plateauing at Day 2. (C) CCL5 concentration in each CM was determined at 48 h. CCL5 expression in MB231-LEC was significantly higher than in n-LEC (**P = 0.0023). One thousand MB231-LEC cells expressed 1.2 ± 0.2 pg hCCL5 in 48 h. (D) SUM149 TCM also induced CCL5 expression in LEC compared to the secretion from n-LEC (**P < 0.01), however, MCF7 TCM was inactive. (E) TCM (50 μl) prepared from MB231, SUM149, and MCF7 cells were subcutaneously dosed into nude mice for 2 weeks. LN and lungs from MB231-TCM treated animals showed mCCL5 (green) expression around mLV (pink). No mCCL5 expression was seen in the LN and lungs from the SFM-treated groups and the hearts from either group. Scale bars, 1 mm. (F) mCCL5 intensity was quantified by ImageJ (**P = 0.0048, ***P = 0.00075). (G) SUM149 TCM treatment induced mCCL5 expression in lungs while MCF7 TCM treatment did not. Scale bars, 500 μm.

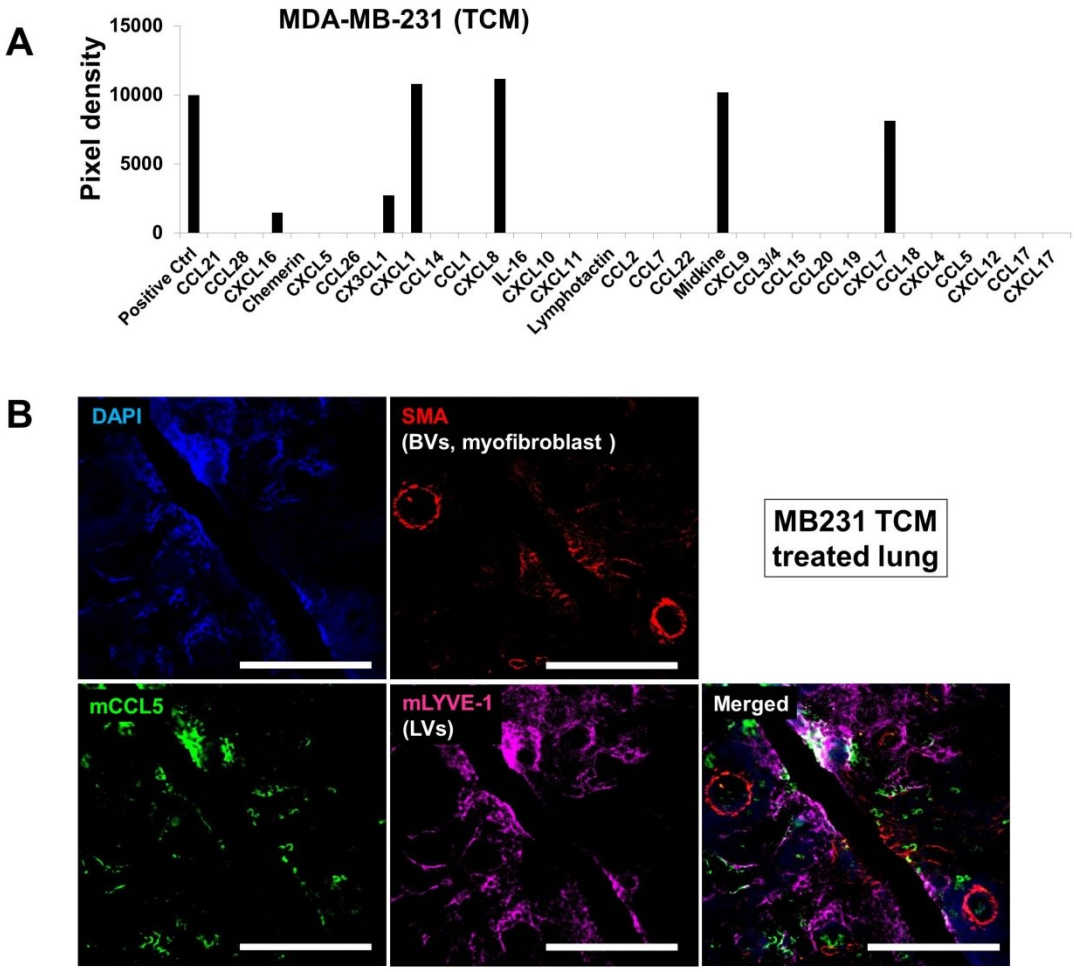

Figure 3.2: CCL5 is exclusively expressed in tumor-educated LEC (MB231-LEC). (A) Chemokine array results with MDA-MB-231 tumor-conditioned media (TCM). CXCL7 is pre-existing in TCM, but CCL5 is not in TCM. (B) Immunostaining of the lungs harvested from MB231 TCM-treated animals with anti-smooth muscle actin (α-SMA, red), anti-mCCL5 (green), and anti-mLYVE-1 (pink) antibodies. mCCL5 (green) was co-localized with mLV (pink), but not with the SMA-positive area which is likely to be occupied by blood endothelial cells, pericytes, or myofibroblasts. Scale bars, 500 μm.

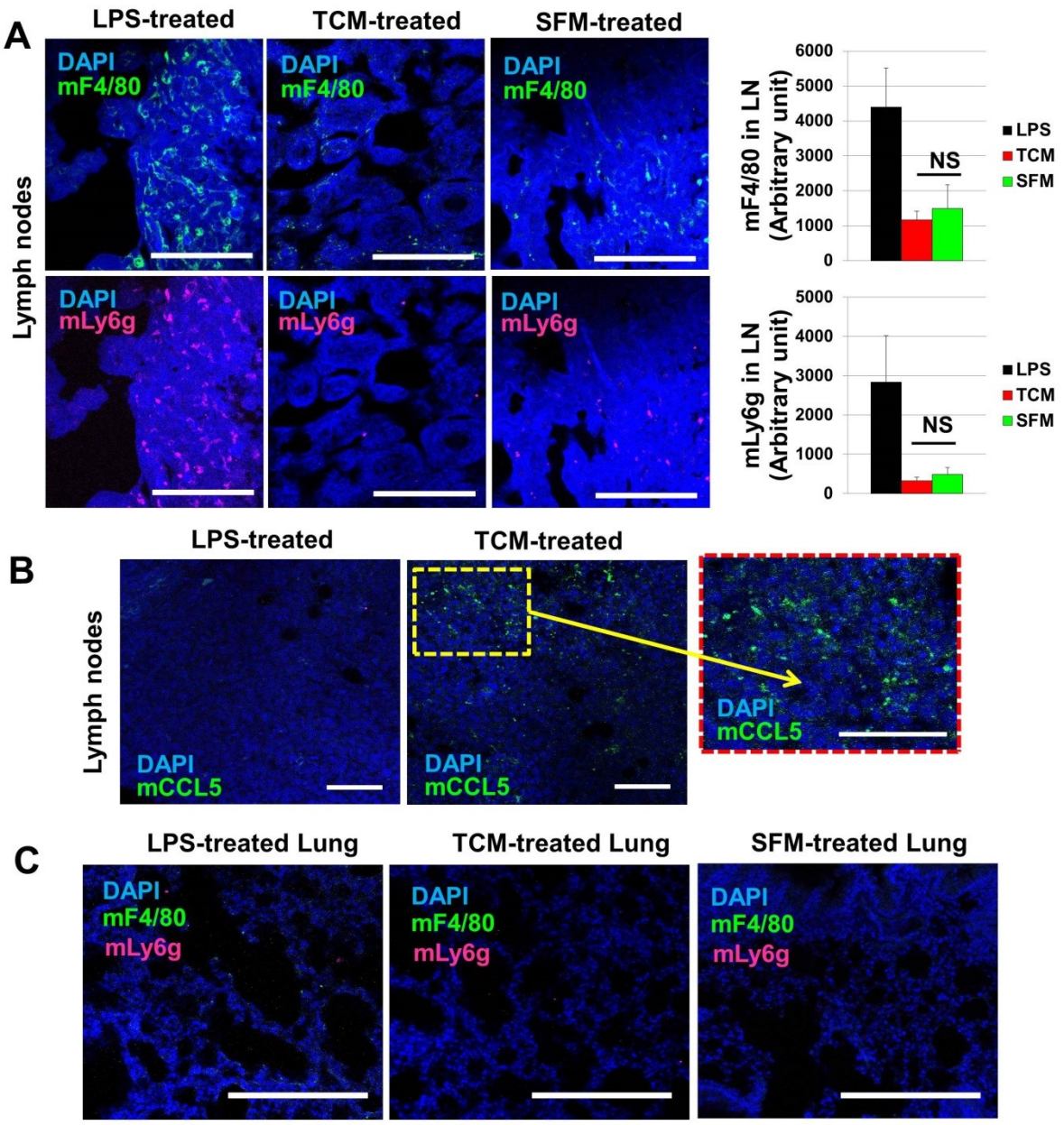

Figure 3.3: Lipopolysaccharide-induced monocyte recruitment in the LN does not induce CCL5 expression. Animals were treated i.p. with 5 mg/kg lipopolysaccharide (LPS) to compare TCM-mediated tumor education with LPS-driven acute inflammatory reaction. After 24 h of the LPS challenge, the LN and the lungs were harvested and stained with anti-mF4/80 and anti-mLY6g antibodies to detect inflammatory monocytes in those organs. For the control, TCM or

SFM-treated organs were observed. (A) LN from LPS-treated animals showed infiltration of mF4/80-positive macrophages (green) and mLy6g-positive neutrophils (pink), compared to LN from TCM or SFM treated animals. Scale bars, 200 μm. (B) Although LPS-induced LN showed monocyte infiltration, CCL5 expression was not detected. Scale bars, 100 μm. (C) Lungs from the LPS-treated animals showed no significant infiltration of mF4/80-positive macrophages (green) or mLy6g-positive neutrophils (pink). Scale bars, 200 μm.

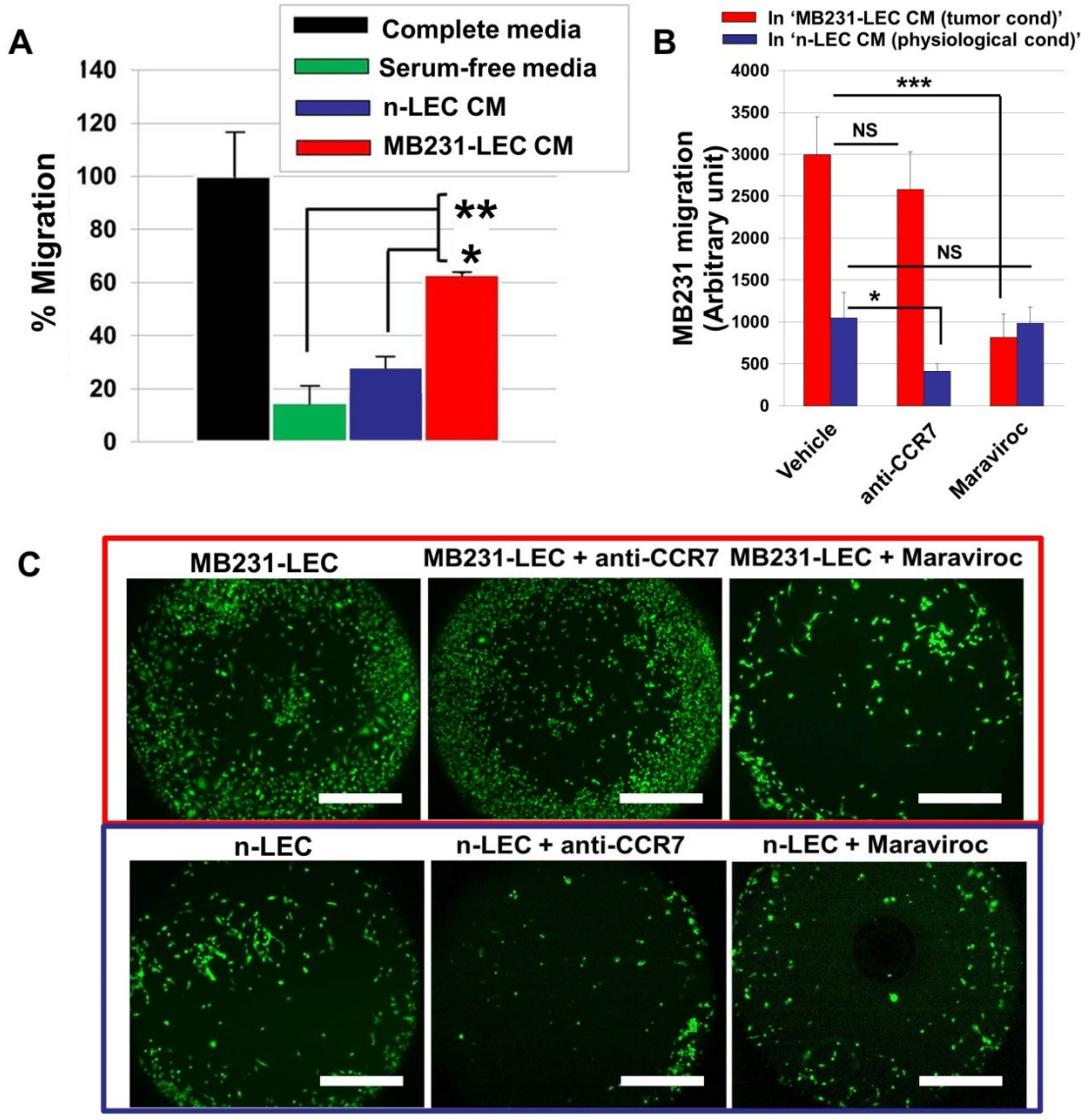

Figure 3.4: LEC-induced MB231 cell migration and roles of the CCR7 and CCR5 chemokine receptors. In vitro MB231 cell migration was studied in two different LEC conditioned media (MB231-LEC CM vs. n-LEC CM) by using the Oris^{TM} cell migration kit. (A) MB231-LEC CM promoted MB231 cell migration, compared to n-LEC CM (*P = 0.031) and serum-free media (SFM) (**P = 0.0072). (B) Anti-CCR7 antibody or maraviroc were added to MB231 cells migrating in response to MB231-LEC CM or n-LEC CM. Maraviroc significantly

blocked MB231 cell migration induced by MB231-LEC CM (***P = 0.00038). Anti-CCR7 antibody did not block MB231 cell migration induced by MB231-LEC CM, but inhibited that in n-LEC CM (*P = 0.033). These results suggest that CCL5-CCR5 axis is central for MB231 cell migration in tumor condition (MB231-LEC CM). CCR7-mediated cell migration is meaningful in physiological condition (n-LEC CM) rather than in tumor condition (MB231-LEC CM). (C) Representative images of (b), Scale bars, 500 μm.

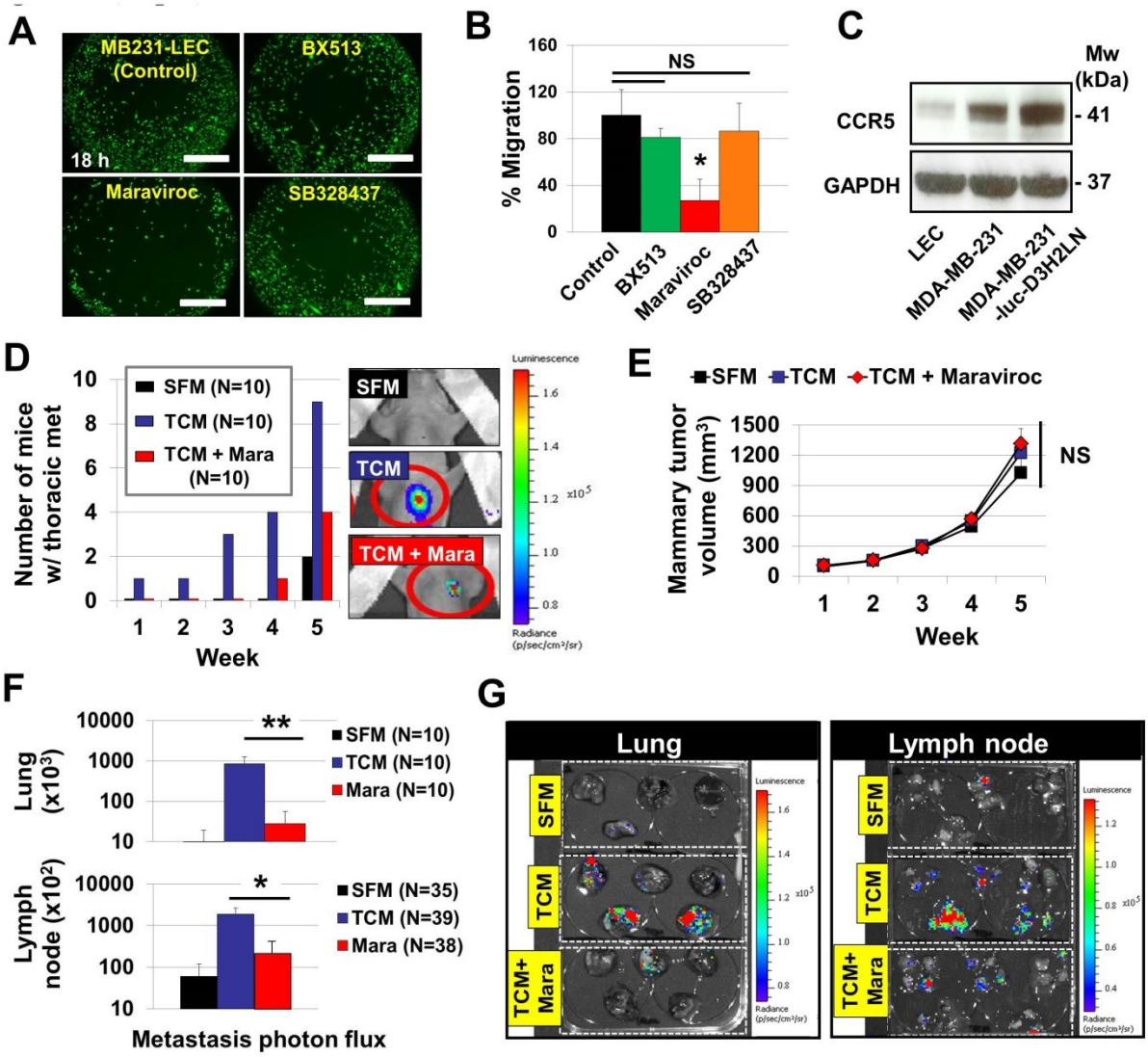

Figure 3.5: Tumor-educated LEC (MB231-LEC) promote metastasis through the CCL5-CCR5 axis. (A) MB231 cell migration assay in vitro. MB231 cells were pre-labeled with Cell Tracker Green and their migration was assessed using the Oris^{TM} cell migration kit. Maraviroc, a CCR5 inhibitor potently blocked MB231 cell migration in the presence of MB231-LEC CM at 18 h. Scale bars, 500 μm. (B) Green fluorescent signal from the migrated cells from (A) was measured at 485/530 nm and quantified. Maraviroc significantly inhibited MB231 cell migration

(*P = 0.013). (C) CCR5 levels in 300,000 LEC, MB231, and luc-MB231 were measured by western blotting. GAPDH was used as a loading control. LEC did not express CCR5 whereas MB231 and luc-MB231 cells did. (D) Athymic nude mice (N=10) were pre-treated with TCM for 2 weeks before inoculation with luc-MB231 tumor cells and initiation of maraviroc (8 mg/kg/day, p.o.) or vehicle treatment. Five weeks later the maraviroc-treated group showed more than 50% inhibition of metastasis compared to vehicle-treated group. Red circles represent thoracic metastasis observed with the IVIS imager. (E) Tumor growth was not influenced by TCM or maraviroc treatment. (F) Quantification of (G), Luciferase-mediated photon flux from the lungs (N=10) and the LN (N=35-39) were obtained by using Living Image® 3D Analysis (Xenogen) (**P = 0.008, *P = 0.042). (G) Representative organ images under the IVIS imager.

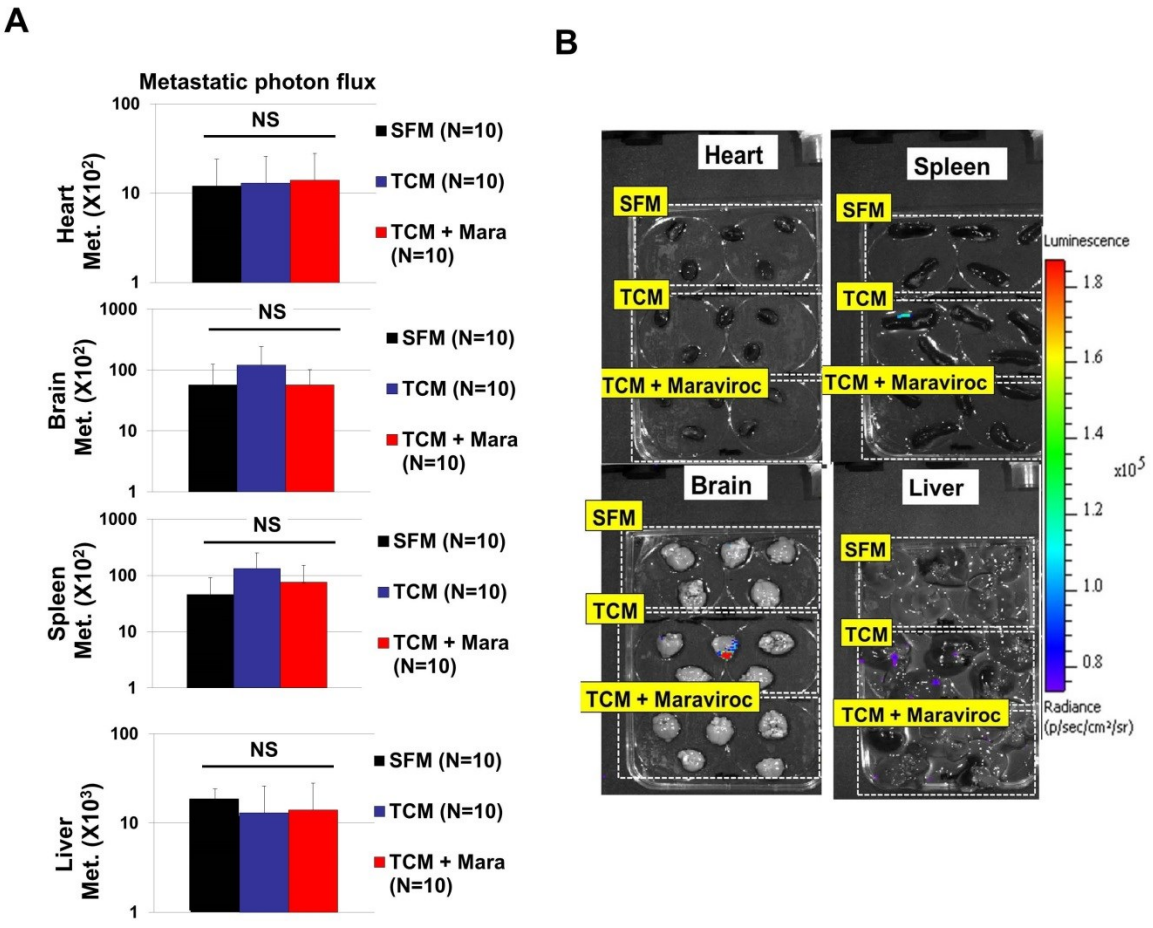

Figure 3.6: TCM-treated animals do not show significant metastases in the hearts, brains, spleens, and livers. (A) Quantification of the photon flux from each group (N=10). (B) Images of the organs under the imager.

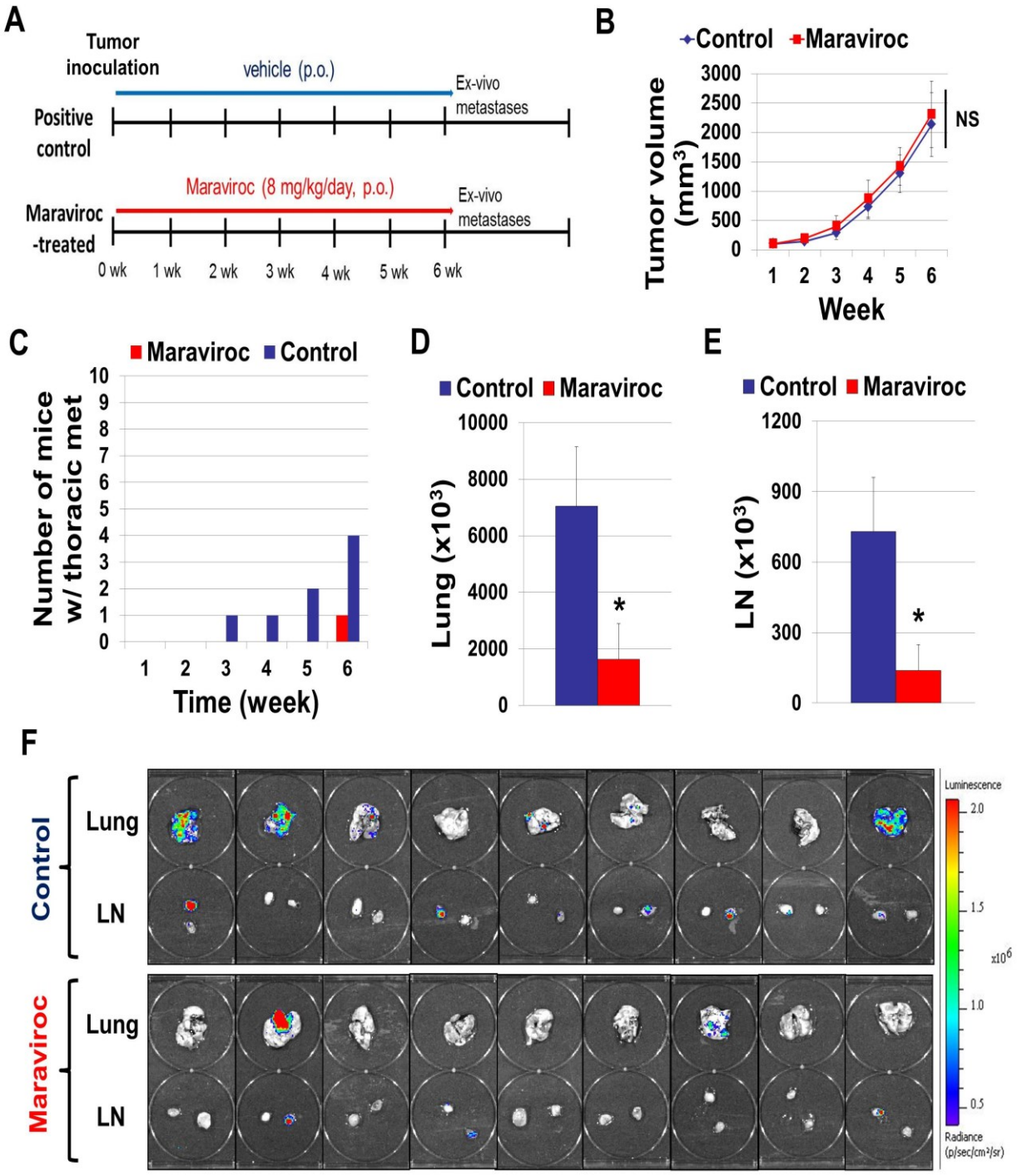

Figure 3.7: Maraviroc in spontaneous metastasis models without TCM pre-treatment. (A) Description of experimental groups. (B) Tumor growth curve. (C) Number of mice with thoracic

metastasis counted every week under the IVIS imager. (D) Quantification of lung metastasis, luciferase-mediated photon flux from the lungs (N=10) were obtained by using Living Image® 3D Analysis (Xenogen) (*P = 0.047). (E) Quantification of LN metastasis (N=20, one axillary and brachial LN from one mouse, total 10 mice/group) (*P = 0.040). (F) Organ images under the IVIS imager.

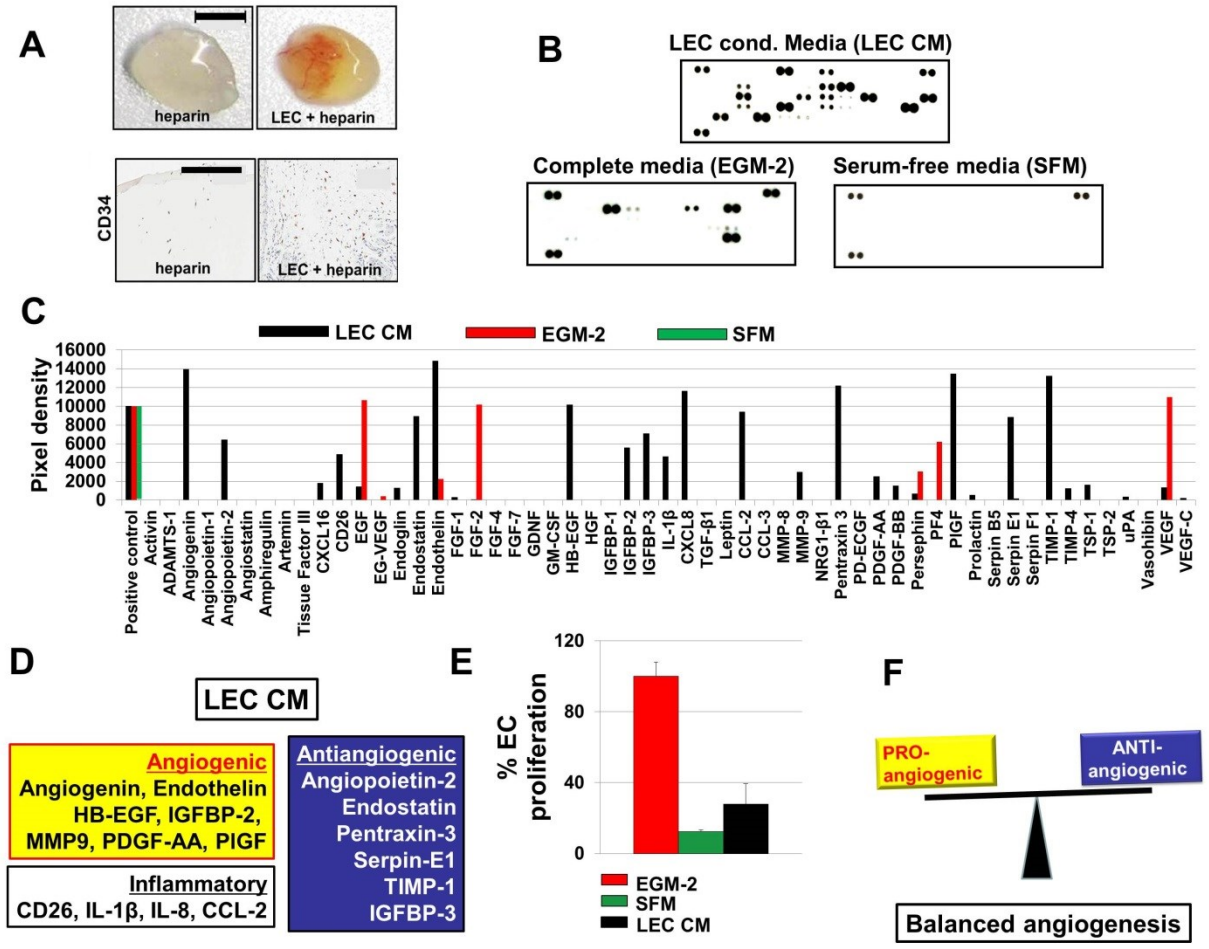

Figure 3.8: Normal LEC secrete angiogenic factors and antiangiogenic factors, maintaining angiogenic homeostasis. (A) Matrigel with or without LEC ($2x10^6$/plug, 500 µl) was subcutaneously injected into the abdomen of athymic nude mice. After 10 day, animals were euthanized and the plugs were removed and analyzed. Representative macroscopic images (scale bar, 5 mm) of two groups of matrigel plugs demonstrate that LEC-matrigel had moderate angiogenesis after 10 days of injection. Anti-mCD34 antibody staining detected mouse blood endothelial cells (mBEC) in the hLEC-included plugs (scale bar, 500 µm). (B) Reverse western assays with the human angiogenesis antibody arrays (R&D systems) detected the relative amounts of 55 angiogenesis factors in LEC conditioned media (LEC CM), endothelial growth

media (EGM-2), and serum-free media (SFM). (C) Bar graphs of (B). (D) Summary of the LEC-secreted factors, categorizing angiogenic, antiangiogenic, and inflammatory factors. (E) WST-1 mediated EC proliferation assays. LEC CM moderately induced EC proliferation, but the activity was much smaller than EGM-2, suggesting that (F) LEC-secreted factors maintain angiogenic homeostasis.

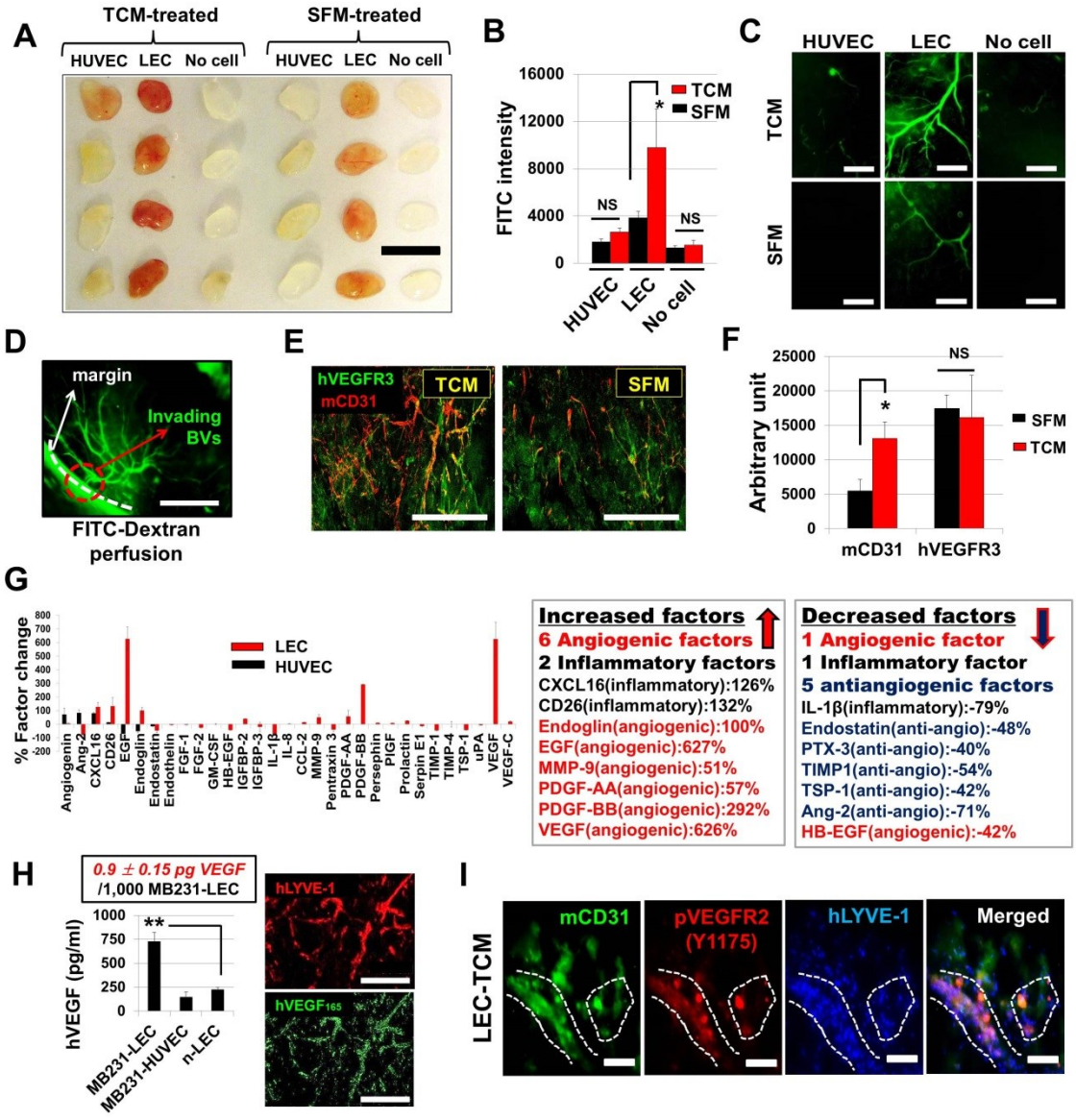

Figure 3.9: Human LEC in TCM (from MB231) treated animals promote angiogenesis. (A) Matrigel plugs with LEC/HUVEC or without cells. LEC-included matrigel plugs in animals that were treated with TCM showed profound angiogenesis. Scale bar, 10 mm. (B) One hour before sacrifice, FITC-dextran (70 kDa) was injected through the tail-vein to visualize blood vessels in the gel plugs. Plugs were homogenized and the intensity of FITC was measured and normalized

to the volume of the plug. (*P = 0.030). (C) Representative FITC images of the gel plugs under the fluorescent microscope. FITC-positive areas represent blood vessels within the plugs. Scale bars, 200 μm. (D) A representative image showing the margin of the plugs as well as mouse blood vessels (mBV) infiltrating the plug. Scale bars, 500 μm. (E) Gel plugs were fixed, frozen, sectioned (10 μm thickness), and stained with anti-hVEGFR3 (green) and anti-mCD31 (red) antibodies to detect hLEC and mBV, Scale bars, 500 μm. (F) Quantification of (E). (*P = 0.037). TCM treatment promotes mouse blood endothelial cell (BEC, mCD31-positive) infiltration into the plugs. (G) Reverse western assays with human angiogenesis antibody arrays (R&D systems) detected the relative changes of 55 angiogenesis factors in LEC and HUVEC after tumor education. The LEC angiogenic secretome was highly perturbed by TCM treatment, showing dramatic increases in EGF (627%) and VEGF (626%), and decrease of several antiangiogenic factors. Profiles of LEC-derived factors (enhanced or down-regulated) are described in the box (the right panel). TCM did not induce any significant changes in HUVEC. (H) hVEGF concentration (pg/ml) in each CM was determined. MB231-LEC showed significantly higher VEGF expression than n-LEC (**P = 0.0084). 1,000 MB231-LEC secreted 0.9 ± 0.15 pg of VEGF. Immunostaining of LEC-Matrigel plugs revealed that $hVEGF_{165}$ (green) expression was colocalized with hLEC (hLYVE-1, red). Scale bars, 200 μm. (I) LEC-Matrigel from TCM treated animals showed phospho-VEGFR2 (Y1175, red) around areas that were positive for mCD31 (green) and hLYVE-1 (blue) signals. Scale bars, 100 μm.

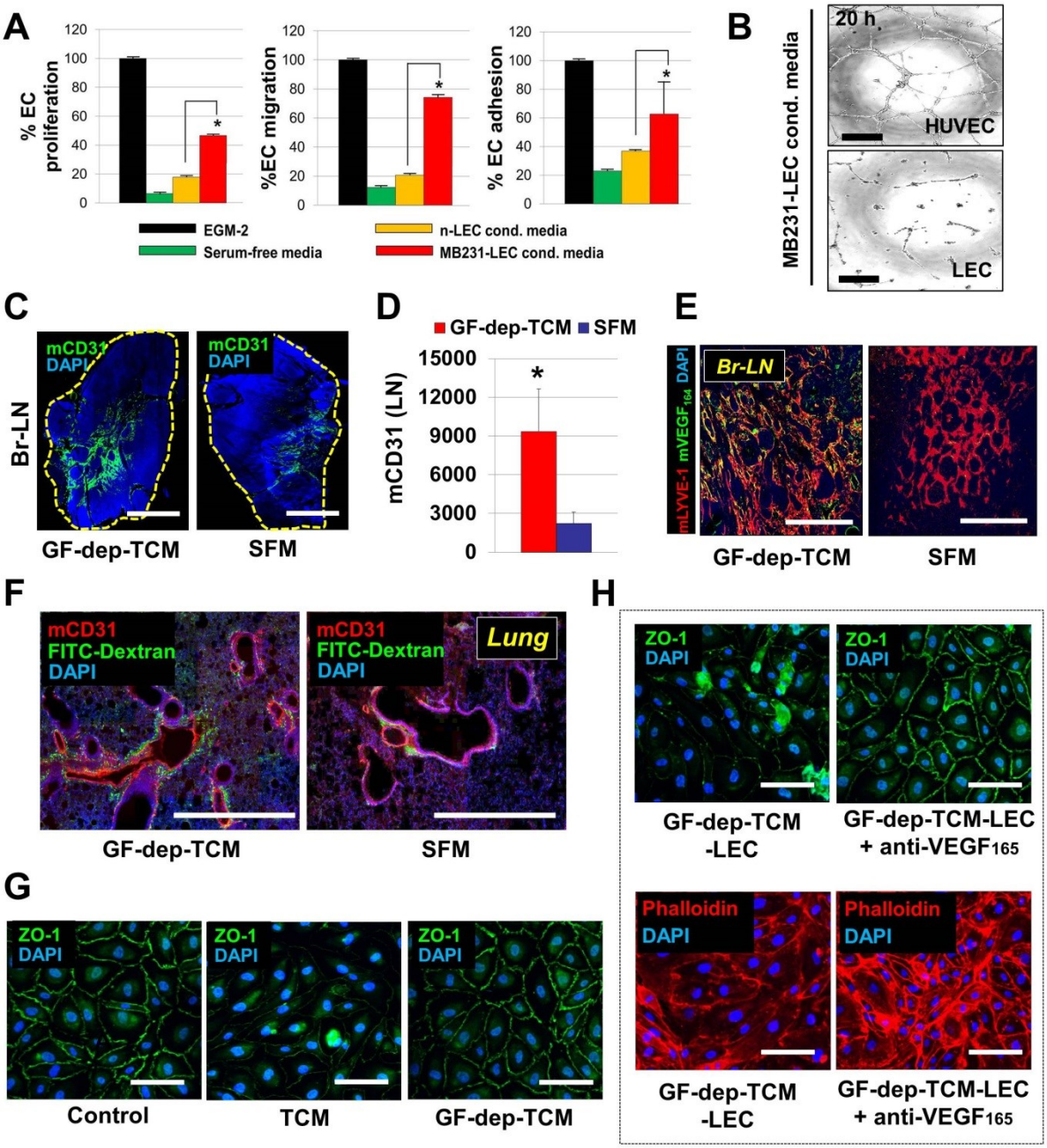

Figure 3.10: Growth factor (VEGF/ EGF) depleted TCM (GF-dep-TCM) promote LN angiogenesis and enhance lung vascular permeability through LEC-secreted local VEGF.

(A) The WST-1 method was used for EC proliferation assays. MB231-LEC CM promoted EC proliferation in 72 h (*P = 0.039). HUVEC migration and adhesion were assessed by using the ACEA instrument and CIM/E-plates. MB231-LEC conditioned media (MB231-LEC CM) promoted HUVEC migration (*P = 0.011, at 18 h) and adhesion (*P = 0.042 at 3 h), compared to normal LEC CM (n-LEC CM). (B) HUVEC tube formation was induced by MB231-LEC CM at 20 h. LEC tube formation was poorly induced in the same media. Scale bars, 200 μm. (C) Brachial LN from GF-dep-TCM treated animals showed increased mCD31. Scale bars, 1 mm. (D) Quantification of (c) (*P = 0.032). (E) Br-LN from GF-dep-TCM treated animals showed $mVEGF_{164}$ (green) expression around mLV (Peinado, Aleckovic et al.). Scale bars, 500 μm. (F) GF-dep-TCM treated animals were perfused with FITC-dextran 1 h before termination. Harvested lungs were stained with anti-mCD31. Higher amount of dextran (green) infiltrated from the blood into the lung tissues in GF-dep-TCM treated animals than in SFM-treated group. Scale bars, 1,000 μm. (G) Anti-ZO-1 antibody staining of HUVEC monolayers treated with SFM (control), TCM, and GF-dep-TCM. TCM disrupted EC junctions while GF-dep-TCM did not because of the absence of $hVEGF_{165}$. Scale bars, 50 μm. (H) Anti-ZO-1 (green) and anti-phalloidin (Peinado, Aleckovic et al.) antibody staining. GF-dep-TCM educated LEC CM (GF-dep-TCM-LEC) promoted disruption of EC junction. This was blocked by anti-$VEGF_{165}$ antibody treatment. Scale bars, 50 μm.

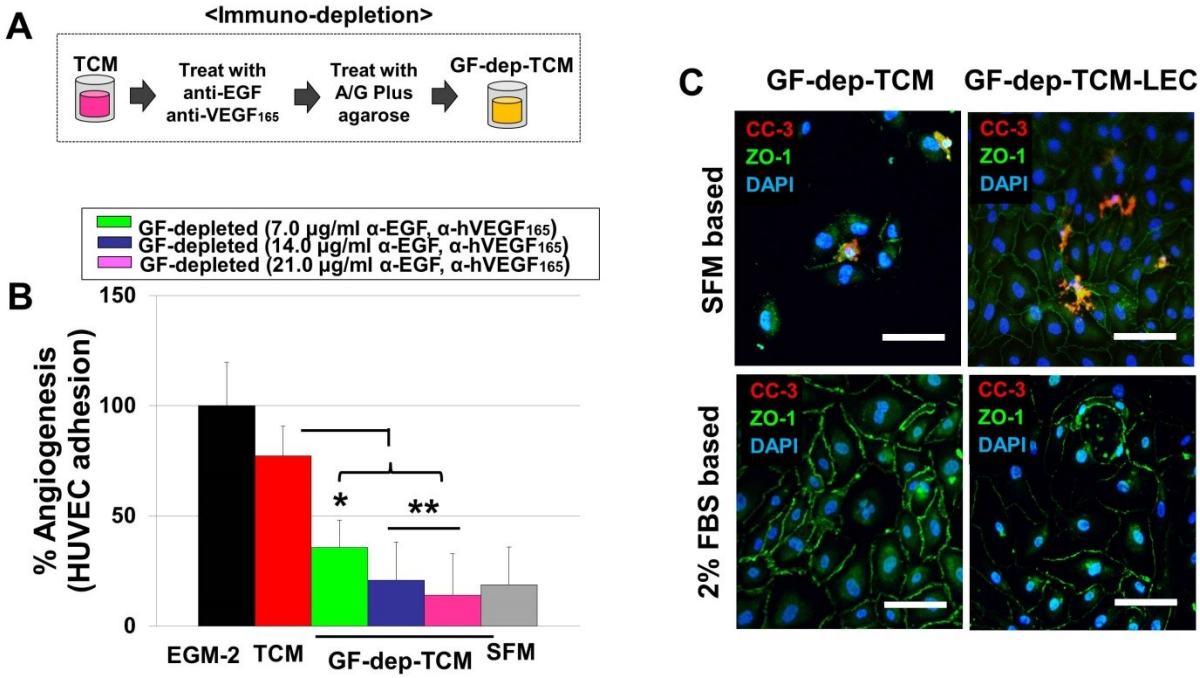

Figure 3.11: Preparation of GF-dep-TCM and HUVEC monolayer assays. (A) Preparation of growth factor depleted TCM (GF-dep-TCM). $hVEGF_{165}$ and hEGF were removed from TCM, using neutralizing antibodies and pull-down methods. (B) HUVEC adhesion assays were performed. HUVEC adhered poorly in GF-dep-TCM (*P = 0.041, **P = 0.0094). (C) Apoptosis disrupts endothelial cell (EC) junction, thus it is necessary to distinguish between EC apoptosis and increases in cell permeability. We clarified that our model in 2% FBS does not involve apoptosis. 2% FBS successfully supported EC to survive without apoptosis, which was confirmed by negative signal of cleaved caspase-3 (CC-3). But, obviously, in the SFM condition, apoptosis was observed, resulting in small number of live EC (blue, DAPI). Upon 2% FBS, HUVEC monolayer treated with GF-dep-TCM did not disrupt EC junction, which is consistent with (B) that GF-dep-TCM has no angiogenic activity. However, CM from LEC educated with GF-dep-TCM (GF-dep-TCM-LEC) disrupted EC junctions. Scale bars, 50 μm.

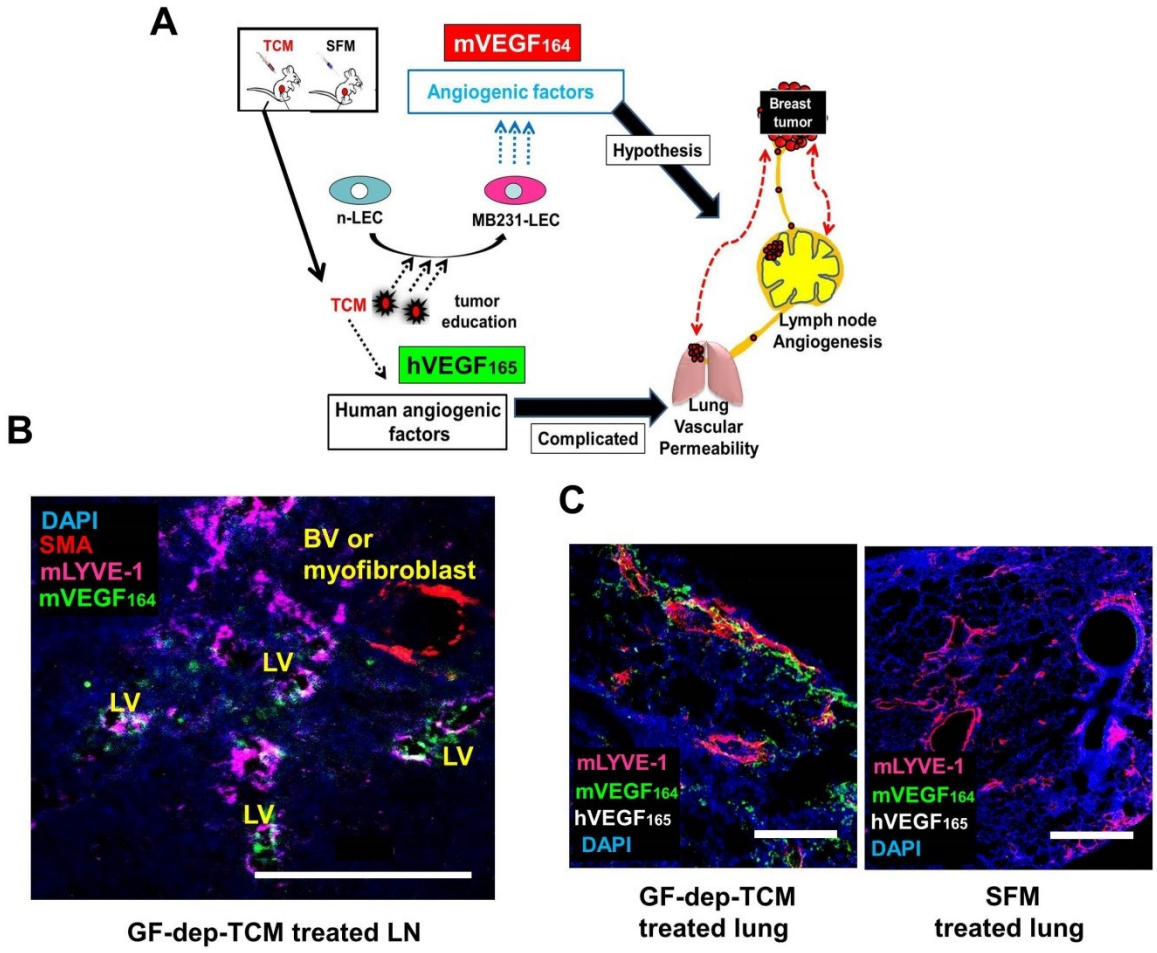

Figure 3.12: GF-dep-TCM induced angiogenic phenotypes are derived from LEC-expressed mVEGF$_{164}$. (A) Any in vivo experiments with TCM treatment would suffer from hVEGF$_{165}$ pre-existing in TCM, because hVEGF$_{165}$ also induces angiogenic phenotypes in vivo, complicating data interpretation. We can evaluate the specific roles of the LEC-secreted mVEGF$_{164}$ in lung vascular permeability or LN angiogenesis, only if we treat with GF-dep-TCM rather than with TCM. (B) LN from GF-dep-TCM showed mVEGF$_{164}$ (green) around mLV (pink), smooth muscle actin (SMA, red) positive cells did not express mVEGF$_{164}$. Scale bar, 200

μm. (c) Lungs from GF-dep-TCM or SFM treated animals. $mVEGF_{164}$ (green) was solely detected around mLV (pink) in GF-dep-TCM treated group, not in SFM-treated group. $hVEGF_{165}$ (Ruddell, Harrell et al.) was not detected in any groups, demonstrating GF-dep-TCM did not include $hVEGF_{165}$. Scale bars, 1,000 μm.

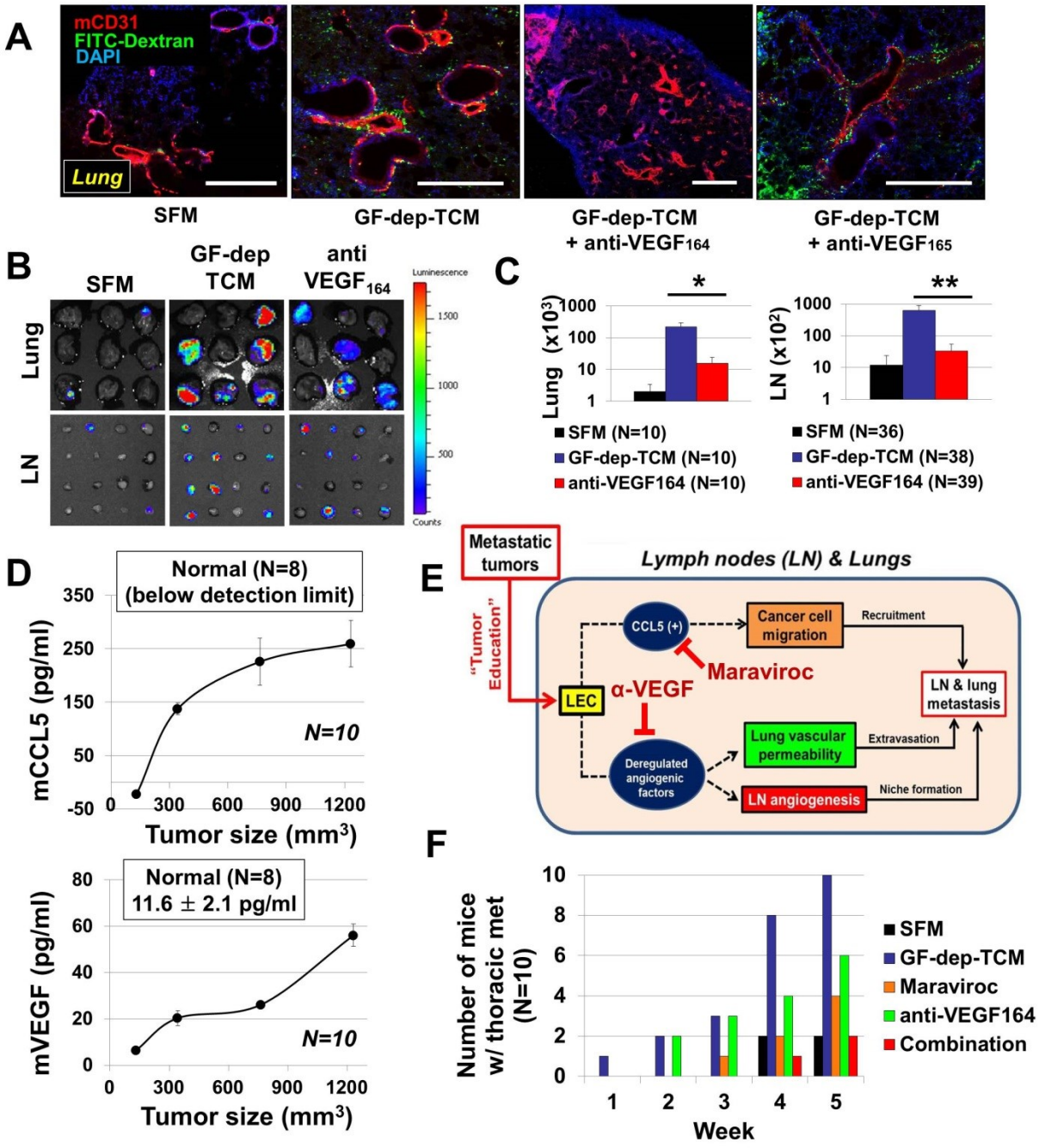

Figure 3.13: Anti-mVEGF$_{164}$ and maraviroc treatment inhibits LN and lung metastasis. (A) GF-dep-TCM treated animals were co-administered anti-hVEGF$_{165}$ and anti-mVEGF$_{164}$

antibodies (i.p. injection, 5 mg/kg, at day 1, 5, 10, 14). FITC-dextran perfusion showed that lung vascular permeability was increased by GF-dep-TCM treatment. The increased permeability was normalized by anti-mVEGF$_{164,}$ not by anti-hVEGF$_{165}$. Scale bars, 1,000 μm. (B) Based on the result in (A), we administered anti-mVEGF$_{164}$ antibodies to inhibit GF-dep-TCM induced metastasis. The anti-VEGF$_{164}$ antibody significantly inhibited metastasis in the LN and lungs as shown in the ex-vivo IVIS images. (C) Averaged photon flux in the lungs (N=10) and LN (N=36-39) (*P = 0.033, **P = 0.006) from (B). (D) Plasma concentration of mCCL5 and mVEGF in mice with (N=10) and without MB231 tumors (N=8). Mouse plasma was obtained at 2, 3, 4 and 5 weeks after tumor inoculation. At week 5, when the tumor size was around 1200 mm^3, the plasma concentration of mCCL5 and mVEGF was approximately 260 and 56 pg/ml, respectively. (E) Conceptual figure of tumor-educated LEC mediated LN and lung metastasis. Tumor-educated LEC express CCL5 which induces tumor cell recruitment, and VEGF which promotes angiogenesis and tumor extravasation. Blocking each target inhibits LN and lung metastasis. (F) Dual inhibition of VEGF and the CCL5-CCR5 axis. Maraviroc and anti-mVEGF$_{164}$ combination therapy completely inhibited thoracic metastasis to levels as low as in the SFM-treated controls (N=10).

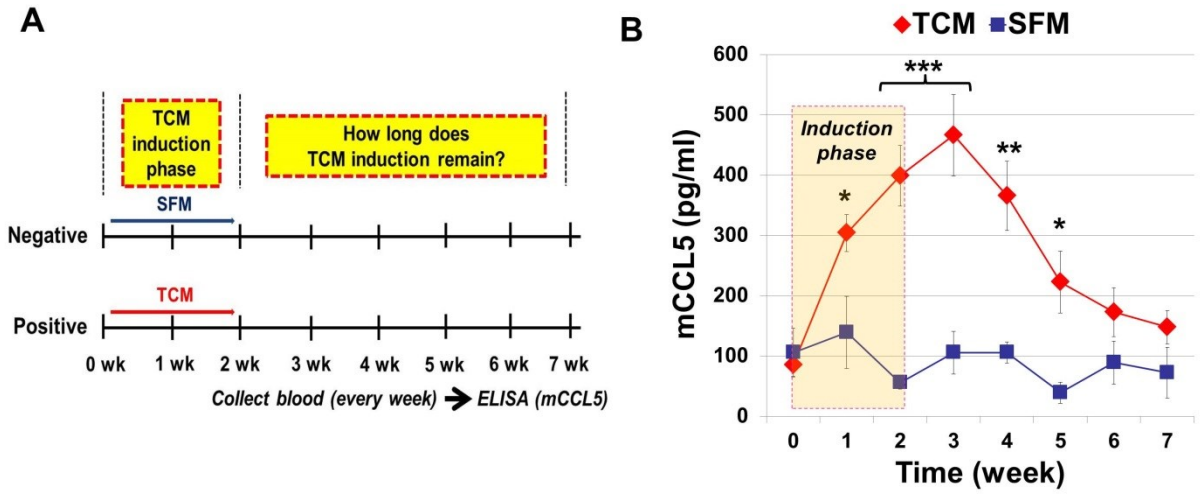

Figure 3.14: Duration of TCM effects in vivo. Mouse CCL5 (mCCL5) concentration was measured in TCM-treated animals to assess duration of the TCM effect. The mCCL5 is a key tumor-recruiting chemokine factor expressed by LEC under TCM treatment. (A) Mice were treated with TCM or serum-free media (SFM) for 2 weeks (week 0 to week 2). From week 0, 50 µl of mouse blood samples (in 10% EDTA) was collected using the retro-orbital bleeding method, every week for up to 7 weeks. (B) The concentration of mCCL5 in plasma in SFM or TCM-treated animals (4-5 animals/group). P-values are based on the comparisons of mCCL5 between SFM and TCM treated groups (*$P < 0.05$, **$P < 0.005$, ***$P < 0.001$).

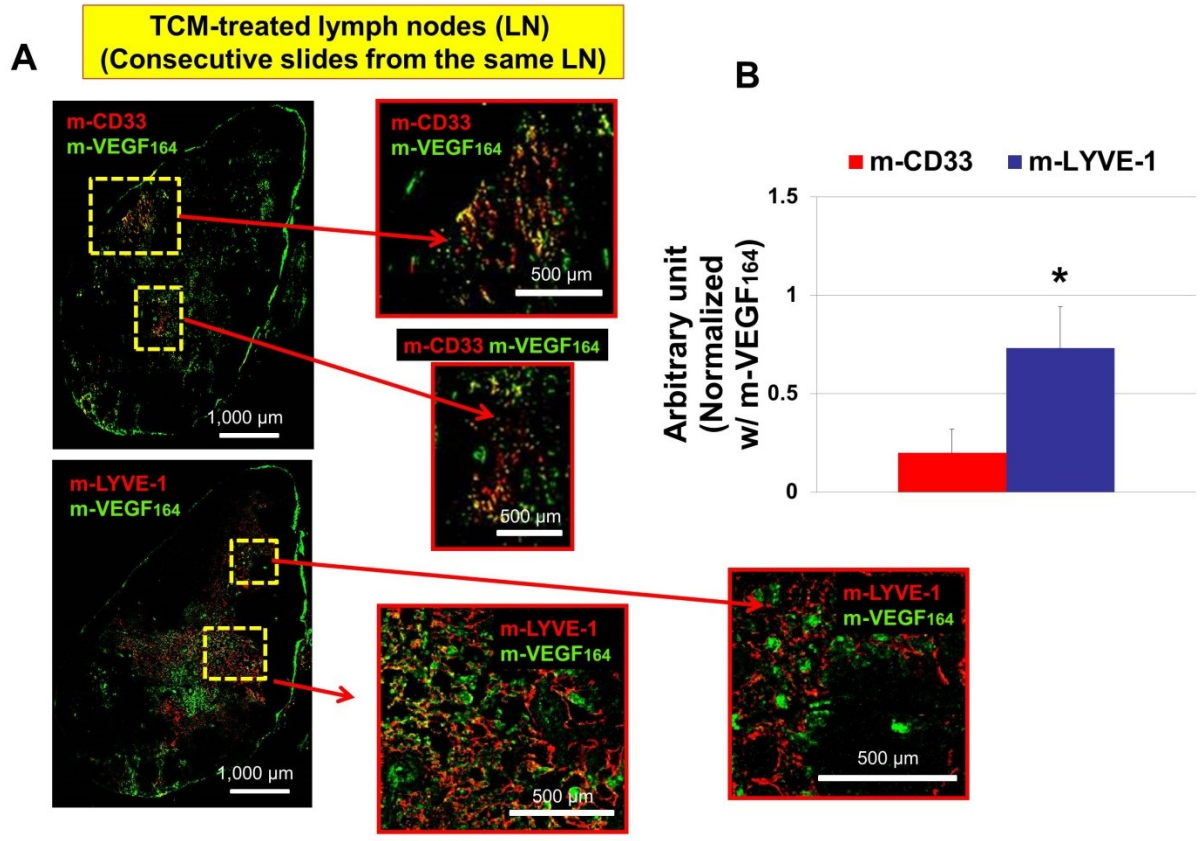

Figure 3.15: Myeloid cells (m-CD33, red) and lymphatic endothelial cells (LEC: m-LYVE-1, red) are detected in the lymph nodes (LN) and contribute to expression of m-VEGF$_{164}$ upon TCM-treatment. (A) LNs from TCM-treated animals were analyzed. Consecutive sections from the same LN were stained with anti-mouse CD33 (red) and anti-mouse VEGF$_{164}$ (green) antibodies or anti-mouse LYVE-1 (red) and anti-mouse VEGF$_{164}$ (green) antibodies to detect the myeloid cells, LEC, and their colocalization with mouse VEGF$_{164}$. After TCM treatment, LEC and myeloid cells were detected in the LN, and both cells were colocalized with mouse VEGF$_{164}$ expression. However, distribution of myeloid cells was local compared to that of LEC, which

was prevalent in the lymph nodes. (B) Pixel density from m-CD31 and m-LYVE-1 staining was normalized to the density of m-$VEGF_{164}$ (*$P = 0.034$).

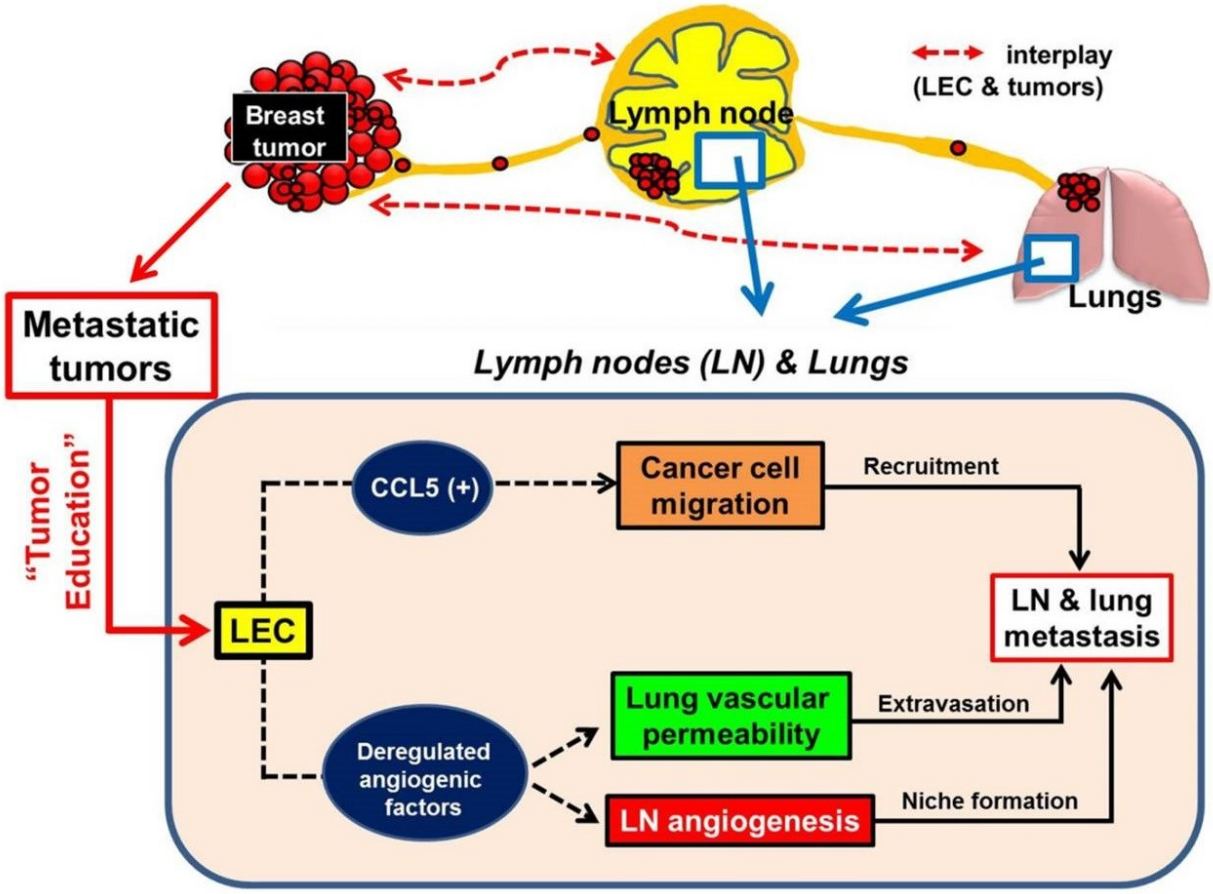

Figure 3.16: Conceptual summary. Metastatic breast tumor secretion educates lymphatic endothelial cells (LEC) within the lymph nodes and the lungs. After tumor education, LEC express CCL5 and VEGF. CCL5 attracts CCR5-positibe cancer cells into the lymphatic system. VEGF enhances lymph node angiogenesis and lung vascular permeability. Finally, these LEC derived factors facilitate tumor recruitment, extravasation, and colonization.

Chapter 4: Interleukin-6: A Key Cytokine for Crosstalk between Lymphatic Endothelial Cells and Cancer Cells for Breast Cancer Metastasis

4.1 RATIONALE

In chapter 3, we described that tumor-conditioned media (TCM) from triple-negative breast cancer (TNBC) cells induce CCL5 and VEGF expression in lymphatic endothelial cells (LEC) within pre-metastatic niches. These two molecular targets have been blocked separately and in combination, using the FDA-approved CCR5 inhibitor and VEGF antibodies: the blockade confirmed that these are crucial signaling molecules to promote breast tumor dissemination and colonization. However, it is still unknown which factors in TCM trigger tumor education of LEC; and which transcription factors in LEC are influenced by the TCM to start CCL5 and VEGF expression. In this chapter, these two important questions will be answered using several in vitro and animal experiments.

4.2 MATERIALS & METHODS

4.2.1 Cell culture

Human umbilical vein endothelial cells (HUVEC) and lymphatic endothelial cells (LEC) were purchased from Lonza, and grown in EGM-2 and EGM-2MV. MDA-MB-231, SUM149, and MCF7 breast cancer cells were gifts from Dr. Zaver Bhujwalla (JHMI, Radiology and Oncology). MDA-MB-231-luc-D3H2LN was purchased from Caliper. MDA-MB-231, MDA-MB-231-luc-D3H2LN, and MCF7 cells were propagated in RPMI-1640 medium supplemented with 10% FBS and 1% penicillin/streptomycin (Sigma). SUM149 cells were cultured in F-12 media supplemented with 5% FBS, 1 ng/ml hydrocortisone, 5 μg/ml insulin (Sigma), and 0.1mM HEPES (Gibco).

4.2.2 Conditioned media

When MDA-MB-231, MCF7 and SUM149 cells were confluent in T175 tissue culture flasks, the normal growth media was replaced with 8 ml serum-free media (SFM). After 24 h incubation, the supernatant was centrifuged and filtered through 0.2 μm syringe filters (Corning). The resulting tumor-conditioned media (TCM) was stored in aliquots at -80°C. When LEC/HUVEC reached 30-40% confluence in T75 tissue culture flasks, EGM was replaced with 30% TCM (TCM:EGM=3:7) to allow the TCM to educate the LEC/HUVEC. LEC/HUVEC were allowed to grow in the media for 4 days then the media was replaced with 3 ml SFM with 2% FBS (not supplemented with bullet kit). After 48 h, the supernatant was centrifuged and filtered. The resulting tumor-educated LEC/HUVEC conditioned media (MB231-LEC or MB231-HUVEC) was stored in aliquots at -80°C to avoid multiple freeze thaws.

4.2.3 TCM-induced metastasis models

Animal protocols described in this study were approved by the Institutional Care and Use Committee at the Johns Hopkins Medical Institutions. Before tumor inoculation, athymic nude mice (female, 5-6 weeks, 18-20 g) were pre-treated by injecting 50 µl tumor-conditioned media (TCM) or growth factor-depleted TCM (GF-dep-TCM), or growth factor/IL6 depleted TCM (GF/IL6-dep-TCM), or serum-free media (SFM) subcutaneously for 2 weeks daily as described previously (Lee, Pandey et al. 2014). After 2 weeks of induction, luc-MB231 cells ($2x10^6$/mouse, 100 µl of 50% matrigel solution) were injected into the upper inguinal mammary fat pad of the animals under anesthesia (50 mg/kg ketamine and 5 mg/kg acepromazine). The tumor size was measured by using a caliper, and the volume was calculated, using the formula: $V = 0.52 \times (\text{length}) \times (\text{width})^2$. Animals were imaged every week to track anterior tumor metastases, using the IVIS Xenogen 200 optical imager (Xenogen) after i.p. injection of D-luciferin (Caliper, 150 mg/kg). After 5 weeks, organs were harvested and bathed in D-luciferin solution for 3 min and placed in the IVIS imager to detect metastases ex vivo. Luciferase-mediated photon flux was quantified by using Living Image® 3D Analysis (Xenogen). S3I-201 (5 mg/kg, Calbiochem) was administered intravenously every 2 days. One hundred microliter of blood was collected from the tail-vein, and EDTA plasma was prepared to perform ELISA.

4.2.4 Immunofluorescence

Tumors, matrigel plugs, LN, and lungs fixed in 3.5% formalin were placed in 30% sucrose (Sigma) in PBS, incubated overnight at 4°C, and frozen in the O.C.T. compound (Sakura). Sections of 10-µm thickness were cut at -20°C. After blocking with 5% normal goat or normal chicken serum (Jackson Immunoresearch) in PBST (0.3% Triton) for 1 h at room temperature

(RT), the sections were treated with one or more of the following primary antibodies overnight at 4°C: rabbit anti-mouse LYVE-1 antibody (1:200, AngioBio), rat anti-mouse CCL5 (1:200, Abcam), rat anti-mouse CD31 (1:100, BD Pharmingen), goat anti-mouse $VEGF_{164}$, mouse anti-human $VEGF_{165}$ (1:300, R&D systems), rabbit anti-pVEGFR2 (1:400, Cell Signaling), mouse anti-smooth muscle actin Cy-3 (1:500, Sigma), goat anti-mouse F4/80 FITC (1:100, Serotec), goat anti-mouse lectin FITC (1:100, Sigma), rabbit anti-mouse CD33 antibody (1:50, Santa-Cruz), and goat anti-mouse Ly6g (1:200, Serotec). After 3 rinses with PBST, sections were incubated for 1 hour at RT with one or more of the following secondary antibodies (1:500): FITC-conjugated goat anti-rat, FITC-conjugated chicken anti-goat, rhodamine-conjugated goat anti-rat, Cy3-conjugated goat anti-rabbit, Alexa Fluor 647 goat anti-rabbit, Alexa Fluor 488 goat anti-rabbit, DyLight405 goat anti-rabbit, and DyLight405 goat anti-mouse antibodies (all from Jackson Immunoresearch). After 3 rinses with PBST, the samples were counterstained with DAPI (1:10,000, Roche) (5 min at RT). The samples were washed with PBST once and mounted with the ProLong Gold anti-fade reagent (Invitrogen) in dark. Fluorescent signals were visualized and digital images were obtained using the LSM-510 confocal microscope (Carl Zeiss).

4.2.5 Histology

LN and lungs were fixed, frozen and sectioned as above. After blocking with 5% goat serum in PBST for 1 hour at RT, the sections were treated with mouse anti-cytokeratin antibodies (1:500, Sigma) overnight at 4°C. The rest of the 3,3' diaminobenzidine (DAB) procedure was performed as previously described (Lee, Pandey et al. 2014).

4.2.6 Electrophoretic Mobility Shift Assays (EMSA)

The 2 strands of the wild type CRE oligonucleotide (5'-3', AAAGAGGAAACTGATGAGCTCACTCTAGAT) and of mutated CRE (5'-3', AAAGAGGAAACTGATACAGCCACTCTAGAT), conjugated with biotin at the 5' end were synthesized (Invitrogen). Equal amounts of both strands in 0.5M NaCl, 10 mM Tris pH7.5 were annealed by boiling for 5 min at 95°C, and very gradually cooling on the hot plate. A DNA retardation gel (6%, Novex) was pre-run at 120 V for 50 min at 4°C. For the binding reaction, 3 μg nuclear extract, and 0.5 μg poly(dI-dC) with or without excess unlabeled CRE oligonucleotide were incubated in binding buffer (10 mM Tris, 1 mM EDTA, 50 mM KCl, 10 mM $MgCl_2$, 5 μg/ml BSA, 0.1 mM DTT) for 10 min at RT, after which oligonucleotide-biotin was added (finally 40 pM) and incubated for 30 min at RT. Ten microliter of binding sample was mixed with 1 μl 5x TBE sample buffer (Invitrogen), loaded on the gel, and run for 1 h at 120 V in 0.5X TBE running buffer. The gel were transferred to a DNA transfer stack (Invitrogen), using the iBlot transfer module (Program 8, 7 min). The nylon membrane was dried and cross-linked under a UV source (305 nm) for 15 min, then probed by the Chemiluminescent Nucleic Acid Detection Module (Pierce).

4.2.7 Immunoblot assays

For reverse western blot, Proteome Profiler Antibody Array Kits for human angiogenesis factor, chemokines, cytokines and phospho-kinases (R&D systems) were used, according to the manufacturer's instructions. For western blot, 400,000 cells/well MDA-MB-231 cells or LEC were starved for 24 h, after which they were treated with Stattic (5-10 μM), S3I-201 (2.5-10 μM), or SP600125 (40 μM) and incubated for 60 min. After that, inducers, including TCM (30%),

EGM, IL6-dep-TCM, IL6 or EGF were added. We followed the standard protocol for the rest of the procedure as described previously (Lee, Koskimaki et al. 2013) applying antibodies of interest, including pStat3, HIF-1α, gp130, pNFkB, NFkB, IkBα, Stat3, pCREB, GAPDH (all from Cell Signaling), pc-Jun, pATF-2 (Sigma), CCR5, and Lamin B1 (Abcam).

4.2.8 Coimmunoprecipitation (Co-IP)

LEC (2 x 10^6) treated with Stattic, SP600125, IL6 or EGM, were used to prepare cell lysates or nuclear extracts. Five hundred microliters of cell lysates or 200 µl nuclear extracts were incubated overnight at 4°C with antibodies suitable for IP (1:100 diluted): pStat3, pc-Jun, pATF-2, pNFkB, and NFkB (Cell Signaling). Ten microliters of Protein A/G Plus Agarose (Santa Cruz Biotech) was added and incubated for 3 h at 4°C. The beads were rinsed 3 times with 500 µl cell lysis buffer for IP (Pierce), supplemented with the protease inhibitor and phosphatase inhibitor cocktail 2/3 (Sigma). The protein complex was reduced and separated by SDS-PAGE and probed with the following antibodies in a Western assay: pStat3, pc-Jun, pATF-2, pNFkB, and NFkB (Sigma).

4.2.9 Bioinformatics analyses of The Cancer Genome Atlas (TCGA) data

All analyses of TCGA primary breast cancer tissues (Infusino and Jacobson 2012) were performed in R (3.0.1). TCGA Level 3, RSEM v2 gene expression measurements from RNA-sequencing for CCL5 and IL6 were obtained from the cBioPortal with the CRAN cgdsr package (Gao, Aksoy et al. 2013). ER and PR status were obtained from cross-platform summaries, and HER2 status from IHC measurements in the TCGA clinical data, with a total of 99 triple negative samples and 326 ER+ PR+ HER2-. Samples were called lymph node positive if at least one lymph node was positive by either IHC or H&E staining, consistent with pathological

staging in the TCGA clinical annotations. There were 50 lymph node negative and 37 lymph node positive samples within the triple negative breast cancer subtype. Expression between subtypes was compared with one-sided t-tests on log transformed RSEM values. Correlation coefficients and corresponding p-values were computed with Pearson's correlation.

4.2.10 Statistical Analysis

Error bars correspond to s.e.m, unless otherwise stated. Differences between two groups are regarded as significant when P is less than 0.05 using the Student's t-test.

4.3 RESULTS

4.3.1 TNBC cell secreted IL6 phosphorylates Stat3 in LEC, inducing lymphatic expression of CCL5 and VEGF

Key targets of tumor-education in LEC, which are specifically phosphorylated by TCM were identified. Among 46 kinase phosphorylation sites screened, both S727 and Y705 of Stat3 were exclusively phosphorylated in LEC by TCM treatment (Figure 4.1.A, B). It was demonstrated that phospho-Stat3 (pStat3) was essential for CCL5 expression in LEC by using Stattic, an inhibitor of phosphorylation of Stat3 (Schust, Sperl et al. 2006). Stattic treatment inhibited TCM-induced CCL5 expression as well as Stat3 phosphorylation (Figure 4.1.C, D). Reverse western assays were done to identify the key factors in TCM in the tumor education. Reverse western blotting for cytokines revealed that interleukin 6 (IL6) is highly expressed in both TNBC cell lines, MB231 and SUM149, but not in MCF7 or LEC (Figure 4.1.E-G). GM-CSF, expressed in TNBC cells (Figure 4.1.F) was not considered as a key factor, because GM-CSF is known to phosphorylate Stat5 (Lehtonen, Matikainen et al. 2002): no pStat5 was shown in TCM-treated LEC (Figure 4.1.A). Also GM-CSF was very weak in MB231 cells, compared to SUM149 (Figure 4.1.E). Only TCM containing IL6 induced pStat3 (Figure 4.1.H and Figure 4.3.A, B), demonstrating that tumor-secreted IL6 is the pivotal factor for Stat3 phosphorylation in LEC. IL6-depleted TCM (IL6-dep-TCM) failed to induce CCL5, but induced some VEGF expression (Figure 4.1.I): CCL5 expression in MB231-LEC is totally IL6-driven, but VEGF expression is induced by IL6 and other factors in the TCM.

4.3.2 pStat3-pc-Jun-pATF-2 ternary complex and pStat3-dependent HIF-1α are crucial for CCL5 and VEGF expression in LEC

Stattic treatment inhibited IL6-induced CCL5 and VEGF expression; SP600125, a JNK inhibitor, blocked IL6-induced expression of CCL5 but not of VEGF in LEC (Figure 4.2.A). Western blots showed that c-Jun and ATF-2 were constitutively phosphorylated in normal LEC (EGM-treated), while Stat3 phosphorylation required IL6 (Figure 4.2.B). Also SP600125 reduced the amount of pc-Jun and pATF-2 but pStat3 was not affected. With Stattic treatment pStat3 disappeared but pc-Jun and pATF-2 were maintained (Figure 4.2.B). Co-immunoprecipitation (Co-IP) experiments showed that pc-Jun and pATF-2 are in a binary complex even in the absence of IL6 in the media while strikingly, pStat3, pc-Jun, and pATF-2 form a ternary complex in response to IL6 treatment (Figure 4.2.C).

LEC nuclear extracts were tested. After treating with SP600125, both the ternary and the binary complexes disappeared. With Stattic treatment, however, only the ternary complex was dissociated (Figure 4.2.D). The cAMP-responsive element (CRE) in the promoter of the CCL5 gene is known to regulate its expression in alveolar epithelial cells (Casola, Garofalo et al. 2001). ATF-2 binds to the CRE (Srebrow, Muro et al. 1993). Moreover, c-Jun and ATF-2 have been observed in a binary complex (van Dam, Duyndam et al. 1993). More interestingly, Stat3 can interact with c-Jun and participate in cooperative transcriptional activation (Zhang, Wrzeszczynska et al. 1999). We hypothesized that the pStat3-pc-Jun-pATF-2 ternary complex would bind to the CRE site in CCL5 promoter. An Electrophoretic Mobility Shift Assay (EMSA) was performed to show binding between the protein complex and the CRE oligonucleotide (Figure 4.2.G). When LEC were treated with IL6, nuclear proteins bound to the CRE oligonucleotide, however Stattic or SP600125 treatment inhibited binding. No binding was

observed on the mutated CRE, and excess unlabeled CRE oligonucleotide inhibited binding. Surprisingly, IL6 also promoted the expression of HIF-1α in LEC nucleus in a dose-dependent manner (Figure 4.2.E). This expression was blocked by Stattic but not by SP600125, demonstrating that nuclear HIF-1α and VEGF expression are IL6-pStat3 dependent and do not require pc-Jun or pATF-2 (Figure 4.2.E, F).

4.3.3 IL6-induced CCL5 expression is NFkB-independent

IL6 or TCM-induced LEC were analyzed to examine whether there is a complex formation between Stat3 and NFkB (Figure 4.3). IL6-depleted TCM was prepared for the experiment using IL6 neutralizing antibodies (Figure 4.3.A). In the IL6-depleted TCM, Stat3 was not phosphorylated, but pNFkB was constitutively observed regardless of IL6 in TCM (Figure 4.3.B). IL6-treated LEC was analyzed by using coimmunoprecipitation (Co-IP) methods with pStat3 or NFkB or p-NFkB antibody. No complex formation was shown between pStat3 and NFkB (or p-NFkB) in IL6-treated LEC and HUVEC; however pStat3 forms complex with pc-Jun and p-ATF-2 in LEC (Figure 4.3.C, D). These results demonstrate that IL6-induced pStat3-pc-Jun-pATF-2 ternary complex, which is independent with NFkB activity, is essential for CCL5 expression.

4.3.4 EGF does not induce CCL5 expression in LEC

EGF was tested in LEC whether it influences CCL5 expression and Stat3 phosphorylation (Figure 4.4). In western blots, IL6 highly phosphorylated Stat3, but EGF did not. ATF-2 and c-Jun were phosphorylated by the induction with both EGF and IL6 (Figure 4.4.A). Stat3 in LEC was only phosphorylated by IL6 in dose responsive manner, but not by EGF even at a very high concentration (Figure 4.4.B). Percent CCL5 expression in LEC was also tested with IL6 and

EGF with different concentrations. Similarly, EGF does not induce any CCL5 expression in LEC (Figure 4.4.C).

4.3.5 IL6-induced CCL5 expression is gp130-positive LEC specific

LEC were treated with EGM, IL6 (1, 10 ng/ml), TCM, and IL6-depleted TCM. Then, pStat3, pgp130, and pJak2 were analyzed by western blotting. IL6 or IL6-included TCM induces phosphorylation of Stat3, gp130, and Jak2 in LEC (Figure 4.5). Upon this result, gp130 and pStat3 were further analyzed in IL6-treated HUVEC and LEC (Figure 4.6.A). HUVEC did not show significant expression of gp130 compared to LEC; also, they did not show Stat3 phosphorylation by IL6-included TCM (Figure 4.6.A). CCL5 or VEGF expression in tumor-educated HUVEC (MB231-HUVEC) was also not significant, compared to normal HUVEC or serum-free media (Figure 4.6.B). Proangiogenic potential of MB231-HUVEC conditioned media (Lee, Pinder et al.) was compared with that of MB231-LEC conditioned media. MB231-HUVEC CM did not induce tube formation, proliferation, migration and adhesion of vascular endothelial cells (Figure 4.6.C, D).

4.3.6 Targeting of IL6 and pStat3 blocks LN and lung metastasis

The results above indicate that the IL6-Stat3 axis is a key inducer of CCL5 and VEGF expression in LEC. Thus IL6 and pStat3 were inhibited in the GF-dep-TCM induced metastasis model in vivo (Figure 4.7.B). The FDA-approved IL6 receptor antibody (tocilizumab) was for human IL6 receptor blockage, thus to block IL6 singly in mice, growth factor and IL6 depleted TCM (GF/IL6-dep-TCM) was prepared by immunodepleting IL6 from previously prepared GF-dep-TCM. S3I-201, a pStat3 inhibitor with the same mechanism of action as Stattic was selected, because S3I-201 has been tested in vivo (Siddiquee, Zhang et al. 2007). S3I-201 was separately

tested in vitro (Figure 4.7.A): S3I-201 inhibited pStat3 in IL6-treated LEC (Figure 4.7.A). All mice pre-treated with GF-dep-TCM for 2 weeks prior to tumor inoculation developed metastases 5 weeks later; 44% of the mice (4/9) treated with S3I-201 during the pre-treatment phase developed metastases; only 22% (2/9) of the mice pre-treated with GF/IL6-dep-TCM had metastases which was less than the 33% (3/9) of mice with metastases in the SFM treated group (Figure 4.8A). Significant reductions in lung and LN metastases after inhibiting IL6 and pStat3 were observed by IVIS imaging, macroscopic morphology, and anti-cytokeratin immunostaining (Figure 4.8.B-D). Tumor size was not influenced by S3I-201 (Figure 4.8.E), as the drug was administered before establishing primary tumors, which is different from a previous study showing primary tumor inhibition with S3I-201 treatment (Siddiquee, Zhang et al. 2007).

4.3.7 TCGA RNA-sequencing data analyses

Motivated by these results, the IL6-CCL5 axis was evaluated by analyzing The Cancer Genome Atlas (TCGA) mRNA-sequencing datasets of breast cancer patients to determine clinical relevance of the targets (Figure 4.9); this analysis was performed in collaboration with Dr. Elana Fertig of the Sidney Kimmel Comprehensive Cancer Center. Both IL6 and CCL5 were significantly overexpressed in primary triple negative breast cancer (TNBC) samples compared to ER+, PR+, HER2- samples. This was consistent with our experimental results that only TNBC (SUM149 and MB231) cell lines express IL6 and induce CCL5 expression in LEC; but MCF7 (ER+ PR+ HER2-) cell line does not (Figure 3.1.D, Figure 4.1.G). In addition, expression of IL6 and CCL5 were not significantly correlated in LN-negative TNBC samples. On the contrary, the correlation between IL6 and CCL5 was significant (P=0.001) in LN-positive TNBC samples, suggesting that the IL6 and CCL5 can be therapeutic and prognostic markers in TNBC metastasis.

4.4 DISCUSSION

This chapter concludes that TNBC cell-secreted IL6 educates LEC in the pre-metastatic lungs and LN to prime them and promotes breast cancer metastasis. Paracrine signals regulated by the IL6-Stat3 axis and operating between cancer cells and LEC play a pivotal role in the induction of CCL5 and VEGF expression in LEC within pre-metastatic organs facilitating tumor cell recruitment, extravasation and colonization (Figure 4.10).

IL6 is an inflammatory cytokine which leads to activation of the Jak kinases and glycoprotein 130 (gp130) to phosphorylate Stat3 (Gerhartz, Heesel et al. 1996) upon interaction with the IL6 receptors. In our experiment using LEC, we showed that gp130, Jak2, and Stat3 were phosphorylated by TCM containing IL6 (Figure 4.5). Stat3 is a transcription factor that contributes to the expression of diverse cytokines and growth factors (Hirano, Ishihara et al. 2000; Takeda and Akira 2000). Thus the IL6-Stat3 axis has been explored in cancer as well (Basolo, Conaldi et al. 1993; Bartsch, Woehrer et al. 2006; Reyes-Gibby, Spitz et al. 2007). The IL6-Stat3 axis promotes tumorigenesis (Niu, Bowman et al. 2002; Wei, Kuo et al. 2003; Corvinus, Orth et al. 2005; Hedvat, Huszar et al. 2009), causes chemo-resistance (Catlett-Falcone, Landowski et al. 1999; Nair, Tolentino et al. 2012; Ara, Nakata et al. 2013; Liu, Cao et al. 2013; Yi, Lee et al. 2013), and contributes to epithelial-mesenchymal transition (EMT) (Xiong, Hong et al. 2012; Balanis, Wendt et al. 2013; Guo, Chen et al. 2013). IL6-Stat3 feed forward loops amplify pro-tumorigenic and pro-metastatic signals using intrinsic and extrinsic pathways (Yu, Pardoll et al. 2009; Chang, Bournazou et al. 2013). The intrinsic pathway is activated by genetic alterations in cancer cells, causing the overexpression of IL6 or the persistent activation of IL6 receptors or phospho-Stat3 (Yu, Pardoll et al. 2009; Lee, Deng et al. 2010). These receptors and transcription factors also can be activated by extrinsic pathways (e.g.,

ultraviolet radiation, infection, chemicals, etc.). However the role and importance of the IL6-Stat3 axis in LEC has not been studied well. This is the first study, showing that LEC can be actively involved in breast tumor metastasis via the IL6-STAT3 axis.

Mechanisms of CCL5 regulation in LEC under TCM condition were studied. In previous studies of CCL5 regulation, vascular smooth muscle cells that expressed CCL5 were shown to activate early inflammation through TNFs (Kovacic, Gupta et al. 2010); NFkB-dependent CCL5 expression has been studied in different types of cells (Genin, Algarte et al. 2000; Yeligar, Machida et al. 2009; Kovacic, Gupta et al. 2010). In this study, however, it was shown that IL6-induced CCL5 is not colocalized with the smooth muscle actin (Schoppmann, Bayer et al.)-positive cells, and is not regulated by an NFkB-Stat3 complex (Figure 3.2 and Figure 4.3). Instead, pStat3 forms a ternary complex consisting of pStat3, pc-Jun, and pATF-2 in response to IL6, which regulates CCL5 expression in the lymphatic system; this mechanism has not been previously discovered. Other molecular details of IL6 dependent induction of CCL5 remain to be elucidated. Interestingly, unlike LEC, HUVEC could not be educated by tumor cells (Figure 4.6). It has been reported that LEC express 3-4 times more gp130, compared to blood endothelial cells (BEC) (Hirakawa, Hong et al. 2003). Consistent with these findings, less gp130 as well as less pStat3 in BEC were observed thus showing no TCM effect.

VEGF expression in TCM-induced LEC is partially IL6-driven (Figure 4.1.I). While IL6-depleted TCM did not induce any CCL5 in LEC, around 60% of total VEGF induced by TCM treatment was still expressed in LEC even in the absence of IL6. This demonstrates that molecules other than IL6 in the TCM, which we have not identified by our analysis, are also involved in metastasis by inducing angiogenesis. Lastly, IL6 and Stat3 were targeted by using anti-IL6 antibodies and S3I-201. Both IL6 depletion and S3I-201 treatment significantly

inhibited LN and lung metastasis (Figure 4.8). This suggests that current anti-IL6 receptor therapy (tocilizumab) for rheumatoid arthritis might help improve metastatic breast cancer treatment. Though we focus on crosstalk between LEC and cancer cells, our tumor education models need to be further tested in other types of stromal cells, such as fibroblasts, bone marrow cells, and other immune cells based on studies suggesting the importance of the influence of tumor-secreted factors on diverse types of cells for tumor progression (Pollard 2004; Kuang, Zhao et al. 2008; Ishii, Hashimoto et al. 2010; Peinado, Aleckovic et al. 2012; Ribeiro, Monteiro et al. 2012; Lu, Ye et al. 2013).

In summary, this chapter proposes a complex molecular crosstalk between TNBC cells and LEC within distal organs for metastasis, and identifies the key players, IL6-Stat3, pStat3-pc-Jun-pATF2 ternary complex and pStat3 dependent HIF1α, which can be targeted to treat breast cancer metastasis.

4.5 FIGURES & TABLES

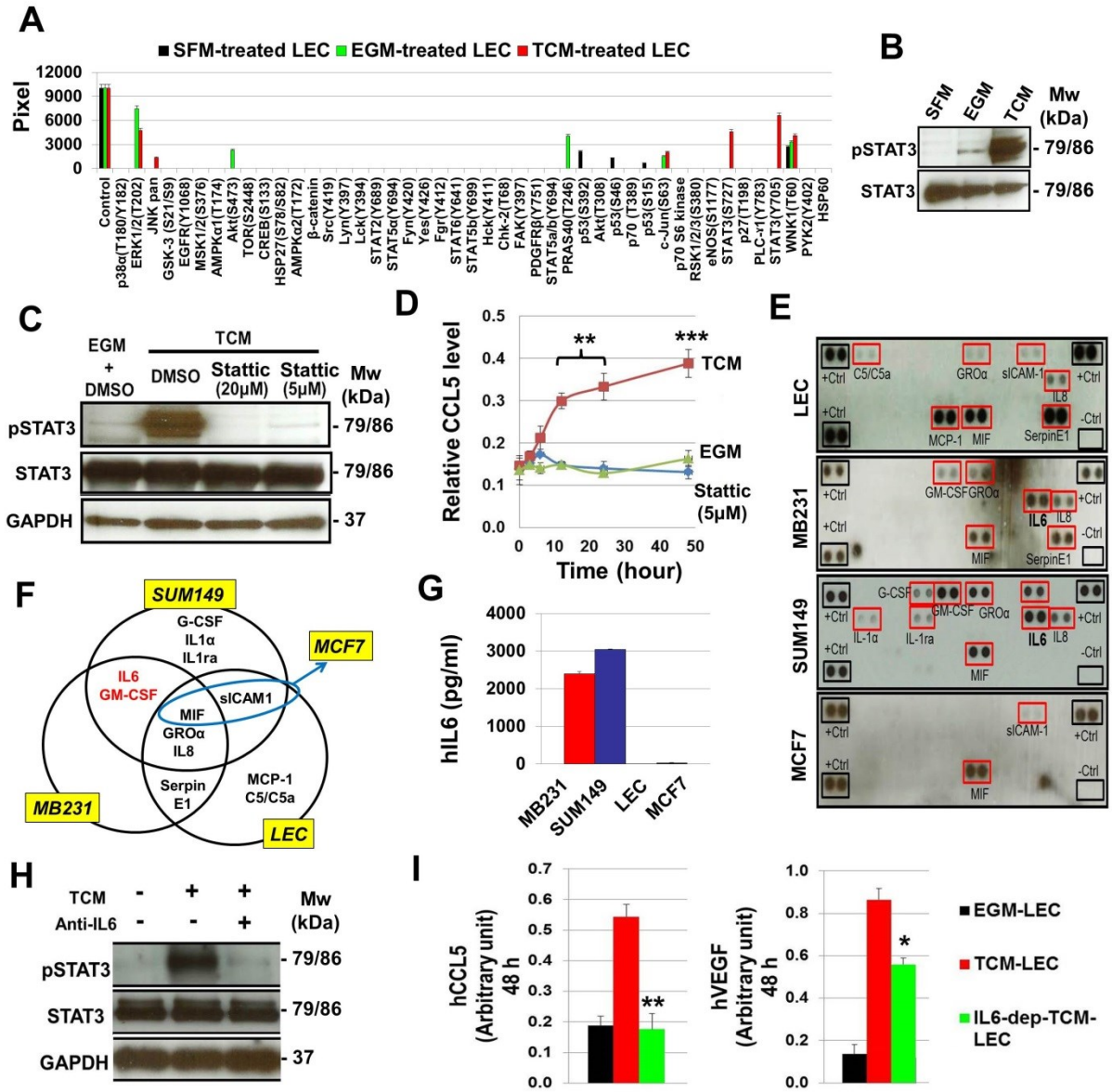

Figure 4.1: Tumor cell secreted IL6 phosphorylates Stat3 which induces CCL5 and VEGF expression in LEC. (A) Reverse western assays with the human phospho-kinase antibody arrays (R&D systems) simultaneously detected the relative amounts of 46 phospho-kinases in LEC. We compared the effects of SFM, EGM, and TCM treatment. Erk1/2 (T202/Y204, T185/Y187),

Stat3 (Y705, S727), c-Jun (S63), JNK pan (T183/Y185, T221/Y223), and WNK1 (T60) were phosphorylated in TCM-treated LEC; Erk1/2 (T202/Y204, T185/Y187), Akt (S473), c-Jun (S63), PRAS40 (T246), WNK1 (T60) were phosphorylated in EGM-treated LEC; p53 (S15, S46, S392) and WNK1 (T60) were phosphorylated in SFM-treated LEC. (B) pStat3 (Y705) in LEC was confirmed in separate western blots. TCM exclusively phosphorylates pStat3. (C) Phosphorylation of Stat3 was completely blocked by Stattic (5, 20 μM) in LEC. GAPDH was used as a loading control. (D) ELISA assay showed that 5 μM Stattic completely inhibited CCL5 secretion (**P < 0.01, ***P = 0.0008). (E) Reverse western assays with the human cytokine antibody arrays (R&D systems) detected the relative amounts of 36 cytokines in MB231, SUM149, MCF7, and LEC conditioned media. Representative images of the cytokine array membranes. (F) Summary of the cytokine array results in (E). IL6 and GM-CSF were expressed only in TNBC cell lines (MB231 and SUM149). MIF, GROα and IL8 were expressed in all the cell lines (MB231, SUM149, MCF7 and LEC). (G) ELISA confirmed that IL6 is highly expressed in MB231 and SUM149 cells. (H) IL6-depleted TCM (IL6-dep-TCM) did not induce Stat3 phosphorylation in LEC. GAPDH was used as a loading control. (I) IL6-depleted TCM (IL6-dep-TCM) was unable to induce CCL5 expression in LEC. VEGF expression was significantly reduced by IL6 depletion, but not completely, suggesting that other factors in TCM are also inducing VEGF expression (**P = 0.0075, *P = 0.032).

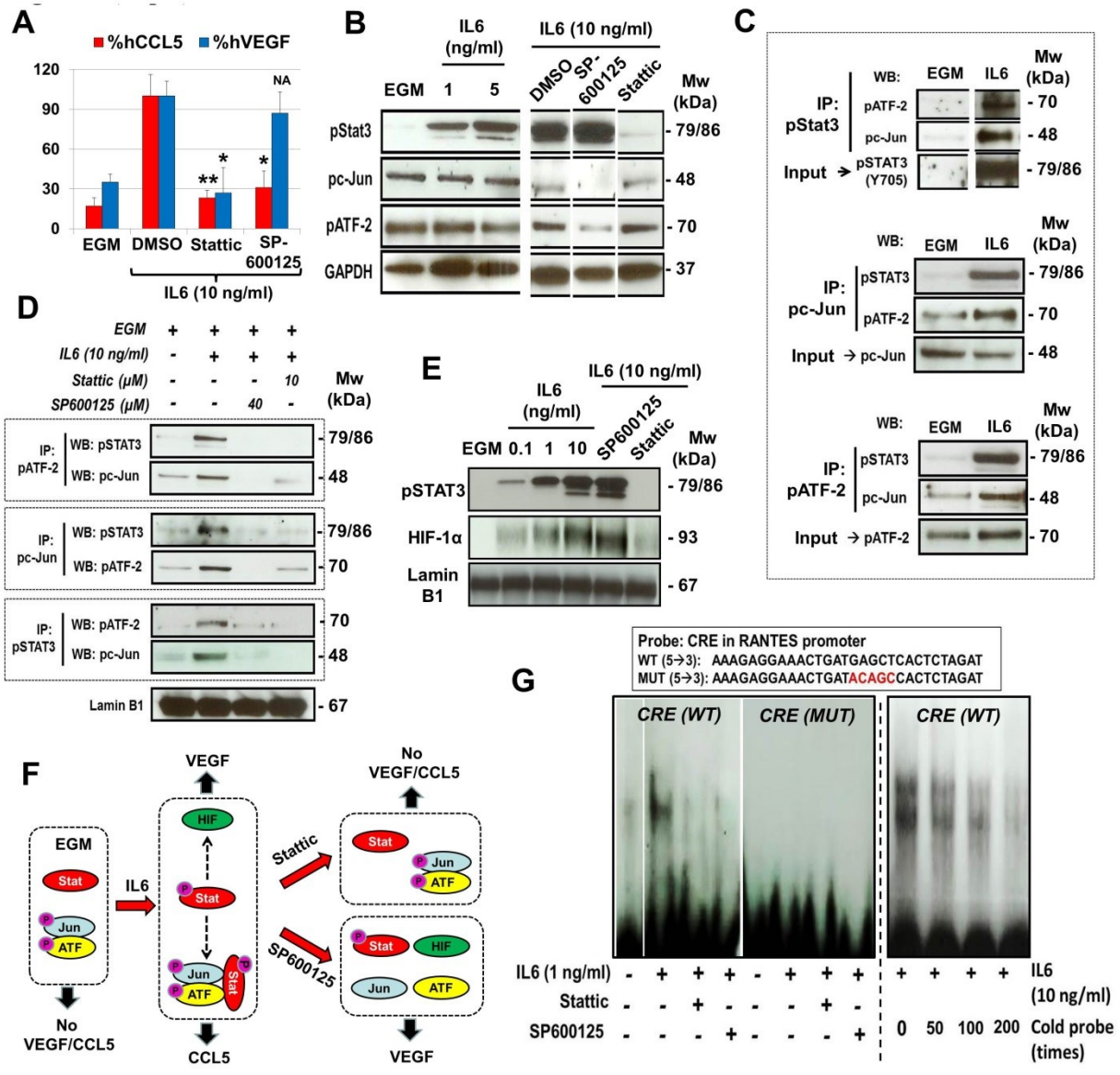

Figure 4.2: The pStat3-pc-Jun-pATF-2 ternary complex is central for CCL5 expression and pStat3-dependent HIF-1α separately induces VEGF expression. (A) IL6-dependent CCL5 expression was inhibited by both Stattic (a pStat3 inhibitor, **P = 0.009) and SP600125 (a JNK inhibitor, *P = 0.028), however, VEGF expression was blocked by Stattic only (*P = 0.041). (B) EGM activated pc-Jun and pATF-2 but not pStat3; only IL6 treatment induced pStat3.

SP600125 blocked pc-Jun and pATF-2 while Stattic selectively blocked pStat3. (C) Coimmunoprecipitation (Co-IP) assays. pStat3 did not form a complex with pc-Jun or pATF-2 in LEC grown in EGM, but a pc-Jun-pATF-2 binary complex was weakly observed. After IL6 treatment, pStat3 associated with the binary complex to form a pStat3-pc-Jun-pATF-2 ternary complex. (D) Co-IP with nuclear extracts. EGM allowed pc-Jun-pATF-2 binary complex to form in the LEC nucleus. IL6 induced a pStat3-pc-Jun-pATF-2 ternary complex which was dissociated by Stattic or SP600125. However, small amounts of the pc-Jun-pATF-2 binary complex remained under Stattic treatment. Lamin B1 was used as a nuclear extract loading control. (E) HIF-1α in the nucleus was increased by IL6 treatment. Though SP600125 did not block pStat3 and HIF-1α, Stattic inhibited both of them, suggesting that HIF-1α is IL6-pStat3 dependent. (F) Graphical summary. pc-Jun-pATF-2 binary complexes and unphosphorylated Stat3 are present in normal LEC (EGM condition) but there is no CCL5/VEGF expression. IL6 induces Stat3 phosphorylation and activates formation of the pStat3-pc-Jun-pATF-2 ternary complex, which is essential for CCL5 expression. pStat3 promotes HIF-1α expression and separately induces VEGF expression. Upon Stattic treatment, pStat3 and the ternary complex disappear, resulting in no expression of CCL5 and VEGF; the pc-Jun-pATF-2 binary complex that remains upon Stattic treatment does not induce either CCL5 or VEGF expression. SP600125 dissociates both ternary and binary complexes, but pStat3 separately induces HIF-1α and VEGF expression. (G) Electrophoretic Mobility Shift Assays (EMSA) showed the binding of LEC nuclear proteins to CRE oligonucleotide in the CCL5 promoter after IL6 treatment. Both Stattic and SP600125 blocked the binding. No nuclear proteins bound to the mutant CRE oligonucleotide. Cold CRE oligonucleotide competed with biotin-conjugated oligonucleotide.

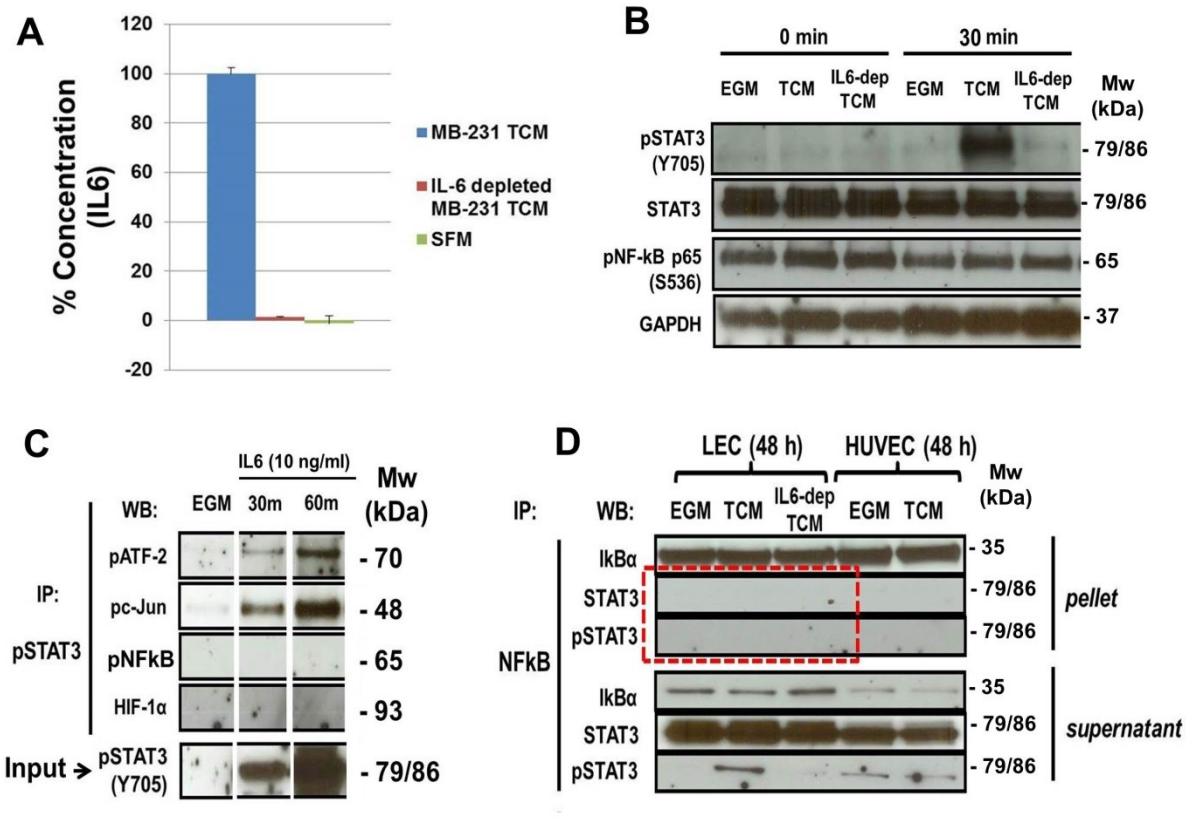

Figure 4.3: Role of IL6 in tumor education. IL6 was depleted from TCM by using an excess of anti-IL6 antibody and pull-down methods. (A) ELISA result shows the IL6 depletion was completed. (B) In 30 min of TCM induction, pStat3 was dramatically increased while IL6-dep-TCM did not induce pStat3. pNFkB (p65) was not influenced by the TCM induction. (C) Upon IL6 treatment, pStat3 formed a protein complex with pATF-2 and pc-Jun while pNFkB and HIF-1α did not associate in the complex. (D) Total NFkB (not pNFkB) and Stat3 (or pStat3) also did not form a complex in response to TCM or IL6-dep-TCM (red-dotted rectangle). pNFkB and pStat3 showed very weak complex formation, but the formation was not directly induced by EGM, TCM, or IL6-dep-TCM (red-dotted rectangle).

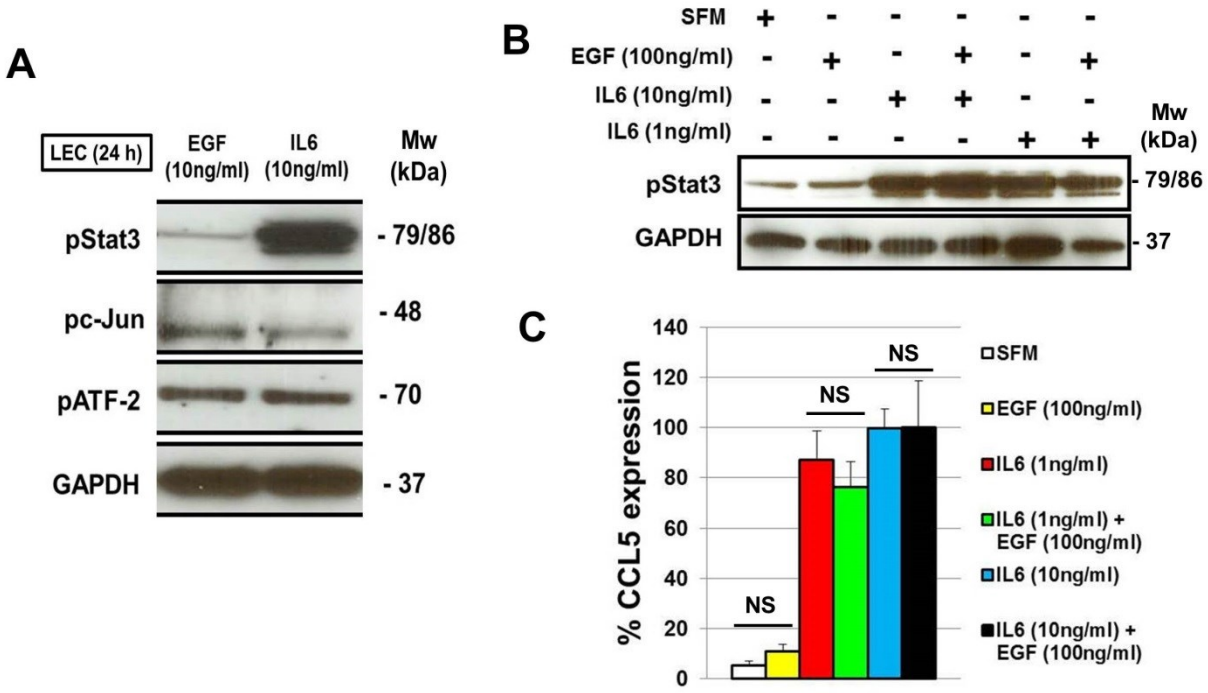

Figure 4.4: EGF induces phosphorylation of c-Jun and ATF-2, but not Stat3, and does not induce CCL5 expression in LEC. (A) Cell lysate prepared from LEC treated with 10 ng/ml EGF or 10 ng/ml IL6 for 24 h was analyzed by western blot. EGF induced phosphorylation of c-Jun and ATF-2, IL6 induced phosphorylation of Stat3, c-Jun, and ATF-2. (B) High concentration of EGF (100 ng/ml) did not cause pStat3. (C) CCL5 expression in LEC was IL6 dependent. 100 ng/ml EGF did not make any change in CCL5 expression in LEC.

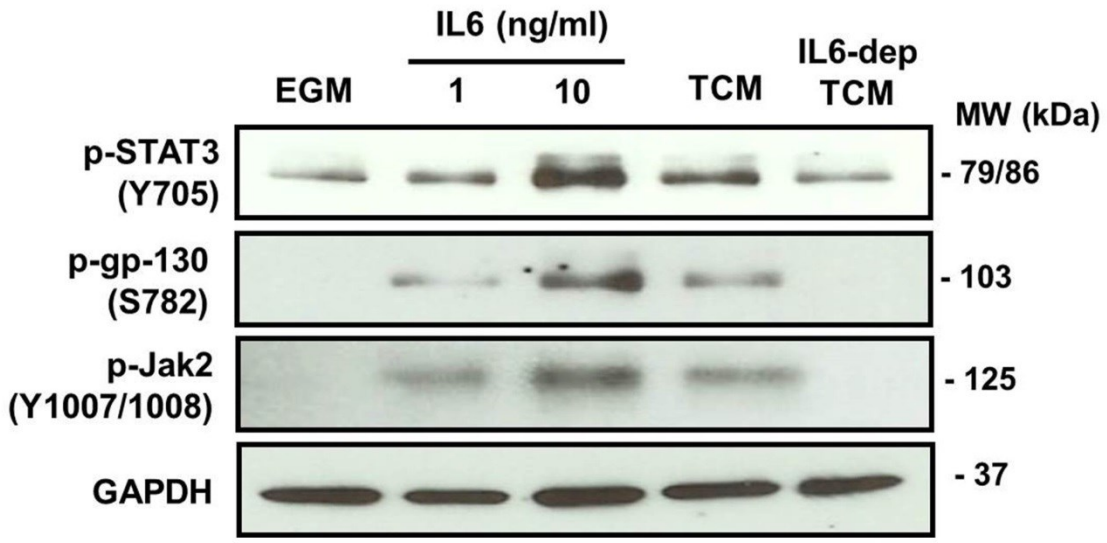

Figure 4.5: The IL6-gp130-Jak2-STAT3 axis is critical for tumor education. Jak2 and gp130 are the important bridges for the IL6-pSTAT3 signaling and would be promising therapeutic targets. LEC treated with EGM (normal LEC growth media), IL6 alone (1, 10 ng/ml), MB231-derived TCM (TCM), and IL6-depleted MB231 TCM (IL6-dep-TCM) were compared. From p-gp130 (S782) and p-Jak2 (Y1007/1008) data, we discovered that IL6 in the TCM was pivotal for the activation of IL6/gp130/Jak2-STAT3 axis. GAPDH was used as a loading control.

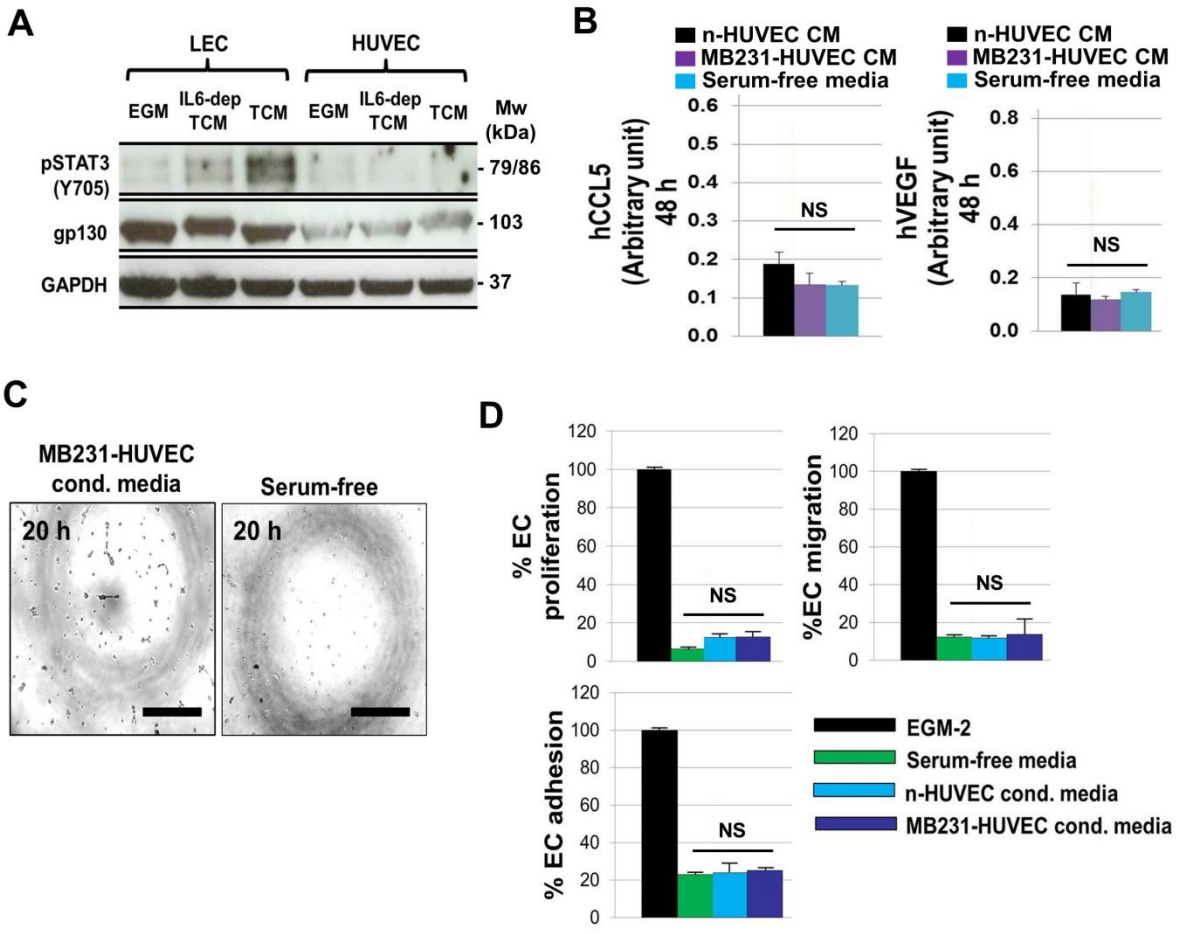

Figure 4.6: IL6-Stat3 mediated tumor education is lymphatic endothelial cell (LEC) specific. Blood endothelial cells (BEC) are not educated by TCM, as BEC do not express glycoprotein 130 (gp130), an IL6 signal transducer. (A) Phospho-Stat3 (pStat3) was only seen in TCM treated LEC, not in TCM-treated HUVEC. gp130 was not expressed in HUVEC so IL6 signaling could not be transduced to Stat3. EGM or IL6-dep-TCM did not induce pStat3 in either cell line. (B) hCCL5/ VEGF expression in HUVEC was not induced by TCM treatment. (C) HUVEC tube formation was not promoted by MB231-HUVEC CM at 20 h showing MB231-HUVEC secretion has no angiogenic activity. Scale bars, 200 μm. (D) EC proliferation, migration, adhesion were not induced by MB231-HUVEC CM.

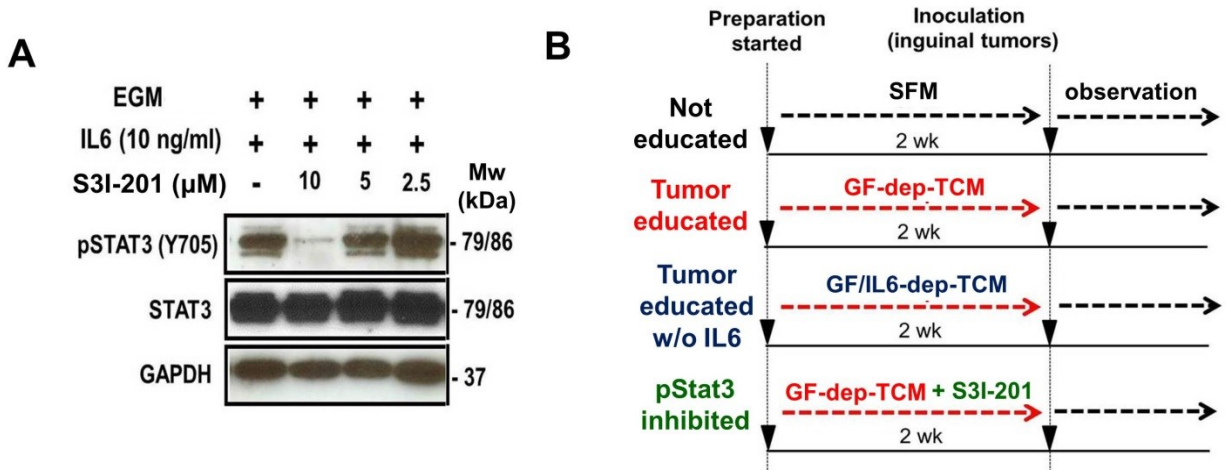

Figure 4.7: Targeting IL6 and pStat3 in vivo.

(A) S3I-201, a pStat3 inhibitor blocked pStat3 in LEC against IL6 induction. (B) Four animal groups described: Not educated (SFM-treated), tumor educated (GF-dep-TCM), tumor-educated w/o IL6 (GF/IL6-dep-TCM), and pStat3 inhibited (GF-dep-TCM + S3I-201). After two weeks of these treatments, primary tumor was established, and thoracic metastasis was monitored for 5 weeks.

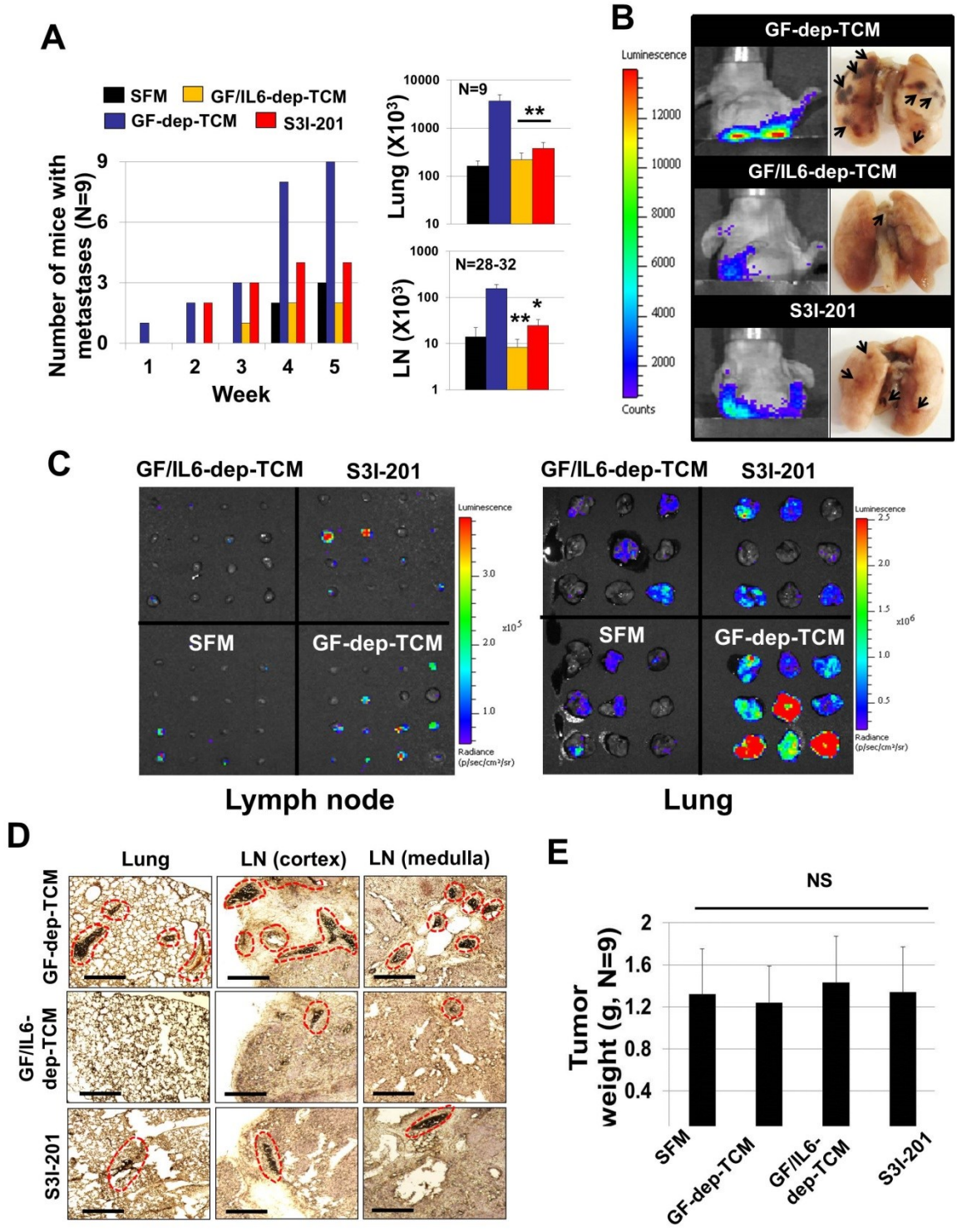

Figure 4.8: Inhibition of IL6 and pStat3 blocks GF-dep-TCM induced LN and lung metastasis. (A) Athymic nude mice pre-treated with GF-dep-TCM showed 100% thoracic

metastasis at week 5 (9/9). IL6 depletion dramatically decreased the number of mice with metastases (2/9) to lower than the metastatic rate in the SFM-treated group (3/9). S3I-201 also inhibited metastasis (4/9). Lungs and LN were harvested and assessed ex vivo under the IVIS imager. Lung metastasis was markedly blocked by both IL6 depletion and S3I-201 (N=9, **P < 0.01). LN metastasis was mostly blocked by IL6 depletion, and significantly inhibited by S3I-201 treatment (N=28-32, *P = 0.027, **P = 0.0007). Data are reported as mean ± s.e.m. (B) Representative images of live animals under the IVIS imager, and images of harvested lungs. Black arrows represent tumor nodules in the lungs. (C) LN and lung images under the IVIS imager. Against the positive control (GF-dep-TCM), there was a dramatic drop in LN and lung metastasis when the animals were treated with GF/IL6-dep-TCM; S3I-201 treatment also inhibited metastasis. (D) Immunohistochemistry with anti-cytokeratin antibodies on the lungs and LN (cortex and medulla). Metastatic colonies are delineated with red-dotted curves. Scale bars, 500 μm. (E) Wet primary tumor weight. Tumor growth was not influenced by the treatments (N=9).

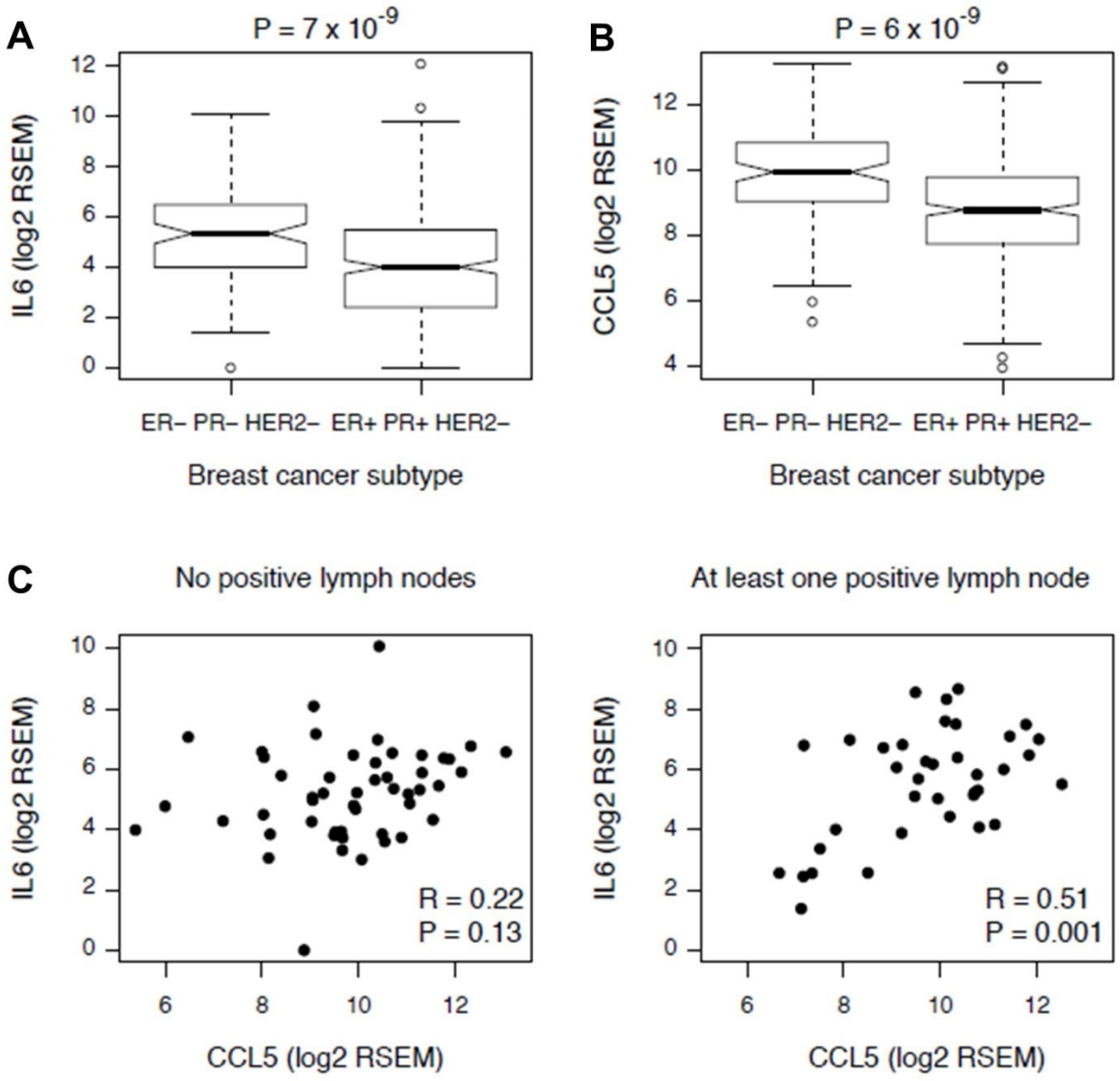

Figure 4.9: Associating IL6 and CCL5 mRNA expression with breast cancer subtypes and lymph node (LN) status. TCGA clinical data with a total of 99 triple negative samples and 326 ER+ PR+ HER2- were analyzed. There were 50 lymph node negative and 37 lymph node positive samples within the triple negative breast cancer subtype. Correlation coefficients and corresponding p-values were computed with Pearson's correlation. (A) Boxplot of log2 RSEM mRNA expression values for IL6 in TCGA samples measured with RNA-seq. (B) As in (A) for CCL5. (C) Association between IL6 and CCL5 mRNA expression in ER- PR- HER2- breast

cancer samples, with no positive LN or at least one positive LN when primary tissue was obtained. R-values represent correlation coefficients.

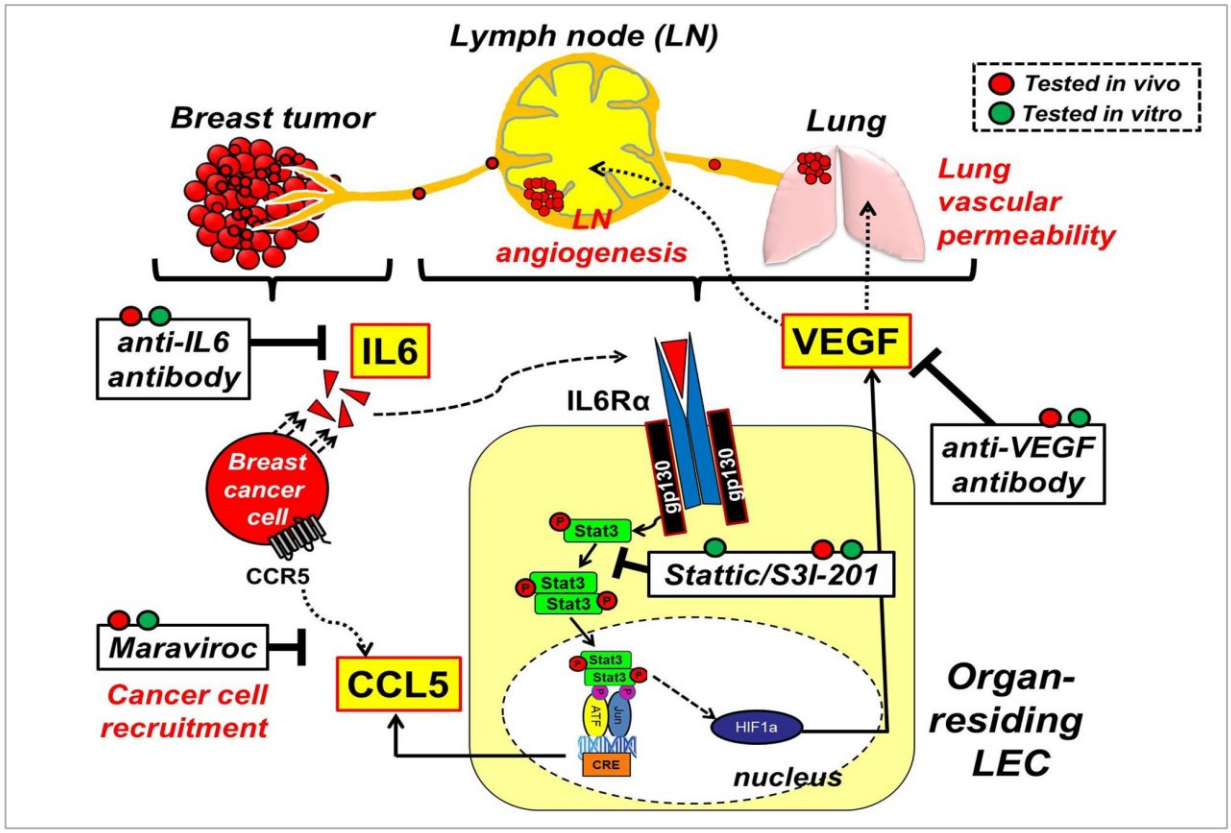

Figure 4.10: Conceptual summary: Breast cancer cells secrete IL6 that interacts with IL6 receptor on LEC within the lungs and LN. Activated IL6 receptors transduce the signals through glycoprotein 130 (gp130), phosphorylating lymphatic Stat3. Phospho-Stat3 (pStat3) translocates into the nucleus to form the pStat3-pc-Jun-pATF-2 ternary complex, which is essential for CCL5 expression by targeting the CRE region in its promoter. Phospho-Stat3 also induces HIF-1α to ultimately express VEGF in LEC. LEC-secreted CCL5 recruits CCR5-positive breast cancer cells into the lymphatic system. The secreted VEGF enhances lung vascular permeability and induces LN angiogenesis to promote metastatic extravasation and colonization. Treatments are marked with red and green circles, which represent "tested in vivo" and "tested in vitro" respectively.

Chapter 5: Roles of Lymphatic and Blood Endothelial Cells in Breast Tumor Microenvironment

5.1 RATIONALE

In chapters 3 and 4, we described that tumor-educated LEC within pre-metastatic organs express CCL5 and VEGF to promote TNBC metastasis into the organs. Although these two factors are essential for metastatic progression in TNBC, other factors expressed in tumor-educated LEC and the other crosstalk between cancer cells and blood endothelial cells remain to be further investigated. In addition, lymphatic vasculature in primary breast tumors have not been considered in the previous chapters, as those chapters mainly focused on organ-residing LEC. Thus, this chapter will investigate roles of LEC and microvascular endothelial cells (MEC) in primary tumor microenvironment by employing in vitro tumor-education models and in vivo EC-included breast tumor xenograft and matrigel plug models.

5.2 MATERIALS & METHODS

5.2.1 Cell culture

Human umbilical vein endothelial cells (HUVEC), lymphatic endothelial cells (LEC), and microvascular endothelial cells (MEC) were purchased from Lonza, and grown in EGM-2 (HUVEC) and EGM-2MV (LEC and MEC). MDA-MB-231 breast cancer cells were gifts from Dr. Zaver Bhujwalla (JHMI, Radiology and Oncology). MDA-MB-231 cells were propagated in RPMI-1640 medium supplemented with 10% FBS and 1% penicillin/streptomycin (Sigma).

5.2.2 Conditioned media

When MDA-MB-231 cells were confluent in T175 tissue culture flasks, the normal growth media was replaced with 8 ml serum-free media (SFM). After 24 h incubation, the supernatant was centrifuged and filtered through 0.2 μm syringe filters (Corning). The resulting tumor-conditioned media (TCM) was stored in aliquots at -80°C. When LEC/HUVEC/MEC reached 30-40% confluence in T75 tissue culture flasks, EGM was replaced with 30% TCM (TCM:EGM=3:7) to allow the TCM to educate the LEC/HUVEC/MEC. LEC/HUVEC/MEC were allowed to grow in the media for 4 days then the media was replaced with 3 ml SFM with 2% FBS (not supplemented with bullet kit). After 48 h, the supernatant was centrifuged and filtered. The resulting tumor-educated LEC/HUVEC/MEC conditioned media (MB231-LEC or MB231-HUVEC or MB231-MEC) was stored in aliquots at -80°C to avoid multiple freeze thaws.

5.2.3 EC-included tumor xenograft models

To evaluate roles of EC (e.g., LEC, MEC, and HUVEC) in primary tumor microenvironment, small number of MDA-MB-231 cells ($3x10^5$/mouse, 100 μl of RPMI-1640 complete media

without addition of matrigel) were orthotopically inoculated into the upper inguinal mammary fat pad of the athymic nude mice (female, 5-6 weeks) with or without two million of LEC or MEC or HUVEC. Though 2 million of MB231 cells in 50% matrigel were inoculated in general tumor xenograft models, here just 300,000 MB231 were mixed with 2,000,000 LEC/MEC/HUVEC; and this model does not employ 50% matrigel to intentionally slow down tumor growth. This system was used to maximize contribution of ECs and to evaluate roles of these ECs in tumor growth and microenvironment. The tumor size was measured by using a caliper, and the volume was calculated, using the formula: $V = 0.52 \times (\text{length}) \times (\text{width})^2$.

5.2.4 Reverse or general western assays

For reverse western blot, Proteome Profiler Antibody Array Kits for human angiogenesis factors (R&D systems) was used, according to the manufacturer's instructions. LEC or MEC or HUVEC conditioned media were compared with tumor-educated LEC (MB231-LEC) or MB231-MEC or MB231-HUVEC. For general western blot, 300,000 cells/well MDA-MB-231 cells were starved in serum-free media for 24 h, after which they were rinsed and re-starved with new SFM overnight. This was done to completely abolish mitogenic and proliferative potential of the cancer cells. They were treated with normal LEC conditioned media or MB231-LEC conditioned media for 1 day. Western assays were performed as described previously (Lee, Koskimaki et al. 2013) applying antibodies of interest, including EGFR, pEGFR, Akt, pAkt, and GAPDH (all from Cell Signaling).

5.2.5 LEC-included matrigel plug assay

High-concentrated matrigel (500 µl, BD Biosciences) containing LEC or HUVEC (2×10^6/gel) and heparin (10 units/gel) was injected subcutaneously on the ventral side of both flanks of

athymic nude mice. TCM or SFM (50 µl/injection) was subcutaneously dosed daily for 10 days, the mice were euthanized, and the gel plugs were excised and analyzed.

5.2.6 Immunofluorescence

Tumors, matrigel plugs fixed in 3.5% formalin were placed in 30% sucrose (Sigma) in PBS, incubated overnight at 4°C, and frozen in the O.C.T. compound (Sakura). Sections of 10-µm thickness were cut at -20°C. After blocking with 5% normal goat or normal chicken serum (Jackson Immunoresearch) in PBST (0.3% Triton) for 1 h at room temperature (RT), the sections were treated with one or more of the following primary antibodies overnight at 4°C: rabbit anti-mouse LYVE-1 antibody (1:200, AngioBio), rat anti-mouse CCL5 (1:200, Abcam), rat anti-mouse CD31 (1:100, BD Pharmingen), goat anti-mouse desmin (Santa-Cruz), mouse anti-smooth muscle actin Cy-3 (SMA, 1:500, Sigma), rabbit anti-pEGFR (Cell Signaling), rabbit anti-cleaved caspase 3 (1:500, Cell Signaling), and goat anti-mouse lectin FITC (1:100, Sigma). After 3 rinses with PBST, sections were incubated for 1 hour at RT with one or more of the following secondary antibodies (1:500): FITC-conjugated goat anti-rat, FITC-conjugated chicken anti-goat, rhodamine-conjugated goat anti-rat, Cy3-conjugated goat anti-rabbit, Alexa Fluor 647 goat anti-rabbit, Alexa Fluor 488 goat anti-rabbit, DyLight405 goat anti-rabbit, and DyLight405 goat anti-mouse antibodies (all from Jackson Immunoresearch). After 3 rinses with PBST, the samples were counterstained with DAPI (1:10,000, Roche) (5 min at RT). The samples were washed with PBST once and mounted with the ProLong Gold anti-fade reagent (Invitrogen) in dark. Fluorescent signals were visualized and digital images were obtained using the LSM-510 confocal microscope (Carl Zeiss).

5.2.7 Cell migration assay

HUVEC migration was assessed using the ACEA Real-Time Cell Analysis (RTCA) system (ACEA Biosciences Inc.) and the Cell Invasion and Migration plates 16 (CIM-plates-16) from Roche Diagnostics (Mannheim, Germany). Briefly, the membrane of the top chamber of a CIM-plate was coated with fibronectin by adding 40 µL of 20 µg/mL fibronectin in PBS solution and incubating at 37°C for 30 min. 180 µL of EGM-2 (complete media for HUVEC) or EBM (serum free media) or MB231-LEC conditioned media was added to the bottom chambers. The equilibrated plate was removed from the incubator and 100 µL of the trypsinized cells (45,000 HUVEC/well) with or without inhibitors (e.g., EGFR-neutralizing antibodies) were added to the top chamber. After 30 min incubation at room temperature, the stabilized chamber was loaded in the RTCA machine and the cell index was measured continuously for 20 h. Cell indices at 20 h were selected for analysis.

5.2.8 Proliferation assay

Proliferation assays were performed using the WST-1 reagent (Roche). Pale yellow colored tetrazolium salt WST-1 can be reduced by mitochondrial dehydrogenases and transformed into dark yellow colored Formazan. In detail, HUVEC was seeded in 96-well plates at a density of 2,000 cells/well in 100 µL of EGM-2 media (100 µL of EGM-2MV was used in MEC and LEC proliferation). The plates were incubated at 37°C in a tissue culture incubator for 20 h to allow cells to adhere and the plates were incubated for 72 h. Media was removed and 100 µL of WST-1 solution (1:10 dilution of WST-1 in serum free EBM media) was added. After incubation for 4 h, the absorbance at 450 nm was measured using a Victor V (Perkin Elmer, Waltham, MA).

5.2.9 Statistical Analysis

Error bars correspond to s.e.m, unless otherwise stated. Differences between two groups are regarded as significant when P is less than 0.05 using the Student's t-test.

5.3 RESULTS

5.3.1 LEC were observed in MDA-MB-231 tumors and express mouse CCL5

MDA-MB-231 breast tumor xenografts were established in athymic nude mice without TCM treatment, after which the tumor was excised and analyzed by immunostaining with anti-mLYVE-1, anti-lectin, and anti-mCCL5 antibodies to detect tumor lymphatic and blood vessels, and mouse CCL5 expression in tumor stroma (Figure 5.1). DAPI staining was performed as background signals. Tumor lymphatic vessels were detected in both intra- and peri-tumoral areas. Some lymphatic vessels had lymphatic lumens, suggesting they are functionally draining lymphatics. Surprisingly, tumor lymphatic vessels also expressed CCL5, showing colocalization of mCCL5 and mLYVE-1 (Figure 5.1.B). The existence of LEC in tumor stroma suggests that roles of LEC and blood endothelial cells within primary tumors need to be studied in tumor progression.

5.3.2 LEC within MB231 tumor stroma promote tumor growth, while MEC suppress it

In a MDA-MB-231 (MB231) breast tumor xenograft model, generally, two million of MB231 cancer cells are orthotopically inoculated with 50% matrigel supplement to optimize tumor growth. In this chapter, this conventional xenograft model was modified as follows: the number of cancer cells was decreased (to 300,000 MB231 cells); a large number of LEC or MEC (2,000,000 cells) were included with 300,000 cancer cells; 50% matrigel was not added in the tumor/EC mixture to remove matrigel effects. In general, matrigel significantly promotes tumor growth rates owing to its scaffold effects. This new xenograft model slows down tumor growth rates, compared to the normal xenograft model; at the same time it gives better sense of understanding of roles of LEC and MEC in tumor growth (Figure 5.2). There were seven arms:

300,000 MB231 only (N=8); 300,000 MB231 + 2,000,000 LEC (N=8); 300,000 MB231 + 2,000,000 MEC (N=8); 300,000 MB231 + 2,000,000 HUVEC (N=8); 2,000,000 LEC only (N=2); 2,000,000 MEC only (N=2); and 2,000,000 HUVEC only (N=2). LEC-included MB231 tumors showed dramatic increases in tumor growth rates, compared to tumors containing only MB231 cells. Interestingly, MEC-included MB231 tumor showed suppression of tumor growth. HUVEC-included MB231 tumors did not show any difference compared to MB231 tumors (Figure 5.2.A, B).

5.3.3 LEC and MEC showed distinctive secretomes after tumor education with TCM

Based on the results shown in Figure 5.2.A, we hypothesized that LEC and MEC secrete different factors in tumor conditioned media (TCM), thus influencing tumor growth rates in different manners. Tumor-educated LEC (MB231-LEC), tumor-educated MEC (MB231-MEC), and tumor-educated HUVEC (MB231-HUVEC) were prepared as previously described in the Materials and Methods in Chapter 3. These tumor-educated LEC, MEC, and HUVEC conditioned media were compared with normal LEC, MEC, and HUVEC conditioned media to assess TCM effects in the endothelial secretomes. A Proteome Profiler Antibody Arrays Kit for Human Angiogenesis (R&D systems, Minneapolis, MN) was used to determine angiogenesis-related factors in these conditioned media. After tumor education, LEC showed high increases in EGF, PDGF-BB, and VEGF; MEC showed high increases in GM-CSF, CD26, and HB-EGF; however HUVEC did not show dramatic changes (Figure 5.2.C).

5.3.4 MB231-LEC express EGF and induce cancer cell proliferation

Human EGF ELISA was performed with MB231-LEC, MB231-HUVEC, and n-LEC conditioned media. EGF was highly expressed in MB231-LEC (Figure 5.3.A). MB231 cell

proliferation was assessed in MB231-LEC conditioned media with or without anti-EGFR antibodies. Anti-EGFR antibodies blocked MB231-LEC induced MB231 cell proliferation (Figure 5.3.B). Confluent MB231 cells were starved with SFM two times, then n-LEC or MB231-LEC conditioned media were applied to the MB231 cells for 1 day. EGFR and Akt were phosphorylated by MB231-LEC conditioned media, demonstrating the EGF in the conditioned media initiate EGFR signaling pathways in the cancer cells (Figure 5.3.C). LEC-included matrigel plugs were treated with TCM and the plugs were analyzed with anti-hLYVE-1 and anti-hEGF antibodies. Colocalization of hLYVE-1 and hEGF suggests that LEC secrete EGF in tumor condition (Figure 5.3.D).

5.3.5 MB231-LEC derived EGF does not induce HUVEC proliferation and migration

MB231-LEC derived EGF promoted MB231 cell proliferation. The same conditioned media was tested in HUVEC migration and proliferation with or without anti-EGFR antibodies. Surprisingly, the antibodies did not block HUVEC proliferation and migration even in high concentration of the antibodies (Figure 5.4). The results in Figure 5.3 and 5.4 suggest that MB231-LEC derived EGF influence MB231 cancer cells in paracrine manner.

5.3.6 MB231 tumors show apoptosis-experiencing pericytes around blood vessels

MB231 tumor xenografts were established and excised tumors were further analyzed. Antibodies for cleaved caspase 3 (CC-3), LYVE-1, CD31, and lectin were used to detect apoptoticcells, considering spatial distribution of lymphatic and blood vessels. Very interestingly, most apoptosis-experiencing cells were located around blood vessels and not around lymphatic vessels (Figure 5.5.A). More precisely, antibodies for CC-3, smooth muscle actin, and lectin were used to detect apoptosis-experiencing cells, pericytes, and blood vessels. The apoptosis-

experiencing cells were alpha SMA positive pericytes residing around blood vessels (Figure 5.5.B).

5.3.7 MB231-LEC express PDGF-BB and recruit pericytes in vivo

The discovery of apoptosis-experiencing pericytes (Figure 5.5.B) leads to a question of whether LEC-secreted PDGF-BB (Figure 5.2.C) in reverse recruits pericytes or maintains survival of the pericytes. First, PDGF-BB in MB231-LEC conditioned media was measured by ELISA, for comparison with MB231-HUVEC, n-LEC, and serum-free media. Remarkably, MB231-LEC express high amount of PDGF-BB (Figure 5.6.A). This was reproduced by using in vivo EC-included matrigel plug models as previously described in Materials and Methods in Chapter 3. A no-cell group and HUVEC group were also included as control groups (Figure 5.6.B). After 10 days of matrigel implantation into the athymic nude mice, the plugs were excised and analyzed with anti-αSMA (alpha smooth muscle actin) and anti-desmin antibodies, as αSMA and a desmin are the markers for pericytes. In αSMA-based immunostaining, LEC-included matrigel from TCM treated animals showed dramatic recruitment of αSMA-positive cells, nevertheless, HUVEC included matrigel or no-cell group showed very little of αSMA-positive population (Figure 5.6.C, D). Anti-desmin and anti-mCD31 antibodies were employed to assess the pericyte coverage on the blood vessels. Notably, the pericyte coverage was much more frequently observed in LEC-matrigel plugs that have been treated with TCM (Figure 5.6.E).

5.4 DISCUSSION

Upon the discovery that 'organ-residing LEC' promote metastasis through CCL5 expression (Figure 3.1) (Lee, Fertig et al. 2014), LEC in primary tumors were also examined. LEC were detected in MB231 tumors by immunohistochemistry with anti-LYVE-1 antibodies (Figure 5.1.A). Moreover, stromal LEC within the tumor also expressed mCCL5, which is similar with that organ-residing LEC express CCL5 when the animals are treated with TCM (Figure 5.1.B, left panel). This could be partially explained by that the tumor-residing LEC were inevitably exposed to tumor-secreted factors owing to their regional adjacency. Thus, the stromal LEC show similar profiles of secretome with that of TCM-influenced organ-residing LEC. CCL5 expression in tumor lymphatic vessels proposes that stromal LEC can form a CCL5 gradient even in the tumor microenvironment, which can trigger very initial recruitment of cancer cells into the lymphatic system via intratumoral and peritumoral lymphatic vessels (Figure 5.1.B, right panel). The presence of LEC in the tumor is due to tumor lymphangiogenesis, driven by cancer cell-secreted lymphangiogenic factors such as VEGFC and VEGFD (Skobe, Hawighorst et al. 2001; Tammela and Alitalo 2010). It is very well studied that VEGFC/D-induced lymphatic vasculatures in the tumors serve as routes of tumor dissemination by leaky nature of the lymphatic vessels, compared to pericyte-covered blood vessels (Mayerson, Patterson et al. 1962; Kim, Park et al. 1988). Tumor interstitial pressure also influences tumor dissemination (Rofstad, Tunheim et al. 2002; Hompland, Ellingsen et al. 2012; Yu, Wang et al. 2013). To this classical understanding of tumor lymphangiogenesis and metastasis, we have added a new concept of the CCL5-expressing LEC within tumors for recruitment of cancer cells (Lee, Fertig et al. 2014; Lee, Pandey et al. 2014). It is also hypothesized that CCL5 derived from the LEC in the primary tumor stroma could drive tumor self-seeding: this hypothesis remains to be further studied.

In addition to CCL5, tumor-educated LEC express EGF and PDGF-BB as well (Figure 5.2.C). ELISA for EGF and PDGF-BB quantitatively confirmed that MB231-LEC express higher amount of these growth factors, compared to normal LEC (Figure 5.3.A and Figure 5.6.A). Using a novel breast tumor xenograft model, it was revealed that LEC-included MB231 tumors exhibit very rapid tumor growth, compared with normal MB231 tumors or MEC/HUVEC-included MB231 tumors (Figure 5.2.A, B). This is possibly related to EGF-induced MB231 cell proliferation in MB231-LEC conditioned media and the inhibition of MB231 proliferation by anti-EGFR antibodies (Figure 5.3.B). The role of EGF in tumor cell proliferation has been well studied in many cancers using experimental and computational approaches (Ozawa, Ueda et al. 1987; Athale and Deisboeck 2006). Assessing the role of LEC in EGF-driven tumor growth with more physiological scenario, human EGF (hEGF) and mouse EGF (mEGF) derived from human MB231 and mouse LEC, respectively, need to be further examined. Using the same model, treatment of anti-human EGF or anti-mouse EGF antibodies would specifically block MB231-derived hEGF or LEC-derived mEGF, thus discerning the role of LEC-derived mEGF in normal tumor models: these experiments would address clinical relevance of the discovery about LEC-expressed EGF. Moreover, the mechanisms of EGF expression in tumor-educated LEC need to be further elucidated, as many of studies have focused on EGF expression in cancer cells (Dazzi, Hasleton et al. 1989; Shima, Sasaguri et al. 1995).

Observation of normal MB231 tumors without any treatments or endothelial cell inclusion provided an interesting insight that the stromal pericytes around blood vessels undergo apoptosis in vivo, without any treatment (Figure 5.5). Two potential mechanisms are proposed. First, tumor angiogenesis would be over-activated by over-expressed proangiogenic factors such as VEGF. Thus, the rate of blood vessel sprouting is too fast for pericytes to follow up to completely cover

the blood vessels so as to allow them to mature. However, there remains a critical question of whether pericytes that are failing to cover blood vessels are more vulnerable to apoptotic signals, compared to blood vessel associated pericytes. Second, tumor microenvironment (TME) might contain unknown TME-derived signals that cause pericytes apoptosis. For instance, tumor-secreted unknown factors or tumor-specific ECM components might influence pericytes to initiate apoptotic signaling. This is quite an attractive idea, because death of pericytes is closely associated with blood vessel mediated metastasis (Xian, Hakansson et al. 2006; Gerhardt and Semb 2008; Garcia-Roman and Zentella-Dehesa 2013), morphologically abnormal immature blood vessels (Raza, Franklin et al. 2010), and tumor drug resistance (Berezowski, Landry et al. 2004). These hypotheses need to be further studied.

MB231-LEC express PDGF-BB, and recruit pericytes in vivo (Figure 5.6). This can partially explain how LEC-included tumors grow faster (Figure 5.2). PDGF-BB is also involved in tumor growth, angiogenesis and tumor drug resistance (Greco, D'Agnano et al. 2006; Nissen, Cao et al. 2007; Xue, Lim et al. 2012). Thus, the LEC expressed PDGF-BB could promote tumor growth. As PDGF receptors are overexpressed in several cancers, targeting PDGFR has been proposed to treat them (Adnane, Trail et al. 2006; Zheng, Chen et al. 2007; Zheng, Chen et al. 2007). In addition to cancers, tissue engineers seek better ways to make mature blood vessels when the tissues are transplanted (Baranski, Chaturvedi et al. 2013). Pericyte coverage is one of criteria to determine whether the transplanted tissues would be successfully grafted to the host (He, Nieponice et al. 2010). In the present study, LEC-included matrigel plugs that were treated with TCM showed improved pericyte infiltration and coverage on the blood vessels. In that sense, PDGF-BB expressing LEC could be an attractive source of growth factors in tissue engineering models, if the key factors in TCM inducing PDGF-BB are determined.

Very interestingly, MEC-included MB231 tumors showed suppression of tumor growth, compared to MB231 tumors. Currently, the role of blood endothelial cells in tumor growth is quite controversial. It has been reported that BEC block tumor growth (Franses, Baker et al. 2011). In that study, perlecan from BEC muted the proliferative and invasive phenotype of lung and breast cancer cells in vitro. BEC perlecan silencing significantly eliminated the ability of BEC to inhibit cancer cell invasiveness via increased IL6 secretion. In contrast, other studies have reported that BEC induce tumor growth via cancer stem cell related mechanisms and tumorigenic crosstalk with TME (Karl, Zhang et al. 2007; Warner, Miyazawa et al. 2008; Kamenova, Braverman et al. 2009). In the present MB231 model, HUVEC was inactive in tumor growth, but MEC suppressed the tumor growth, suggesting that different BEC lines could result in different phenotypes though they are derived from vascular endothelium. MB231-MEC showed a distinctive secretome, including CD26 and GM-CSF expression. These two factors are related to tumor inhibitory mechanisms. CD26 (also called DPPIV) inhibitors extended GLP-2 mediated tumor promoting effects on intestinal cancer cells (Masur, Schwartz et al. 2006). CD26 inhibited malignant phenotype of prostate cancer cells by blocking basic fibroblast growth factor signaling pathway (Wesley, McGroarty et al. 2005). GM-CSF inhibited breast cancer growth and metastasis by invoking an anti-angiogenic program in tumor-educated macrophages (Eubank, Roberts et al. 2009). GM-CSF also involved in anti-tumor immunity (Emens, Armstrong et al. 2004; Borrello, Levitsky et al. 2009; Emens 2009). MEC secreted factors need to be further investigated in primary tumors.

In summary, in this chapter we investigated lymphatic and blood endothelial cell mediated changes of primary breast tumor microenvironment. In terms of tumor growth, LEC induced tumor growth by expressing EGF and PDGF-BB. MEC-induced tumor suppression was observed,

and further mechanistic studies are remaining. LEC derived PDGF-BB also contribute to pericyte infiltration, which can be applied in cancer therapies as well as tissue engineering.

5.5 FIGURES & TABLES

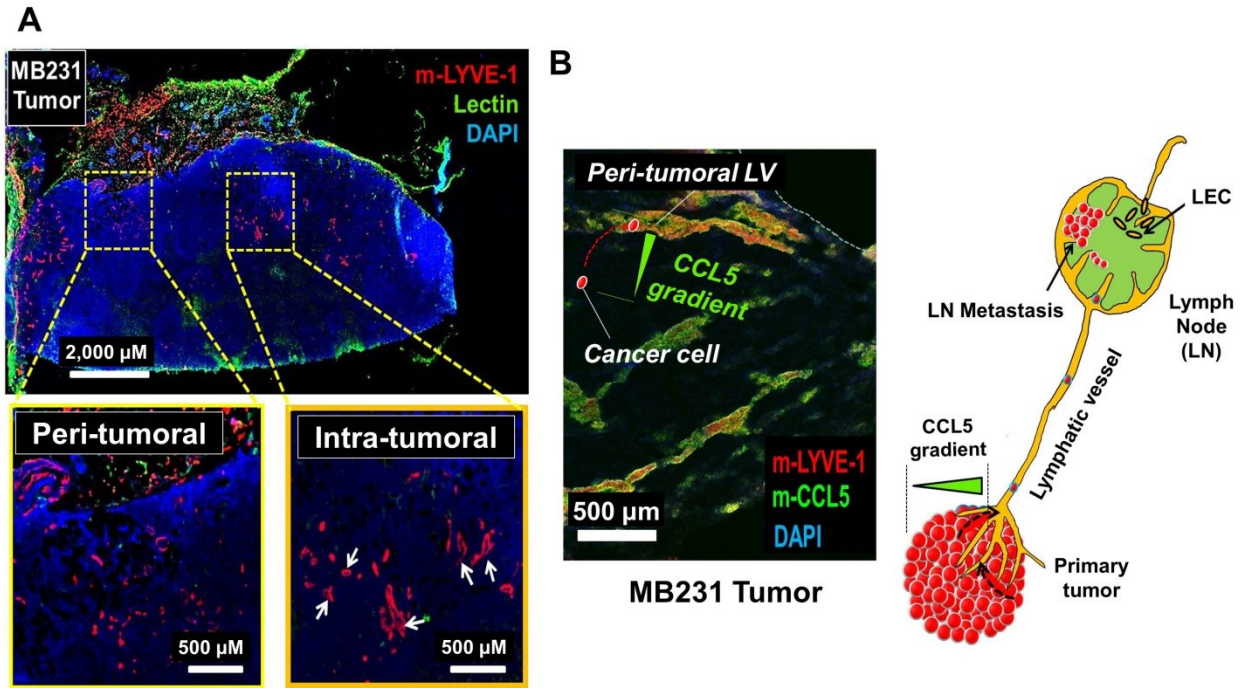

Figure 5.1: Presence of lymphatic endothelial cells in MDA-MB-231 tumors. (A) MDA-MB-231 (MB231) tumors were fixed, frozen, sectioned and stained with anti-mouse LYVE-1 (red) and anti-lectin (green) antibodies to detect lymphatic and blood endothelial cells (LEC & BEC) in the tumor. DAPI was used to stain cell nuclei. Peri-tumoral and intra-tumoral lymphatic vessels (red) were detected. Lumens in lymphatic vessels were observed (white arrows). (B) MB231 tumor tissues were stained with anti-mouse LYVE-1 (red) and anti-mouse CCL5 (green) antibodies to detect mouse lymphatic vessels and mouse CCL5 (the left panel). A colocalization of those two proteins demonstrates that tumor stromal LEC express mouse CCL5 to initially recruit CCR5-positive cancer cells in the tumor to the lymphatic vessels. A conceptual figure (the right panel) describes how cancer cells potentially sense the CCL5 gradient and migrate from tumor stroma to the lymphatic system.

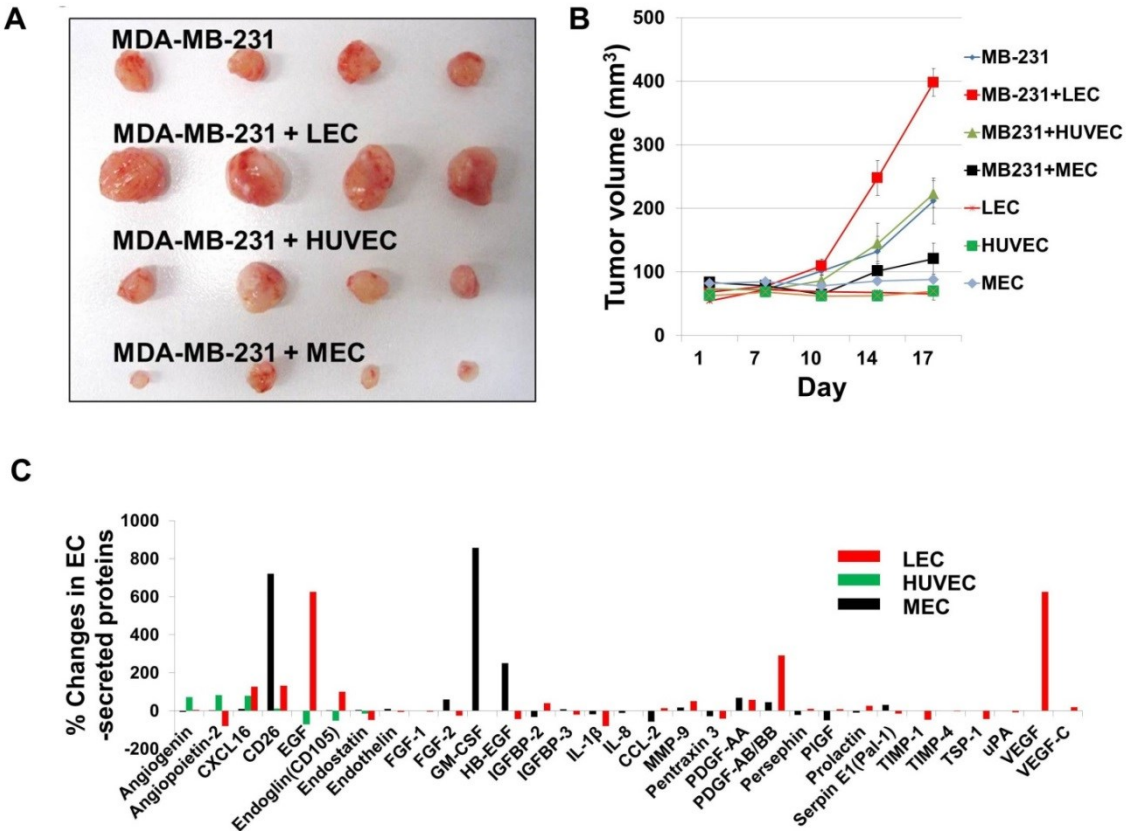

Figure 5.2: Lymphatic endothelial cells (LEC) and microvascular endothelial cells (MEC) influence breast tumor growth in opposite manners. (A) Two million of LEC, HUVEC, and MEC were mixed with 300,000 MB231 cells respectively, after which, the cell mixtures were orthotopically inoculated into the thoracic part (2nd mammary site from the top) of athymic nude mice without supplementing matrigel (N=8). For control, just 300,000 MB231 (N=8) or just 2,000,000 ECs (LEC; MEC; HUVEC, N=2 each EC) were inoculated. (B) Tumor growth curve. (C) Fifty five angiogenesis related factors from tumor-educated LEC/MEC/HUVEC were examined using reverse western blots. Factors secreted from LEC, MEC, and HUVEC before or after incubating them in 30% TCM were analyzed. Tumor-educated LEC (MB231-LEC) shows high expression of EGF, PDGF-BB, and VEGF compared to normal LEC. MB231-MEC shows

high expression in CD26 and GM-CSF, compared to normal MEC. HUVEC does not show dramatic changes.

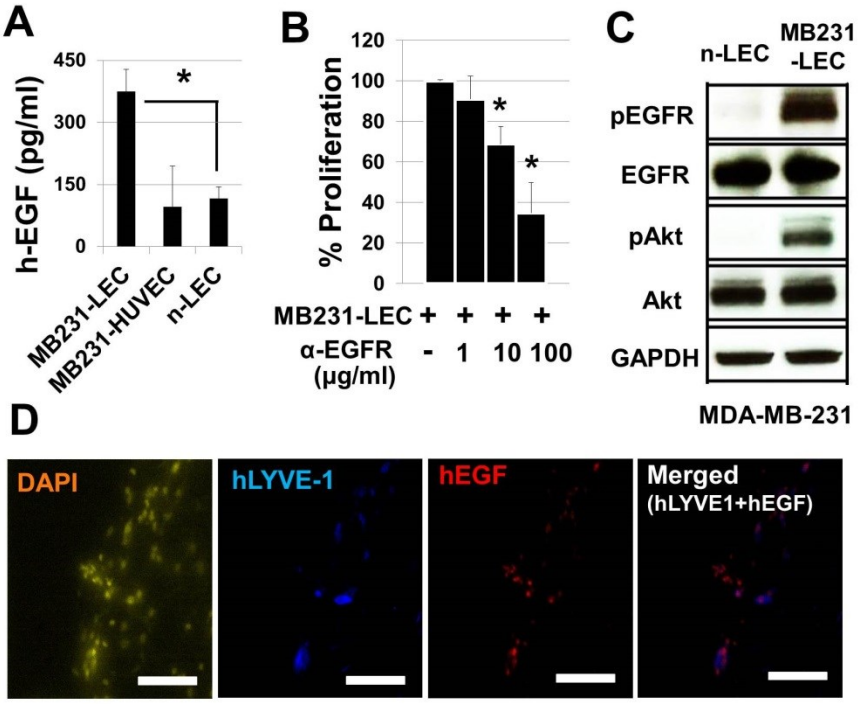

Figure 5.3: Tumor-educated LEC (MB231-LEC) express EGF and induce TNBC cell proliferation. (A) EGF ELISA with MB231-LEC, MB231-HUVEC, and normal LEC conditioned media. MB231-LEC express high amount of EGF, compared to normal LEC (*P=0.042). (B) MB231 cell proliferation induced by MB213-LEC was blocked by using EGFR antibodies (*P<0.05). (C) Western blots with double-starved MB231 cancer cells. Confluent MB231 cells were starved with serum-free media (SFM) for 24 h, rinsed, and re-starved with the same SFM to completely remove cell growth related signals. MB231-LEC conditioned media induced phosphorylation of EGFR and Akt while normal LEC did not. GAPDH was used as loading control. (D) Human LEC (hLEC) included matrigel plugs from TCM-treated athymic nude mice were analyzed after 10 day of matrigel implantation. Human LYVE-1 positive hLEC express human EGF (hEGF) in vivo. Scale bars represent 100 μM.

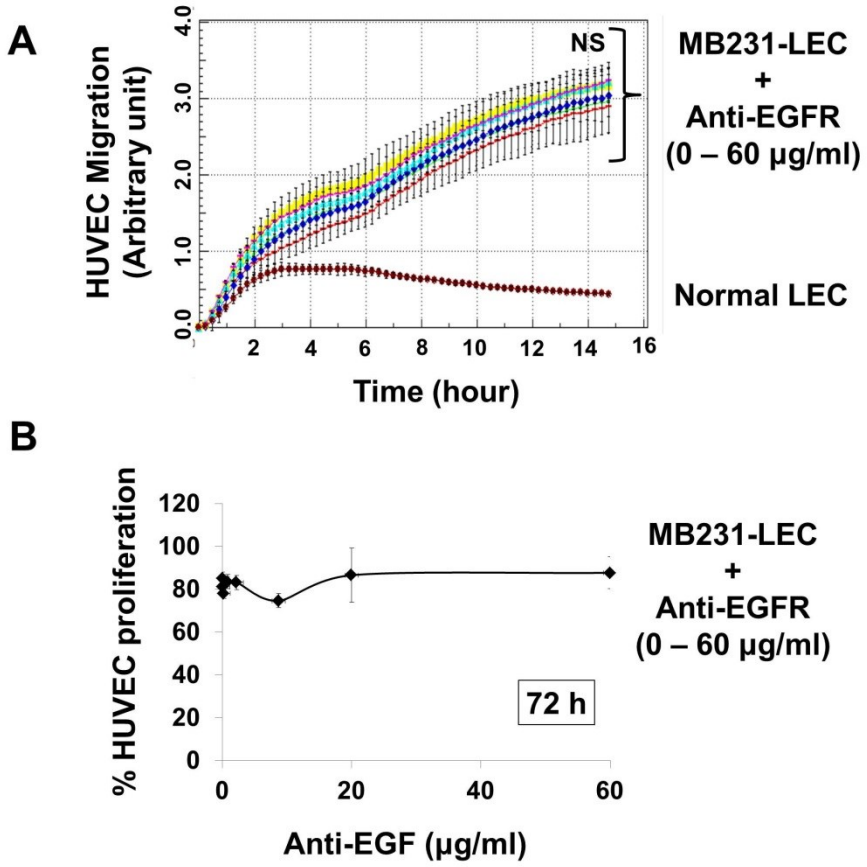

Figure 5.4: Epidermal growth factor (EGF) is expressed in tumor-educated LEC (MB231-LEC), but does not contribute to HUVEC migration and proliferation. (A) MB231-LEC induced HUVEC migration, but the migration was not inhibited even by up to 60 µg/ml anti-EGFR antibody. (B) Anti-EGFR antibody (0-60 µg/ml) did not inhibit MB231-LEC induced HUVEC proliferation, at 72 h.

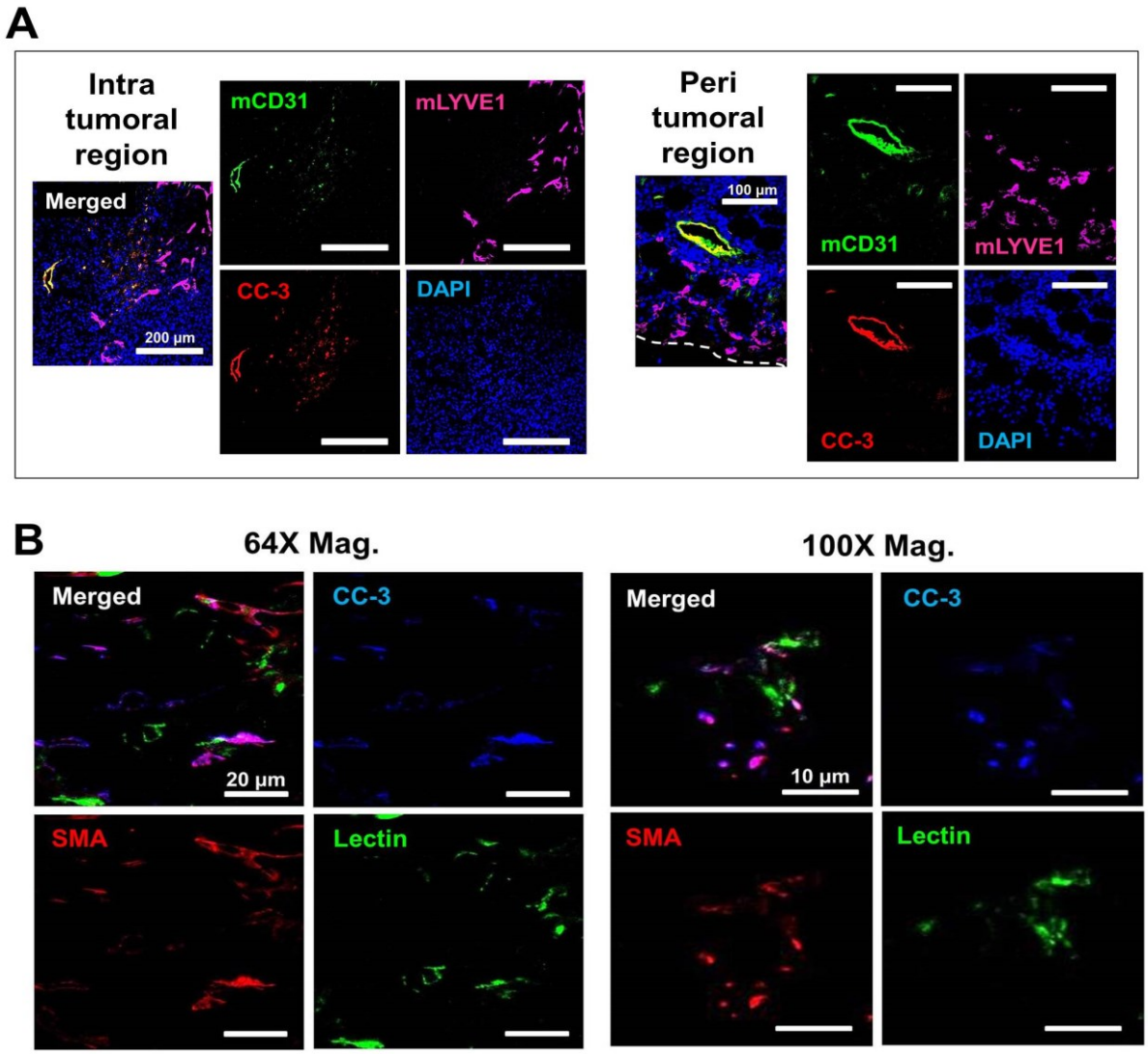

Figure 5.5: Pericytes around blood vessels experience apoptosis in MB231 tumors, but lymphatic vessel areas did not show apoptosis. (A) MB231 tumors were analyzed. Intra- and peri-tumoral regions were stained with anti-cleaved caspase 3 (CC-3), mCD31, and mLYVE-1 antibodies to detect apoptotic cells, blood and lymphatic vessels (BV and LV). In both regions, CC-3 were only positive around BV not around LV. (B) MB231 tumors were further analyzed by staining with anti-cleaved caspase 3 (CC-3), smooth muscle actin (SMA), and lectin antibodies.

More precise observation (64x and 100x mag.) reveals that the CC-3 proteins are exactly colocalized with SMA-positive pericytes around peripheries of BV (lectin-positive).

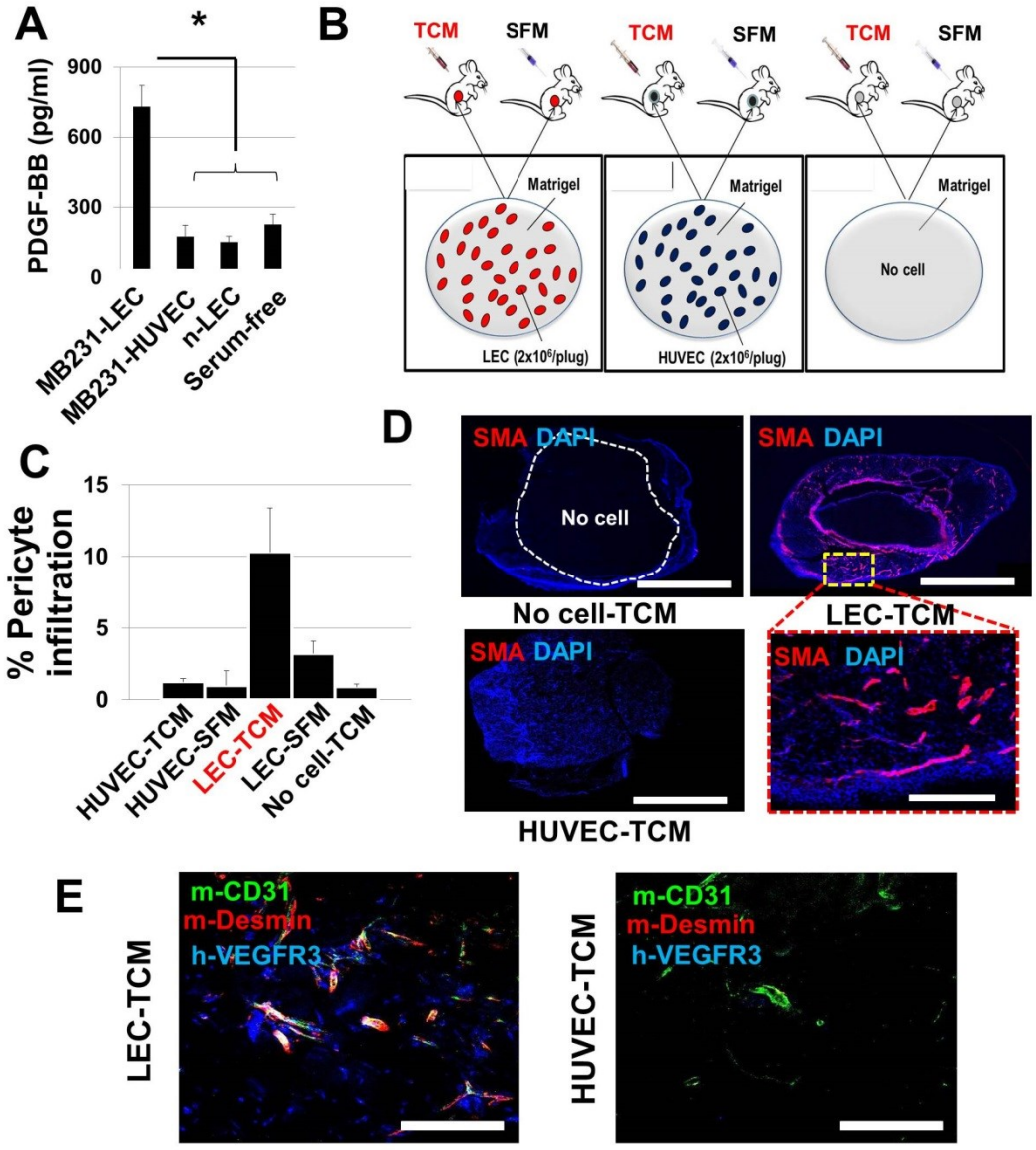

Figure 5.6: Tumor-educated LEC express PDGF-BB and recruit pericytes in matrigel plug assays in vivo. (A) PDGF-BB ELISA with MB231-LEC, MB231-HUVEC, normal LEC conditioned media, and serum-free media (SFM). MB231-LEC express high amount of PDGF-BB, compared to other groups (*P<0.05). (B) LEC-included matrigel plug assay. High-concentrated matrigel containing LEC or HUVEC (2×10^6/gel) and heparin (10 units/gel) was

injected subcutaneously. TCM or SFM (50 μl/injection) was subcutaneously dosed daily for 10 days, the mice were euthanized, and the gel plugs were excised and analyzed. (C) Pericyte recruitment in the plugs. (D) Representative confocal images for smooth muscle actin (SMA) positive area in the plugs. Scale bars represent 500 μm. (E) Confirming that the SMA-positive cells are pericytes, samples were co-stained with anti-desmin and anti-mCD31 antibodies. TCM-treated LEC included matrigel plugs showed higher coverage of pericytes on the blood vessels, compared to TCM-treated HUVEC included plugs.

Chapter 6: Somatotropin-derived Peptides with Anti-lymphangiogenic and Anti-angiogenic Activity

6.4 DISCUSSION

6.5 FIGURES & TABLES

6.1 RATIONALE

Angiogenesis is the process of new blood vessel formation from pre-existing blood vasculature (Folkman and Klagsbrun 1987). Thus the angiogenesis is required for tumors to continue the growth. A number of therapeutic angiogenesis inhibitors have been developed. These include FDA approved monoclonal antibodies bevacizumab and ranibizumab targeting vascular endothelial growth factor (VEGF), small molecule tyrosine kinase inhibitors involved in angiogenesis-related signal transduction (erlotinib, sunitinib, sorafenib, pazopanib), and mammalian target of rapamycin (mTOR) inhibitors (temsirolimus and everolimus) (Moschetta, Cesca et al. 2010; El-Kenawi and El-Remessy 2013). Many peptide angiogenesis inhibitors are in preclinical development or clinical trials (Rosca, Koskimaki et al. 2011).

In contrast, there are relatively few effective inhibitors of lymphangiogenesis compared to those of angiogenesis. This is because molecular studies in lymphatic biology have only been conducted since the late 1990s after lymphatic endothelial cell markers including vascular endothelial growth factor receptor 3 (VEGFR-3) (Kaipainen, Korhonen et al. 1995), lymphatic vessel endothelial hyaluronan receptor 1 (LYVE-1) (Banerji, Ni et al. 1999), prospero homeobox protein 1 (Prox-1) (Wigle and Oliver 1999), neuropilin 2 (NRP-2) (Yuan, Moyon et al. 2002), and podoplanin (Schacht, Ramirez et al. 2003) were identified. VEGFC/D (Joukov, Pajusola et al. 1996; Achen, Jeltsch et al. 1998), VEGFR3 (He, Kozaki et al. 2002), cyclooxygenase 2 (COX-2) (Timoshenko, Chakraborty et al. 2006), and matrix metalloproteinase 2/9 (MMP-2/9) (Daniele, Zito et al. 2010) have been proposed as potential molecular targets for regulating lymphangiogenesis. Large proteins or antibodies including a VEGFR3 antibody, a soluble VEGFR-3 fusion protein (a VEGF-C/D trap), and a neuropilin-2 antibody (Lin, Lalani et al. 2005; Caunt, Mak et al. 2008; Nakamura, Matsui et al. 2010) have been reported to inhibit

lymphangiogenesis in vitro and in vivo. However no FDA approved anti-lymphangiogenic agent has yet been developed and no anti-lymphangiogenic peptide agents have been identified.

This chapter investigates anti-lymphangiogenic and anti-angiogenic activity of novel endogenous 14-mer somatotropin domain-derived peptides; to our knowledge, these are the first short peptide agents with anti-lymphangiogenic activity exhibiting a potency of inhibiting lymphatic endothelial cell proliferation, migration, adhesion and tube formation. Using bioinformatics, the Popel laboratory has previously identified over 100 anti-angiogenic peptides derived from conserved domains of several classes of proteins: type IV collagen, CXC chemokines, thrombospondin 1 (TSP1) repeat-containing proteins, somatotropins and serpins (Karagiannis and Popel 2008). The basis for this analysis was homology to known anti-angiogenic protein fragments that allowed us to identify several anti-angiogenic motifs in the human proteome.

Among these novel peptides, 14-mer peptides derived from the somatotropin conserved domain were tested on lymphatic and blood endothelial cells in vitro. The tested peptides are derived from the endogenous proteins interleukin 17 (IL-17) receptor C (the peptide denoted SP5001, its sequence is RLRLLTLQSWLL), brush border myosin-1 (SP5028, LMRKSQILISSWF), neuropeptide FF receptor 2 (SP5029, LLIVALLFILSWL), chorionic somatomammotropin (SP5030, LLRLLLLIESWLE), transmembrane protein 45A (SP5031, LLRSSLILLQGSWF), chorionic somatomammotropin-like 1 (SP5032, LLHISLLLIESRLE) and placental lactogen (SP5033, LLRISLLLIESWLE). Proliferation, migration, adhesion and tube formation assays were performed on lymphatic and blood endothelial cells to identify anti-lymphangiogenic and anti-angiogenic peptides. Lymphangiogenesis or angiogenesis involves multiple steps including lymphatic or blood endothelial cell attachment and adhesion to the

extracellular matrix, cell migration, cell proliferation, tube formation as well as matrix remodeling. When a peptide inhibits any one or more of these steps, it can serve as a prototype for anti-lymphangiogenic or anti-angiogenic drug development.

Portions of this chapter have previously been published (Lee, Rosca et al. 2011) and were reproduced with permission from the publishers of the journals: copies of permission were included in the Appendix.

6.2 MATERIALS & METHODS

6.2.1 Peptide synthesis and handling

The peptides were produced by a commercial manufacturer (Bachem, Torrance, CA) using a solid-phase synthesis technique (Table 6.1). HPLC and MS analyses of each peptide were provided by the manufacturer to demonstrate greater than 95% purity. The peptides were stored at -80°C and thawed at room temperature just before use. For preparation of peptide stock solutions, dimethyl sulfoxide (DMSO) was used as a solvent at a maximum concentration of 5 or 10% (vol/vol) in PBS due to their hydrophobic profile. The final concentration of DMSO was less than 0.6% when the peptide stock solutions were more diluted in media for in vitro experiments. Experimental groups including controls and peptide treated groups were controlled as they contained same amount of DMSO to eliminate solvent effects.

6.2.2 Cell culture

Human umbilical vein endothelial cells (HUVEC), microvascular endothelial cells (MEC) and lymphatic endothelial cells (LEC) were purchased from Lonza (Walkersville, MD). HUVEC were grown and maintained according to the vendor's recommendation using Endothelial Basal Media (EBM-2) supplemented with the Bullet Kit (EGM-2) from Lonza. The MEC and LEC were propagated in Microvascular Endothelial Cell Growth Medium-2 (EGM-2MV, Lonza). Breast cancer cells, MDA-MB-231 were supplied by Dr. Zaver Bhujwalla (JHMI, Radiology and Oncology). MDA-MB-231 were propagated in RPMI-1640 medium (Gibco, Carlsbad, CA) supplemented with 10% FBS and antibiotics (1% penicillin/streptomycin). Cells were maintained under standard conditions of 37°C and 5% CO_2 and the passage numbers of all the endothelial cells were between 3 and 6.

6.2.3 Specific staining for LEC marker

Western blotting and an immunohistochemistry assay using antibodies against the lymphatic endothelium specific markers podoplanin and LYVE-1 were performed on LEC and HUVEC to confirm the lineage of LEC. HUVEC were used as controls. In the western blotting assay cell extracts were prepared from HUVEC and LEC by incubation of cells in cell lysis buffer (150mM NaCl, 1mM EDTA, 100 µL/mL Protease Inhibitors (Sigma), 10 µL/mL Phosphatase inhibitors (Sigma) and 0.1% Triton) for 2 h. Extracts were centrifuged (14,000 g for 15 min) and protein concentration was assessed by Bradford Assay (BioRad, CA). The extracts were separated by gel electrophoresis and transferred to nitrocellulose membrane for antibody staining. A typical immunohistochemistry protocol was followed for staining using the LEC specific anti-podoplanin antibody D2-40 (Covance, IN).

In the immunohistochemistry assay each well of an 8-well plate was coated with 0.1% gelatin solution and incubated at room temperature for 2 h. 35,000 HUVEC or LEC were seeded and the plate was incubated at 37°C in a tissue culture incubator for 20 h to allow cells to adhere. Media was removed and 100 µL of 1:4 dilution of BD Cytofix fixation buffer (BD Bioscience, CA) was added and incubated at room temperature for 15 min. The fixation buffer was removed and 100 µL of binding media (EBM-2, 1mM 1,10-phenanthroline, 200 µg/mL bacitracin, 0.5 µg/ml leupeptin and 3% BSA) was added for 1 h to prevent non-specific binding. LYVE-1 antibody (Fitzgerald) (4 µg/ml) was added and the plate was incubated at 4°C for 20 h. After rinsing three times with 200 µL/well washing buffer (0.1 L 10xTris buffer + 0.9 L distilled water + 10 mL 10% tween per 1L buffer), anti-mouse IgG Fab 2 labeled with Alexa fluor 488 molecular probes (1:1000 dilution, Cell Signaling) and 5 µg/ml of 4',6-diamidino-2-phenylindole (DAPI, Roche, IN) were added and the plate was incubated at room temperature for 1 h. After 3 rinses with 200

μL/well washing buffer (for 10 min each time), 200 μL of PBS with Ca^{++}/Mg^{++} was added and the cells were imaged using a Nikon microscope (Nikon Instruments Inc.).

6.2.4 Proliferation assay

Proliferation assays in the presence or absence of the peptides were performed using the WST-1 reagent (Roche). Pale yellow colored tetrazolium salt WST-1 can be reduced by mitochondrial dehydrogenases and transformed into dark yellow colored Formazan. In detail, HUVEC were seeded in 96-well plates at a density of 2,000 cells/well in 100 μL of EGM-2 media (100 μL of EGM-2MV was used in MEC and LEC proliferation). The plates were incubated at 37°C in a tissue culture incubator for 20 h to allow cells to adhere. The prepared peptide solutions were added and the plates were incubated for 72 h. Media was removed and 100 μL of WST-1 solution (1:10 dilution of WST-1 in serum free EBM media) was added. After incubation for 4 h, the absorbance at 450 nm was measured using a Victor V (Perkin Elmer, Waltham, MA). IC_{50} values of each peptide were calculated by using GraphPAD Prism 5 (GraphPad Software Inc.).

6.2.5 Cytotoxicity and apoptosis assay

Peptide cytotoxicity was determined using CytoTox-ONE Homogeneous Membrane Integrity assay (Promega, WI). This assay is for detecting the lactate dehydrogenase released from cells with damaged membranes. HUVEC, MEC and LEC were plated at 5,000 cells per well in 96-well plates and the plates were incubated overnight to allow cells to adhere. Then media were replaced with normal media with or without peptide. After 72 h the CytoTox-ONE substrate (100 μL/well) was added. After incubating cells for 10 min at room temperature the stop solution was

added to each well and fluorescence was measured with a Victor V plate reader (Perkin Elmer, MA). Serum-free media (EBM, Lonza), which can be cytotoxic to cells was used as a control.

Apoptosis was detected by using a Caspase-Glo 3/7 apoptosis detection assay kit (Promega, WI). HUVEC, MEC and LEC were plated at 10,000 cells per well in opaque 96-well plates and incubated overnight to allow cells to adhere. Then the media was replaced with complete media with or without peptide. After 72 h the Caspase-Glo chemiluminescent substrate (100 μL/well) was added and the plates were incubating 1.5 h at room temperature. Luminescence was determined with a Victor V plate reader (Perkin Elmer, MA). Serum-free media (EBM-2, Lonza) was used as a control.

6.2.6 Migration assay

HUVEC, MEC, LEC and MDA-MB-231 migration was assessed using the ACEA Real-Time Cell Analysis (RTCA) system (ACEA Biosciences Inc.) and the Cell Invasion and Migration plates 16 (CIM-plates-16) from Roche Diagnostics (Mannheim, Germany). The ACEA RTCA system measures cell electrical impedance expressed as cell index in real time. The cell index indicates the extent of cell migration from the top compartment of a two-chamber system to the bottom compartment in response to chemoattractant factors. In detail, the membrane of the top chamber of a CIM-plate was coated with fibronectin by adding 40 μL of 20 μg/mL fibronectin in PBS solution and incubating at 37°C for 30 min. 180 μL of EGM-2 (complete media for HUVEC) or EGM-2MV (complete media for MEC and LEC) or EBM (serum free media) was added to the bottom chambers. For MDA-MB-231 migration, 180 μL of RPMI-1640 media (Gibco) supplemented with 10% FBS and antibiotics (1% penicillin/streptomycin) was added to the bottom chamber well. The two chambers were assembled together, 30 μL of serum free

media was added to the top chamber and the assembled plate was incubated in a tissue culture incubator at 37°C for at least 1 h. The equilibrated plate was removed from the incubator and 100 µL of the trypsinized cells (45,000 HUVEC/well; 30,000 MEC/well; 120,000 LEC/well; 200,000 MDA-MB-231 cells/well) were added to the top chamber. After 30 min incubation at room temperature, the stabilized chamber was loaded in the RTCA machine and the cell index was measured continuously for 20 h. Cell indices at 20 h were selected for analysis.

Inhibition of migration by one peptide (SP5031) was also investigated in a wound healing type assay to validate the migration data from the RTCA system. This assay was performed using the Oris^{TM} Pro Cell Migration assay (Platypus Technologies, WI). Briefly, 25,000 cells/well in complete media were added to the 96-well plate containing stoppers to prevent the cells from settling in the center region of the wells. Cells were allowed to adhere for 4 h, after which the stoppers were removed. Fully supplemented media with or without peptide was added to the wells to allow migration to the previously blocked area in the center of the wells. After 18 h cells were stained with Calcein AM (0.5 µg/ml) (Invitrogen, CA) in PBS supplemented with Ca^{2+} and Mg^{2+} and the cells that migrated to the center of the well were quantified by reading fluorescence at 485/530 nm on a Victor V plate reader (Perkin Elmer, MA) and also imaged using a Nikon microscope (Eclipse T-100); images were acquired with the CCD Sensicam mounted on a Nikon microscope (Cooke Company, MI). The detection of only the cells that migrated into the previously restricted region is made possible by using a detection mask at the bottom of the plate which obstructs the other parts of the well.

6.2.7 LEC adhesion assay

ACEA E-plates (Roche Diagnostics) were used to measure the extent of LEC adhesion in the RTCA system. Cell impedance is expressed as cell index that indicates the degree of cell adhesion to the electrodes. In detail, 100 µL of 2X concentrated peptide solutions were added to the appropriate wells of an E-plate. LEC (25,000 cells/well) in 100 µL of EGM-2MV media were added next to each well diluting the peptides to the appropriate final concentrations. After equilibrating at room temperature for 30 min, the E-plate was loaded into the RTCA personal system. Cell indices at 1 h were analyzed.

For the validation of adhesion data from the RTCA system a conventional cell adhesion assay was performed. LEC were labeled with Cell Tracker Green (Invitrogen, CA) according to the manufacturer's protocol. Briefly, cells were incubated with complete media containing 10µM Cell Tracker Green for 30 min under normal growth conditions. Labeling media was replaced with complete growth media and cells were allowed to incubate at 37ºC with 5% CO_2 for an additional 30 minutes to complete the labeling process. Following labeling, cells were plated at a density of 10,000 cells/well in a black 96-well plate with a clear bottom. While cells were labeled the well surface was incubated with peptide at concentrations matching the future cell incubation to keep the peptide on the well surface from depletion after PBS washing. Cells were added to wells containing peptide in media or media with matching concentration of DMSO (< 0.2%) and incubated for 2 h. Cells were washed three times with PBS after which the fluorescence intensity was measured using the Victor V plate reader. Images of one randomly selected view per well were acquired using CCD Sensicam mounted on the Nikon microscope.

6.2.8 LEC capillary-like tube formation assay

A LEC capillary-like tube formation assay was performed to determine the effect of the somatotropin peptides on lymphangiogenesis. Basement membrane extracellular matrix (Matrigel, BME, BD Bioscience) was thawed at 4°C overnight. A 96-well plate and 200 µL pipette tips were also kept at 4°C overnight and both the plate and tips were placed on ice during the entire experiment. 50 µL of Matrigel was loaded in each well of the 96-well plate and the plate was incubated at 37°C in a tissue culture incubator for 30 min to allow the matrix to polymerize. Trypsinized LEC were mixed with the peptide making the appropriate cell density (15,000 cells/well) and peptide concentrations (100, 50, 25µM). 100 µL of cell and peptide mixture was added on top of the gel in the 96-well plate. The plate was then incubated at 37°C in a tissue culture incubator and the formation of the capillary-like tubes was observed after 0, 6, 12 and 24 h. At 24 h, the wells were imaged using a Nikon microscope. Quantification of tube formation was assisted by S.CORE, a web based image analysis system (S.CO BioLifescience). Tube formation indices represent the degree of tube formation. The indices were calculated using the equation below. The values of the variables used in the equation were obtained automatically by S.CORE.

(Tube Formation Index) = (Mean Single Tube Index) ^{2} x (1-Confluent Area) x (Number of Branching Points / Total Length Skeleton)

6.2.9 Statistical analysis

Error bars correspond to SEM, unless otherwise stated. Differences between a control and a peptide treated group are regarded as significant when P is less than 0.05 using the Student's t test.

6.3 RESULTS

6.3.1 D2-40, the podoplanin antibody and the LYVE-1 antibody positively identify LEC

Western blotting and an immunohistochemistry assay were carried out on LEC and HUVEC. The western blotting result showed the absence of the specific band for podoplanin, the LEC marker in HUVEC extracts. However, the specific band was present in high amounts in the LEC extracts (Figure 6.1.A). An immunohistochemistry assay showed that the LYVE-1 was only expressed in LEC and not in HUVEC (Figure 6.1.B).

6.3.2 Somatotropin peptides have anti-proliferative effects on both lymphatic and blood endothelial cells

To investigate the anti-proliferative activity of somatotropin peptides a WST-1 based proliferation assay was performed on HUVEC, MEC and LEC. Neuropeptide FF receptor 2 (SP5029), chorionic somatomammotropin (SP5030), chorionic somatomammotropin-like 1 (SP5032) and placental lactogen (SP5033) were potent inhibitors of HUVEC proliferation exhibiting IC_{50} values below 50μM. A peptide from brush border myosin-1 (SP5028) inhibited the proliferation of MEC with IC_{50} below 30μM. Finally in the LEC proliferation assay two peptides, one derived from the IL-17 receptor C (SP5001) and the other derived from the placental lactogen (SP5033) were potent with IC_{50} values below 60μM (Table 6.2).

6.3.3 Somatotropin peptides exhibit cytotoxic and apoptotic activities

Cytotoxic effects of the peptides on HUVEC, MEC and LEC were determined by measuring the lactate dehydrogenase released from damaged cell membranes with CytoTox-ONE Homogeneous Membrane Integrity assay kit (Promega, WI). The normal level of LDH released

from cells incubated in complete media for 72 h was set as 100%. The amount of LDH released from cells incubated in serum free media after the same time was more than 150% of the amount seen when cells were grown in complete media presumably because of the cytotoxic stress from starvation. A concentration of 100μM of all the peptides tested in cells grown in complete media except SP5031 showed more than 150% LDH activity compared to the control when HUVEC were tested. Among them SP5030, SP5032 and SP5033 had significant cytotoxic activity at 10μM (Figure 6.2.A). 100μM of SP5001, SP5028 and SP5033 exhibited more than 200% LDH activity compared to the control on MEC. Even at 10μM these three peptides showed more than 150% LDH level (Figure 6.2.B). However only SP5001 and SP5033 showed significant LDH activity compared to the control on LEC (Figure 6.2.C).

Peptide mediated apoptosis of HUVEC, MEC and LEC were tested with a Caspase-3/7 Glo apoptosis detection reagent (Promega, WI). Apoptosis assays are in general more specific than the LDH cytotoxicity assay. 100μM of SP5028, SP5030 and SP5033 induced significant caspase-3/7 activity compared to the control on HUVEC (Figure 6.2.D). SP5028, SP5030, SP5032 and SP5033 were active against MEC in the apoptosis assay (Figure 6.2.E). Finally only SP5033 induced significant apoptosis on LEC (Figure 6.2.F).

6.3.4 Somatotropin peptides inhibit migration of lymphatic and blood endothelial cells

Real time cell analysis (RTCA) system and ACEA CIM-plates (Roche diagnostics) were used to measure the potency of inhibition of migration of HUVEC, MEC and LEC by the various peptides. 50μM of almost all the peptides showed statistically significant migration inhibitory effects on HUVEC, MEC and LEC (Figure 6.3). Four peptides: SP5028, SP5030, SP5031 and SP5032 inhibited the migration of HUVEC by more than 65% from control (% inhibition of

73.8%, 65.3%, 65.5% and 74.6%, respectively) (Figure 6.3.A). All peptides tested except SP5001 and SP5033, dramatically inhibited the migration of MEC (Figure 6.3.B). Three peptides: SP5028, SP5030 and SP5032 strongly inhibited the migration of LEC (76.1%, 68.7% and 71.3%, respectively). The 14-mer peptide from the transmembrane protein 45A human (SP5031) was the most potent inhibitor of LEC migration (more than 93.6%) (Figure 6.3.C). Real-time LEC migration was determined with RTCA system for 20 h with different concentrations of SP5031. The IC_{50} for inhibition of LEC migration by SP5031 was 25.1μM at 20 h after migration (Figure 6.3.D, E). The wound healing cell migration assay was performed on LEC with SP5031 to validate the data from RTCA system. The results showed a dose response similar to the impedance based migration data from the RTCA system (Figure 6.3.F, G).

6.3.5 Somatotropin peptides block LEC adhesion

The ACEA E-plates (Roche) were used to evaluate LEC adhesion with or without peptides. All peptides were screened at a concentration of 50μM and the most potent peptide was subsequently tested at concentrations of 100, 33, 11, 3.7, 1.2μM to obtain an IC_{50} value. SP5001, SP5028 and SP5029 inhibited the LEC adhesion only slightly (19.5%, 18.4% and 21.8%, respectively). However, SP5030, SP5031 and SP5032 showed strong inhibition of LEC adhesion inhibition (49%, 58% and 46%, respectively) (Figure 6.4.A). Among them the peptide derived from the transmembrane protein 45A human (SP5031) inhibited LEC adhesion most potently with an IC_{50} value of 24.2μM (Figure 6.4.B, C). The conventional cell adhesion assay was carried out on LEC with SP5031 peptide to validate the LEC adhesion data from RTCA system. The result showed that SP5031 blocked LEC adhesion in a dose-dependent manner (Figure 6.4.D, E). However the conventional cell adhesion method was less sensitive than the RTCA system at the low concentrations (below 33μM) of SP5031. These experiments demonstrate that the results

from the E-plate based RTCA adhesion assay are reliable and that it may be a more sensitive methodology to measure cell adhesion than the conventional adhesion assay.

6.3.6 Somatotropin peptides inhibit LEC tube formation

Non-reduced matrigel with EGM-2MV complete media was used in the LEC capillary-like tube formation assay because it promotes robust tube formation allowing us to test the inhibitory effects of the peptides. All peptides were tested at 100μM to show their anti-tube formation activities. SP5030, SP5031 and SP5032 showed pronounced activities so that tube formation was completely blocked (Figure 6.5.A). Three selected candidates (SP5030, 5031, 5032) were tested at lower concentrations of 50μM and 25μM to obtain the minimum concentration for complete tube inhibition. The peptide from transmembrane protein 45A (SP5031) blocked LEC tube formation most effectively showing a dose response (Figure 6.5.B). The tube formation index was decreased by 89%, 67% and 22% by 100, 50 and 25μM of the SP5031 respectively.

6.4 DISCUSSION

Small peptides are emerging and promising agents in developing new therapeutics for different diseases (Saladin, Zhang et al. 2009; Rosca, Koskimaki et al. 2011). Peptide agents have significant merits compared to conventional proteins and large synthetic molecules. The advantages of peptides as drugs over proteins are high specificity, low immunogenicity and toxicity, better solubility in water and stable product quality between batches (Sulochana and Ge 2007). One disadvantage is short half-life in vivo, which could be overcome by peptide modification, conjugation to a macromolecule, or combination with a delivery vehicle (Bhise, Shmueli et al. 2011; Rosca, Koskimaki et al. 2011)

Previously several anti-angiogenic peptides were identified, derived from endogenous proteins such as thrombospondin-1, collagen, laminin, decorin, platelet factor-4, kininostatin, and VEGFR. Among them a number of anti-angiogenic peptides are in clinical trials (Sulochana and Ge 2007; Rosca, Koskimaki et al. 2011). Although many trials have been conducted for anti-angiogenic peptides, peptide agents for inhibiting lymphangiogenesis have not been reported. In this study the anti-lymphangiogenic effects of small somatotropin peptides were investigated. The peptides from IL-17 receptor C (SP5001) and placental lactogen (SP5033) potently inhibited LEC proliferation (Table 2). Four peptides derived from brush border myosin-1 (SP5028), chorionic somatomammotropin (SP5030), transmembrane protein 45A (SP5031) and chorionic somatomammotropin-like 1 (SP5032) strongly inhibited LEC migration and adhesion (Figure 6.3 and Figure 6.4). SP5030, SP5031 and SP5032 were strong inhibitors of the LEC capillary-like tube formation. Among them SP5031 was the most active LEC tube formation inhibitor (Figure 6.5).

In the present study two classes of lymphangiogenesis inhibitors were identified. The first class which includes SP5001 and SP5033 inhibit lymphangiogenesis by inhibiting proliferation of lymphatic endothelial cells and the second class which includes SP5030, SP5031 and SP5032 inhibit lymphangiogenesis by mainly inhibiting lymphatic endothelial cell migration and adhesion (Figure 6.7). SP5033 showed significant apoptotic activity on HUVEC, LEC and MEC exhibiting caspase-3/7 activity (Figure 6.2.D, E, F). Interestingly the amino acid sequence of SP5033 (LLRISLLLIESWLE) was very similar to the previously studied 14-mer tilted peptide (LLRISLLLIQSWLE) from 16-kDa fragments of prolactin (PRL) with a difference only in the 10^{th} amino acid (Nguyen, Tabruyn et al. 2006). The glutamic acid (Glu, E) in SP5033 is replaced with the glutamine (Gln, Q) in the tilted PRL peptide. It has been reported that the tilted PRL peptide led to cell apoptosis (Nguyen, Tabruyn et al. 2006). These results with prolactin (PRL) peptide and protein suggest that the PRL protein has active domains which may include the sequence of SP5033 exhibiting apoptotic activity. Also the apoptotic property of SP5033 may be associated with its structure that may be conserved regardless of the 10^{th} amino acid replacement. However SP5001, the other peptide in this class, was not associated with caspase-3/7 activity even though it showed potent proliferation inhibitory effect as seen by increased LDH levels (Figure 6.2). This suggests that SP5001 has anti-proliferative activity through other pathways such as arresting the cell cycle or other cytotoxic pathways that are different from the caspase-3/7 dependent apoptosis pathway. The second class peptides comprising SP5030, SP5031 and SP5032 inhibited LEC migration and adhesion and were potent lymphatic tube formation inhibitors compared to the first class of peptides (Figure 6.3-5). These two classes of peptides allow one to manipulate endothelial cell proliferation and migration separately via independent

pathways. The receptors and signaling pathways targeted by the two classes of peptides resulting in the control of cell proliferation and migration remain to be identified.

Several anti-lymphangiogenic sequences derived from various proteins were identified, which includes IL-17 receptor C, brush border myosin-1, neuropeptide FF receptor 2, transmembrane protein 45A: they have not been associated with angiogenesis or lymphangiogenesis. These findings may contribute to the understanding of the poorly understood physiological roles of these proteins. For example, SP5001, a peptide derived from IL-17 receptor C protein, could lead us to hypothesize that there might be lymphangiogenesis-related physiological roles of the IL-17 receptor C protein which is known as a receptor for IL-17A and F. Recently it was reported that a ligand IL-17 promotes the expression of VEGFC in non-small-cell lung carcinomas inducing lymphangiogenesis and inflammation (Chen, Wan et al. 2010). This correlation between IL-17 and lymphangiogenesis has not been expected before the identification of the SP5001 peptide. We hypothesize that IL-17 receptor C might work as an endogenous scavenger of IL-17 and the active site for anti-lymphangiogenic and anti-inflammatory activity could be closely related to the peptide sequence identified here; further studies are required to validate this hypothesis.

When it comes to anti-angiogenic efficacy of the peptides, three leading peptides have been identified: peptides derived from brush border myosin-1 (SP5028), chorionic somatomammotropin (SP5030) and chorionic somatomammotropin-like 1 (SP5032). Interestingly both SP5030 and SP5032 are derived from chorionic somatomammotropin related proteins. Their amino acid sequences are very similar: 10 of 13-14 amino acids are identical between the two sequences. These anti-angiogenic peptides could be applied to the treatment of different angiogenesis dependent diseases such as cancer, age-related macular degeneration (AMD), or rheumatoid arthritis.

Angiogenesis and lymphangiogenesis are both important processes in health and disease. Somatotropin peptides are active in both inhibiting lymphangiogenesis and angiogenesis (Figure 6.6). These properties are expected be useful for modulating those processes in diseases. In particular these peptides would be applied to prevent the deadly spread of cancer cells by inhibiting not only tumor growth but also peritumoral lymphatics. Alternatively, a single compound that targets both tumor-associated blood vessels and tumor-associated lymphatic vessels may decrease tumor size and decrease the incidence of local and distant metastases. Thus these peptides should be further tested in vivo for their simultaneous inhibition of tumor growth and metastasis and other angiogenesis- and lymphangiogenesis-dependent diseases.

6.5 FIGURES & TABLES

Peptide name	Peptide origin	Accession #	Peptide Sequence
SP-5001	IL-17 receptor C	NP703191 (376-387)	RLRLLTLQSWLL
SP-5028	Brush border myosin-1	AAD31189 (719-731)	LMRKSQILISSWF
SP-5029	Neuropeptide FF receptor 2	AAG41398 (276-288)	LLIVALLFILSWL
SP-5030	Chorionic somatomammotropin	AAA52116 (101-113)	LLRLLLLIESWLE
SP-5031	Transmembrane protein 45A	NP060474 (181-194)	LLRSSLILLQGSWF
SP-5032	Chorionic somatomammotropin-like 1	Q14406 (83-96)	LLHISLLLIESRLE
SP-5033	Placental Lactogen	AAA98621 (101-114)	LLRISLLLIESWLE

Table 6.1: The amino acid sequences of the tested somatotropin peptides.

Peptide name	IC_{50} (μM ± 95% Cl)		
	HUVEC	MEC	LEC
SP-5001	50.7 ± 31.8	52.4 ± 27.8	27.3 ± 19.6
SP-5028	58.2 ± 35.2	27.7 ±17.4	>200
SP-5029	34.9 ± 15.4	>200	>200
SP-5030	17.7 ± 11.2	93.2 ± 42.3	>200
SP-5031	96.9 ± 34.3	83.4 ± 21.9	157.6 ± 122.2
SP-5032	36.5 ± 25.1	80.1 ± 47.9	Not converged
SP-5033	14.7 ± 8.1	81.1 ± 37.2	59.8 ± 27

Table 6.2: IC_{50} values in proliferation assay with somatotropin peptides.

Somatotropin peptides were tested against HUVEC, MEC and LEC using WST-1 cell proliferation reagent.

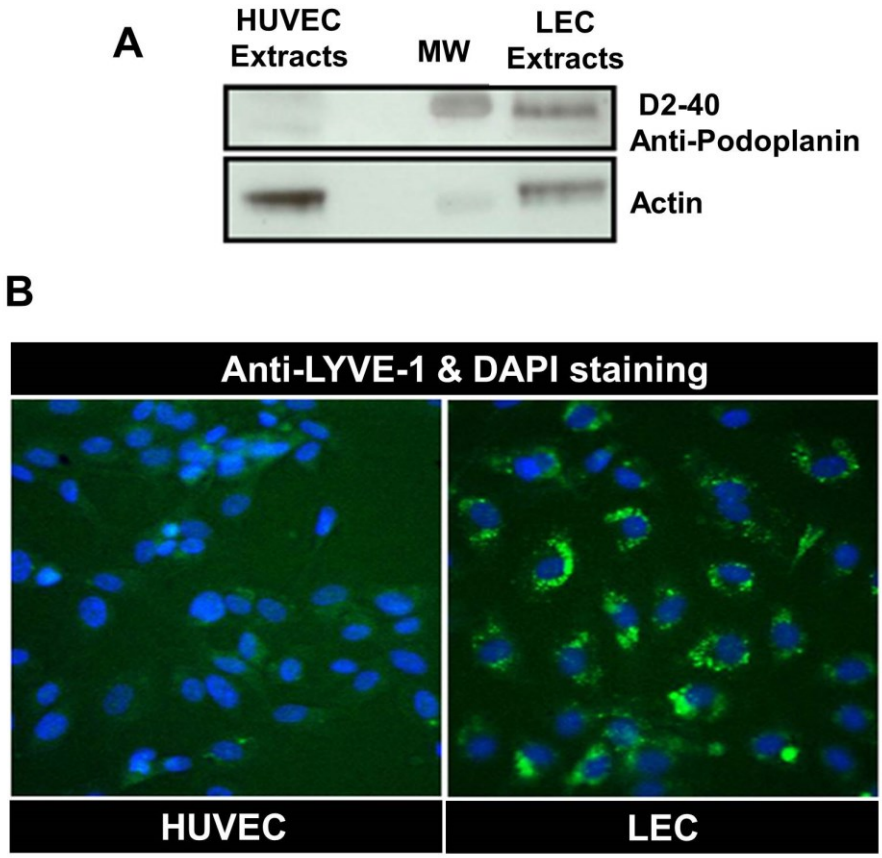

Figure 6.1: Specific staining for LEC markers. (A) Western blotting with D2-40, podoplanin antibody on HUVEC and LEC. Lane 1 demonstrates the absence of the specific band for D2-40 LEC marker in HUVEC extracts while the band is strongly visible in the LEC extracts (Lane 4). (B) An immunohistochemistry assay with LYVE-1 antibody on HUVEC and LEC. The immunohistochemistry assay shows that LEC is positive for anti-LYVE-1 LEC marker (green colored), however HUVEC is not. A merged image with DAPI staining (blue colored) shows that LYVE-1 receptor proteins (green colored) are expressed in LEC membranes specifically not in HUVEC membranes.

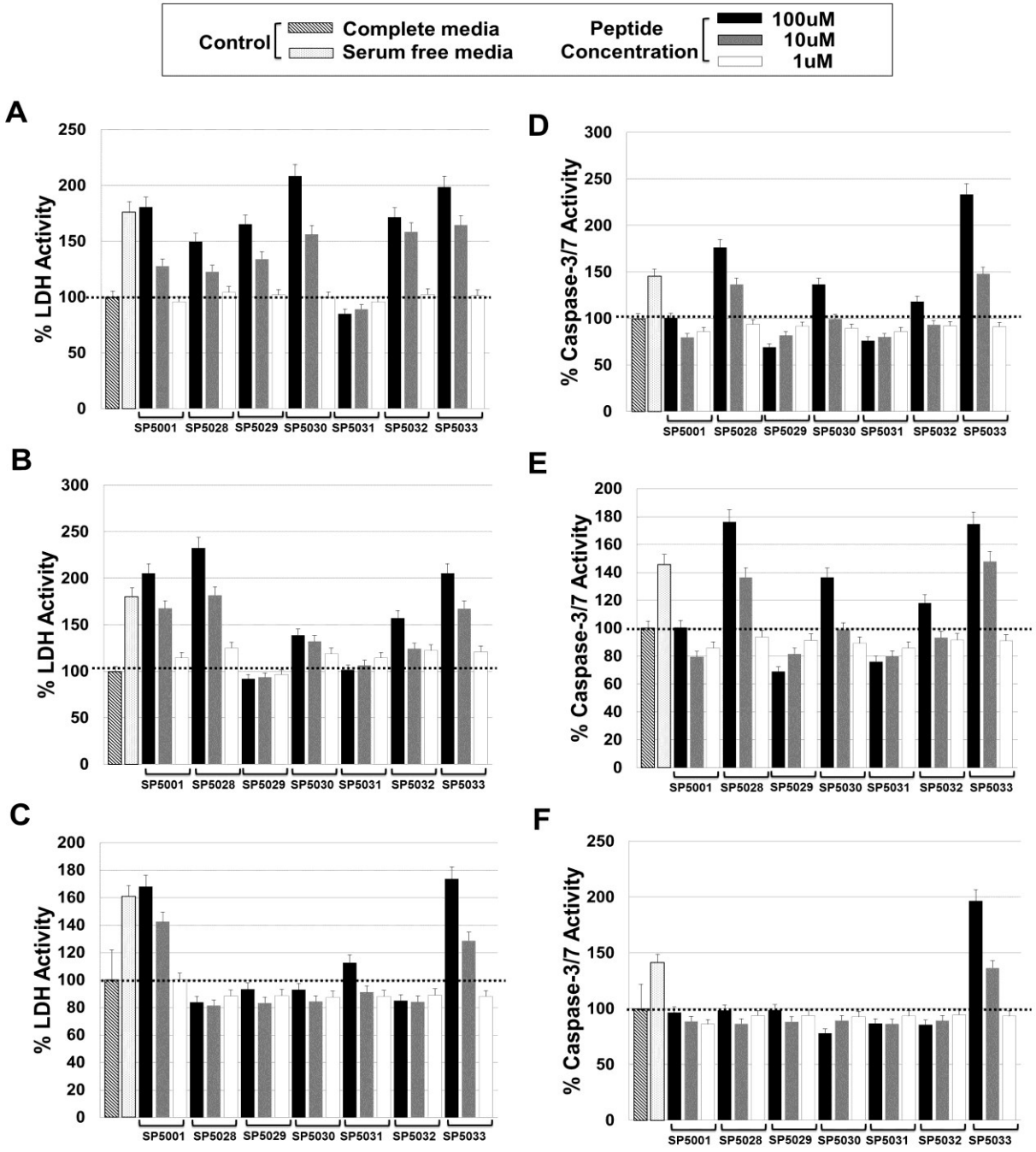

Figure 6.2: The cytotoxic and apoptotic activity of the peptides.

The cytotoxic effect of the peptides was determined by using CytoTox-ONE Homogeneous Membrane Integrity assay kit detecting lactate dehydrogenase (Dieu, Vanbervliet et al.) released

from damaged cells. Peptide induced apoptotic activity was detected by using a Caspase-Glo 3/7 apoptosis detection assay kit. HUVEC, MEC and LEC were incubated at 37°C in complete media with or without peptides for 72 h before these two assays. The LDH or caspase-3/7 signals in the normal condition with only complete media were defined as negative control with 100% LDH or caspase-3/7 activity (black dotted lines). Starved condition with serum free media or peptide treatment induced more LDH or caspase-3/7 activity. (A) Percent LDH activity after treating HUVEC with somatotropin peptides. (B) Percent LDH activity on MEC. (C) Percent LDH activity on LEC. (D) Percent caspase-3/7 activity after treating HUVEC with somatotropin peptides. (E) Percent caspase-3/7 activity on MEC. (F) Percent caspase-3/7 activity on LEC.

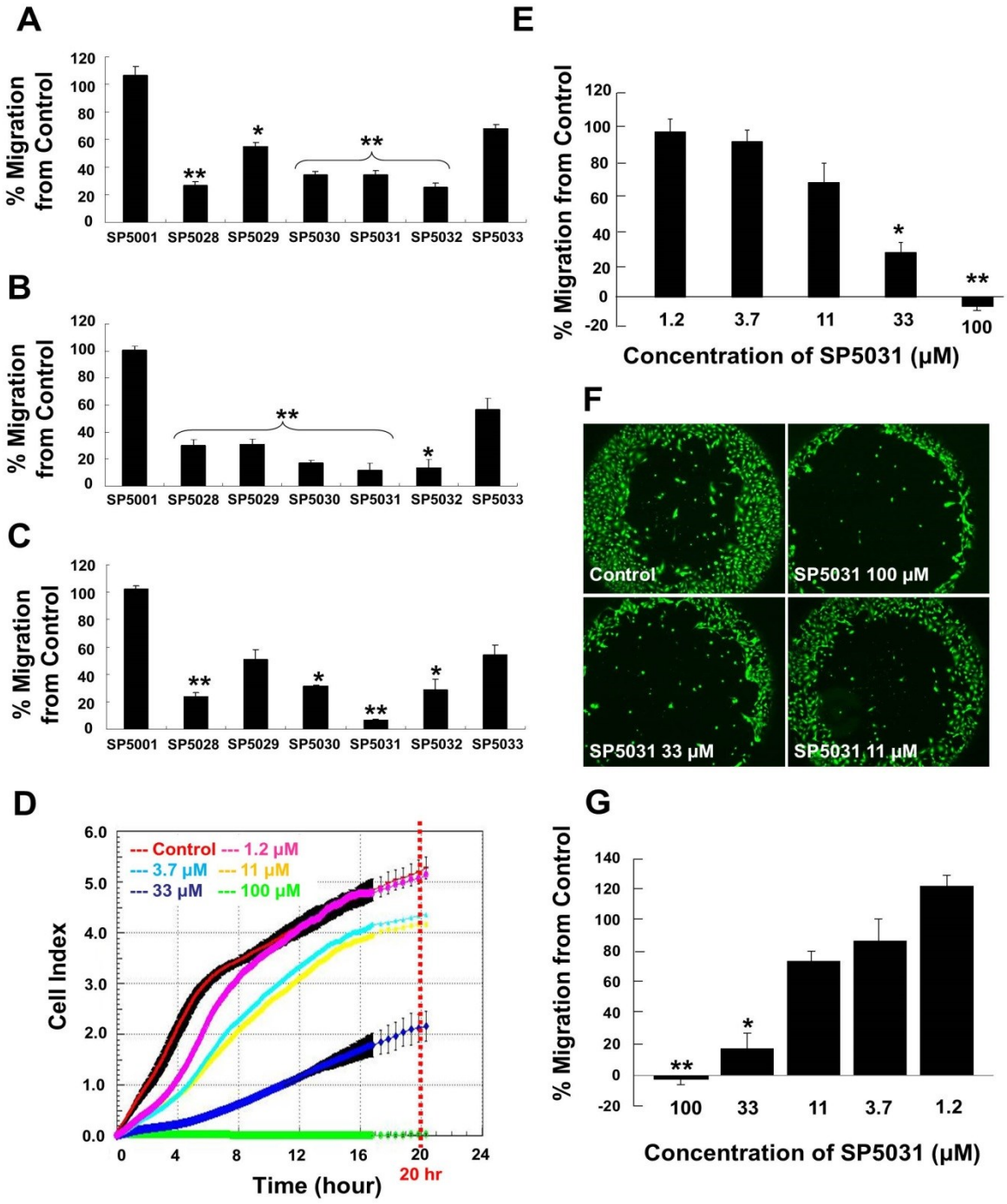

Figure 6.3: Migration inhibitory activity of the somatotropin peptides.

Somatotropin peptides were tested against HUVEC, MEC and LEC for their anti-migratory activity. The peptide concentration was 50µM and cell indices at 20 h were used for data analysis.

(A) Percent HUVEC migration. * $P < 0.05$ versus control and ** $P < 0.03$ versus control. (B) Percent MEC migration. * $P < 0.05$ versus control, ** $P < 0.03$ versus control. (C) Percent LEC migration. * $P < 0.05$ versus control and ** $P < 0.02$ versus control. (D) Real-time migration data with SP5031 (0, 1.2, 3.7, 11, 33 and 100μM) on LEC. (E) Percent LEC migration with SP5031 after 20 h of migration using RTCA migration assay. * $P < 0.05$ versus control and ** $P < 0.01$ versus control. (F) The image of the wound healing LEC migration assay with SP5031. (G) The quantified percent LEC migration with SP5031 using the wound healing cell migration assay. * $P < 0.05$ versus control and ** $P < 0.02$ versus control.

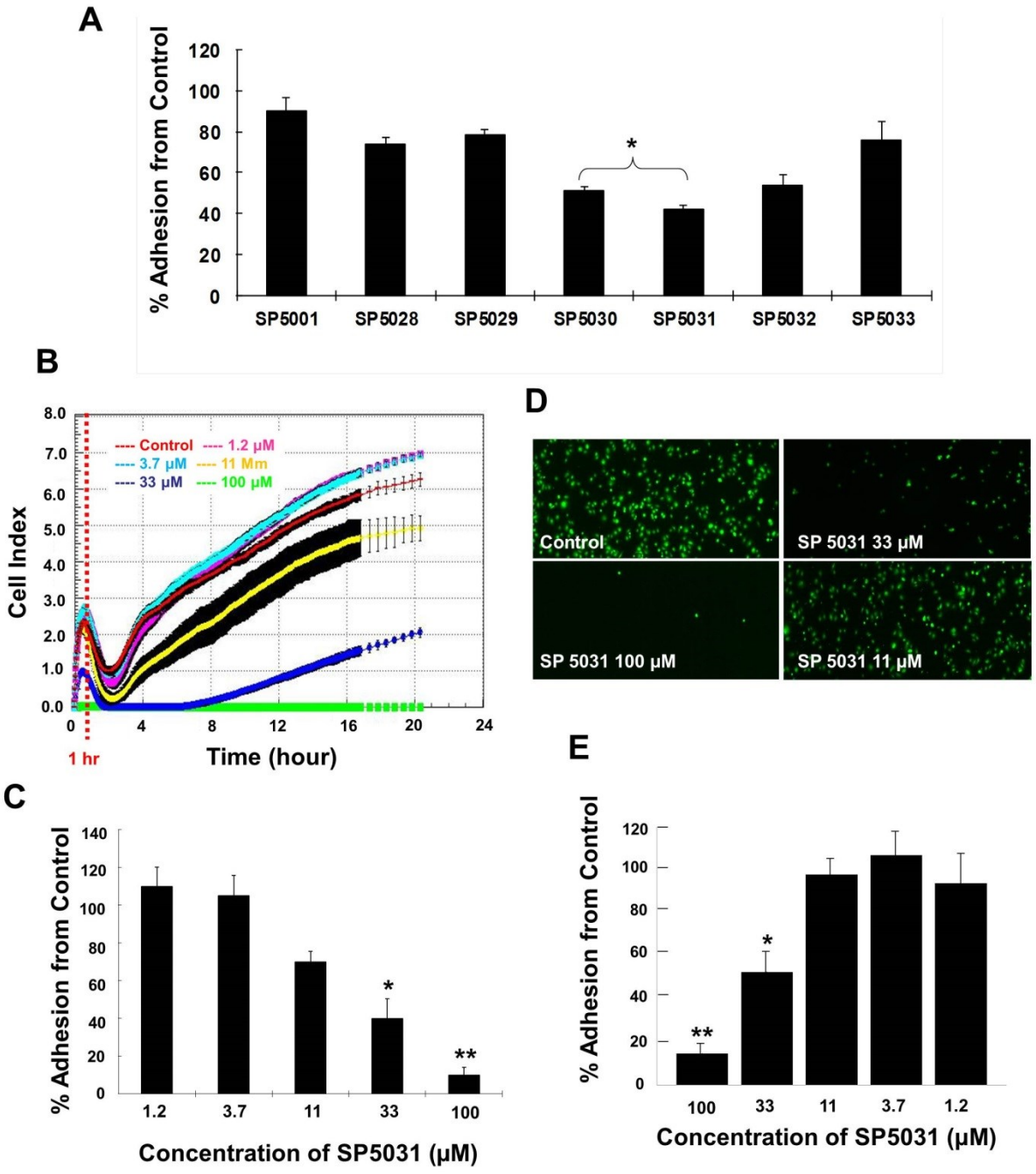

Figure 6.4: Adhesion inhibitory activity of the somatotropin peptides on LEC.

(A) LEC adhesion in the presence of 50µM of somatotropin peptides at 1 h using the RTCA method. * $P < 0.05$ versus control. (B) Real-time LEC adhesion data in the presence of different

concentrations of SP5031 (0, 1.2, 3.7, 11, 33, 100μM). (C) LEC adhesion with SP5031 after 1 h of adhesion using RTCA. * $P < 0.05$ versus control and ** $P < 0.02$ versus control. (D) The image of LEC adhesion with different concentrations of SP5031. (E) The quantified percent LEC adhesion. * $P < 0.05$ versus control and ** $P < 0.02$ versus control.

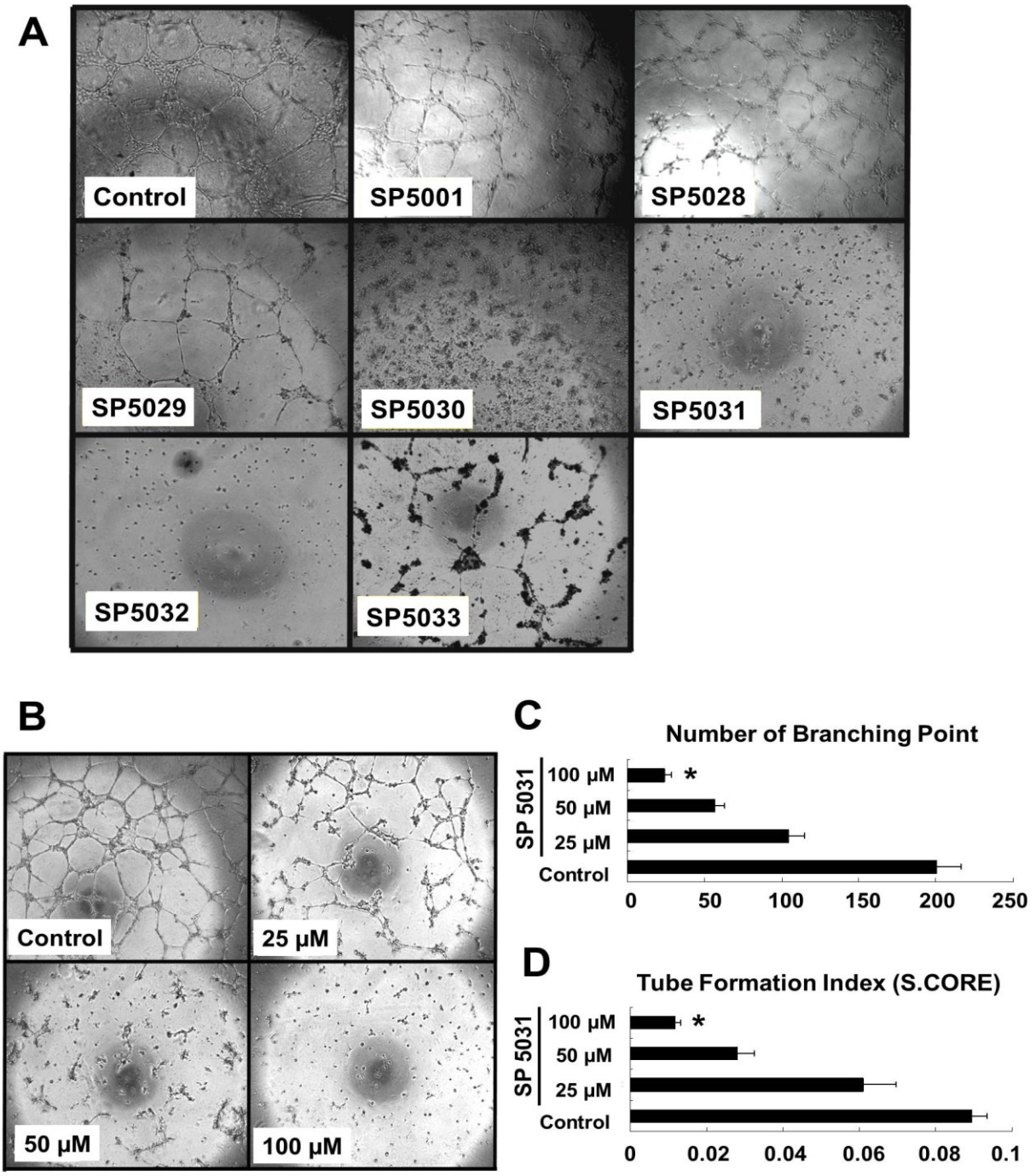

Figure 6.5: Capillary-like tube formation assay with somatotropin peptides on LEC.

(A) LEC tube formation in the presence of 100μM of the peptides at 24 h. (B) LEC tube formation in the presence of different concentrations (0, 25, 50, 100μM) of SP5031 at 24 h.

(C) Number of branching point. * $P < 0.01$ versus control. (D) Tube formation index (S.CORE). * $P < 0.01$ versus control. Quantification of tube formation was assisted by S.CORE web based image analysis system.

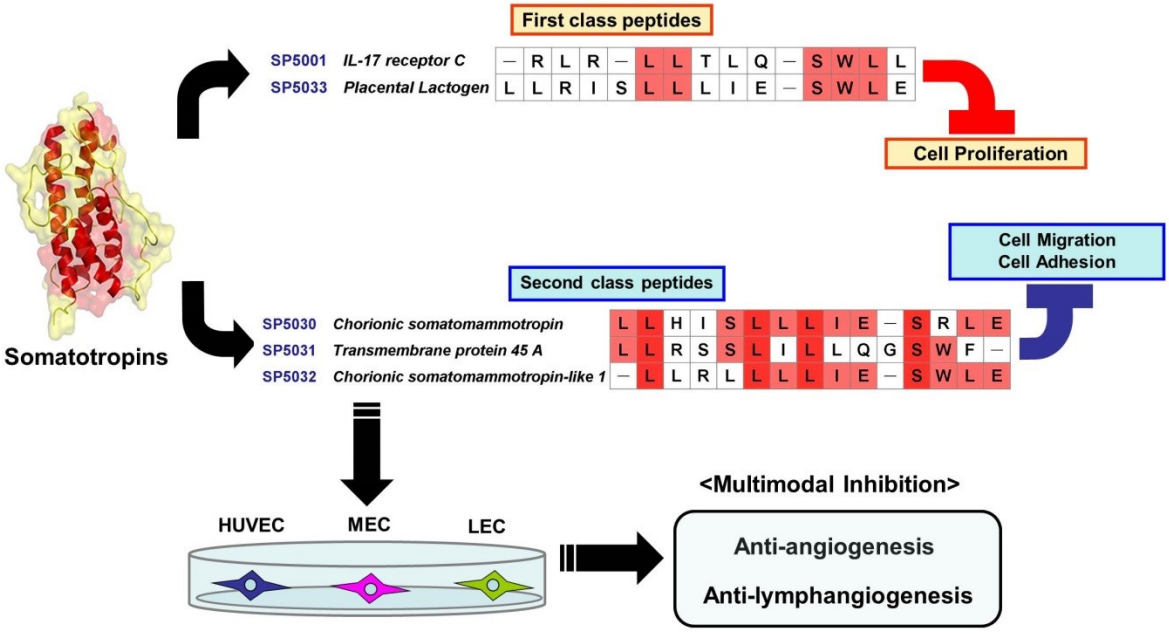

Figure 6.6: Classification of somatotropin peptides.

Two classes of somatotropin peptides were determined. The first class of peptides, SP5001 and SP5033, mainly inhibit the proliferation of both lymphatic and blood endothelial cells. The second class of peptides including SP5030, SP5031 and SP5032, potently inhibit migration and adhesion of lymphatic and blood endothelial cells. Their sequences are shown and the conserved amino acids within each class are highlighted. Dark red colored amino acids represent common residues of all these peptides in the two classes.

Chapter 7: Transmembrane Protein 45A-derived Peptide Shows Anti-lymphangiogenic and Anti-angiogenic Activity in Breast Tumor Xenografts and Lymph Nodes.

7.3.2 SP5031 exhibits anti-lymphangiogenic and anti-angiogenic activity in MDA-MB-231 tumor xenografts

7.3.3 SP5031 shows anti-lymphangiogenic and anti-angiogenic activity in tumor-conditioned regional LN

7.3.4 SP5031 blocks TCM-induced VEGFR2 phosphorylation

7.3.5 SP5031 exhibits anti-lymphangiogenic and anti-angiogenic activity in Matrigel plug assays

7.3.6 SP5031 inhibits VEGFA/C-dependent VEGFR2/3 signals, resulting in inhibition of activation of downstream proteins

7.3.7 Neuropilin 1/2 are the target receptors of SP5031

7.3.8 SP5002, a peptide homologous to SP5031, is inactive

7.4 DISCUSSION

7.5 FIGURES & TABLES

7.1 RATIONALE

Angiogenesis is a process that tumors employ to promote their growth and spread (Carmeliet and Jain 2011). Although blood vessels contribute to cancer cell dissemination, tumor metastasis is significantly facilitated by the lymphatic system as well (Tammela and Alitalo 2010). Studies in micrometastases of melanoma, gastric cancer, and breast cancer have shown that 16-20% of cancer patients showed lymphatic invasion, whereas 3-5.4% showed blood vessel invasion, bypassing the lymphatic system (Hyung, Lee et al. 2002; Lee, Pinder et al. 2006; Doeden, Ma et al. 2009). Lymphatic vessels offer several advantages over blood vessels for cancer cell dissemination. The lymphatic vessels have a discontinuous basement membrane that facilitates intravasation and extravasation of cancer cells. The lymphatic vessels have a much slower flow rate of lymphatic fluid with lower shear stress, resulting in less tumor cell death, and a higher lymphatic concentration of hyaluronic acid, a molecule with potent cancer cell-protecting properties (Ran, Volk et al. 2010).

Metastasis is significantly enhanced by an increase in lymphangiogenesis in primary tumors and regional lymph nodes: these pathological phenomena at the two different sites are referred to as tumor lymphangiogenesis and lymph node lymphangiogenesis (Cueni, Hegyi et al. 2010). In terms of tumor lymphangiogenesis, peritumoral or intratumoral lymphatic vessels play a role as initial routes of cancer cell dissemination from the primary tumor to the lymphatic system. Lymph node (LN) lymphangiogenesis is also central for lymphatic metastasis; as shown pre- or post-metastatic LN feature highly enhanced lymphangiogenesis (Tobler and Detmar 2006). Before invasion, primary tumors overexpress lymphangiogenic factors, deliver these factors to tumor-draining LN through lymphatic vessels thus inducing neo-lymphangiogenesis in the LN (Hirakawa, Brown et al. 2007). Additionally, the LN lymphangiogenesis is maintained, and

further enhanced after cancer cells metastasize to the LN (Duong, Koopman et al. 2012). These suggest that tumor lymphangiogenesis and LN lymphangiogenesis would be crucial targets of anti-metastatic agents.

Breast cancer is the most commonly diagnosed female malignancy in the United States (DeSantis, Siegel et al. 2011). Though anti-angiogenic or hormonal therapies combined with other agents are in development to treat breast cancer (Doyle and Miller 2008), many patients with metastatic breast cancer (e.g., triple-negative breast cancer subtypes) have suffered from recurrence of secondary tumors in regional LN and distant organs (Kerbel 2011; Martin 2011). Avastin (Bevacizumab), a VEGFA monoclonal antibody, was revoked by the Food and Drug Administration (FDA) from clinical indications for advanced breast cancer, since it had not improved overall survival rates of metastatic breast cancer patients (Tanne 2011). This limitation of Avastin can be interpreted based on the evidence that anti-angiogenic therapies result in a hypoxic condition in tumors, overexpression of lymphangiogenic factors, enhancing tumor metastasis through the lymphatics (Paez-Ribes, Allen et al. 2009; Ribatti 2011). Thus, lymphatic metastasis is an alternative way of tumor resistance to current anti-angiogenic therapies.

Previously, in Popel lab, bioinformatics approach using peptides known to have anti-angiogenic activity as the input resulted in the identification of more than 100 novel anti-angiogenic endogenous peptides in the human proteome. These peptides are parts of larger proteins of different classes, including type IV collagen, thrombospondin-1, CXC chemokines, serpins, and somatotropins (Karagiannis and Popel 2008). Recently, it has been discovered that small peptides from somatotropin domain-containing proteins are anti-lymphangiogenic and anti-angiogenic in cell-based experiments (Lee, Rosca et al. 2011). Based on these findings, in vivo activity of one of the most potent somatotropin peptides will be investigated in breast tumor

xenograft and tumor-conditioned regional LN models. The peptide is derived from a transmembrane protein 45A (TMEM45A), denoted SP5031 (amino acid sequence: LLRSSLILLQGSWF-NH_2).

Portions of this chapter have previously been published (Lee, Koskimaki et al. 2013) and were reproduced with permission from the publishers of the journals: copies of permission were included in the Appendix.

7.2 MATERIALS & METHODS

7.2.1 Peptide synthesis and handling

Peptides were produced by Bachem (Torrance, CA) by using a solid-phase synthesis technique. HPLC and MS analyses of the peptides were provided by the manufacturer to indicate a purity of more than 95%. In preparation of peptide stock solution, DMSO was used as a solvent at a maximum concentration of 5% (vol/vol) in distilled water. All experiments were carried out with < 0.3% concentrations of DMSO so as not to harm cells. Theoretical isoelectric points (p.I.) of the peptides were calculated, using the Compute pI/Mw on-line software in ExPASy provided by Swiss Institute of Bioinformatics.

7.2.2 Cell culture

Lymphatic endothelial cells (LEC), microvascular endothelial cells (MEC), and human umbilical vein endothelial cells (HUVEC) were purchased from Lonza (Walkersville, MD). LEC and MEC were propagated in microvascular endothelial cell growth medium-2 (EGM-2MV, Lonza). HUVEC were propagated in endothelial cell growth medium-2 (EGM-2, Lonza). MDA-MB-231 triple-negative human breast cancer cells, and MCF-7 estrogen receptor-positive human breast cancer cells were supplied by Dr. Zaver Bhujwalla (JHMI, Radiology and Oncology), and propagated in RPMI-1640 medium (Gibco, Carlsbad, CA) supplemented with 10% fetal bovine serum (Gibco), and 1% penicillin streptomycin (Gibco). Cells were maintained under standard conditions of 37°C and 5% CO_2 and the passage numbers of endothelial cells were kept between 3 and 6.

7.2.3 Preparation and characterization of tumor-conditioned media (TCM)

MDA-MB-231 cells in complete growth media (RPMI-1640) were plated on 175 mm^2 tissue culture plates. When the cell number reached 10 X 10^6 (confluent monolayer) the complete media was removed, and the cells were carefully rinsed with serum-free media (RPMI-1640 without supplements), then, 5 ml of serum-free media was added. After 24 h of incubation at 37°C, TCM was carefully gathered, centrifuged, and filtered through 0.2 µm sterile syringe filters (Corning, Germany) to remove cells. The TCM was stored in aliquots at -80°C to avoid multiple freeze thaws. A Proteome Profiler Antibody Arrays Kit for Human Angiogenesis (R&D systems, Minneapolis, MN) was used to determine angiogenesis-related factors in TCM. Array membranes were blocked with 2 ml blocking buffer provided in the kit for 1 h at room temperature on a rocking platform. 1,000 µl TCM was mixed with 500 µl dilution buffer provided in the kit. The prepared sample was added to the blocked membrane and the membrane was incubated overnight at 4˚C. After three rinses with washing buffer provided in the kit, 1.5 ml HRP-conjugated detection antibody in the kit was added for signal detection.

7.2.4 Migration and adhesion assays

Cell migration and adhesion assays were performed, using Real-Time Cell Analysis (RTCA) system (ACEA Biosciences, San Diego, CA) as described previously (Lee, Rosca et al. 2011). To evaluate cell migration, Cell Invasion and Migration plates (CIM-plates) (Roche, Indianapolis, IN), and a RTCA system were used. The membrane of the top chamber of a CIM-plate was pre-coated with 20 µg/ml fibronectin (Sigma Aldrich, St. Louis, MO). 180 µl of TCM was added to the bottom chamber as a chemoattractant. Cells (45,000 HUVEC; 120,000 LEC/well) were added to the top chamber with or without peptides. After stabilizing CIM-plates for 30 min at

room temperature, the chamber was loaded in the RTCA machine, and the cell indices were measured continuously for 24 h. Cell indices at 20 h were selected for analysis. For adhesion assays, 100 µl of 2X concentrated peptide solution was added to the appropriate wells of an E-plate (Roche). LEC and HUVEC (25,000 cells/well) in TCM were added next to each well diluting peptides to the appropriate final concentration. After equilibrating at room temperature for 30 min, the E-plate was loaded into the RTCA system. Cell indices at 3 h were analyzed.

7.2.5 Tube formation assay

50 µl Matrigel (BD Biosciences, Bedford, MA) was loaded in each well of a 96-well plate, and the plate was incubated at 37°C for 30 min. 100 µl LEC and HUVEC in TCM with or without peptides were added on top of the matrix in the 96-well plate (15,000 cells/well). The plate was then incubated at 37°C, and the wells were imaged using a Nikon microscope at 20 h (Nikon Instruments Inc., Melville, NY). Quantification of tube formation was assisted by S.CORE, a web based image analysis system (S.CO Life Science, Germany). Tube formation indices represent the degree of tube formation. The indices were calculated using the equation below. The values of the variables used in the equation below were obtained automatically by S.CORE.

(Tube Formation Index) = (Mean Single Tube Index) ^{2} x (1-Confluent Area) x (Number of Branching Points / Total Length Skeleton)

7.2.6 Cell proliferation assay

Cell proliferation assay was carried out by using cell proliferation reagent WST-1 (Roche) as described previously (Lee, Rosca et al. 2011). For the proliferation assay, 2,000 cells were plated in a 96-well plate, allowed to attach for 4 h and the media was replaced with media with peptides.

After 72 h at 37°C the number of viable cells was measured after adding WST-1, a reagent that is converted to a formazan whose absorbance at 450nm is measured in a plate reader.

7.2.7 In vivo MDA-MB-231 xenograft models

Animal protocols were approved by the Institutional Care and Use Committee at the Johns Hopkins Medical Institutions. 2 X 10^6 MDA-MB-231 cells were orthotopically inoculated into the lower thoracic mammary fat pad of severe combined immunodeficiency (SCID) mice under anesthesia (50 mg/kg ketamine + 5 mg/kg acepromazine in PBS), and the tumors were allowed to grow until they reached around 100 mm^3. 15 mg/kg peptide solution in PBS, or PBS (vehicle) was injected intraperitoneally, and continued for 27 days. The tumor size was measured and the volume was calculated as previously described (Tomayko and Reynolds 1989), using the formula: $V = 0.52 \times a \times b^2$, where 'a' is the long axis, and 'b' is the short axis of the tumor. Each group has 8 to 10 mice.

7.2.8 In vivo tumor-conditioned regional lymph node models

50 µl MDA-MB-231 tumor-conditioned media (TCM) or serum-free media (SFM) was subcutaneously administered through the scruff of athymic nude mice. These animals were either treated with SP5031 or with the vehicle (PBS) (intraperitoneal administration, 15 mg/kg) for 14 days. After 14 days, animals were euthanized, the axillary and brachial LN were excised and the LN volumes were measured. The LN volumes (V) were calculated according to the formula: $V = 0.52 \times a \times b^2$ where 'a' is the long axis, and 'b' is the short axis of the LN. The LN were rinsed in PBS and fixed in 4% formalin for 16 h for immunohistochemistry. Each group has 4 mice, giving 16 regional LN (8 axillary LN + 8 brachial LN) per experimental group.

7.2.9 Matrigel plug assay

Growth factor reduced Matrigel (High Concentration) (BD Biosciences, Bedford, MA) containing rh-$VEGF_{165}$ (380 ng/ml, R&D systems), rh-bFGF (380 ng/ml, R&D systems) and heparin (10 IU/plug, Sigma Aldrich) were mixed with or without the peptide (200 μg/ml) in a total volume of 400 μl. The Matrigel mixtures were subcutaneously injected on both flanks on the abdominal side of athymic nude mice under anesthesia. After 10 days the gels were removed, imaged and analyzed via immunohistochemistry.

7.2.10 Immunohistochemistry

Axillary and brachial lymph nodes (LN) fixed in 4% formalin were placed in 30% sucrose solution in PBS, incubated overnight at 4°C, and frozen in the Tissue-Tek Optimal Cutting Temperature (O.C.T.) compound (Sakura, Japan). Serial sections of 10-μm thickness were cut parallel to the long axis of the LN at -20°C. After blocking with 5% normal chicken serum in PBST (5% chicken serum, 0.1% cold fish gelatin, 0.1% Triton X-100, 0.05% Tween 20, and 0.05% Sodium azide in PBS) for 1 h at room temperature, the sections were treated with rat monoclonal anti-mouse MECA-79 antibody (Santa Cruz Biotechnology, Inc. Santa Cruz, CA) overnight at 4°C. After 3 rinses with PBST, sections were incubated with Alexa Fluor 647 chicken anti-rat IgG in the dark (Invitrogen, Grand Island, NY) for 1 h at room temperature. After 3 rinses, the second blocking agent (5% normal donkey serum in PBST) was added and incubation at room temperature in the dark was continued for another hour. Goat polyclonal anti-mouse LYVE-1 antibody was added and incubation was continued overnight after switching to 4°C, and Alexa Fluor 488 donkey anti-goat IgG (Invitrogen) were added and processed as above. The samples were mounted with the ProLong Gold anti-fade reagent (Invitrogen). Matrigel plugs

and breast tumor tissues were fixed in 4% formalin fixative solution for 16 h and sent to a commercial vendor (Covance Inc., Princeton, NJ) to probe with CD34 and LYVE-1 antibodies, assessing blood vessels and lymphatic vessels. MECA-79, CD34 and LYVE-1 were analyzed using the FRiDA software (Johns Hopkins University, Baltimore, MD) and ImageJ (National Institutes of Health, Bethesda, MD), measuring the pixel intensity/4X frame of randomly selected 12 images in each group. Images shown are magnified to 10X or 20X to visually show greater surface area, and the fluorescent images from the LN were merged, using the ImageJ software.

7.2.11 Histopathology

Hematoxylin and Eosin (H & E) staining was carried out on lungs, liver, spleen, and kidney of animals that are treated with vehicle (PBS) or SP5031 for 27 days, assessing peptide toxicity in the animals. Lungs, liver, spleen, and kidney were harvested, rinsed with DPBS, and fixed in 4% formalin for 16 h at room temperature. The organs were placed in 30% sucrose solution in DPBS, incubated overnight at 4°C, and frozen in the Tissue-Tek Optimal Cutting Temperature (O.C.T.) compound. Sections of 10-μm thickness were cut at -20°C. The sections were rehydrated in PBS for 5 min (X3) and immersed in the filtered 0.1% Mayer's Hematoxylin solution (Sigma Aldrich) for 10 min. Then, the slides were rinsed with tap water for 5 min. Next, the stained sections were co-stained with Eosin by immersing the slides in 0.5% Eosin Y solution (Sigma Aldrich) for 1 min. The slides were dipped in distilled water 10 times (X10). The sections were dehydrated in ascending ethanol (EtOH) solutions: 50% EtOH X10 dips, 70% EtOH X10 dips, 30 sec incubation in 95% EtOH, and 1 min incubation in 100% EtOH. The slides were rinsed with xylene two times. The slide was mounted with mounting media (50% Glycerin), and covered

with a slide glass. The slides were observed by using Olympus BX51TF with DP70 color camera (Olympus, Japan).

7.2.12 Phospho-Receptor Tyrosine Kinase (p-RTK) proteome analysis

A Proteome Profiler Antibody Arrays Kit for human p-RTK (R&D systems) was used to determine which of the RTKs that are phosphorylated in the presence of TCM phosphorylation were inhibited by SP5031. Briefly, 2 X 10^6 LEC treated with or without 50 μM SP5031 for 90 min, were stimulated by TCM (3X-concentrated) for 10 min at 37˚C. To prepare the concentrated-TCM (3X), 3.6 ml of RPMI serum-free media and 20 X 10^6 cancer cells in plates were used: other conditions were the same as the protocol for preparation of TCM described above. Treatments were stopped by adding cold PBS, the cells were lysed in cold lysis buffer (150 mM NaCl, 1 mM EDTA, 100 μl/ml protease inhibitors (Sigma Aldrich), 10 μl/ml phosphatase inhibitors (Sigma) and 1% Triton X-100) for 2 h at 4˚C, and then scraped to collect the lysates. Cell lysates were spun at 14,000 g for 15 min to remove cell debris. Array membranes were blocked with blocking buffer provided in the kit. Cell lysate was mixed with dilution buffer, the prepared sample was added to the blocked membrane, and the membrane was incubated overnight at 4˚C. After three rinses, anti-phospho-tyrosine-HRP detection antibody (diluted by 1:2000 with dilution buffer in the kit) was added, and the antibody-bound streptavidin-HRP complex was detected by using a chemiluminescence detection reagent (GE Healthcare, United Kingdom).

7.2.13 Western blot assay

HUVEC, MEC and LEC were grown in complete growth media and plated on tissue culture-treated 6-well plates at 400,000 cells/well in CM. Cells were starved in serum-free media for 24

h after which SP5031 was added for 90 min. VEGFA (20 ng/ml) or VEGFC (100 ng/ml) was added and the incubation was continued for 10 min at 37˚C. Treatments were stopped by adding cold PBS and cell lysates were prepared as described above. Cell lysates were separated by SDS-PAGE and transferred to nitrocellulose blots (Invitrogen, Carlsbad, CA). Membranes were blocked for 1 h with 5% non-fat milk + 1% BSA in TBST and probed with antibodies of interest including pVEGFR2 (Y1175), VEGFR2, pMKK3/6 (S189/S207), pp38MAPK (T180/Y182), p-MAPKAPK2 (T334), pHSP27 (S82), pSrc (Y416), Src, GAPDH (Cell Signaling Technology, Inc.) and 4G10 pan-tyrosine phosphorylation antibody (Santa Cruz Biotechnology, Inc., Santa Cruz, CA). GAPDH was used as a loading control. Secondary antibodies were added at 1:2000 dilution and protein bands detected with a chemiluminescence detection reagent (GE Healthcare).

7.2.14 Sulfo-SBED crosslinking assay

A crosslinking strategy with Sulfo-SBED crosslinking reagent was used to identify target receptors of SP5031 on BEC and LEC. A Sulfo-SBED Biotin Label Transfer Reagent (Thermo Scientific Inc., Rockford, IL) has three functional groups, including an amine-reactive NHS-ester group, a UV-activatable aryl azide group and a biotin group. The peptide was reacted with Sulfo-SBED at ratio of 1 to 3 in PBS at room temperature for 2 h, in the dark. After the reaction, unreacted Sulfo-SBED was quenched with excess Tris-HCl. HUVEC or LEC were rapidly gathered from cell culture plates, using a non-enzymatic cell dissociation reagent (Sigma-Aldrich), and rinsed with PBS to remove serum proteins on the cell surface. 15 μM probe-conjugated peptide (30 μl) was added to 1 X 10^7 HUVEC or LEC in 1 ml PBS in a 24-well plate and the mixture was incubated at room temperature for 1 h on a rocker. The 24-well plate was exposed in UV (365 nm) without a lid for 15 min. UV-exposed cells were rinsed with 1 ml cold PBS twice (centrifuged at 3,000 rpm, 4°C for 5 min) to remove unreacted probes and dead cells.

The rinsed cells were resuspended in 500 µl cell lysis buffer, incubated in an ice bath for 1 h, with vortexing every 20 min. 15 µl streptavidin sepharose bead (Cell Signaling Technologies) was added in the cell lysates, and the mixture was incubated at 4°C for 2 h. Beads were rinsed 3 times with 500 µl lysis buffer. The beads were collected by a brief spin in a microfuge tube. The collected beads were boiled for 10 min with sample reducing buffer (4X). The reduced sample was centrifuged at 14,000 g for 15 min, and the supernatant was separated by SDS-PAGE, and probed with anti-biotin, anti-NRP1, anti-NRP2, anti-CD44, anti-VEGFR-2, and anti-VEGFR3 (Cell signaling technologies). For competition assays, 10x molar excess of unlabeled-SP5031 or 10x unlabeled-SP5002 was added in the wells containing LEC/BEC and the SP5031-probe. After the same crosslinking process as above, LEC or BEC cell lysates were immunoprecipitated with anti-NRP1 or anti-NRP2 (Cell signaling technologies) antibodies plus Protein A/G Plus Agarose (Santa Cruz Biotechnologies) as above, the immunoprecipitated proteins were separated, and probed with anti-biotin (HRP-linked) antibodies.

7.2.15 Co-immunoprecipitation

Co-immunoprecipitation (co-IP) was performed to investigate molecular interaction between NRP1 and VEGFR2 in HUVEC or between NRP2 and VEGFR3 in LEC. To optimize conditions for co-IP, cell lysis buffers with different ionic strengths and detergents (50, 100 and 150 mM NaCl; 0.1 and 1% Triton X-100) were tested in VEGFA-induced VEGFR2-NRP1 complex formation in HUVEC lysates. To determine SP5031 activity, 4 X 10^6 HUVEC or 1.2 X 10^7 LEC was treated with SP5031 for 90 min followed by induction with VEGFA (40 ng/ml) or VEGFC (100 ng/ml). Optimized cell lysis buffer (50 mM NaCl, 20 mM Tris HCl, 1 mM EDTA, 100 µl/ml Protease Inhibitors (Sigma, St. Louis, MO), 10 µl/ml Phosphatase inhibitors (Sigma) and 1% Triton X-100 (Sigma)) was used to conserve the receptor complex. 500 µl cell lysates were

incubated overnight at 4°C with antibodies suitable for IP: rabbit anti-VEGFR-2 antibody; rabbit anti-NRP1 antibody; rabbit anti-NRP2 antibody (Cell Signaling Technology, Inc.); mouse anti-VEGFR3 (EMD Millipore, Billerica, MA). Protein A/G Plus Agarose (Santa Cruz Biotechnologies) was added and the tubes rocked for 3 h at 4°C. The beads were rinsed 3 times with 500 µl cell lysis buffer and the protein complex was reduced and separated by SDS-PAGE and probed with the following antibodies: mouse anti-NRP1, mouse anti-VEGFR2 (R&D Systems), mouse anti-NRP2, rabbit anti-NRP2, rabbit anti-VEGFR3 (Cell Signaling Technology), and mouse anti-VEGFR3 (EMD Millipore).

7.2.16 Statistical analysis

Error bars correspond to SEM, unless otherwise stated. Differences between a control and a peptide treated group are regarded as significant when P is less than 0.05 using the Student's t-test.

7.3 RESULTS

7.3.1 SP5031 blocks migration, adhesion, and tube formation of LEC and BEC in tumor-conditioned media (TCM)

The Real-Time Cell Analysis (RTCA) system was used to measure TCM-induced migration and adhesion of lymphatic and blood endothelial cells (LEC and BEC) with or without SP5031. SP5031 peptide significantly inhibited TCM-induced migration of LEC and BEC. TCM contains multiple angiogenesis-related factors as will be presented below. 50 μM SP5031 inhibited LEC migration by 83.5% ($P < 0.01$), and BEC migration by 56.0% from control (Figure 7.1.B, C). SP5031 also inhibited LEC adhesion (30.0% inhibition with 10 μM SP5031; 61.0% inhibition with 50 μM SP5031), and BEC adhesion (17.2% inhibition with 10 μM SP5031; 42.4% inhibition with 50 μM SP5031) (Figure 7.1.D, E). SP5031 limited TCM-induced LEC tube formation (33.5% inhibition with 10 μM SP5031; 93.0% inhibition with 50 μM SP5031, $P < 0.01$), also inhibited TCM-induced BEC tube formation (32.2% inhibition with 10 μM SP5031; 58.0% inhibition with 50 μM SP5031, $P < 0.05$) (Figure 7.1.F, G).

7.3.2 SP5031 exhibits anti-lymphangiogenic and anti-angiogenic activity in MDA-MB-231 tumor xenografts

Next the activity of SP5031 was examined in an MDA-MB-231 orthotopic xenograft model. SP5031 (15 mg/kg) administered i.p. daily delayed tumor growth compared to a PBS-treated control group. At the end of the experiment, the SP5031-treated group showed 51.0% less tumor growth than the control group ($P < 0.05$) (Figure 7.2.A). Immunostaining with mouse anti-CD34 and mouse anti-LYVE-1 demonstrated that SP5031 blocked formation of stromal blood and lymphatic vessels in both intratumoral and peritumoral areas (Figure 7.2.D). There were 35.7%

fewer blood vessels and 62.0% fewer lymphatic vessels ($P < 0.05$) in tumor tissues from animals treated with SP5031 (Figure 7.2.B, C).

7.3.3 SP5031 shows anti-lymphangiogenic and anti-angiogenic activity in tumor-conditioned regional LN

A tumor-conditioned regional lymph node (LN) model was developed by injecting TCM subcutaneously into animals for 14 days to simulate the conditioning of tumor-draining LN by primary tumor-secreted factors which are transported to the LN through lymphatic vessels (Mumprecht and Detmar 2009; Duong, Koopman et al. 2012). The axillary and brachial LN of TCM-treated animals were 2-3 times larger than those of serum-free media (SFM)-treated animals. Next SP5031 was coadministered in TCM-treated animals. The SP5031-treated group showed significant normalization of the LN volume ($P < 0.05$) (Figure 7.3.A, B). Anti-mouse LYVE-1, and anti-mouse MECA-79 antibodies were used to detect lymphatic vessels (LV), and high endothelial venules (HEV, lymph node-specific vascular endothelium) in the LN. TCM treatment enhanced lymphatic vessel density (LVD) by 87.7% in axillary LN and by 66.0% in brachial LN, and blood vessel density (BVD) by 101.0% in axillary LN and by 98.2% in brachial LN. SP5031 normalized both TCM-enhanced LVD and BVD significantly ($P < 0.05$) (Figure 7.3.C, D). These results demonstrate that SP5031 blocks both LN lymphangiogenesis and LN angiogenesis in tumor-conditioned axillary and brachial LN.

7.3.4 SP5031 blocks TCM-induced VEGFR2 phosphorylation

The pro-angiogenic and pro-lymphangiogenic factors present in TCM were determined using Proteome Profiler Human Angiogenesis Array kits. MDA-MB-231 cells expressed pro-angiogenic factors, including Angiogenin, chemokine ligand 16 (CXCL16), heparin-binding

EGF-like growth factor (HB-EGF), matrix metalloproteinase 8 and 9 (MMP-8/9), PDGF-AA, Endothelin-1, interleukin 8 (IL-8), vascular endothelial growth factor A (VEGFA), and placental growth factor (PlGF). Interestingly, TCM contained anti-angiogenic factors as well, including Serpin E1, Serpin F1, tissue inhibitor of metalloproteinase 1 (TIMP-1), and thrombospondin 1 (TSP-1). However, a well-known lymphangiogenic factor, VEGFC was not detected in TCM (Figure 7.4.A). Two million LEC pre-treated with or without 50 μM SP5031 were stimulated by TCM. Lysates from these LEC were analyzed by phospho-RTK Proteome Array kits to determine the phosphorylation status of multiple receptor tyrosine kinases. SP5031 specifically inhibited the phosphorylation of VEGFR2 by 87.0% compared to control, however, phosphorylation of VEGFR1 was not influenced by peptide treatment (Figure 7.4.B, C). Thus the inhibition of VEGFR2 phosphorylation by SP5031 must be a result of activity against the VEGFA that is present in TCM (Figure 7.4.A).

7.3.5 SP5031 exhibits anti-lymphangiogenic and anti-angiogenic activity in Matrigel plug assays

Next, matrigel plugs containing VEGFA with or without SP5031 were implanted into athymic nude mice (Figure 7.4.D). bFGF and heparin were additionally included in the matrigel plugs, as bFGF supports survival of endothelial cells, and heparin enhances the interaction between VEGFA and VEGFR2. After 10 days, plugs containing VEGFA, bFGF, and heparin (positive control group) showed pronounced angiogenesis which SP5031 significantly inhibited: CD34-positve area was decreased by 74.0% compared to the growth factor-treated control group (Figs. 4D and 4F). LYVE-1, a marker for lymphatic vessels (LV) was used to measure VEGFA induced lymphangiogenesis in the plugs (Hirakawa, Kodama et al. 2005). SP5031 inhibited LV by 65.4% compared to the control (Figure 7.4.E, G). These results demonstrate that the anti-

lymphangiogenic and anti-angiogenic activities of SP5031 are achieved by targeting VEGFA in the plugs.

7.3.6 SP5031 inhibits VEGFA/C-dependent VEGFR2/3 signals, resulting in inhibition of activation of downstream proteins

Given the result that SP5031 blocks the phosphorylation of VEGFR2 experiments were expanded to test for its effect on phosphorylation of VEGFR3 on LEC. VEGFR3, which is activated by VEGFC, is one of the major receptors for lymphangiogenic signaling on LEC. SP5031 on LEC and BEC stimulated by VEGFC or VEGFA was tested separately (Figure 7.6). As shown in Figure 7.6, SP5031 potently inhibited VEGFA-induced phosphorylation of VEGFR2, FAK, MKK3/6, p38MAPK, MAPKAPK2 and HSP27 in BEC (HUVEC and MEC). VEGFC-dependent phosphorylation of VEGFR3, VEGFR2 and FAK in LEC were also blocked by SP5031 (Figure 7.6.B). This result was confirmed in a VEGFC-induced LEC migration assay in which 50 μM SP5031 inhibited LEC migration by 80.0% ($P < 0.05$) (Figure 7.6.C). These results demonstrate that SP5031 inhibits the phosphorylation of VEGFR2, VEGFR3, and downstream proteins on LEC and BEC.

7.3.7 Neuropilin 1/2 are the target receptors of SP5031

A crosslinking strategy was used to identify potential receptors of SP5031. SP5031 was conjugated to the trivalent Sulfo-SBED biotin-carrying reagent (Figure 7.5). The conjugated SP5031-Sulfo-SBED (SP5031-probe) was applied to BEC or LEC followed by exposure to UV light to allow crosslinking to occur. Given that SP5031 inhibits VEGFR2 and VEGFR3 phosphorylation, we asked whether target proteins could be NRP1, NRP2, CD44, VEGFR2 or VEGFR3 in immunoblotting experiments using the corresponding antibodies. NRP1 and NRP2

were suspected because of their role as co-receptors of VEGFA and VEGFC in activation of VEGFR2 and VEGFR3 respectively (Caunt, Mak et al. 2008; Kawamura, Li et al. 2008). CD44 was also suspected because of the role of CD44v3 and CD44v6 in endothelial cell migration and adhesion via VEGFR2 signaling in the presence of VEGFA (Forster-Horvath, Meszaros et al. 2004; Tremmel, Matzke et al. 2009). Surprisingly, NRP1 and NRP2 but not CD44 and VEGFR2/3 cross-linked to SP5031 on LEC and BEC (Figure 6.6.D). Next, co-immunoprecipitation (co-IP) experiments were performed with VEGFR2/3 and NRP1/2 antibodies in the presence of VEGFA/C with or without SP5031 as described previously (Caunt, Mak et al. 2008). It was shown that upon activation with VEGFA, VEGFR2 and NRP1 formed a receptor complex (Figure 7.6.E). SP5031 treatment hindered VEGFA-induced VEGFR2/NRP1 complex formation in BEC, and VEGFC-induced VEGFR3 and NRP2 complex formation in LEC (Figure 7.6.F, G). However, VEGFR2 and CD44 complex formation in BEC was not inhibited by SP5031 treatment consistent with the finding that CD44 is not a target receptor of SP5031 (Figure 7.7). These results demonstrate that the peptide binding to NRP1/2 hinders receptor complex formation between VEGFR2/3 and NRP1/2 which results in suppression of VEGFA/C signal transduction.

7.3.8 SP5002, a peptide homologous to SP5031, is inactive

A sham peptide, SP5002, which is homologous to wild type SP5031, was generated (Figure 7.8). In a previous screen of a number of somatotropin peptides on cell proliferation, migration and adhesion of LEC, MEC, and HUVEC, we discovered that SP5001 (amino acid sequence: RLRLLTLQSWLL-NH_2) had anti-proliferative but no anti-migratory activity (Figure 7.8.B) (Lee, Rosca et al. 2011). An alanine scan of SP5001 was performed to determine the amino acids that are crucial for its anti-proliferative activity. SP5002, SP5003, SP5005, SP5006, and SP5011

did not inhibit LEC proliferation (Figure 7.8.A). Among them, SP5002 has a nearly identical isoelectric point (p.I. = 9.75) to SP5031 (Figure 7.8.C), suggesting that the overall surface charge and peptide solubility of SP5002 are comparable to those of SP5031 under the same experimental conditions. First, the effect of SP5002 and SP5031 on TCM-induced migration of LEC and BEC was evaluated. Even at 50 μM, SP5002 did not significantly inhibit migration of either cell type. SP5031 potently inhibited migration of both cell types under the same conditions (Figure 7.8.E, F). Next, SP5002 did not significantly inhibit VEGFA-induced phosphorylation of VEGFR2 on BEC and VEGFC-induced phosphorylation of VEGFR3 on LEC (Figure 7.8.G, H). SP5002 also did not hinder VEGFC-induced complex formation between VEGFR3 and NRP2 unlike SP5031 (Figure 7.8.I). A crosslinking experiment in the presence of excess peptide as a competitor was performed with the SP5002-probe and the SP5031-probe (Figure 7.8.D). SP5031-probe was efficiently crosslinked to NRP1 (120, 80 kDa), and NRP2 (130 kDa) on BEC and LEC (Figure 7.8.D, lane 1). When unconjugated SP5031 at a 10-fold excess to SP5031-probe was included in the crosslinking assay, crosslinking of SP5031-probe to the target receptors was significantly reduced (Figure 7.8.D, lane 2). These results demonstrate specific binding of SP5031 to these target receptors. SP5002-probe showed no binding to NRP1, and NRP2 in BEC and LEC (Figure 7.8.D, lane 3). Very importantly in a competition assay a 10-fold excess of SP5002 was not able to compete for binding to receptors of SP5031 (Figure 7.8.D, lane 4). These results demonstrate that the activity of SP5031 is not because of nonspecific binding due to its overall surface charge but because of sequence specific interactions with the target receptors.

7.4 DISCUSSION

Most malignant tumors exploit adaptive-evasive responses to the VEGF monoclonal antibody (bevacizumab) by switching their dependence to alternative pro-angiogenic signals and enhancement of distant metastasis mediated by lymphatics (Paez-Ribes, Allen et al. 2009; Kerbel 2011). Sunitinib, a multi-targeted tyrosine kinase inhibitor (TKI), however, exhibited anti-angiogenic activity and allowed less lymphatic metastasis, as it targets both angiogenesis and lymphangiogenesis by inhibiting a large number of receptor tyrosine kinases, including the VEGF receptors and platelet-derived growth factor receptors (PDGFRs) (Kodera, Katanasaka et al. 2011). In addition to those receptors, sunitinib blocks more than 70 tyrosine kinases with other activities, which are thought to lead to several side-effects (e.g., hand-foot syndrome, stomatitis, hypothyroidism, and dermatologic toxicities) (Karaman, Herrgard et al. 2008). The two different examples discussed above (bevacizumab and sunitinib) suggest that single-target drugs are inadequate as therapeutics and also that agents that inhibit multiple common targets such as tyrosine kinases or GPCRs are problematic as effective therapeutics because of toxicity. However, SP5031 is expected to be an effective cancer therapeutic because it inhibits angiogenesis and lymphangiogenesis, two of the primary drivers of tumor growth and metastasis, highly specifically, thus minimal toxicity is expected.

In terms of cytotoxicity of SP5031, apoptotic and cytotoxic activities of SP5031 were previously evaluated, using caspase-3/7 and lactate dehydrogenase tests (Lee, Rosca et al. 2011). In this study, no cytotoxicity or apoptosis was observed at 1, 10, 100 μM of SP5031 in HUVEC, microvascular endothelial cells (MEC), and LEC. After treating with SP5031 for 27 days, mouse organs, including lungs, liver, spleen, and kidney were harvested for H&E staining (Figure 7.9). Any significant changes were observed in SP5031-treated groups and vehicle (PBS)-treated

group. We hypothesized that SP5031 which is primarily blocking cell migration and adhesion, but not proliferation, may have advantage over cell death-inducing conventional chemotherapeutics.

In this study, SP5031 selectively suppressed VEGFC/VEGFA-induced VEGFR3/VEGFR2 signaling pathways by targeting NRP2 and NRP1 on LEC and BEC. VEGFC-dependent VEGFR3 activation is a major pro-lymphangiogenic signal in LEC (Hirakawa, Kodama et al. 2005). In addition, VEGFR2 is a validated target for VEGFA-dependent angiogenesis and lymphangiogenesis (Hirakawa, Kodama et al. 2005). Thus, SP5031 has the potential to simultaneously inhibit lymphangiogenesis and angiogenesis. Recent studies with combination therapies, blocking both lymphangiogenesis and angiogenesis have shown better outcomes in several experimental models. Targeting COX-2 and prostaglandin E receptors (EPs) decreased angiogenesis and lymphangiogenesis, improving overall survival rates in breast tumor xenograft models (Xin, Majumder et al. 2012). A combination therapy with short interfering RNAs (siRNAs) against VEGFC and VEGFA suppressed lymphogenous as well as hematogenous metastasis in mammary tumor models (Shibata, Morimoto et al. 2008). Bevacizumab combined with a genetic blockade of insulin-like growth factor 1 (IGF-1) reduced angiogenesis and lymphangiogenesis in gastric cancer models (Li, Adachi et al. 2011). Accordingly, multi-targeted anti-lymphangiogenic and anti-angiogenic agents have a potential to generate better therapeutics to efficiently inhibit tumor progression and metastasis. To our knowledge, this is the first study targeting tumor-induced lymphangiogenesis and angiogenesis with one short peptide. Previous studies utilized combination of two (or more) antibodies, genetic modifications, large proteins, and siRNAs (Shibata, Morimoto et al. 2008; Li, Adachi et al. 2011; Xin, Majumder et al. 2012).

The peptide needs to be further modified with sequence mutations for an improved in vivo stability as we discussed previously (Rosca, Koskimaki et al. 2011).

SP5031 activity in vivo was assessed in a breast tumor xenograft study. SP5031 slowed down tumor growth and blocked lymphangiogenesis and angiogenesis in peritumoral and intratumoral areas of primary tumors in MDA-MB-231 xenograft models (Figure 7.2). These results suggest that SP5031 could inhibit tumor cell dissemination via stromal lymphatic and blood vessels in addition to delaying primary tumor growth facilitated by blood vessels (Figure 7.10, the upper panel). In vivo activity of SP5031 was further investigated in tumor-conditioned regional LN (Figure 7.3). In this LN model, 2-3 times larger, more pro-angiogenic and pro-lymphangiogenic axillary and brachial LN were observed in TCM-treated animals. SP5031 treatment inhibited the increase in the LN volume and the lymphatic and blood vessel densities in the LN. As shown in Figure 7.10 (the upper panel), the inhibition of LN lymphangiogenesis by SP5031 could delay tumor invasion into the LN by limiting lymphatic flow (Mumprecht and Detmar 2009). At the same time, the inhibition of LN angiogenesis by SP5031 could block the conditioning of metastatic niches in the LN thus depriving tumor cells that may have metastasized to the LN of sufficient oxygen and nutrients (Carlini, De Lorenzo et al. 2011).

In the proposed mechanism of action of SP5031 (Figure 7.10, the lower panel), SP5031 blocks the activities of VEGFR2/3 by binding to NRP1/2. Recently, it have been reported that VEGFR2 is expressed on both blood endothelial cells and lymphatic endothelial cells, and blockade of VEGFR2 by SP5031 showed dual inhibition of LEC and BEC (Koskimaki, Lee et al. 2013). With the present data that SP5031 blocks VEGFR3 that are expressed predominantly on LEC, SP5031 mostly targets VEGFR2 via the binding to NRP1, and partially blocks VEGFR3 via NRP2. NRP1 and NRP2 have three common structural motifs: two CUB homology domains,

two coagulation factor V/VIII homology domains, and a MAM domain. In addition to having similar motifs, NRP1 and NRP2 share 44% amino acid sequence identity (Bagri, Tessier-Lavigne et al. 2009). Peptide binding to NRP1 and NRP2 blocks complex formation between VEGFR2 and NRP1 (on BEC), and VEGFR3 and NRP2 (on LEC) indirectly inhibiting signaling from VEGFR2 and VEGFR3 in the presence of VEGFA and VEGFC. NRP1/2-mediated inhibition of VEGFR2/3 suggests that SP5031 may synergize with the currently used VEGFA monoclonal antibody (bevacizumab), and the VEGFR2 monoclonal antibody, ramucirumab (Spratlin 2011). At the intracellular level (Figure 7.10, the lower panel), SP5031 inhibits focal adhesion kinase (FAK) and p38MAPK-related proteins. It is known that p38MAPK and HSP27 activate actin reorganization, inducing endothelial cell migration (Nguyen, Chen et al. 2004). FAK is central for focal adhesion turnover which is required for endothelial cell adhesion and migration. Thus, the anti-migratory and anti-adhesive activities of SP5031 can be explained by its inhibition of FAK and p38MAPK.

In summary, this chapter shows that SP5031 is capable of directly tuning lymphangiogenesis and angiogenesis via multi-modal inhibitory mechanisms to improve current anti-angiogenic strategies in cancer treatment.

7.5 FIGURES & TABLES

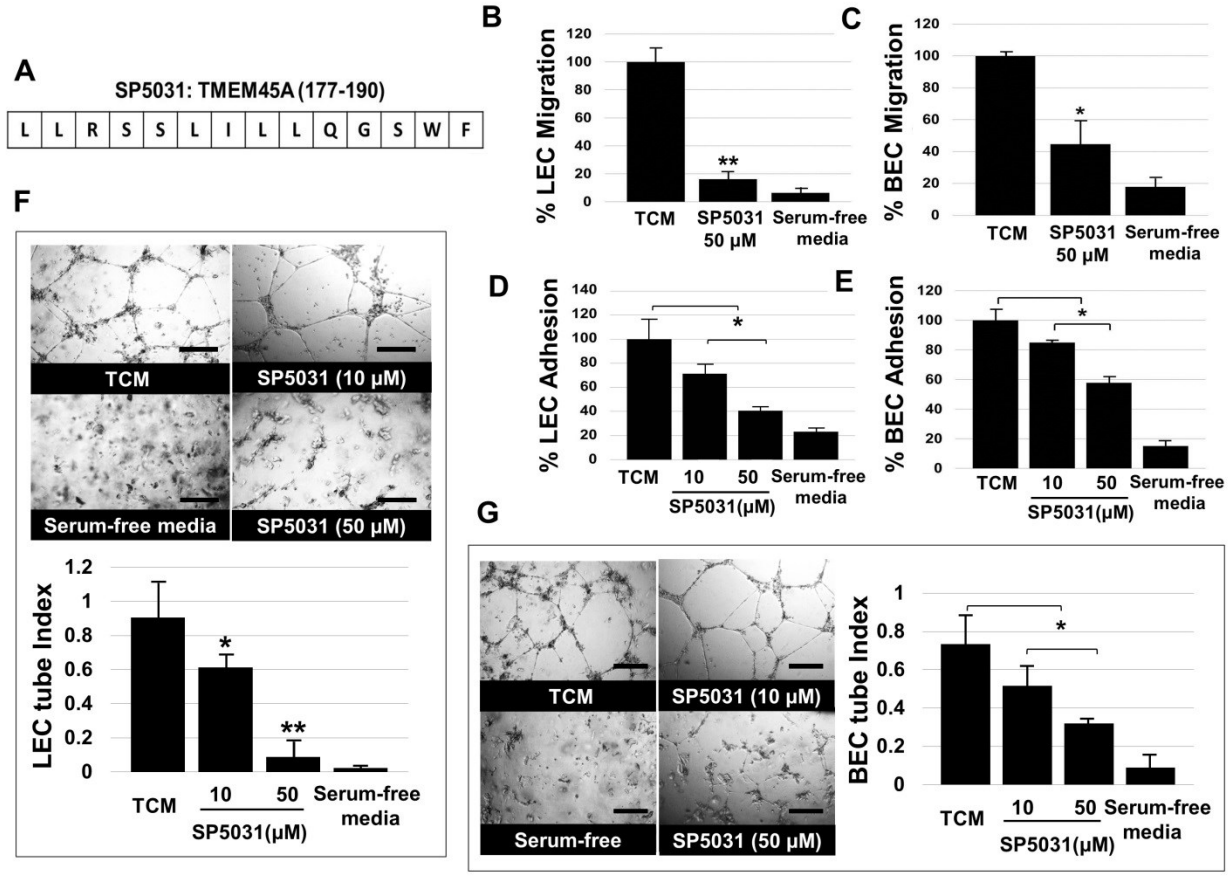

Figure 7.1: In vitro activity of SP5031 on LEC and BEC. (A) Amino acid sequence of the SP5031 peptide. (B) Percent LEC migration at 20 h. **P < 0.01 versus TCM-treated control. (C) Percent BEC migration (*P < 0.05). (D) Percent LEC adhesion (*P < 0.05). (E) Percent BEC adhesion (*P < 0.05). (F) SP5031 inhibits TCM-induced LEC tube formation. LEC tube index (S.CORE quantification) shows dose response of SP5031 (*P < 0.05 and **P < 0.01). S.CORE (S.CO Life Science, Germany) is a web based image analysis system(Lee, Rosca et al. 2011). Scale bars represent 200 µm. (G) BEC tube formation (*P < 0.05). Scale bars represent 200 µm.

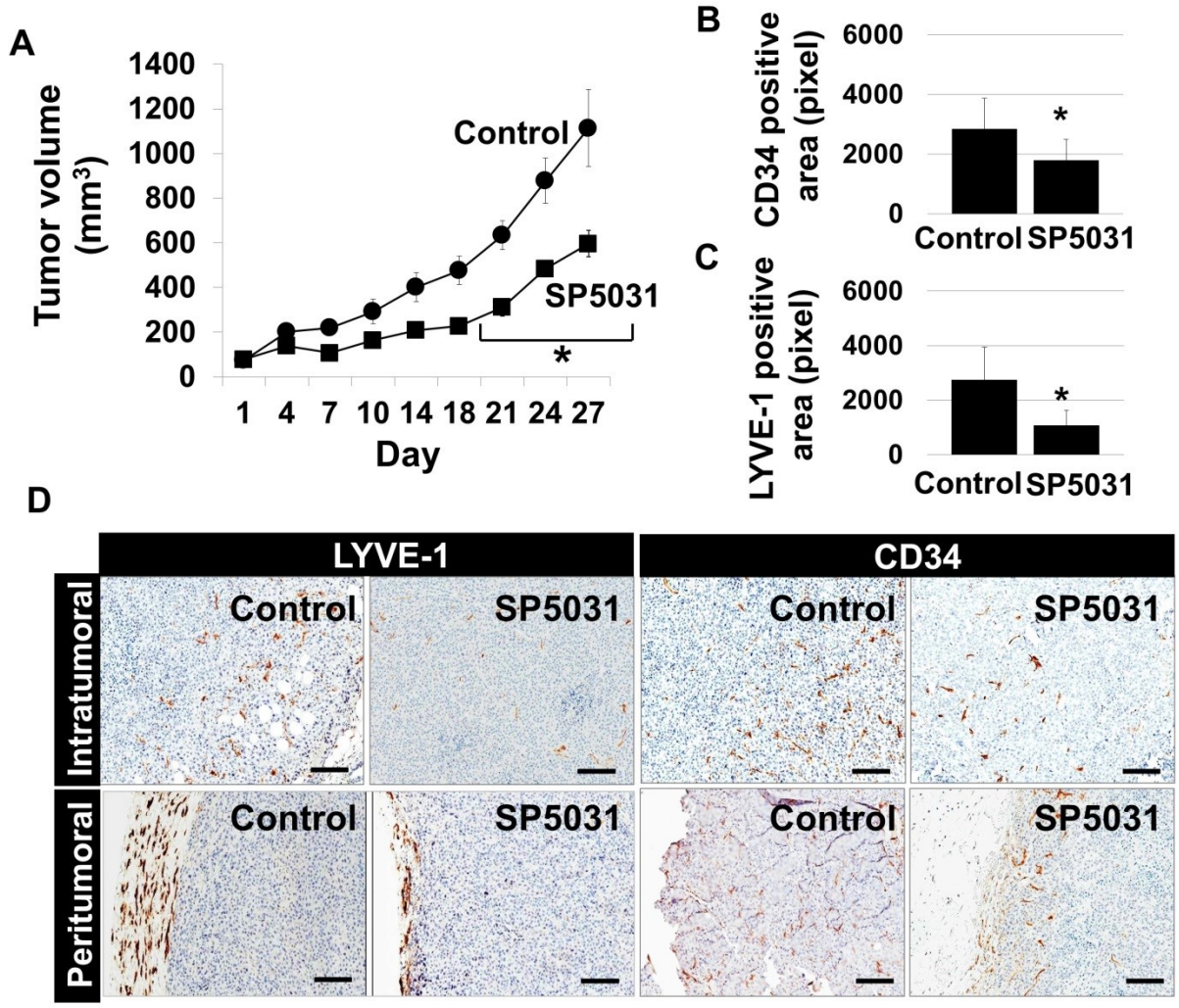

Figure 7.2: MDA-MB-231 xenografts with SP5031 treatment. SP5031 blocks lymphangiogenesis and angiogenesis in MDA-MB-231 xenografts. (A) Changes in tumor volume of the PBS or SP5031-treated groups. After day 21, SP5031 significantly delayed tumor growth compared to control (*$P < 0.05$). (B) Quantification of blood vessels in the tumors (*$P < 0.05$). (C) Quantification of lymphatic vessels (*$P < 0.05$). (D) Representative immunohistochemistry images from intratumoral and peritumoral regions of the tumor. Scale bars represent 100 μm.

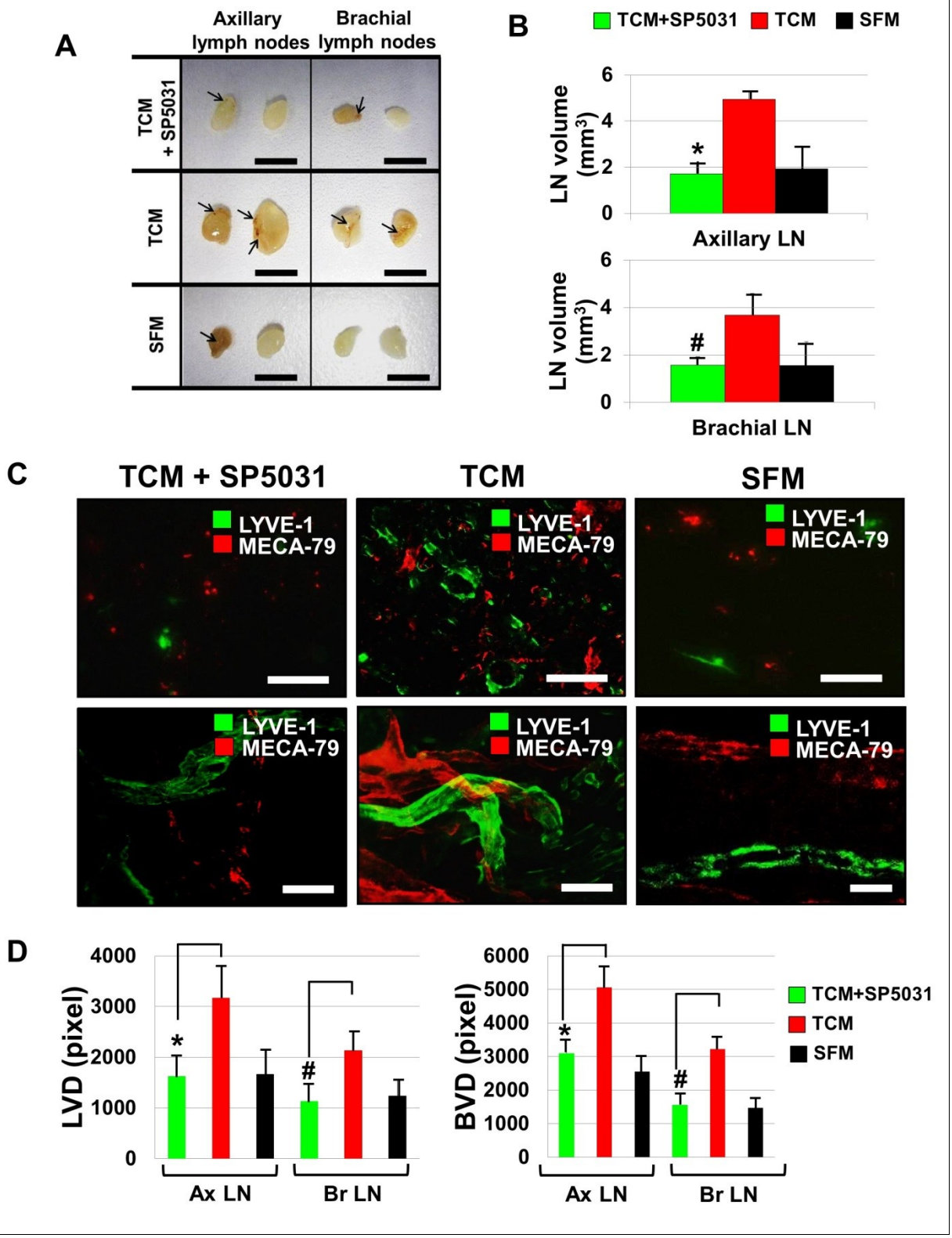
A
Axillary lymph nodes
Brachial lymph nodes
TCM + SP5031
TCM
SFM
B
TCM+SP5031
TCM
SFM
LN volume (mm3)
Axillary LN
Brachial LN
C
TCM + SP5031
TCM
SFM
LYVE-1
MECA-79
D
LVD (pixel)
BVD (pixel)
Ax LN
Br LN
TCM+SP5031
TCM
SFM

Figure 7.3: Tumor-conditioned regional lymph node (LN) models with SP5031 treatment. SP5031 inhibits lymphangiogenesis and angiogenesis in axillary and brachial LN induced by TCM treatment. (A) Representative images of axillary and brachial LN. Arrows represent macroscopically detectable blood vessels. Scale bars represent 3 mm. (B) LN from TCM-treated mice show an increase in LN volumes. SP5031 treatment normalized the volume of the LN. *$P < 0.05$, and $^{\#}P < 0.05$ versus the TCM-treated group. (C) Representative immunofluorescence images for lymphatic vessels (green), and high endothelial venules (Harrell, Dye et al.). Scale bars represent 100 μm. (D) Quantification of LVD, and BVD in LN. TCM enhances LVD by 87.7% in axillary LN (ax-LN), by 66.0% in brachial LN (br-LN); BVD by 101.0% in ax-LN, by 98.2% in br-LN. SP5031 treatment normalized the LVD and BVD in the LN in TCM treated animals significantly. *$P < 0.05$ (ax-LN), $^{\#}P < 0.05$ (br-LN) in LVD, and $^{*}P < 0.05$ (ax-LN), $^{\#}P < 0.05$ (br-LN) in BVD.

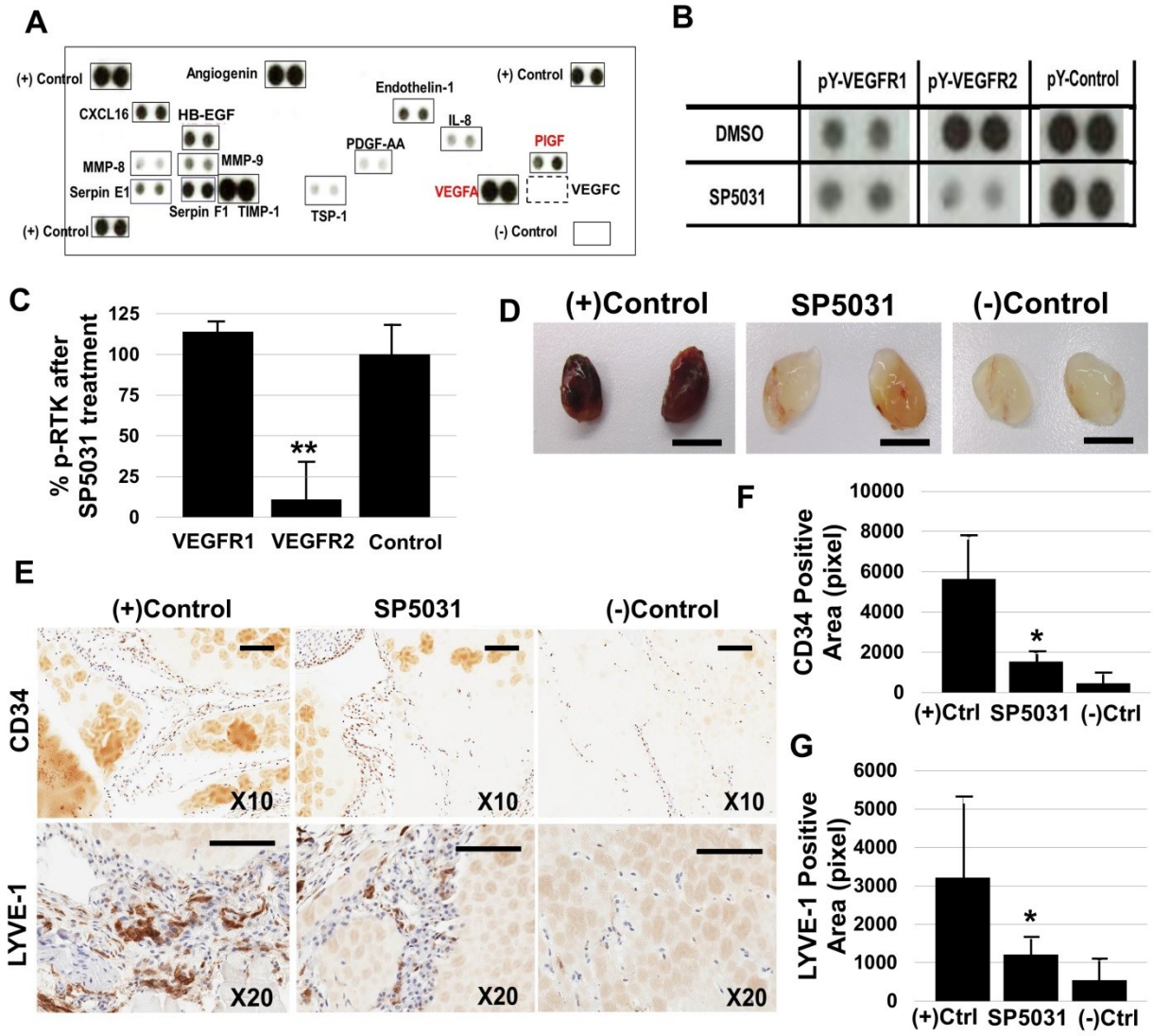

Figure 7.4: TCM-induced p-RTK analysis and VEGFA-induced Matrigel plug assays. (A) Angiogenesis factors in MDA-MB-231 tumor-conditioned media (TCM). (B) 50 μM SP5031 inhibits phosphorylation of VEGFR2, not VEGFR1. (C) Percent phospho-RTK after treatment with SP5031, compared to control. SP5031 treatment lowers the phosphorylation of VEGFR2. **P < 0.01 versus control. (D) Representative Matrigel plugs with VEGFA plus or minus SP5031. Scale bars represent 10 mm. (E) Representative immunohistochemistry images from the

Matrigel plugs. Images show that SP5031 treatment blocks VEGFA-induced angiogenesis (CD34), and lymphangiogenesis (LYVE-1) in vivo. Scale bars represent 100 μm. (F) Quantification of blood vessels in the plugs (*P < 0.05). (G) Quantification of lymphatic vessels in the plugs (*P < 0.05).

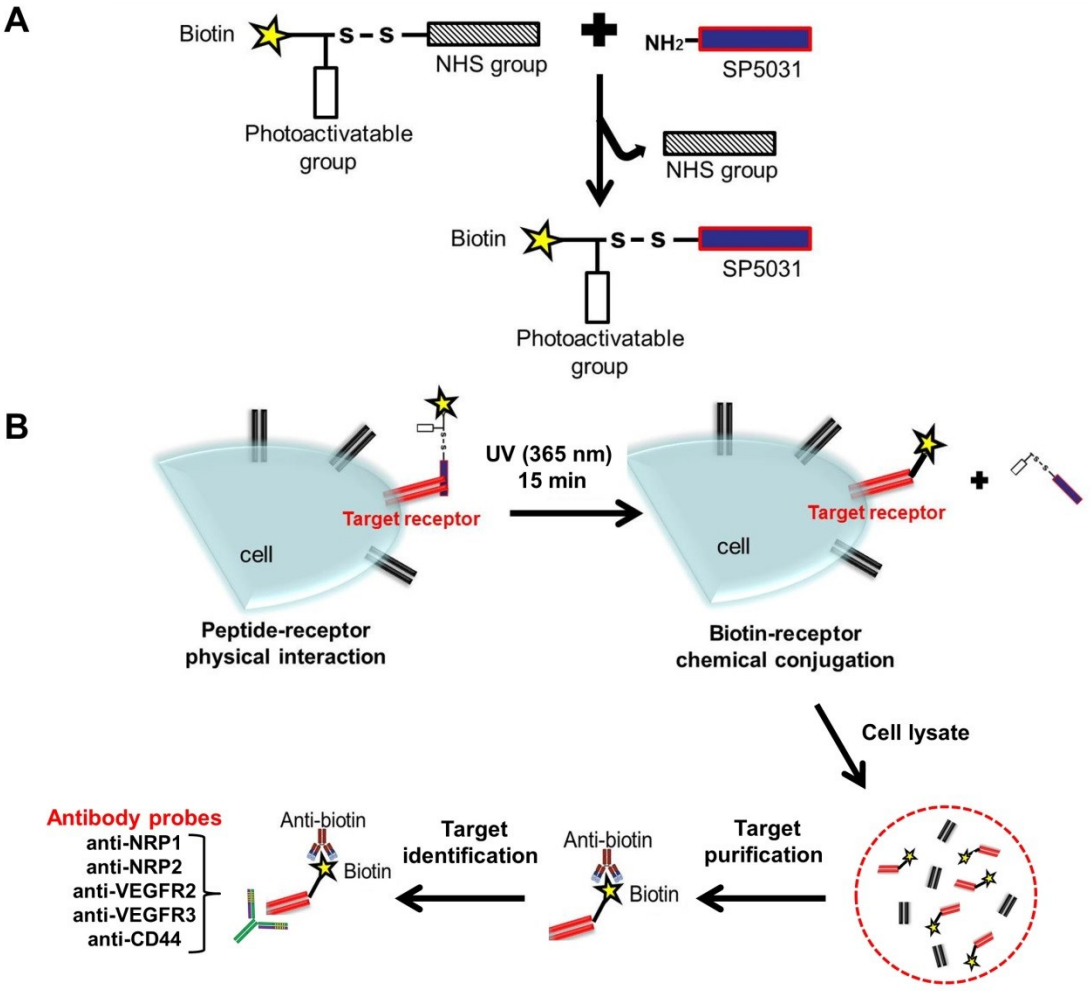

Figure 7.5: Sulfo-SBED crosslinking methodology. (A) A Sulfo-SBED Biotin Label Transfer Reagent (Thermo Scientific Inc., Rockford, IL) has three functional groups, including an amine-reactive NHS-ester group, a UV-activatable aryl azide group and a biotin group. The peptide was reacted with Sulfo-SBED in PBS at room temperature for 2 h, in the dark. (B) Probe-conjugated peptide was added to HUVEC or LEC in PBS in a 24-well plate and the plate was exposed in UV (365 nm) for 15 min. Then the biotin groups are reacted with target receptors, making

chemical bonds: the biotinylated target receptors were purified by using anti-biotin then probed by target receptor antibodies.

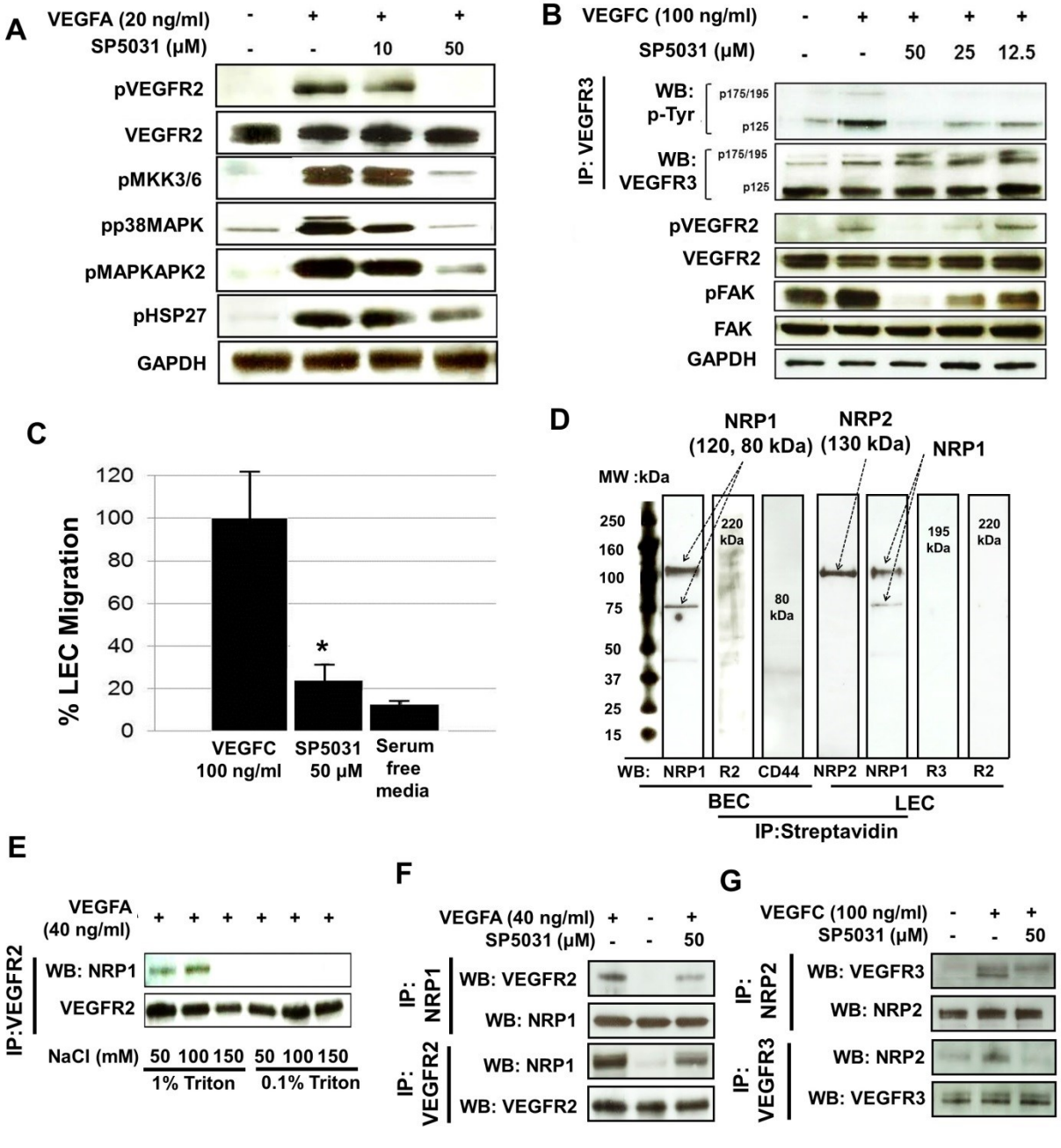

Figure 7.6: Inhibition of VEGFC and VEGFA signaling by SP5031 binding to NRP2 and NRP1. (A) SP5031 blocks VEGFA-induced phosphorylation of VEGFR2 (Y1175), and p38MAPK signaling proteins, including MKK3/6 (S189, S207), p38MAPK (T180, Y182), MAPKAPK2 (T334), and HSP27 (S82). (B) VEGFC-dependent phosphorylation of VEGFR3 (p-

Tyr), VEGFR2 (Y1175), and FAK (4G10) were inhibited by SP5031 in LEC. GAPDH levels were used to control for the amount of total proteins in all cases. (C) VEGFC-induced LEC migration with or without SP5031 (*$P < 0.05$). (D) Target receptors of SP5031 were identified by using a crosslinking strategy. Biotinylated (crosslinked) proteins are purified, and probed using antibodies: the biotinylated target proteins were found to be NRP1 (80, 120 kDa), and NRP2 (130 kDa). (E) Co-immunoprecipitation (co-IP) assays were performed to optimize complex formation between VEGFR2 and NRP1 in the presence of VEGFA. (F) Treatment with SP5031 hindered VEGFA-induced complex formation between NRP1 and VEGFR2 in HUVEC. (G) Treatment with SP5031 blocked VEGFC-induced complex formation between NRP2 and VEGFR3 in LEC.

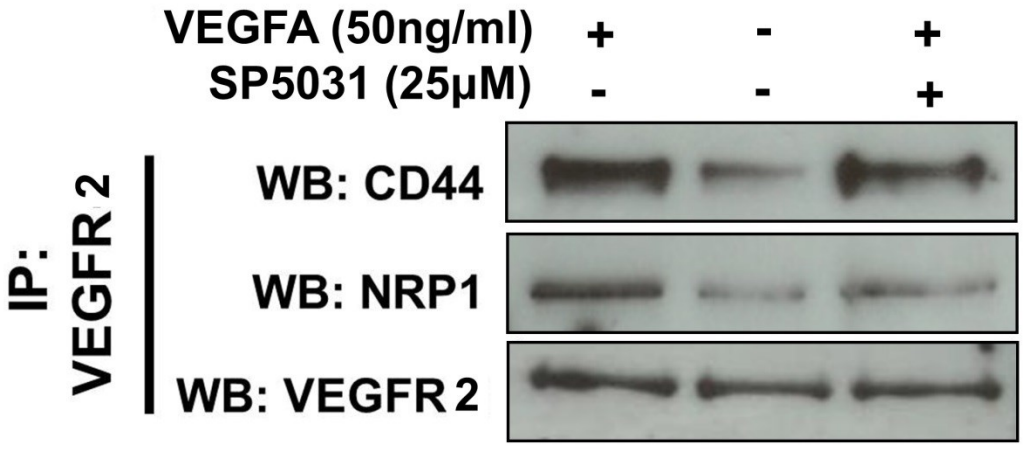

Figure 7.7: VEGFR2/CD44 or VEGR2/NRP1 complex formation with SP5031 treatment. VEGFA induces VEGFR2 and CD44 complex formation as well as VEGFR2 and NRP1 complex in HUVEC. SP5031 binds to NRP1 and dissociates the VEGFR2 and NRP1 complex formation. However, SP5031 does not inhibit VEGFR2 and CD44 complex formation, as SP5031 has no interaction with CD44.

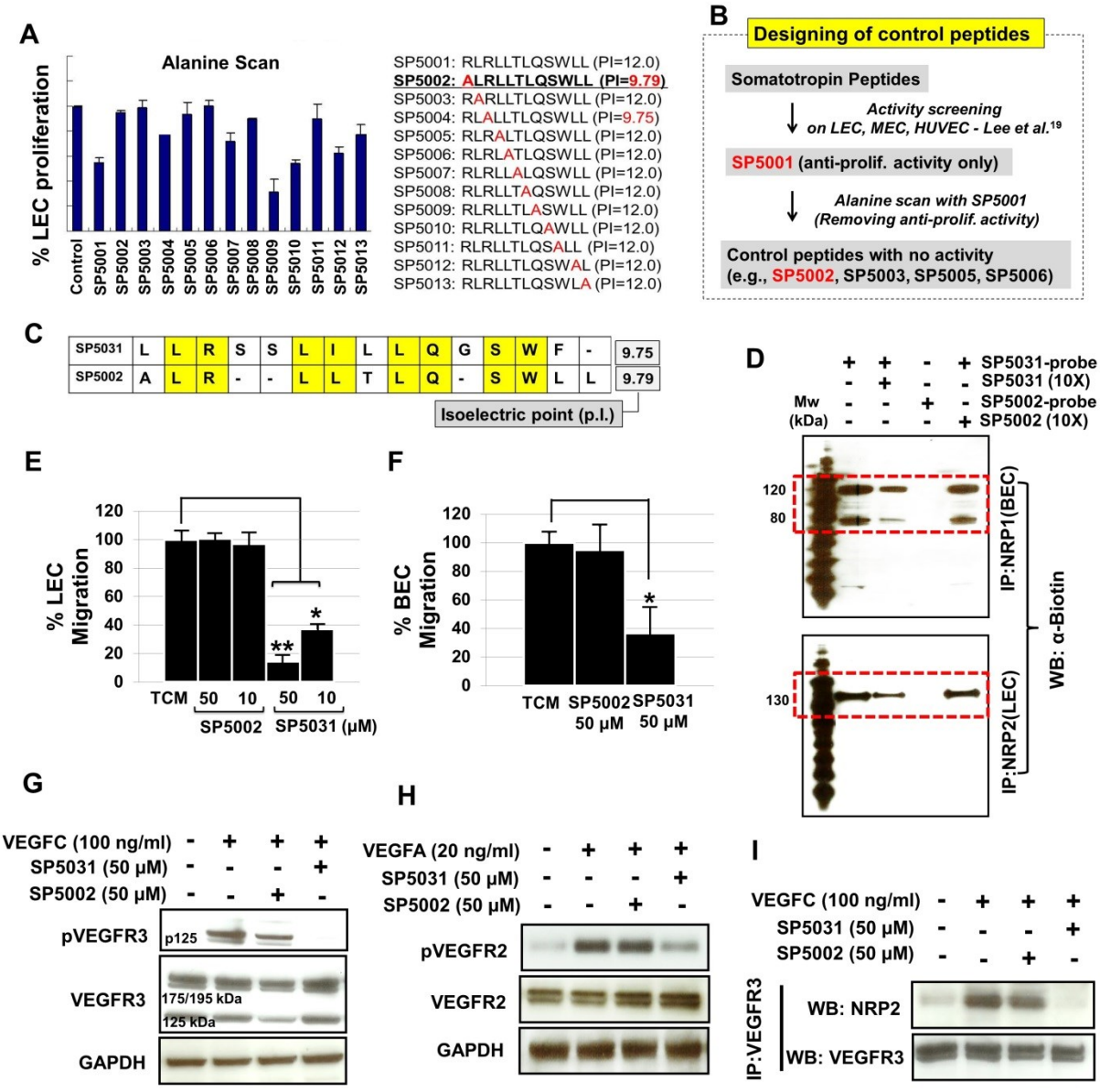

Figure 7.8: SP5031 binding to its receptors is specific. (A) Alanine scan of SP5001 to eliminate proliferation inhibitory activity of SP5001. (B) The flow chart for the identification of control peptides (C) Peptide sequence comparison between SP5031 and SP5002. (D) SP5031-probe bound to NRP1 and NRP2 on BEC and LEC (lane 1). Competition with 10X unlabeled-SP5031 lowered the amount of binding of SP5031-probe to its target receptors (lane 2). SP5002-probe did not bind to the same target receptors (lane 3). Competition with 10X unlabeled-

SP5002 did not hinder the binding of SP5031-probe to its target receptors (lane 4). (E) Percent LEC migration. SP5002 did not cause inhibition of LEC migration. However, SP5031 showed potent inhibition (*$P < 0.05$, and **$P < 0.01$). (F) Percent BEC migration (*$P < 0.05$). (G) VEGFC-induced phosphorylation of VEGFR3 was not significantly inhibited by SP5002 compared to SP5031. (H) VEGFA-induced phosphorylation of VEGFR2 was not inhibited by SP5002. (I) VEGFC-dependent complex formation between VEGFR3 and NRP2 was significantly dissociated by SP5031, however, not by SP5002.

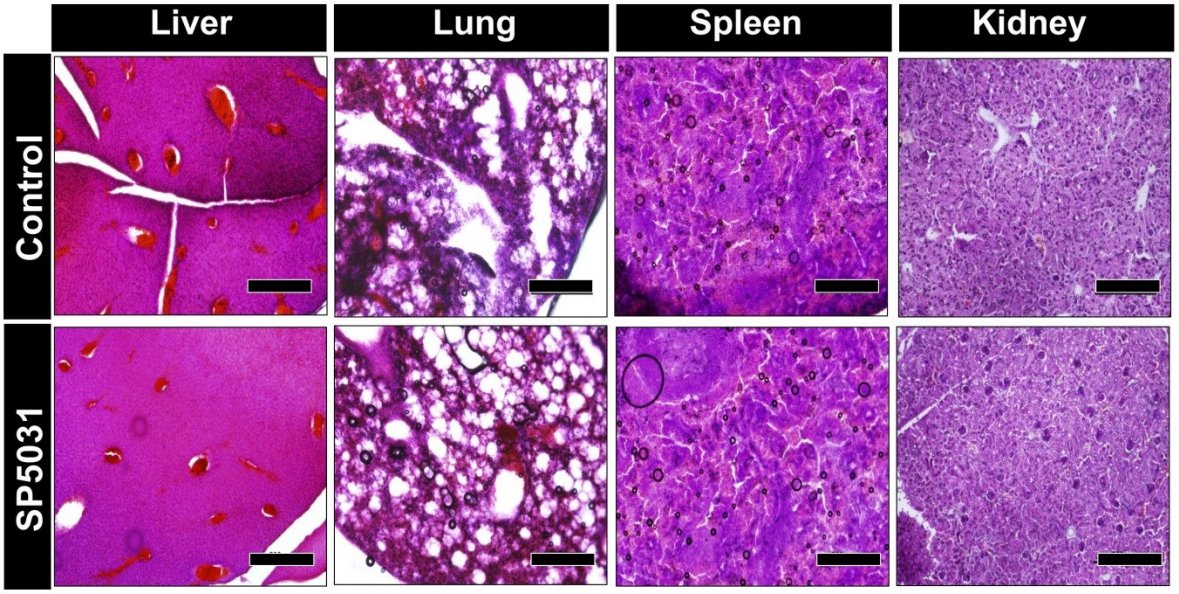

Figure 7.9: SP5031 is not toxic to normal tissues as seen by histopathology. Histopathological examination of liver, lung, spleen, and kidney was performed by H&E staining. No significant morphologic changes were seen in these organs from animals treated with SP5031, compared to the organs from the control group of animals. Scale bars represent 500 μm.

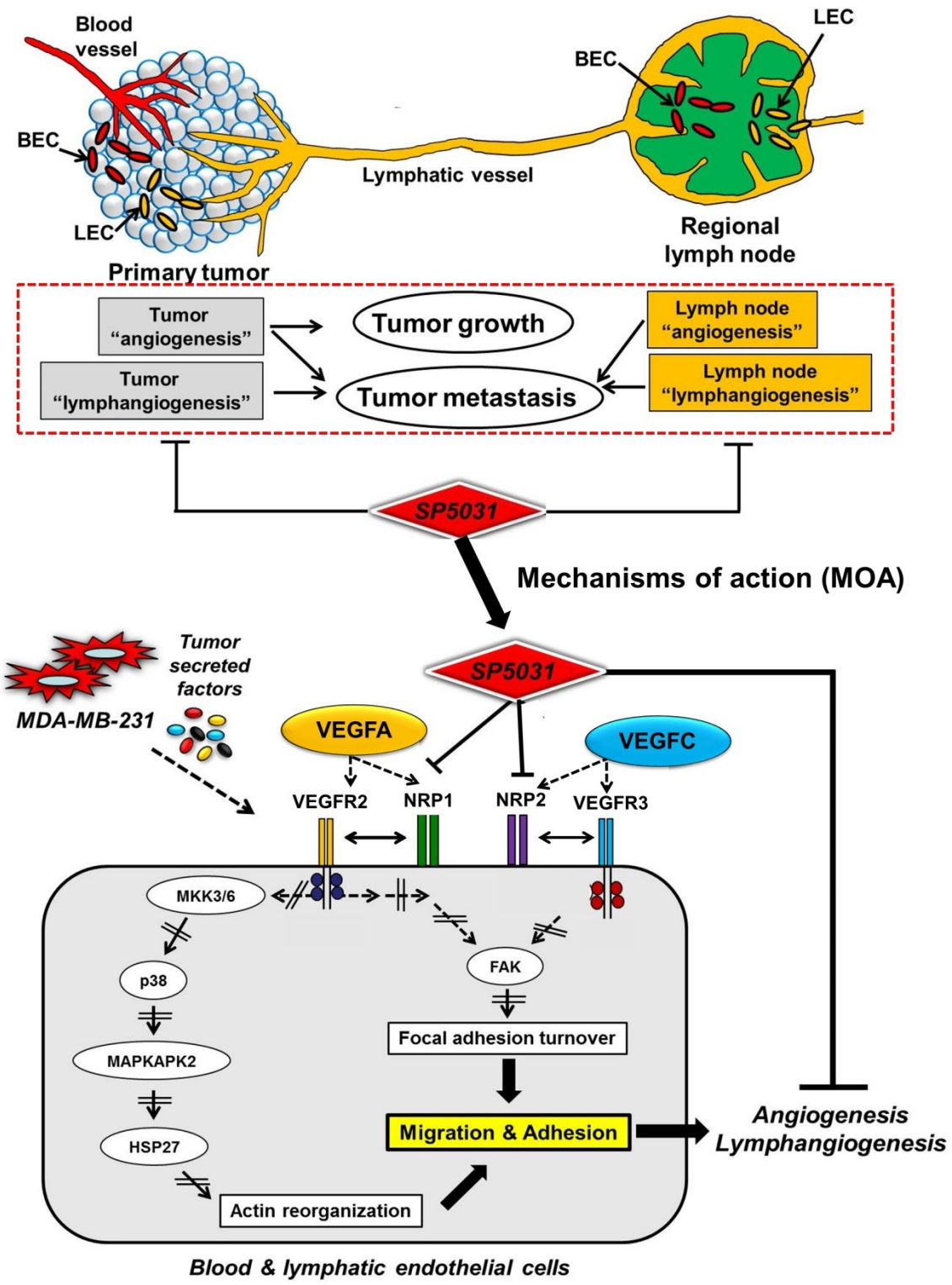
Blood vessel
BEC
LEC
Primary tumor
Lymphatic vessel
BEC
LEC
Regional lymph node
Tumor "angiogenesis"
Tumor "lymphangiogenesis"
Tumor growth
Tumor metastasis
Lymph node "angiogenesis"
Lymph node "lymphangiogenesis"
SP5031
Mechanisms of action (MOA)
Tumor secreted factors
MDA-MB-231
SP5031
VEGFA
VEGFC
VEGFR2
NRP1
NRP2
VEGFR3
MKK3/6
p38
MAPKAPK2
HSP27
Actin reorganization
FAK
Focal adhesion turnover
Migration & Adhesion
Angiogenesis
Lymphangiogenesis
Blood & lymphatic endothelial cells

Figure 7.10: Mechanisms of Action of SP5031. SP5031 inhibits lymphangiogenesis and angiogenesis in primary tumors and tumor-conditioned regional LN. This suggests the potential of SP5031 to prevent both tumor growth and tumor metastasis (the upper panel, hypothetical mechanisms are shown in a red dotted-rectangle). At the cellular level, SP5031 targets LEC and BEC (the lower panel). NRP1 (on BEC) and NRP2 (on LEC) are the target receptors. Peptide binding to NRP1 and NRP2 indirectly inhibits signaling from VEGFR2 and VEGFR3 in the presence of VEGFA and VEGFC. SP5031 further inhibits VEGF-induced phosphorylation of p38MAPK signaling molecules and FAK, element proteins for endothelial cell migration and adhesion.

Chapter 8: Collagen IV-derived Peptide Shows Anti-lymphangiogenic and Anti-angiogenic Activity Inhibiting Breast Tumor Growth and Metastasis.

8.1 RATIONALE

Tumor angiogenesis is one of widely recognized targets to treat cancers, as solid tumors require newly formed and extended blood vessels in tumor stroma to efficiently supply the tumor cells with nutrients and oxygen (Jain and Carmeliet 2012). Although anti-angiogenic strategy has been used for treating several cancers in clinic, overall survival in advanced breast cancer patients has not been improved well (Shamloo, Chhabra et al. 2012), because breast tumor metastasis involves lymphatic dissemination in addition to hematogenous spreading (Schoppmann, Bayer et al. 2004). Thus, there is unmet need to develop agents to block tumor lymphangiogenesis as well as angiogenesis.

The Popel laboratory has identified several endogenous peptides to inhibit lymphangiogenesis by using bioinformatics-aided methodologies and in vitro and animal experiments (Karagiannis and Popel 2008; Lee, Rosca et al. 2011; Koskimaki, Lee et al. 2013; Lee, Koskimaki et al. 2013). Lee et al. (2011) have reported that short peptides derived from somatotropin domain-containing proteins inhibit lymphatic endothelial cell proliferation, migration, adhesion and tube formation (Lee, Rosca et al. 2011). Lee et al. (2013) also have documented that 14-mer peptide derived from transmembrane protein 45A (TMEM45A), among the somatotropin peptides, exhibits potent anti-lymphangiogenic activity in breast tumor xenograft and tumor-conditioned lymph node models (Lee, Koskimaki et al. 2013). Recently, Koskimaki et al. (2013) have showed synergy between a collagen IV mimetic peptide and the TMEM45A peptide as lymphangiogenesis inhibitors (Koskimaki, Lee et al. 2013). Notably, the collagen IV derived peptide shows potent anti-angiogenic activity as well (Rosca, Koskimaki et al. 2011; Rosca, Koskimaki et al. 2012; Koskimaki, Lee et al. 2013). Testing those peptides separately, the collagen IV peptide was much more potent than TMEM45A peptide in a blockage of

angiogenesis; but was comparable to TMEM45A peptide in an inhibition of lymphangiogenesis (Koskimaki, Lee et al. 2013). Based on these findings, the collagen IV peptide has been selected and optimized to be soluble, easy to synthesize and stable by using bioinformatics and amino acid mutation methodology (Rivera, Rosca et al. 2011; Rosca, Koskimaki et al. 2012). This chapter will discuss synergy between a collagen IV derived peptide and a TMEM45A derived peptide in inhibiting of lymphangiogenesis; and will also focus on the latest version of collagen IV mimetic peptides, SP2043, whose amino acid sequence is LRRFSTAPFAFIDINDVINF, investigating efficacy to block lymphangiogenesis and angiogenesis in vitro; and therapeutic potential in breast tumor xenograft and tumor-conditioned media (TCM) induced spontaneous metastasis models in vivo. The TCM-induced spontaneous metastasis model shows rapid formation of metastases in mice within one month (Lee, Pandey et al. 2014) and the molecular mechanisms of the metastatic acceleration was previously investigated (Lee, Fertig et al. 2014).

Portions of this chapter have previously been published (Koskimaki, Lee et al. 2013) and were reproduced with permission from the publishers of the journals: copies of permission were included in the Appendix.

8.2 MATERIALS & METHODS

8.2.1 Peptide synthesis and handling

Peptides were produced by New England Peptide (Gardner, MA) by using a solid-phase synthesis technique. HPLC and MS analyses of the peptides were provided by the manufacturer to indicate a purity of more than 95%. The peptides have an amine at the N-terminus and an amide at the C-terminus. In preparation of peptide stock solution, DMSO was used as a solvent at a maximum concentration of 5% (vol/vol) in distilled water. All in vitro experiments were carried out with < 0.3% concentrations of DMSO so as not to harm cells.

8.2.2 Cell culture

Microvascular endothelial cells (MEC), human umbilical vein endothelial cells (HUVEC), and lymphatic endothelial cells (LEC) were purchased from Lonza (Walkersville, MD). MEC and LEC were propagated in microvascular endothelial cell growth medium-2 (EGM-2MV, Lonza). HUVEC were propagated in endothelial cell growth medium-2 (EGM-2, Lonza). MDA-MB-231 human breast cancer cells were supplied by Dr. Zaver Bhujwalla (JHMI, Radiology and Oncology), and MDA-MB-231-luc-D3H2LN was purchased from Caliper (Hopkinton, MA). The breast cancer cells were propagated in RPMI-1640 medium (Gibco, Carlsbad, CA) supplemented with 10% fetal bovine serum, and 1% streptomycin. The passage numbers of all the endothelial cells were kept between 3 and 6 and cells were maintained under standard conditions of 37°C and 5% CO_2.

8.2.3 Proliferation assay

Colorimetric based proliferation assay using WST-1 (Roche, Indianapolis, IN) proliferation reagent was carried out using HUVEC. 2,000 cells/well were plated in 96-well plates and allowed to adhere overnight. On the following day the media was exchanged with fully supplemented media containing SP2043 peptide or equivalent DMSO vehicle for the controls. Three days later the media containing the peptide was replaced with serum-free media (EBM-2) containing WST-1 reagent and the plates were incubated for four hours. Changes in color due to the formazan dye resulted from the cleavage of the tetrazolium salt WST-1 by the mitochondrial succinate-tetrazolium reductase, were read on a Victor V fluorescence plate reader (Perkin Elmer, MA) by measuring the absorbance at 450 nm.

8.2.4 Migration and adhesion assays

Cell migration and adhesion assays were performed by using Real-Time Cell Analysis (RTCA) system (ACEA) as described previously (Lee, Rosca et al. 2011). To evaluate cell migration, a membrane of the top chamber of a CIM-plate (Roche, Indianapolis, IN) was pre-coated with 20 µg/ml fibronectin (Sigma Aldrich) for 30 min at 37°C. 180 µl of complete endothelial growth media (HUVEC, EGM-2) was added to the bottom chamber as a chemoattractant. Cells (45,000 HUVEC) were added to the top chamber with or without SP2043 peptide. The chamber was loaded in the RTCA machine, and the cell indices were measured continuously for 24 h. Cell indices at 20 h were selected for analysis. For adhesion assays, 100 µl of 2X concentrated peptide solution was added to the appropriate wells of an E-plate (Roche). LEC, MEC and HUVEC (25,000 cells/well) in EGM-2 (HUVEC) or EGM-2MV (LEC, MEC) were added next to each well diluting peptides to the appropriate final concentration. After

equilibrating at room temperature for 30 min, the E-plate was loaded into the RTCA system. Cell indices at 3 h were analyzed.

8.2.5 Tube formation assay

50 µl matrigel (BD Biosciences, Bedford, MA) was loaded in each well of a 96-well plate, and the plate was incubated at 37°C for 30 min. 100 µl LEC, MEC, and HUVEC in EGM-2 (HUVEC) or EGM-2MV (LEC, MEC) with or without SP2043 peptide were added on top of the matrix in the 96-well plate (15,000 cells/well). The plate was then incubated at 37°C, and the wells were imaged using a Nikon microscope at 20 h (Nikon Instruments Inc., Melville, NY).

8.2.6 Synergy Calculations

The Chou-Talalay method (Chou 2010) commonly used in drug combination studies provided the standard for drug synergy in cell assays using the calculation by combination index (CI). CI<1 indicates synergy, CI=1 indicates additivity, and CI>1 indicates antagonism. The CI can be expressed as:

$$CI = [(D)_1/(D_x)_1]+ [(D)_2/(Dx)_2]$$

$(D)_1$ is the tested dose of SP2012 (1, 5 or 25 µM) and $(D)_2$ is the tested dose of SP5031 (1, 5 or 25 µM). $(D_x)_{1/2} =(D)_m[f_a/(1-f_a)]^{1/m}$ where $(D)_m$ is the median-effect dose (IC_{50} value), m= the slope or hill coefficient, and f_a is the fraction affected, in this case activity of the compound in adhesion, migration or proliferation. IC_{50} values were used and slope values were measured for LEC for each compound (SP2012, SP5031) in each cell assay (adhesion, migration, and proliferation), calculated with GraphPad Prism 5 Software (GraphPad Software, Inc. San Diego, CA). Normalized isobolograms were constructed using the dose reduction index (Corvinus, Orth

et al.) for SP2012 and SP5031, defined as (Corvinus, Orth et al.)$_1$=$(D_X)_1/(D)_1$ and (Corvinus, Orth et al.)$_2$=$(D_X)_2/(D)_2$, plotted on the x- and y-axes.

8.2.7 Western blot assay

MEC and LEC were grown in complete endothelial growth media (EGM-2MV) and plated on tissue culture-treated 100 mm dishes at 1,500,000 cells/dish in EGM-2MV. After a day for cell attachment on the bottom, cells were starved in serum-free media for 24 h after which SP2043 (10, 30 μM) was added for 90 min. HGF (50 ng/ml) or IGF1 (100 or 50 ng/ml) was added and the incubation was continued for 10 – 30 min at 37˚C. Treatments were stopped by adding cold PBS and cell lysates were prepared as described above. Cell lysates were separated by SDS-PAGE and transferred to nitrocellulose blots (Invitrogen, Carlsbad, CA). The membranes were blocked for 1 h with 5% non-fat milk + 1% BSA in TBST and probed with antibodies of interest including p-Met (Y1234/1235), p-Met (Y1349), p-Gab1 (Y307), p-Akt (S473), Akt, p-MAPK (T202/Y204), MAPK, p-IGF1R (Y1135/1136), IGF1R, and GAPDH (Cell Signaling Technology, Inc.). GAPDH was used as a loading control. Secondary antibodies were added at 1:2000 dilution and protein bands detected with a chemiluminescence detection reagent (GE Healthcare).

8.2.8 MDA-MB-231 tumor xenografts

Two million of MDA-MB-231 cells were orthotopically inoculated into the second thoracic mammary fat pad of 4-5 week old female severe combined immunodeficiency (SCID) mice under anesthesia (50 mg/kg ketamine + 5 mg/kg acepromazine in PBS, i.p. injection), and the tumors were allowed to grow until they reached around 100 mm^3. 10 or 20 mg/kg SP2043 peptide solution or the vehicle was injected intraperitoneally, and continued for 33 days. The tumor size and mouse body weight were measured every four days using a caliper and a

weighing machine for small animals. The tumor volume was calculated by using the formula: V = 0.52 x ('long axis' of the tumor) x ('short axis' of the tumor)^2. After sacrificing animals, the tumors were excised and rinsed in PBS and fixed in 4% formalin for 16 h for immunohistochemistry.

8.2.9 Tumor-conditioned media induced spontaneous metastasis models

Tumor-conditioned media (TCM) induced spontaneous metastasis models were used to show accelerated metastasis in a short time and to evaluate anti-metastatic effects of the SP2043 peptide compared to a control group. MDA-MB-231-luc-D3H2LN tumor-conditioned media (TCM) was prepared as previously described (Lee, Pandey et al. 2014). Briefly, MDA-MB-231-luc-D3H2LN cells in complete growth media (RPMI-1640) were plated on 175 mm^2 tissue culture plates. When the cells are confluent, the complete media was removed, and the cells were carefully rinsed with serum-free media. 8 ml of serum-free media was added and the cells were incubated for 24 h at 37°C. The supernatant was carefully gathered, centrifuged, and filtered through 0.2 µm sterile syringe filters (Corning, Germany). The resulting TCM was stored in aliquots at -80°C to avoid multiple freeze thaws. 50 µl tumor-conditioned media (TCM) or serum-free media (SFM) was daily administered subcutaneously through the scruff of 4-5 week old female athymic nude mice for two weeks. TCM treated animals were either treated with SP2043 (10 mg/kg, i.p.) or with the vehicle during the 2-week of TCM induction phase. Then, 2 x 10^6 MDA-MB-231-luc-D3H2LN cells in 100 µl of 50% matrigel were orthotopically inoculated into the upper inguinal mammary fat pad of 4-5 week old female athymic nude mice under anesthesia (50 mg/kg ketamine + 5 mg/kg acepromazine in PBS, i.p. injection). After two weeks, primary tumor size was measured by using a caliper as described above, and thoracic metastasis was assessed every week by using the In Vivo Imaging System (IVIS) Xenogen 200

optical imager (Xenogen) up to week 5. Photon flux from the thoracic region was monitored to determine metastases 5-10 min after intraperitoneal injection of 150 mg/kg D-luciferin (Caliper). After 5 weeks, the lungs, brains, livers, lymph nodes, and bones (humerus/ulna and femur/tibia) were harvested and bathed in D-luciferin solution for 3 min and placed in the IVIS imager to detect metastases ex vivo. After the imaging, the organs were rinsed in PBS and fixed in 4% formalin for 16 h for immunohistochemistry.

8.2.11 Identification of IGF1R/c-Met binding proteins

We hypothesized that the SP2043 peptide binds to unknown 3rd receptor proteins on endothelial cells and interrupts both IGF1R and c-Met. Experiments were designed to determine which receptor proteins make a complex with IGF1R or c-Met in the presence of IGF-1 or HGF; which receptor proteins are dissociated from IGF1R or c-Met after treating with SP2043 against IGF-1 and HGF. MEC were grown in complete endothelial growth media (EGM-2MV) and plated on tissue culture-treated 100 mm dishes at 1,500,000 cells/dish in EGM-2MV. After a day for cell attachment on the bottom, cells were starved in serum-free media for 24 h after which SP2043 (30 μM) was added for 90 min. HGF (100 ng/ml) or IGF1 (100 ng/ml) was added and the incubation was continued for 60 min at 37˚C. Treatments were stopped by adding cold PBS and cell lysates were prepared. The cell lysates were incubated with anti-IGF1R (1:50, Cell Signaling) or anti-c-Met (1:50) antibody overnight. Then A/G agarose plug (Santa-Cruz) was added to pull-down the antibody protein complex. After removing supernatant pellets were rinsed with PBS. The pellets were treated with Glycine (pH 2, 10ml) for 2 h to dissociate all the bound proteins of the beads and the beads were removed by centrifugation. Recovering protein structure and maintaining normal pH, 0.5 ml of Tris (pH 8) was added. The mixture was dialyzed with membrane (3K) removing glycine and Tris. Resulting mixture has all the proteins that were

bound to IGF1R or c-Met. The mixture was analyzed using antibody arrays for soluble receptors (Proteome Profiler Antibody Arrays Kit for human soluble receptors, R&D systems). Array membranes were blocked with blocking buffer provided in the kit. Protein mixture samples were mixed with dilution buffer, and the diluted protein mixture sample was added to the blocked membrane, and the membrane was incubated overnight at 4˚C. After three rinses, anti-phospho-tyrosine-HRP detection antibody (diluted by 1:2000 with dilution buffer in the kit) was added, and the antibody-bound streptavidin-HRP complex was detected by using a chemiluminescence detection reagent (GE Healthcare, United Kingdom).

8.2.12 Statistical analysis

Error bars correspond to SEM, unless otherwise stated. Differences between a control and a peptide treated group are regarded as significant when P is less than 0.05 using the Student's t-test.

8.3 RESULTS

8.3.1 Synergistic activity between SP2012 and SP5031 in vitro

Migration and adhesion are necessary for the formation of both blood and lymphatic vessels inside and around tumors. It has been shown that SP2012 and SP5031, whose sequences are described in Figure 8.1.A, individually block blood endothelial cell adhesion and lymphatic endothelial cell migration (Lee, Rosca et al. 2011; Rosca, Koskimaki et al. 2011). It was shown that these peptides behave similarly in lymphatic endothelial cell migration assays and show similar synergy (Figure 8.1.B). After observing the synergistic effect of the two peptides in migration, SP2012 and SP5031 were tested in LEC adhesion. Figure 8.1.C shows a similar synergy in LEC with SP20102 and SP5031 tested alone or in combination at indicated doses. All CI are <1 in tested doses indicating synergy by the Chou-Talalay method, and tested doses show a statistical improvement over single doses. These results are shown graphically (Figure 8.1.D) and are highly synergistic with all CI<1. Western blot was performed to see $VEGF_{165}$ signaling in LEC with these two peptides (Figure 8.2). Both peptides synergistically blocked pVEGFR2 (Figure 8.2.A) and pFAK (Figure 8.2.B) in the presence of $VEGF_{165}$ in LEC.

8.3.2 In vitro tube formation and in vivo matrigel plug assays

The combination of SP2012 and SP5031 was examined in in vitro tube formation and in vivo matrigel plug assays. For tubules and networks to form in vitro and in vivo endothelial cells must adhere, migrate and remain viable. In vitro, a mild response for SP2012 25 μM and SP5031 5 μM was observed. Tubules are most fragmented and broken in LEC when the peptides are applied in combination at tested doses (Figure 8.3.A). Next, matrigel plugs were implanted with or without peptides (singular and combinatorial manners) into athymic nude mice with $VEGF_{165}$

and heparin as the positive control. To show the anti-lymphangiogenic response immunohistochemistry was performed by staining cross sections for mLYVE-1, a marker for mouse lymphatic vessels. Figure 8.3.B shows representative cross sections, quantified in Figure 8.3.C. SP2012 and SP5031 together showed a significant decrease in lymphatic vessel density, statistically lower than each peptide alone.

8.3.3 SP2043 blocks proliferation, migration, adhesion, and tube formation of the lymphatic and blood endothelial cells in vitro

Human umbilical vein endothelial cells (HUVEC) were tested with SP2043 (Figure 8.4.A), a mimetic collagen IV peptide, in cell proliferation, migration, adhesion, and tube formation to evaluate anti-angiogenic activity of the peptide (Figure 8.4). The WST-1 proliferation reagent was applied to HUVEC with or without SP2043. SP2043 inhibits HUVEC proliferation with an IC_{50} value of 7.0±2.1 μM (Figure 8.4.B). The real time cell analysis (RTCA) system was employed to measure HUVEC adhesion and migration. SP2043 potently inhibited HUVEC adhesion (IC_{50} value of 0.93±0.56 μM) and migration against EGM-2 complete endothelial growth media (Figure 8.4.C, D). HUVEC tube formation was also blocked by SP2043 (Figure 8.4.E). HUVEC are routinely used in angiogenesis in vitro assays, but due to their venous origin may not adequately replicate microcapillaries of tumors. As an additional study the effect of SP2043 in microvascular endothelial cells (MEC) was assessed (Figure 8.5). SP2043 blocked MEC adhesion and tube formation (Figure 8.5.A, B). Lymphatic endothelial cells were also tested, similarly SP2043 inhibited LEC adhesion and tube formation (Figure 8.5.C, D).

8.3.4 SP2043 blocks IGF1R and c-Met signals in lymphatic and blood endothelial cells

IGF1R and c-Met signaling pathways were studied in lymphatic and blood endothelial cells with SP2043 treatment. In HGF-induced MEC, SP2043 blocked phospho-c-Met (Y1234/1235/1349), and phosphorylation of the downstream proteins: Gab1, Akt, MAPK, and FAK (Figure 8.6.A). In IGF1 induced MEC, SP2043 blocked phospho-IGF1R (Y1135/1136) and phosphorylation of the MAPK and Akt (Figure 8.6.B). LEC were activated with HGF and IGF1 and the SP2043 effects were observed. Similar to MEC, LEC induced by HGF showed phospho-c-Met, p-Akt, and p-MAPK, but the c-Met signaling was blocked by SP2043 in a dose response manner. In IGF1 induced LEC, SP2043 blocked phospho-IGF1R (Y1135/1136) and phosphorylation of Akt and MAPK (Figure 8.6.C).

8.3.5 CD58, CD155, and ADAM17 are dissociated from IGF1R and c-Met receptor complex after SP2043 treatment

To understand the bimodal inhibition of IGF1R and c-Met by the SP2043 peptide, IGF1R or c-Met binding receptor proteins were determined in the presence of IGF1 or HGF. Then, it was determined which receptor proteins are dissociated from IGF1R or c-Met complex after SP2043 treatment. Proteome Profiler Antibody Arrays Kit for human soluble receptors (R&D systems) was employed to identify receptor proteins in the receptor complex. In IGF1 induced MEC, 11 receptor proteins form receptor complex with IGF1R (CD58, CD155, CD31, CD36, CD44, CD147, RECK, ADAM17, Galectin-3, Integrin β1, Integrin β2). After SP2043 treatment, 8 proteins (CD31, CD147, Integrin β1, RECK, Galectin-3, CD58, CD155, ADAM17) were dissociated from the receptor complex (Figure 8.7.A). In HGF-induced MEC, 8 receptor proteins form receptor complex with c-Met (CD58, CD155, TIMP3, CD36, CD154, CD44, ADAM17,

Integrin β2). After SP2043 treatment, 7 proteins (CD58, CD155, TIMP3, CD36, CD154, CD44, ADAM17) were dissociated from the receptor complex (Figure 8.7.B). Taken together, very interestingly, CD58, CD155, and ADAM17 were targeted by SP2043 and dissociated from the receptor complex of IGF1R and c-Met (Figure 8.7.C).

8.3.6 SP2043 inhibits MDA-MB-231 tumor growth

MDA-MB-231 tumor xenografts were established in SCID mice as previously described (Lee, Koskimaki et al. 2013; Lee, Fertig et al. 2014; Lee, Pandey et al. 2014). After tumor formation with a volume around 100 mm^3, SP2043 (10, 20 mg/kg) was treated i.p. every day up to 33 days: the tumor size and mouse body weight were measured every four days. Both 10 and 20 mg/kg SP2043 showed significant inhibition of tumor growth, compared to the vehicle treated control (Figure 8.8.A). SP2043 (10 mg/kg) showed a saturated activity compared to 20 mg/kg SP2043 group, demonstrating that 20 mg/kg SP2043 is overdosed. But in both cases, mouse body weights were statistically identical showing no severe toxicity in high dose treatment (Figure 8.8.B).

8.3.7 SP2043 inhibits MDA-MB-231 tumor metastasis in the tumor-conditioned media induced spontaneous metastasis model

We have reported that tumor-conditioned media (TCM) pre-treatment followed by tumor inoculation facilitated spontaneous metastasis by influencing lymphangiogenesis and angiogenesis in the primary tumors and pre-metastatic organs (Lee, Fertig et al. 2014; Lee, Pandey et al. 2014). Surprisingly, TCM-induced lymphatic and blood vessel formation in the lymph nodes was inhibited by treating the animals with the peptide from transmembrane protein 45A (SP5031) (Lee, Koskimaki et al. 2013). We hypothesized that SP2043 would show similar

inhibitory effects, preventing pre-metastatic niche formation and metastasis in these organs. Here SP2043 was evaluated in the TCM-induced metastasis model. TCM was pre-treated with or without SP2043 (10 mg/kg, i.p.) for two weeks, after which luc-MDA-MB-231 tumors were established in inguinal mammary fat pads. Up to 5 week thoracic tumor metastasis and primary tumor size were monitored (Figure 8.9.A). Primary tumor size was not influenced by either peptide treatment or TCM pre-treatment, as the cancer cells were inoculated after finishing all of the TCM and peptide pre-treatment (Figure 8.9.B). However, metastatic progression was significantly affected by those treatments. In 5 week, serum-free media (SFM) treated group showed 3 mice with metastases, but the TCM treated group showed 9 mice with metastases (90%). Upon TCM treatment, SP2043 prevented more than 50% of metastasis from the positive control group. This is comparable with the SFM treated negative control group (Figure 8.9.C). At week 5, the lymph nodes, lungs, livers, brains and bones were harvested, bathed in D-luciferin for 5-10 min and imaged under the IVIS imager. The lymph nodes, lungs, and livers from TCM treated animals showed dramatic acceleration of metastasis. The peptide treatment inhibited the metastatic progression (Figure 8.9.D, E).

8.4 DISCUSSION

This chapter demonstrates that a collagen IV derived peptide, SP2012, and a transmembrane protein 45A derived peptide, SP5031 show synergy in inhibition of lymphangiogenesis in lymphatic endothelial cell migration, adhesion, tube formation and in vivo matrigel plug assays. This chapter also focuses on that a mimetic, collagen IV derived peptide, SP2043 exhibits potent anti-lymphangiogenic and anti-angiogenic activity, inhibiting breast tumor growth and preventing tumor-conditioned media (TCM) induced metastasis. MDA-MB-231 (or luciferase-expressing MDA-MB-231) cell line, one of triple-negative breast cancer (TNBC) cell lines (Lehmann, Bauer et al. 2011) was employed in these animal models. TNBC exhibits strong metastatic potential and currently effective drug agents are very limited.

In vitro assays with SP2012 and SP5031 showed synergy in blockage of lymphatic endothelial cell adhesion, migration and tube formation. Previously, it has been shown that SP2012 binds to β1 integrins and shows anti-angiogenic activity (Rosca, Koskimaki et al. 2011). Integrin receptor biology is central to endothelial cell attachment to the extracellular matrix, and is regulated by different combinations of alpha and beta integrin subunits to different matrices (Shattil and Ginsberg 1997). We have also reported that SP5031 binds to neuropilin 1/2 and interferes with VEGFR2/3 signaling in blood and lymphatic endothelial cells (Lee, Koskimaki et al. 2013). Although the integrin signaling and the neuropilin signaling appear to be independent, they have been investigated together and some interactions have been reported. For example, neuropilin 2 promoted extravasation and metastasis of cancer cells by interacting with endothelial α5 integrin on blood vessels (Cao, Hoeppner et al. 2013). Enhancement of the integrin function by VEGF/neuropilin signaling has also been reported (Goel and Mercurio 2012). In western blot assays with VEGF-treated LEC, VEGFR2 and FAK were inhibited by

SP2012 and SP5031, showing synergy (Figure 8.1 and 2). This chapter describes how combining two peptides with knowledge of their mechanisms of action can produce a therapeutic combination with enhanced activity (Koskimaki, Lee et al. 2013). These synergy effects need to be further assessed with other growth factors, because VEGF was the only growth factor tested with these peptides. In vivo, two peptides synergistically blocked lymphangiogenesis in matrigel plug assays (Figure 8.3). In vivo results with the peptides are promising, as clinically peptide-peptide combination therapies may also be advantageous to chemotherapeutic regimens or to monoclonal antibodies and small molecules due to lower toxicity and enhanced specificity (Rosca, Koskimaki et al. 2011). Optimal peptide-peptide dosing combinations, dose intervals, and which disease-specific lymphangiogenesis-based models to apply SP20XX and SP5031 treatment are further areas that should be tested and refined in subsequent studies.

SP2043 (amino acid sequence: LRRFSTAPFAFIDINDVINF) was designed by replacing some natural or synthetic amino acids ('M' to 'A'; 'Abu' to 'I'; 'N' to 'D') from SP2012 (LRRFSTMPFMF-Abu-NINNV-Abu-NF). These modifications deleted the synthetic amino acid Abu (2-aminobutyric acid) and alkyl chain M (methionine), maintaining water solubility by replacing hydrophobic N (asparagine) with negatively charged D (aspartic acid). These were performed based on previous expertise in SAR (Structure & Activity Relationship) analysis in the lab (Rivera, Rosca et al. 2011; Rosca, Koskimaki et al. 2012). The SP2043 peptide exhibits both anti-angiogenic and anti-lymphangiogenic activity in blood and lymphatic endothelial cell based assays (Figure 8.4 and 8.5) and the activity was much more potent than SP5031 or SP2012 peptide. Interestingly, SP2043 targets two different receptor tyrosine kinases (Balz, Bartkowiak et al.) on blood and lymphatic endothelial cells: IGF1R and c-Met (Figure 8.6). These two RTK have been studied in cancers. The IGF1R and its contributions to metastatic tumor growth have

been studied (Bahr and Groner 2005). Roles of IGF1-PI3K/Akt signaling have been shown in skin tumor (Wilker, Lu et al. 2005). It has been reported that IGF1 regulates the expression of the pituitary tumor transforming gene (PTTG), an oncogene in breast tumor (Thompson and Kakar 2005). c-Met has also been widely recognized as a target of metastatic progression of cancers. An inhibition of c-Met reduced lymphatic metastasis in RIP-Tag2 transgenic mice (Sennino, Ishiguro-Oonuma et al. 2013). Gene silencing of c-Met led to brain metastasis inhibitory effects (Lee, Seol et al. 2013). Thus, the multimodal inhibition of IGF1R and c-Met could improve current mono targeting therapies that usually elicit tumor drug resistance and adaptive behavior of cancer cells to be more invasive and metastatic. Suppression of tumor invasion and metastasis by concurrent inhibition of c-Met and VEGF in pancreatic neuroendocrine tumors was reported (Sennino, Ishiguro-Oonuma et al. 2012). It also has been reported that the collagen IV peptide inhibits VEGF signaling (Koskimaki, Lee et al. 2013), thus this finding of c-Met inhibition could improve the outcome.

Mechanistically, the SP2043 peptide disrupts co-receptor complex formation of IGF1R and c-Met in the presence of IGF1 and HGF (Figure 8.7). Innovative combination of coimmunoprecipitation and reverse western assay detecting diverse soluble receptors revealed that IGF1R forms co-receptor complex with CD31, CD147, β1 integrin, RECK, Galectin 3, CD58, CD155 and ADAM17 (Figure 8.7.A); and c-MET forms co-receptor complex with TIMP3, CD154, CD44, CD58, CD155, and ADAM17 (Figure 8.7.B). Very interestingly, CD58, CD155, and ADAM17 were completely gone after SP2043 treatment in both co-receptor complexes in the presence of IGF1 an HGF (Figure 8.7.C). One notable point is that the β1 integrin, which was known as the target of collagen IV peptide SP2012, is found only in IGF1 activation, not in the HGF induction in endothelial cells. Thus previously understood target of

collagen IV peptides can be more than one, at least in the case of SP2043 as these experiments suggest. We speculate that ADAM17 could be an important target of the SP2043 peptide, as ADAM17 has been widely studied in angiogenesis and cancers (Lin, Lemke et al. 2011; Das, Czarnek et al. 2012), and specifically in breast cancer (Glunde and Stasinopoulos 2009; Zheng, Jiang et al. 2009; Gao, Kim et al. 2013). However CD58 and CD155 have not been implicated in angiogenesis or lymphangiogenesis: they could be novel targets for angiogenesis and lymphangiogenesis, if the mechanisms are elucidated. SP2043 peptide binding to/interacting with those receptors and functional assays of angiogenesis and lymphangiogenesis with neutralizing antibodies of those receptors remain for future investigation.

SP2043 was tested in animal models of TNBC tumor growth and metastasis. MDA-MB-231 tumor xenografts were treated with SP2043 (10, 20 mg/kg, i.p.) and it was observed that the tumor growth was dramatically inhibited without significant body weight changes (Figure 8.8). It is speculated that the blockade of tumor growth was derived from the anti-angiogenic activity of the SP2043 peptide. In terms of metastasis models, as conventional spontaneous metastasis models take more than 2 months to show significant metastasis as positive controls, TCM-induced metastasis models (Lee, Pandey et al. 2014) were employed. This model requires 2 week of TCM induction phase before luc-MB231 tumor inoculation (Figure 8.9.A). After establishing orthotopic tumor xenografts in inguinal mammary fat pads, the model results in dramatic distal metastasis within 4-5 weeks. SP2043 (10 mg/kg) was administered i.p. in the 2 weeks of TCM induction phase only, after tumor inoculation, the peptide treatment was ceased. This was because that the model should give the peptide efficacy in only the metastatic dissemination and colonization by specifically disrupting pre-metastatic niche formation within organs before tumor inoculation. If the peptide were still injected even after tumor inoculation, the peptide

would significantly inhibit tumor growth as well, thus the followed decrease in metastases would makes it difficult to interpret the results. Generally small size tumors would result in less metastasis, as the tumor cell sources are not as abundant compared to well-developed big tumors. This model confirmed that tumor sizes were identical within all the experimental groups (Figure 8.9.B). Upon the same degree of tumor mass, only the metastatic dissemination and colonization was potently inhibited by the SP2043 peptide treatment (Figure 8.9.C-E).

In this chapter, the anti-angiogenic and anti-lymphangiogenic peptides showed their activities in vitro and in vivo, specifically breast tumor growth and metastasis models. Targeting angiogenesis through endothelial cell adhesion, migration and proliferation, in addition to lymphangiogenesis would yield the more efficacious result of limiting functional vessel formation in tumors and should be considered as a treatment strategy in angiogenesis and lymphangiogenesis-dependent diseases. As angiogenesis and lymphangiogenesis are central to metastatic cell dissemination and metastatic disease is the primary cause of death in cancer, these compounds applied in combination should be considered as a potential treatment for metastatic disease.

8.5 FIGURES & TABLES

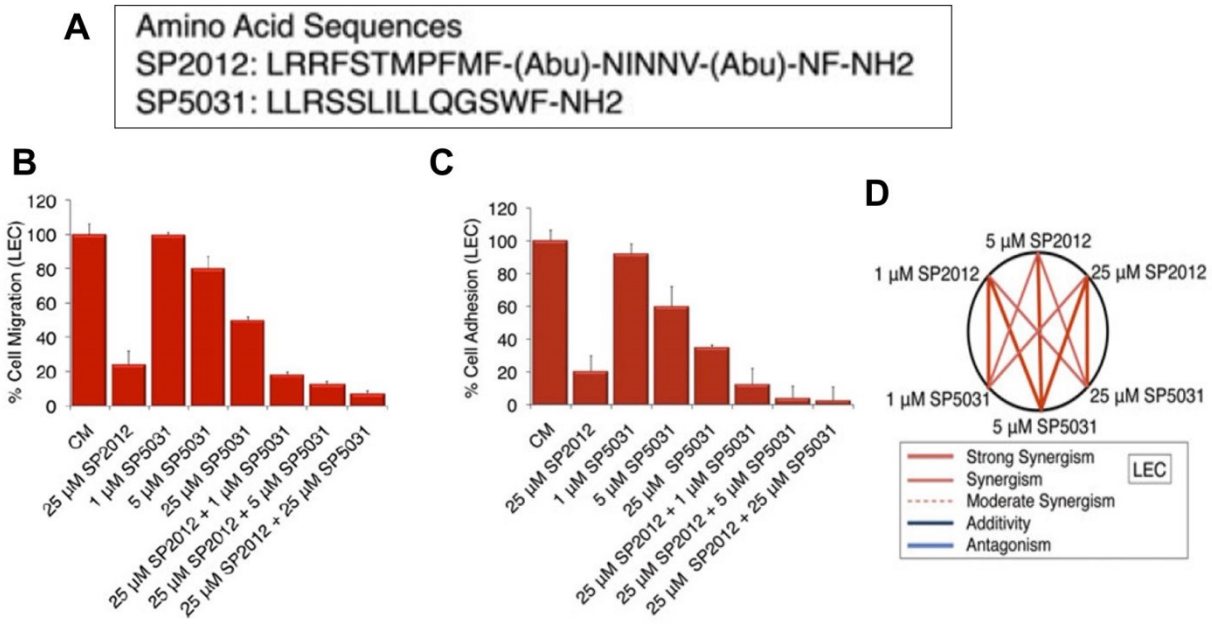

Figure 8.1: SP2012 and SP5031 block lymphatic endothelial cell migration and adhesion alone and synergistically in combination. (A) Sequences of selected peptides: SP2012, a collagen IV mimetic peptide and SP5031, a somatotropin-domain derived peptide. (B) SP2012 and SP5031 synergistically block LEC migration. (C) SP2012 and SP5031 synergistically block LEC adhesion. (D) Graphical representation of peptide doses on LEC.

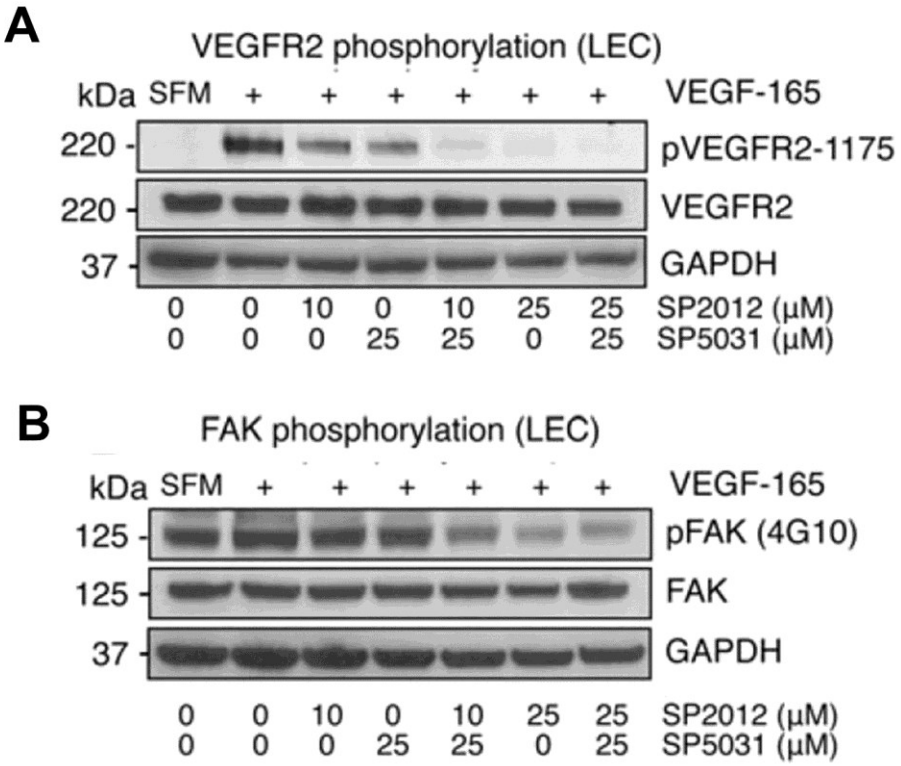

Figure 8.2: Effects of SP2012 and SP5031 on vascular endothelial growth factor receptor 2 and focal adhesion kinase in LEC. (A). SP2012 and SP5031 block phosphorylation of VEGFR2 in LECs. This effect is additive at low and high doses of SP2012. (B). SP2012 and SP5031 block phosphorylation of FAK in LECs at low and high doses of SP2012.

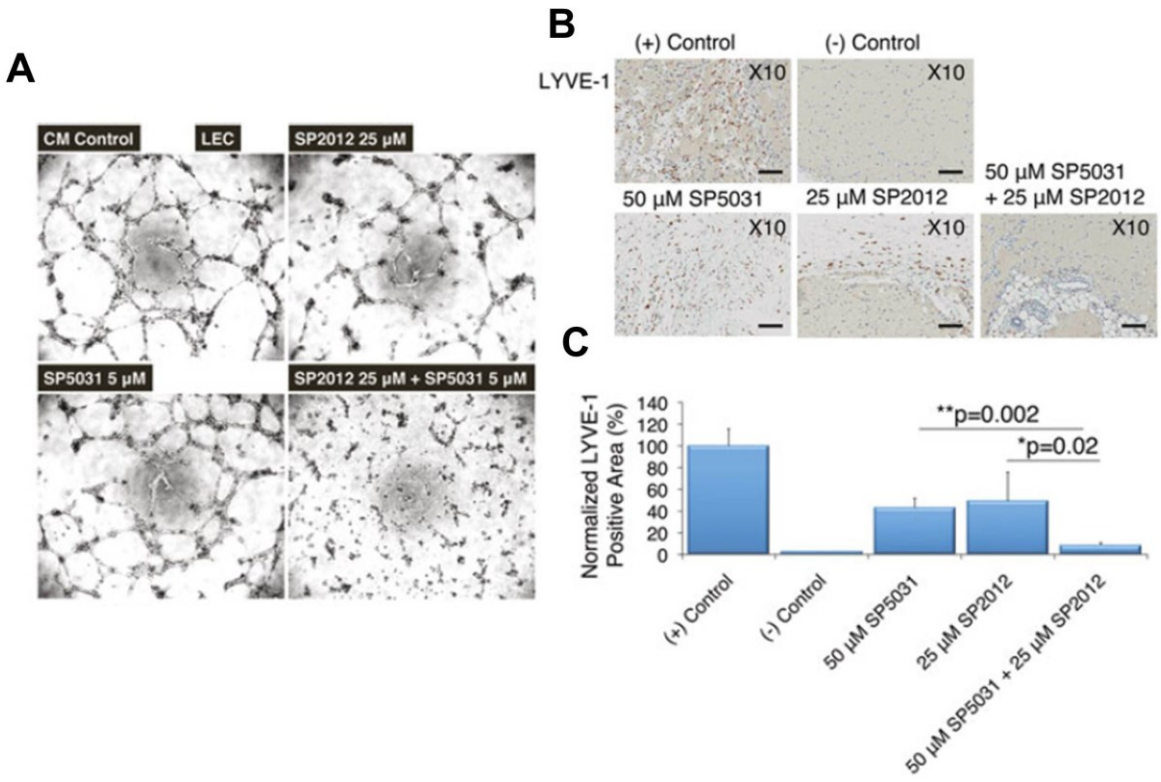

Figure 8.3: In vitro capillary-like tubule formation assay and in vivo Matrigel Plug assay.

(A) LEC tube formation assay. SP2012 and SP5031 in combination show enhanced activity in blocking tubule formation. (B). Matrigel plug assays: LYVE-1 immunohistochemical staining for lymphatic cell vasculature. SP2012 and SP5031 applied in combination significantly reduce lymphatic vessel formation (brown color). Images shown are at 10X magnification, and scale bars represent 100 µM. (C). Quantification of LYVE-1 staining. The combination of SP2012 25 µM and SP5031 50 µM statistically significantly reduce lymphatic vessel formation into plugs over either compound alone (**$p<0.01$, and *$p<0.05$). The standard deviation (+/-) is shown.

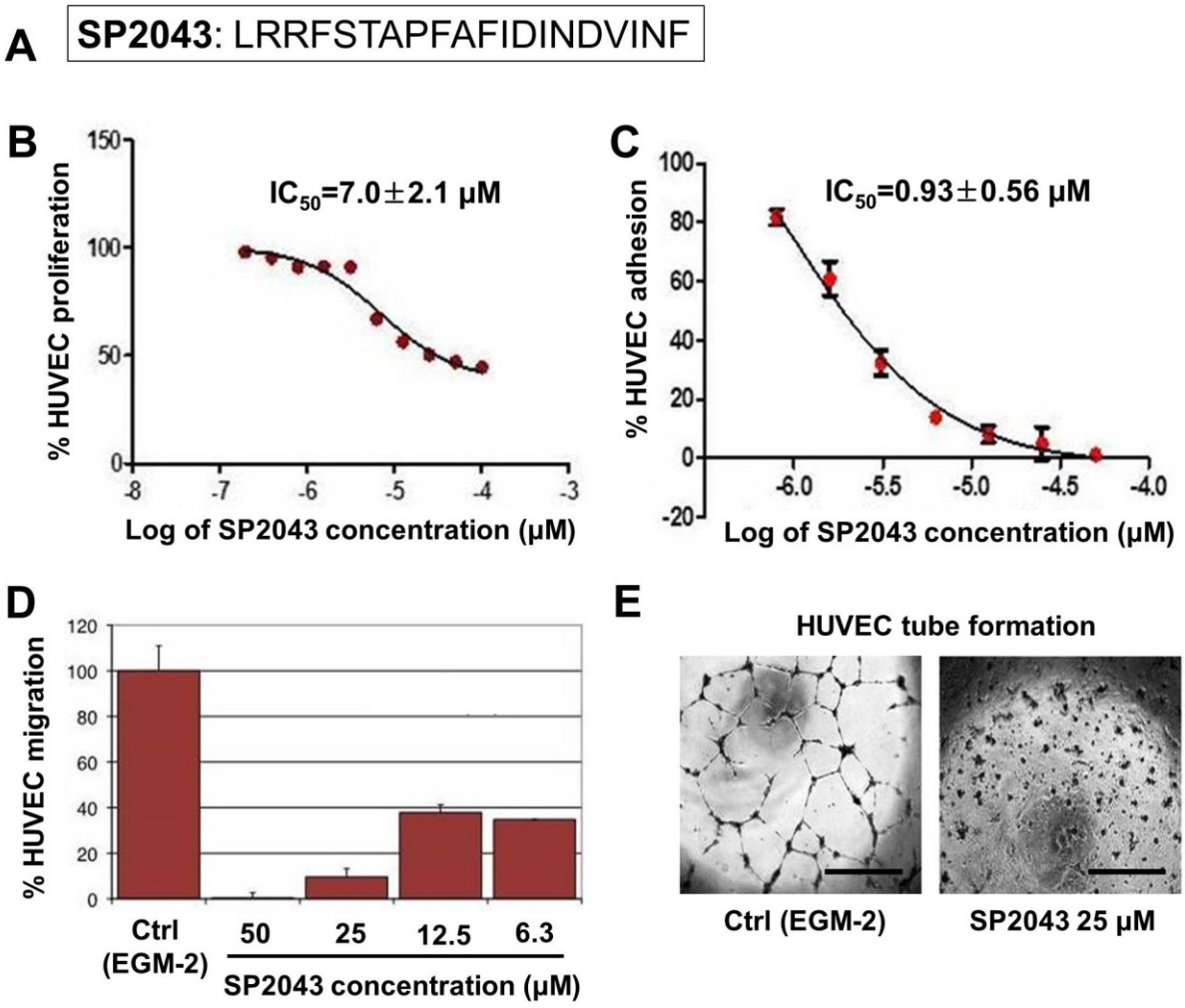

Figure 8.4: In vitro activity of SP2043 on HUVEC. SP2043 potently blocks angiogenesis in vitro against HUVEC growth media (EGM-2). (A) Amino acid sequence of the SP2043 peptide. (B) Percent HUVEC proliferation. (C) Percent HUVEC adhesion. (D) Percent HUVEC migration. (E) HUVEC tube formation. Scale bars represent 200 μm.

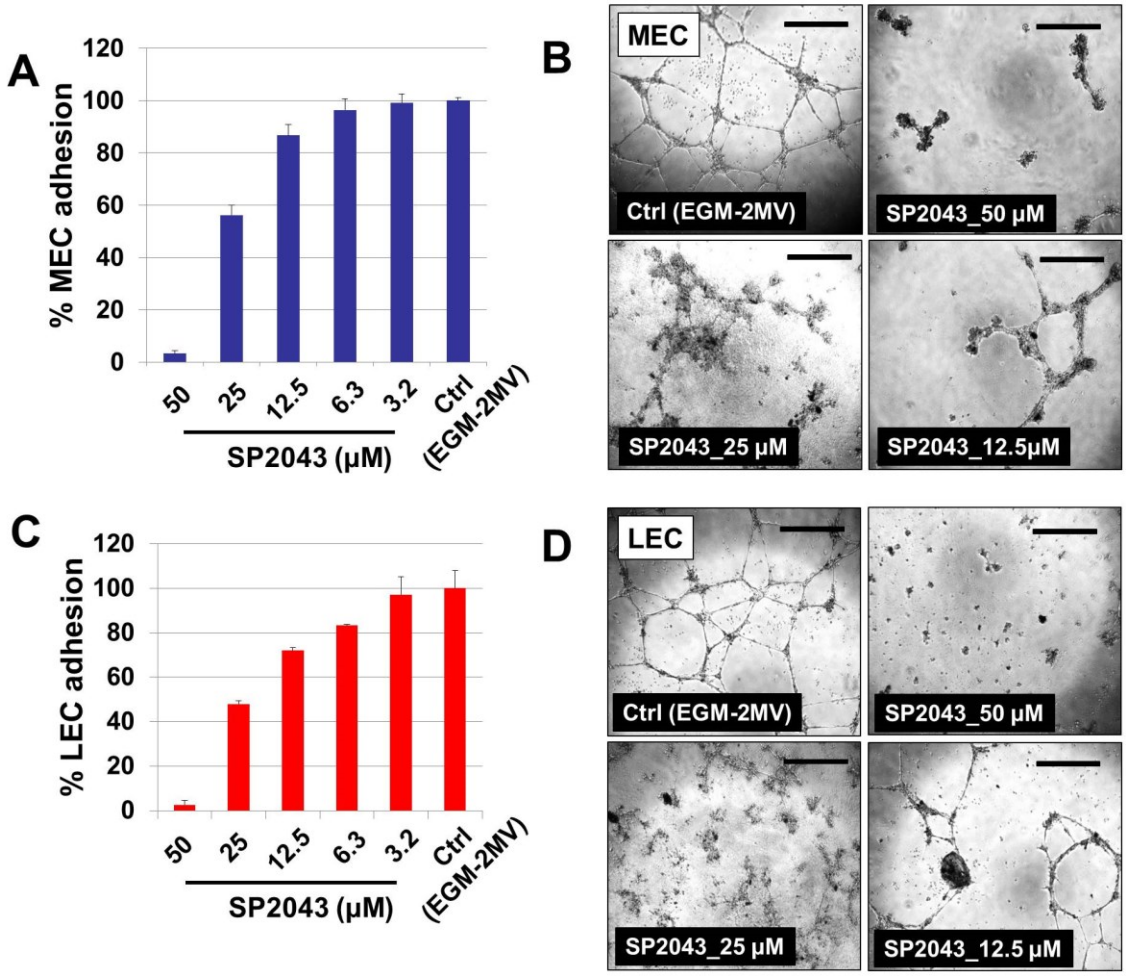

Figure 8.5: In vitro activity of SP2043 on MEC and LEC. SP2043 blocks lymphangiogenesis and angiogenesis in vitro against MEC/LEC growth media (EGM-2MV). (A) Percent MEC adhesion. (B) MEC tube formation. Scale bars represent 200 μm. (C) Percent LEC adhesion. (B) LEC tube formation. Scale bars represent 200 μm.

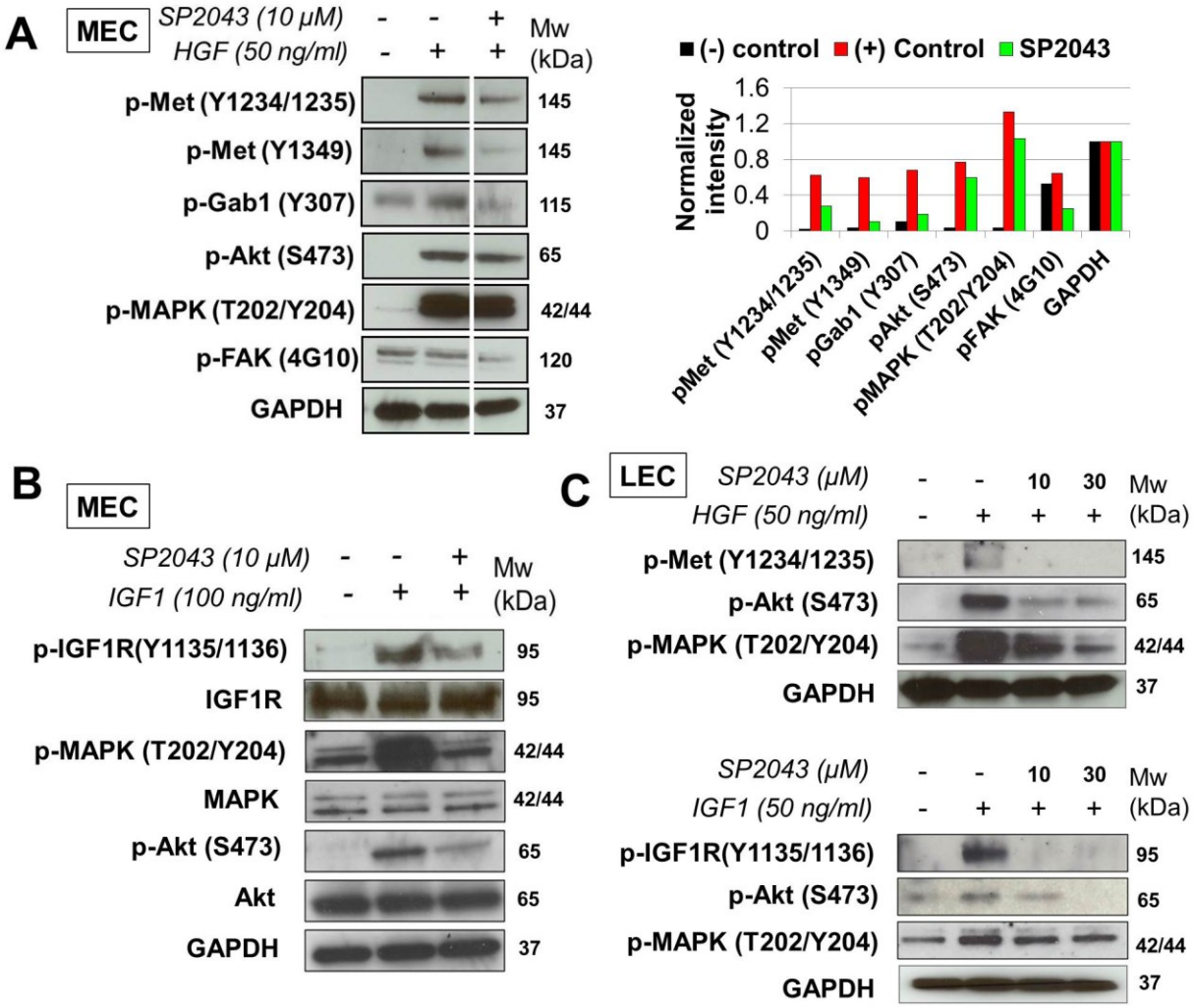

Figure 8.6: Inhibition of HGF and IGF-1 signaling by SP2043 in MEC and LEC. (A) Left panel: SP2043 blocks HGF-induced phosphorylation of c-Met (Y1234/1235/1349), and downstream proteins, including Gab1 (Y307), Akt (S473), MAPK (T202/204) in MEC. Right panel: GAPDH normalized western intensity from (A). (B) SP2043 blocks IGF-1 induced phosphorylation of IGF1R (Y1135/1136), and downstream proteins, including Akt (S473) and MAPK (T202/204) in MEC. (C) SP2043 blocks HGF-induced phosphorylation of c-Met

(Y1234/1235), Akt (S473), and MAPK (T202/204) in LEC. SP2043 also blocks IGF-1 induced phosphorylation of IGF1R (Y1135/1136), Akt (S473), and MAPK (T202/204) in LEC.

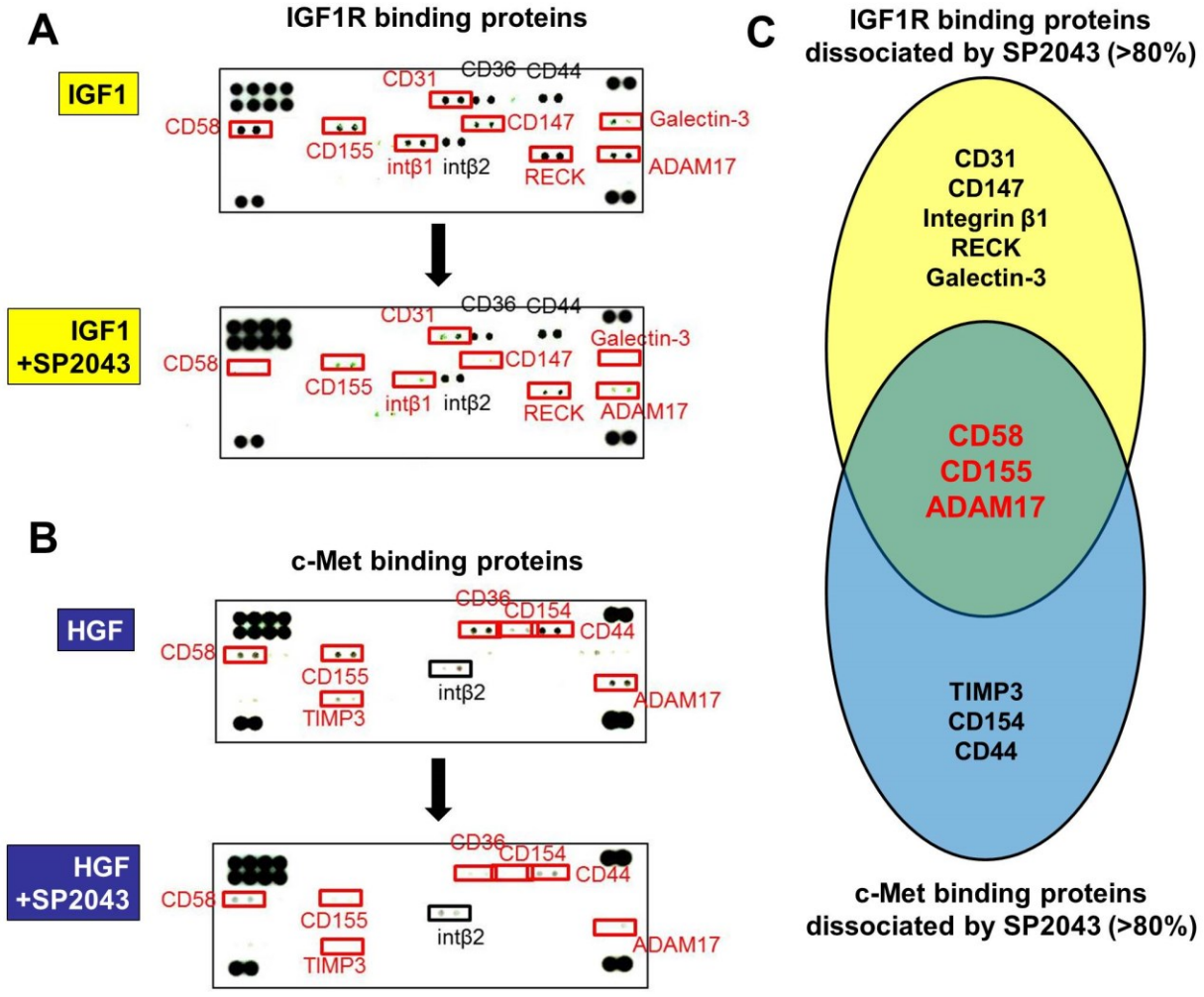

Figure 8.7: Identification of the IGF1R and c-Met binding receptor proteins that are induced to make a complex by growth factors (IGF-1 and HGF) as well as that are inhibited by SP2043 treatment. (A) It was determined which receptor proteins are involved in IGF1R receptor complex formation and dissociated from the IGF1R complex by SP2043 treatment. Proteome Profiler Antibody Arrays Kit for human soluble receptors (R&D systems) was employed to identify receptor proteins. Eleven receptor proteins newly formed receptor complex with IGF1R (CD58, CD155, CD31, CD36, CD44, CD147, RECK, ADAM17, Galectin-3, Integrin β1, Integrin β2) in a response of IGF-1 treatment. After SP2043 treatment, 8 proteins

(CD31, CD147, Integrin β1, RECK, Galectin-3, CD58, CD155, ADAM17) were dissociated from the receptor complex. (B) Eight receptor proteins formed receptor complex with c-Met (CD58, CD155, TIMP3, CD36, CD154, CD44, ADAM17, Integrin β2). After SP2043 treatment, 7 proteins (CD58, CD155, TIMP3, CD36, CD154, CD44, ADAM17) were dissociated. (C) CD58, CD155, ADAM17 were targeted by SP2043 to dissociate from the receptor complex.

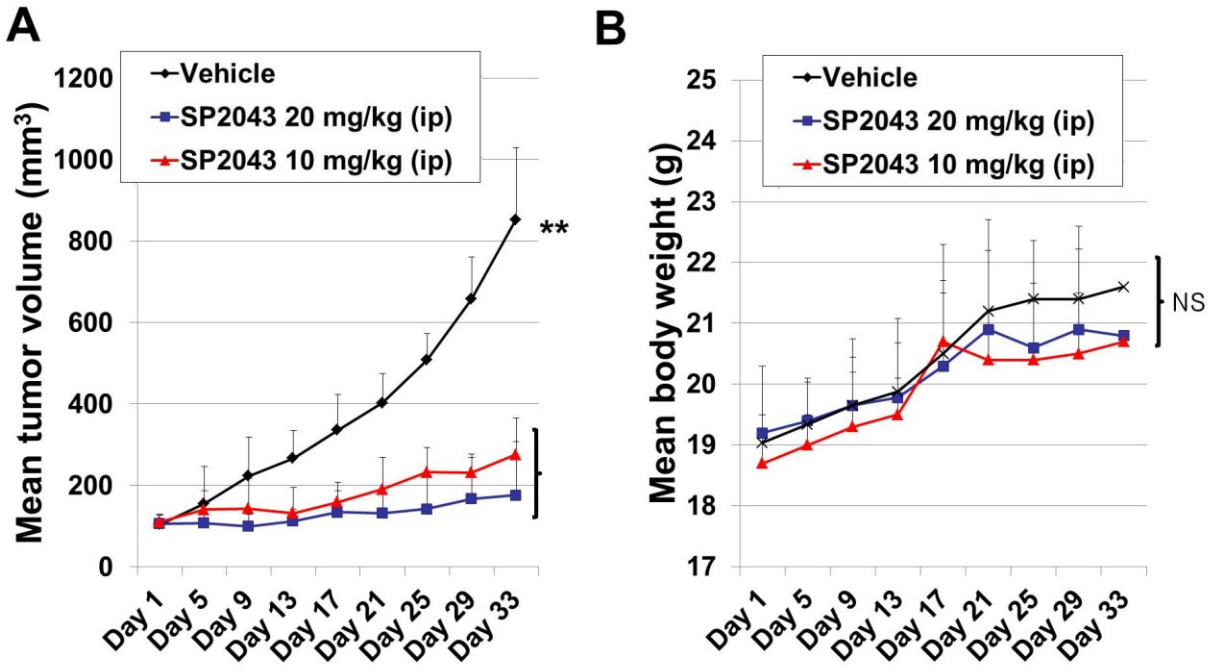

Figure 8.8: MDA-MB-231 xenograft models with SP2043 treatment. SP2043 inhibits MDA-MB-231 primary breast tumor growth. (A) Mean tumor volume. **P <0.01. (B) Mean mouse body weight.

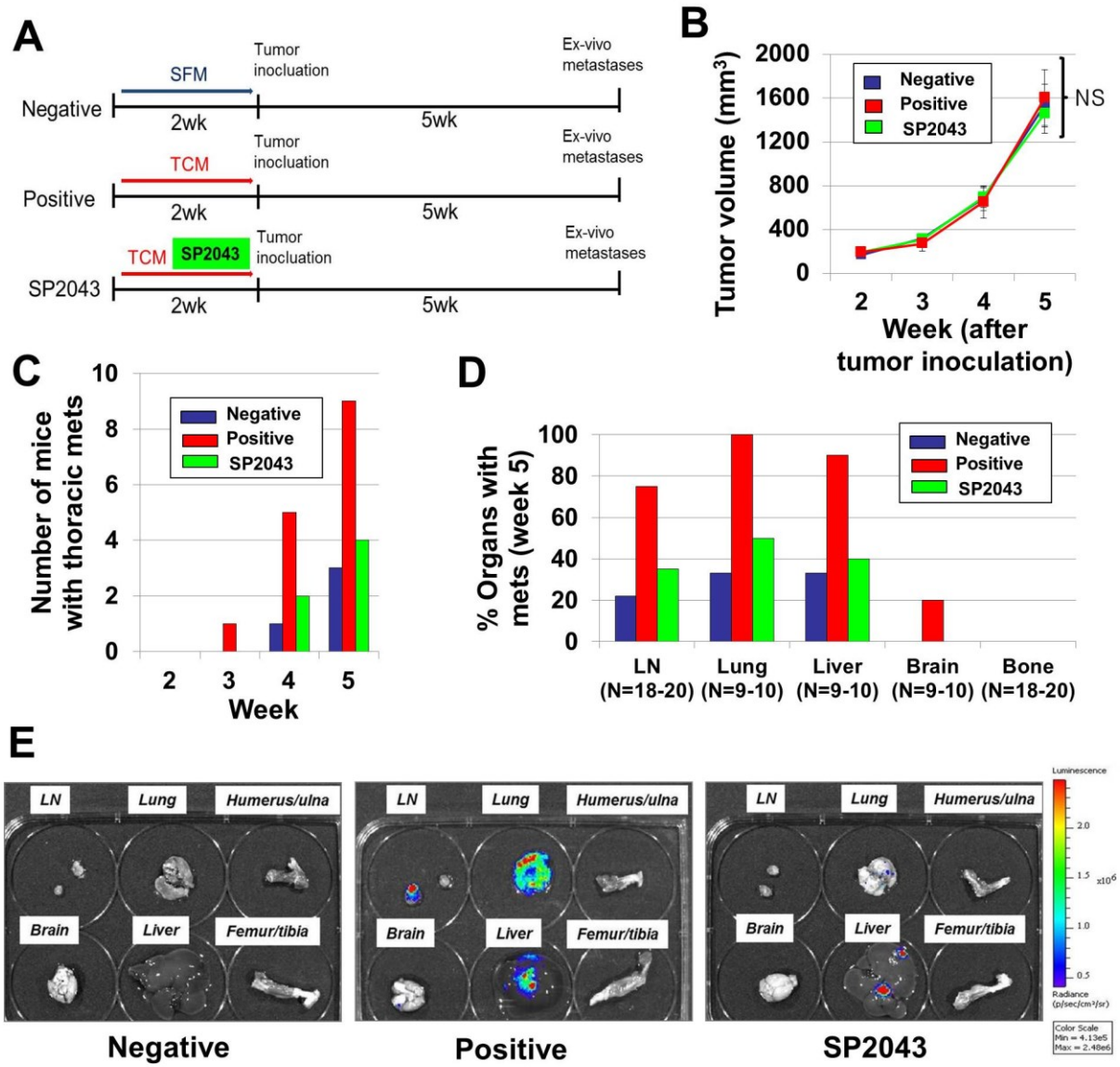

Figure 8.9: Tumor-conditioned media induced spontaneous metastasis models with SP2043 treatment. Tumor-conditioned media (TCM) pre-treatment and tumor inoculation induce rapidly formed metastasis. SP2043 was treated in the TCM induction phase and compared with other groups. Data shows that SP2043 inhibits MDA-MB-231 breast tumor metastasis in the lymph nodes and lungs. (A) Experimental group description. (B) Mean tumor volume. (C) Number of

mice with thoracic metastasis determined every week. (D) Number of organs with metastases ex vivo at week 5. (E) Representative organ images under the IVIS imager.

Chapter 9: Conclusion

9.1 SUMMARY

9.2 CONCLUDING STATEMENT

9.1 SUMMARY

The dissertation investigated mechanisms of breast cancer growth and metastasis by focusing on lymphatic and blood vasculatures in tumor and organ microenvironment. Specifically, cell-to-cell communication between cancer cells and the lymphatic and blood endothelial cells revealed that secretomes of these cells are the key way of communication to prime pre-metastatic niches in distant organs as well as to condition tumor promoting microenvironment in primary sites. The dissertation also documented development of novel anti-lymphangiogenic and anti-angiogenic peptides to treat breast cancer.

In the first step, a new spontaneous breast cancer metastasis model was developed based on the discovery that pre-treatment of animals with tumor-conditioned media (TCM) accelerates spontaneous metastasis in the corresponding tumor xenograft models. The pre-metastatic organs in TCM-treated animals showed enhanced lymphangiogenesis. Thus, **the second step** of the research focused on molecular crosstalk between lymphatic endothelial cells and breast cancer cells. The dissertation examined how the secretome of lymphatic endothelial cells within pre-metastatic niches are influenced by cancer cell secretome to accelerate metastasis. The dissertation revealed that lymphatic endothelial cells within pre-metastatic organs are educated by TCM, and express CCL5 and VEGF, facilitating tumor cell recruitment, extravasation and colonization. **In the third step**, the research examined which factors in TCM dysregulate LEC secretome, and which transcription factors in LEC are phosphorylated by the TCM to trigger the machinery of CCL5 and VEGF expression in LEC. The dissertation elucidated the mechanism: IL6 secreted by the cancer cells activates Stat3 phosphorylation in LEC, causing the formation of a pStat3-pc-Jun-pATF2 ternary complex and inducing HIF-1α expression in LEC. These changes finally result in expression of CCL5 and VEGF in LEC. **In the fourth step**, the dissertation

examined other crosstalks between cancer cells and lymphatic and blood endothelial cells in primary tumor sites. The dissertation revealed that lymphatic endothelial cells expressed EGF and PDGF-BB promoted tumor proliferation, but microvascular endothelial cells showed an opposite effect by suppressing tumor growth. Upon the understanding that the lymphatic endothelial cells facilitate tumor growth and metastasis in the tumor and organ microenvironment, **in the fifth step**, novel peptides to inhibit lymphangiogenesis were screened and developed. Specifically, the peptides derived from somatotropin or collagen IV domain conserved proteins showed bimodal inhibition of angiogenesis and lymphangiogenesis. Their mechanisms of action were examined using molecular biology methodologies and the inhibitory effects were evaluated using several in vitro and in vivo assays of angiogenesis and lymphangiogenesis. **In the last step**, the optimized mimetic peptide was tested in vivo in breast tumor xenograft models, tumor conditioned lymph node models, and TCM-induced spontaneous metastasis models.

9.2 CONCLUDING STATEMENT

The dissertation provides evidence that lymphatic endothelial cells in the tumor and distant organ microenvironment communicate with breast cancer cells to regulate metastatic dissemination, colonization, and tumor growth. The dissertation also highlights two novel anti-lymphangiogenic and anti-angiogenic peptides to effectively treat breast cancer growth and metastasis and possibly other angiogenesis- and lymphangiogenesis-dependent diseases.

Appendix

: Permission from publishers

This is a License Agreement between ESAK LEE ("You") and Elsevier ("Elsevier"). The license consists of your order details, the terms and conditions provided by Elsevier, and the payment terms and conditions.

Get the printable license.

License Number	3332020448505
License date	Feb 18, 2014
Licensed content publisher	Elsevier
Licensed content publication	The International Journal of Biochemistry & Cell Biology
Licensed content title	Small peptides derived from somatotropin domain-containing proteins inhibit blood and lymphatic endothelial cell proliferation, migration, adhesion and tube formation
Licensed content author	Esak Lee,Elena V. Rosca,Niranjan B. Pandey,Aleksander S. Popel
Licensed content date	December 2011
Licensed content volume number	43
Licensed content issue number	12
Number of pages	10
Type of Use	reuse in a thesis/dissertation
Portion	full article
Format	both print and electronic
Are you the author of this Elsevier article?	Yes
Will you be translating?	No
Title of your thesis/dissertation	NOVEL ROLE OF LYMPHATIC AND BLOOD VASCULATURES IN BREAST CANCER GROWTH AND METASTASIS AND PEPTIDE AGENTS WITH ANTI-LYMPHANGIOGENIC AND ANTI-ANGIOGENIC ACTIVITY
Expected completion date	Mar 2014
Estimated size (number of pages)	290
Elsevier VAT number	GB 494 6272 12
Permissions price	0.00 USD
VAT/Local Sales Tax	0.00 USD / 0.00 GBP

This is a License Agreement between ESAK LEE ("You") and Springer ("Springer"). The license consists of your order details, the terms and conditions provided by Springer, and the payment terms and conditions.

Get the printable license.

License Number	3332020331894
License date	Feb 18, 2014
Licensed content publisher	Springer
Licensed content publication	Angiogenesis
Licensed content title	Synergy between a collagen IV mimetic peptide and a somatotropin-domain derived peptide as angiogenesis and lymphangiogenesis inhibitors
Licensed content author	Jacob E. Koskimaki
Licensed content date	Jan 1, 2012
Volume number	16
Issue number	1
Type of Use	Thesis/Dissertation
Portion	Full text
Number of copies	50
Author of this Springer article	Yes and you are the sole author of the new work
Title of your thesis / dissertation	NOVEL ROLE OF LYMPHATIC AND BLOOD VASCULATURES IN BREAST CANCER GROWTH AND METASTASIS AND PEPTIDE AGENTS WITH ANTI-LYMPHANGIOGENIC AND ANTI-ANGIOGENIC ACTIVITY
Expected completion date	Mar 2014
Estimated size(pages)	290
Total	**0.00 USD**

This is a License Agreement between ESAK LEE ("You") and Springer ("Springer"). The license consists of your order details, the terms and conditions provided by Springer, and the payment terms and conditions.

Get the printable license.

License Number	3332020372344
License date	Feb 18, 2014
Licensed content publisher	Springer
Licensed content publication	Angiogenesis
Licensed content title	Synergy between a collagen IV mimetic peptide and a somatotropin-domain derived peptide as angiogenesis and lymphangiogenesis inhibitors
Licensed content author	Jacob E. Koskimaki
Licensed content date	Jan 1, 2012
Volume number	16
Issue number	1
Type of Use	Thesis/Dissertation
Portion	Figures
Author of this Springer article	Yes and you are the sole author of the new work
Title of your thesis / dissertation	NOVEL ROLE OF LYMPHATIC AND BLOOD VASCULATURES IN BREAST CANCER GROWTH AND METASTASIS AND PEPTIDE AGENTS WITH ANTI-LYMPHANGIOGENIC AND ANTI-ANGIOGENIC ACTIVITY
Expected completion date	Mar 2014
Estimated size(pages)	290
Total	**0.00 USD**

Edassist Jan 24

to me

Dear Esak,

Neoplasia Press is happy to give permission for the use of your recent article for your doctoral dissertation. Any figures or tables from the publication should be used without significant modification and Neoplasia should be cited as source of the material within the figure legend.

Edassist,
Neoplasia

On Thu, Jan 23, 2014 at 5:24 PM, Esak Lee <elee530@gmail.com> wrote:

> To whom it may concern,
>
> This is Esak Lee, a Ph.D. candidate at Johns Hopkins University, MD, USA. I am writing this E-mail to ask permission to use contents of the publication. In writing my dissertation, I need to include figures, tables, or text passages that have already been published in Neoplasia below. I have contributed as a first author to that work.
>
> **Lee, E.**, Koskimaki, J.E., Pandey, N.B., Popel, A.S., Inhibition of lymphangiogenesis and angiogenesis in breast tumor xenografts and lymph nodes by a peptide derived from transmembrane protein 45A. ***Neoplasia***, 15(2):112-24, 2013
>
> I would like to get a permission from you before I use the contents of the publication, as now you have a copyright. A copy of the permission will be included in my dissertation.

This is a License Agreement between ESAK LEE ("You") and Springer ("Springer"). The license consists of your order details, the terms and conditions provided by Springer, and the payment terms and conditions.

Get the printable license.

License Number	3332010426841
License date	Feb 18, 2014
Licensed content publisher	Springer
Licensed content publication	Clinical & Experimental Metastasis
Licensed content title	Pre-treatment of mice with tumor-conditioned media accelerates metastasis to lymph nodes and lungs: a new spontaneous breast cancer metastasis model
Licensed content author	Esak Lee
Licensed content date	Jan 1, 2013
Volume number	31
Issue number	1
Type of Use	Thesis/Dissertation
Portion	Full text
Number of copies	50
Author of this Springer article	Yes and you are the sole author of the new work
Title of your thesis / dissertation	NOVEL ROLE OF LYMPHATIC AND BLOOD VASCULATURES IN BREAST CANCER GROWTH AND METASTASIS AND PEPTIDE AGENTS WITH ANTI-LYMPHANGIOGENIC AND ANTI-ANGIOGENIC ACTIVITY
Expected completion date	Mar 2014
Estimated size(pages)	290
Total	**0.00 USD**

This is a License Agreement between ESAK LEE ("You") and Springer ("Springer"). The license consists of your order details, the terms and conditions provided by Springer, and the payment terms and conditions.

Get the printable license.

License Number	3332020263617
License date	Feb 18, 2014
Licensed content publisher	Springer
Licensed content publication	Clinical & Experimental Metastasis
Licensed content title	Pre-treatment of mice with tumor-conditioned media accelerates metastasis to lymph nodes and lungs: a new spontaneous breast cancer metastasis model
Licensed content author	Esak Lee
Licensed content date	Jan 1, 2013
Volume number	31
Issue number	1
Type of Use	Thesis/Dissertation
Portion	Figures
Author of this Springer article	Yes and you are the sole author of the new work
Title of your thesis / dissertation	NOVEL ROLE OF LYMPHATIC AND BLOOD VASCULATURES IN BREAST CANCER GROWTH AND METASTASIS AND PEPTIDE AGENTS WITH ANTI-LYMPHANGIOGENIC AND ANTI-ANGIOGENIC ACTIVITY
Expected completion date	Mar 2014
Estimated size(pages)	290
Total	**0.00 USD**

Bibliography

Achen, M. G., M. Jeltsch, et al. (1998). "Vascular endothelial growth factor D (VEGF-D) is a ligand for the tyrosine kinases VEGF receptor 2 (Flk1) and VEGF receptor 3 (Flt4)." Proc Natl Acad Sci U S A **95**(2): 548-553.

Achen, M. G., G. B. Mann, et al. (2006). "Targeting lymphangiogenesis to prevent tumour metastasis." Br J Cancer **94**(10): 1355-1360.

Adnane, L., P. A. Trail, et al. (2006). "Sorafenib (BAY 43-9006, Nexavar), a dual-action inhibitor that targets RAF/MEK/ERK pathway in tumor cells and tyrosine kinases VEGFR/PDGFR in tumor vasculature." Methods Enzymol **407**: 597-612.

Alderton, G. K. (2012). "Metastasis. Exosomes drive premetastatic niche formation." Nat Rev Cancer **12**(7): 447.

Alitalo, K. and P. Carmeliet (2002). "Molecular mechanisms of lymphangiogenesis in health and disease." Cancer Cell **1**(3): 219-227.

Angeli, V., F. Ginhoux, et al. (2006). "B cell-driven lymphangiogenesis in inflamed lymph nodes enhances dendritic cell mobilization." Immunity **24**(2): 203-215.

Ara, T., R. Nakata, et al. (2013). "Critical Role of STAT3 in IL-6-Mediated Drug Resistance in Human Neuroblastoma." Cancer Res **73**(13): 3852-3864.

Araki, C. (1968). "[Organs with low incidence of neoplasm metastasis through blood circulation]." Nihon Rinsho **26**(11): 3217-3221.

Athale, C. A. and T. S. Deisboeck (2006). "The effects of EGF-receptor density on multiscale tumor growth patterns." J Theor Biol **238**(4): 771-779.

Bagri, A., M. Tessier-Lavigne, et al. (2009). "Neuropilins in tumor biology." Clin Cancer Res **15**(6): 1860-1864.

Bahr, C. and B. Groner (2005). "The IGF-1 receptor and its contributions to metastatic tumor growth-novel approaches to the inhibition of IGF-1R function." Growth Factors **23**(1): 1-14.

Balanis, N., M. K. Wendt, et al. (2013). "Epithelial to Mesenchymal Transition Promotes Breast Cancer Progression via a Fibronectin-dependent STAT3 Signaling Pathway." J Biol Chem **288**(25): 17954-17967.

Balz, L. M., K. Bartkowiak, et al. (2012). "The interplay of HER2/HER3/PI3K and EGFR/HER2/PLC-gamma1 signalling in breast cancer cell migration and dissemination." J Pathol **227**(2): 234-244.

Banerji, S., J. Ni, et al. (1999). "LYVE-1, a new homologue of the CD44 glycoprotein, is a lymph-specific receptor for hyaluronan." J Cell Biol **144**(4): 789-801.

Baranski, J. D., R. R. Chaturvedi, et al. (2013). "Geometric control of vascular networks to enhance engineered tissue integration and function." Proc Natl Acad Sci U S A **110**(19): 7586-7591.

Bartsch, R., S. Woehrer, et al. (2006). "Serum interleukin-6 levels in patients with gastric MALT lymphoma compared to gastric and pancreatic cancer." Anticancer Res **26**(4B): 3187-3190.

Basolo, F., P. G. Conaldi, et al. (1993). "Normal breast epithelial cells produce interleukins 6 and 8 together with tumor-necrosis factor: defective IL6 expression in mammary carcinoma." Int J Cancer **55**(6): 926-930.

Berezowski, V., C. Landry, et al. (2004). "Contribution of glial cells and pericytes to the mRNA profiles of P-glycoprotein and multidrug resistance-associated proteins in an in vitro model of the blood-brain barrier." Brain Res **1018**(1): 1-9.

Bergfeld, S. A. and Y. A. DeClerck (2010). "Bone marrow-derived mesenchymal stem cells and the tumor microenvironment." Cancer Metastasis Rev **29**(2): 249-261.

Bhise, N. S., R. B. Shmueli, et al. (2011). "Drug delivery strategies for therapeutic angiogenesis and antiangiogenesis." Expert Opin Drug Deliv **8**(4): 485-504.

Borrello, I. M., H. I. Levitsky, et al. (2009). "Granulocyte-macrophage colony-stimulating factor (GM-CSF)-secreting cellular immunotherapy in combination with autologous stem cell transplantation (ASCT) as postremission therapy for acute myeloid leukemia (AML)." Blood **114**(9): 1736-1745.

Brantley-Sieders, D. M., C. M. Dunaway, et al. (2011). "Angiocrine factors modulate tumor proliferation and motility through EphA2 repression of Slit2 tumor suppressor function in endothelium." Cancer Res **71**(3): 976-987.

Bromley, S. K., S. Y. Thomas, et al. (2005). "Chemokine receptor CCR7 guides T cell exit from peripheral tissues and entry into afferent lymphatics." Nat Immunol **6**(9): 895-901.

Burgess, L. C. and J. O. Hall (2001). "Conditioned media from solid tumor cell lines treated with retinoic acids both decreases and increases proliferation of capillary endothelial cells." Life Sci **69**(24): 2819-2831.

Butler, J. M., H. Kobayashi, et al. (2010). "Instructive role of the vascular niche in promoting tumour growth and tissue repair by angiocrine factors." Nat Rev Cancer **10**(2): 138-146.

Cabioglu, N., M. S. Yazici, et al. (2005). "CCR7 and CXCR4 as novel biomarkers predicting axillary lymph node metastasis in T1 breast cancer." Clin Cancer Res **11**(16): 5686-5693.

Calvo, F. and E. Sahai (2011). "Cell communication networks in cancer invasion." Curr Opin Cell Biol **23**(5): 621-629.

Campos, M. S., K. G. Neiva, et al. (2012). "Endothelial derived factors inhibit anoikis of head and neck cancer stem cells." Oral Oncol **48**(1): 26-32.

Cao, Y., L. H. Hoeppner, et al. (2013). "Neuropilin-2 promotes extravasation and metastasis by interacting with endothelial alpha5 integrin." Cancer Res **73**(14): 4579-4590.

Carlini, M. J., M. S. De Lorenzo, et al. (2011). "Cross-talk between tumor cells and the microenvironment at the metastatic niche." Curr Pharm Biotechnol **12**(11): 1900-1908.

Carmeliet, P. and R. K. Jain (2011). "Molecular mechanisms and clinical applications of angiogenesis." Nature **473**(7347): 298-307.

Carmeliet, P. and R. K. Jain (2011). "Principles and mechanisms of vessel normalization for cancer and other angiogenic diseases." Nat Rev Drug Discov **10**(6): 417-427.

Casola, A., R. P. Garofalo, et al. (2001). "Multiple cis regulatory elements control RANTES promoter activity in alveolar epithelial cells infected with respiratory syncytial virus." J Virol **75**(14): 6428-6439.

Catalano, V., A. Turdo, et al. (2013). "Tumor and its microenvironment: a synergistic interplay." Semin Cancer Biol **23**(6 Pt B): 522-532.

Catlett-Falcone, R., T. H. Landowski, et al. (1999). "Constitutive activation of Stat3 signaling confers resistance to apoptosis in human U266 myeloma cells." Immunity **10**(1): 105-115.

Caunt, M., J. Mak, et al. (2008). "Blocking neuropilin-2 function inhibits tumor cell metastasis." Cancer Cell **13**(4): 331-342.

Chang, Q., E. Bournazou, et al. (2013). "The IL-6/JAK/Stat3 Feed-Forward Loop Drives Tumorigenesis and Metastasis." Neoplasia **15**(7): 848-862.

Chen, X., J. Wan, et al. (2010). "Increased IL-17-producing cells correlate with poor survival and lymphangiogenesis in NSCLC patients." Lung Cancer **69**(3): 348-354.

Chou, T. C. (2010). "Drug combination studies and their synergy quantification using the Chou-Talalay method." Cancer Res **70**(2): 440-446.

Corvinus, F. M., C. Orth, et al. (2005). "Persistent STAT3 activation in colon cancer is associated with enhanced cell proliferation and tumor growth." Neoplasia **7**(6): 545-555.

Cueni, L. N., I. Hegyi, et al. (2010). "Tumor lymphangiogenesis and metastasis to lymph nodes induced by cancer cell expression of podoplanin." Am J Pathol **177**(2): 1004-1016.

Daniele, A., A. F. Zito, et al. (2010). "Expression of metalloproteinases MMP-2 and MMP-9 in sentinel lymph node and serum of patients with metastatic and non-metastatic breast cancer." Anticancer Res **30**(9): 3521-3527.

Das, S., M. Czarnek, et al. (2012). "ADAM17 silencing in mouse colon carcinoma cells: the effect on tumoricidal cytokines and angiogenesis." PLoS One **7**(12): e50791.

Dazzi, H., P. S. Hasleton, et al. (1989). "Expression of epidermal growth factor receptor (EGF-R) in non-small cell lung cancer. Use of archival tissue and correlation of EGF-R with histology, tumour size, node status and survival." Br J Cancer **59**(5): 746-749.

De Marco, R., M. L. Di Gioia, et al. (2010). "A new non-natural arginine-like amino acid derivative with a sulfamoyl group in the side-chain." Amino Acids **38**(3): 691-700.

DeSantis, C., R. Siegel, et al. (2011). "Breast cancer statistics, 2011." CA Cancer J Clin **61**(6): 409-418.

Dietrich, T., F. Bock, et al. (2010). "Cutting edge: lymphatic vessels, not blood vessels, primarily mediate immune rejections after transplantation." J Immunol **184**(2): 535-539.

Dieu, M. C., B. Vanbervliet, et al. (1998). "Selective recruitment of immature and mature dendritic cells by distinct chemokines expressed in different anatomic sites." J Exp Med **188**(2): 373-386.

Ding, B. S., D. J. Nolan, et al. (2010). "Inductive angiocrine signals from sinusoidal endothelium are required for liver regeneration." Nature **468**(7321): 310-315.

Ding, B. S., D. J. Nolan, et al. (2011). "Endothelial-derived angiocrine signals induce and sustain regenerative lung alveolarization." Cell **147**(3): 539-553.

Doeden, K., Z. Ma, et al. (2009). "Lymphatic invasion in cutaneous melanoma is associated with sentinel lymph node metastasis." J Cutan Pathol **36**(7): 772-780.

Donlon, T. A., A. M. Krensky, et al. (1990). "Localization of a human T-cell-specific gene, RANTES (D17S136E), to chromosome 17q11.2-q12." Genomics **6**(3): 548-553.

Dos Santos, L. A., K. Garg, et al. (2011). "Incidence of lymph node and adnexal metastasis in endometrial stromal sarcoma." Gynecol Oncol **121**(2): 319-322.

Doyle, D. M. and K. D. Miller (2008). "Development of new targeted therapies for breast cancer." Breast Cancer **15**(1): 49-56.

Duong, T., P. Koopman, et al. (2012). "Tumor lymphangiogenesis as a potential therapeutic target." J Oncol **2012**: 204946.

Edel, M. J., J. M. Harvey, et al. (2000). "Comparison of vascularity and angiogenesis in primary invasive mammary carcinomas and in their respective axillary lymph node metastases." Clin Exp Metastasis **18**(8): 695-702.

El-Kenawi, A. E. and A. B. El-Remessy (2013). "Angiogenesis inhibitors in cancer therapy: mechanistic perspective on classification and treatment rationales." Br J Pharmacol **170**(4): 712-729.

Elkin, M. and I. Vlodavsky (2001). "Tail vein assay of cancer metastasis." Curr Protoc Cell Biol **Chapter 19**: Unit 19 12.

Emens, L. A. (2009). "GM-CSF-secreting vaccines for solid tumors." Curr Opin Investig Drugs **10**(12): 1315-1324.

Emens, L. A., D. Armstrong, et al. (2004). "A phase I vaccine safety and chemotherapy dose-finding trial of an allogeneic GM-CSF-secreting breast cancer vaccine given in a specifically timed sequence with immunomodulatory doses of cyclophosphamide and doxorubicin." Hum Gene Ther **15**(3): 313-337.

Eubank, T. D., R. D. Roberts, et al. (2009). "Granulocyte macrophage colony-stimulating factor inhibits breast cancer growth and metastasis by invoking an anti-angiogenic program in tumor-educated macrophages." Cancer Res **69**(5): 2133-2140.

Ferrara, N., K. J. Hillan, et al. (2004). "Discovery and development of bevacizumab, an anti-VEGF antibody for treating cancer." Nat Rev Drug Discov **3**(5): 391-400.

Festuccia, C., M. Bologna, et al. (1999). "Osteoblast conditioned media contain TGF-beta1 and modulate the migration of prostate tumor cells and their interactions with extracellular matrix components." Int J Cancer **81**(3): 395-403.

Folkman, J. and M. Klagsbrun (1987). "Angiogenic factors." Science **235**(4787): 442-447.

Forster-Horvath, C., L. Meszaros, et al. (2004). "Expression of CD44v3 protein in human endothelial cells in vitro and in tumoral microvessels in vivo." Microvasc Res **68**(2): 110-118.

Forster, R., A. C. Davalos-Misslitz, et al. (2008). "CCR7 and its ligands: balancing immunity and tolerance." Nat Rev Immunol **8**(5): 362-371.

Francia, G., W. Cruz-Munoz, et al. (2011). "Mouse models of advanced spontaneous metastasis for experimental therapeutics." Nat Rev Cancer **11**(2): 135-141.

Franses, J. W., A. B. Baker, et al. (2011). "Stromal endothelial cells directly influence cancer progression." Sci Transl Med **3**(66): 66ra65.

Franses, J. W. and E. R. Edelman (2011). "The evolution of endothelial regulatory paradigms in cancer biology and vascular repair." Cancer Res **71**(24): 7339-7344.

Galan-Moya, E. M., A. Le Guelte, et al. (2011). "Secreted factors from brain endothelial cells maintain glioblastoma stem-like cell expansion through the mTOR pathway." EMBO Rep **12**(5): 470-476.

Gao, D. and V. Mittal (2009). "The role of bone-marrow-derived cells in tumor growth, metastasis initiation and progression." Trends Mol Med **15**(8): 333-343.

Gao, D., D. J. Nolan, et al. (2008). "Endothelial progenitor cells control the angiogenic switch in mouse lung metastasis." Science **319**(5860): 195-198.

Gao, J., B. A. Aksoy, et al. (2013). "Integrative analysis of complex cancer genomics and clinical profiles using the cBioPortal." Sci Signal **6**(269): pl1.

Gao, M. Q., B. G. Kim, et al. (2013). "Human breast cancer-associated fibroblasts enhance cancer cell proliferation through increased TGF-alpha cleavage by ADAM17." Cancer Lett **336**(1): 240-246.

Garcia-Roman, J. and A. Zentella-Dehesa (2013). "Vascular permeability changes involved in tumor metastasis." Cancer Lett **335**(2): 259-269.

Genin, P., M. Algarte, et al. (2000). "Regulation of RANTES chemokine gene expression requires cooperativity between NF-kappa B and IFN-regulatory factor transcription factors." J Immunol **164**(10): 5352-5361.

Gerhardt, H. and H. Semb (2008). "Pericytes: gatekeepers in tumour cell metastasis?" J Mol Med (Berl) **86**(2): 135-144.

Gerhartz, C., B. Heesel, et al. (1996). "Differential activation of acute phase response factor/STAT3 and STAT1 via the cytoplasmic domain of the interleukin 6 signal transducer gp130. I. Definition of a novel phosphotyrosine motif mediating STAT1 activation." J Biol Chem **271**(22): 12991-12998.

Ghajar, C. M., H. Peinado, et al. (2013). "The perivascular niche regulates breast tumour dormancy." Nat Cell Biol **15**(7): 807-817.

Glunde, K. and I. Stasinopoulos (2009). "ADAM17: the new face of breast cancer-promoting metalloprotease activity." Cancer Biol Ther **8**(11): 1055-1057.

Goel, H. L. and A. M. Mercurio (2012). "Enhancing integrin function by VEGF/neuropilin signaling: implications for tumor biology." Cell Adh Migr **6**(6): 554-560.

Greco, C., I. D'Agnano, et al. (2006). "c-MYC deregulation is involved in melphalan resistance of multiple myeloma: role of PDGF-BB." Int J Immunopathol Pharmacol **19**(1): 67-79.

Guerin, E., S. Man, et al. (2013). "A model of postsurgical advanced metastatic breast cancer more accurately replicates the clinical efficacy of antiangiogenic drugs." Cancer Res **73**(9): 2743-2748.

Guidi, A. J., D. A. Berry, et al. (2000). "Association of angiogenesis in lymph node metastases with outcome of breast cancer." J Natl Cancer Inst **92**(6): 486-492.

Guo, L., C. Chen, et al. (2013). "Stat3-coordinated Lin-28-let-7-HMGA2 and miR-200-ZEB1 circuits initiate and maintain oncostatin M-driven epithelial-mesenchymal transition." Oncogene.

Gupta, G. P., D. X. Nguyen, et al. (2007). "Mediators of vascular remodelling co-opted for sequential steps in lung metastasis." Nature **446**(7137): 765-770.

Hale, J. S., M. Li, et al. (2012). "The malignant social network: cell-cell adhesion and communication in cancer stem cells." Cell Adh Migr **6**(4): 346-355.

Hamada, J., P. G. Cavanaugh, et al. (1992). "Separable growth and migration factors for large-cell lymphoma cells secreted by microvascular endothelial cells derived from target organs for metastasis." Br J Cancer **66**(2): 349-354.

Harrell, J. C., W. W. Dye, et al. (2006). "Estrogen receptor positive breast cancer metastasis: altered hormonal sensitivity and tumor aggressiveness in lymphatic vessels and lymph nodes." Cancer Res **66**(18): 9308-9315.

Hayashida, T., F. Takahashi, et al. (2010). "HOXB9, a gene overexpressed in breast cancer, promotes tumorigenicity and lung metastasis." Proc Natl Acad Sci U S A **107**(3): 1100-1105.

He, W., A. Nieponice, et al. (2010). "Pericyte-based human tissue engineered vascular grafts." Biomaterials **31**(32): 8235-8244.

He, Y., K. Kozaki, et al. (2002). "Suppression of tumor lymphangiogenesis and lymph node metastasis by blocking vascular endothelial growth factor receptor 3 signaling." J Natl Cancer Inst **94**(11): 819-825.

Hedvat, M., D. Huszar, et al. (2009). "The JAK2 inhibitor AZD1480 potently blocks Stat3 signaling and oncogenesis in solid tumors." Cancer Cell **16**(6): 487-497.

Hirakawa, S., L. F. Brown, et al. (2007). "VEGF-C-induced lymphangiogenesis in sentinel lymph nodes promotes tumor metastasis to distant sites." Blood **109**(3): 1010-1017.

Hirakawa, S., Y. K. Hong, et al. (2003). "Identification of vascular lineage-specific genes by transcriptional profiling of isolated blood vascular and lymphatic endothelial cells." Am J Pathol **162**(2): 575-586.

Hirakawa, S., S. Kodama, et al. (2005). "VEGF-A induces tumor and sentinel lymph node lymphangiogenesis and promotes lymphatic metastasis." J Exp Med **201**(7): 1089-1099.

Hirano, T., K. Ishihara, et al. (2000). "Roles of STAT3 in mediating the cell growth, differentiation and survival signals relayed through the IL-6 family of cytokine receptors." Oncogene **19**(21): 2548-2556.

Hirasawa, T., T. Gotoda, et al. (2009). "Incidence of lymph node metastasis and the feasibility of endoscopic resection for undifferentiated-type early gastric cancer." Gastric Cancer **12**(3): 148-152.

Hompland, T., C. Ellingsen, et al. (2012). "Interstitial fluid pressure and associated lymph node metastasis revealed in tumors by dynamic contrast-enhanced MRI." Cancer Res **72**(19): 4899-4908.

Hong, Y. K. and M. Detmar (2003). "Prox1, master regulator of the lymphatic vasculature phenotype." Cell Tissue Res **314**(1): 85-92.

Hood, J. L., R. S. San, et al. (2011). "Exosomes released by melanoma cells prepare sentinel lymph nodes for tumor metastasis." Cancer Res **71**(11): 3792-3801.

Hyung, W. J., J. H. Lee, et al. (2002). "Prognostic impact of lymphatic and/or blood vessel invasion in patients with node-negative advanced gastric cancer." Ann Surg Oncol **9**(6): 562-567.

Infusino, G. A. and J. R. Jacobson (2012). "Endothelial FAK as a therapeutic target in disease." Microvasc Res **83**(1): 89-96.

Irigoyen, M., E. Anso, et al. (2007). "Hypoxia alters the adhesive properties of lymphatic endothelial cells. A transcriptional and functional study." Biochim Biophys Acta **1773**(6): 880-890.

Ishida, Y., A. Kimura, et al. (2012). "Pivotal role of the CCL5/CCR5 interaction for recruitment of endothelial progenitor cells in mouse wound healing." J Clin Invest **122**(2): 711-721.

Ishii, G., H. Hashimoto, et al. (2010). "Fibroblasts associated with cancer cells keep enhanced migration activity after separation from cancer cells: a novel character of tumor educated fibroblasts." Int J Oncol **37**(2): 317-325.

Jain, R. K. and P. Carmeliet (2012). "SnapShot: Tumor angiogenesis." Cell **149**(6): 1408-1408 e1401.

Jain, R. K. and T. P. Padera (2002). "Prevention and treatment of lymphatic metastasis by antilymphangiogenic therapy." J Natl Cancer Inst **94**(11): 785-787.

Jenkins, D. E., Y. S. Hornig, et al. (2005). "Bioluminescent human breast cancer cell lines that permit rapid and sensitive in vivo detection of mammary tumors and multiple metastases in immune deficient mice." Breast Cancer Res **7**(4): R444-454.

Joukov, V., K. Pajusola, et al. (1996). "A novel vascular endothelial growth factor, VEGF-C, is a ligand for the Flt4 (VEGFR-3) and KDR (VEGFR-2) receptor tyrosine kinases." EMBO J **15**(2): 290-298.

Kaipainen, A., J. Korhonen, et al. (1995). "Expression of the fms-like tyrosine kinase 4 gene becomes restricted to lymphatic endothelium during development." Proc Natl Acad Sci U S A **92**(8): 3566-3570.

Kamenova, B., A. S. Braverman, et al. (2009). "Effective treatment of the brachial plexus syndrome in breast cancer patients by early detection and control of loco-regional metastases with radiation or systemic therapy." Int J Clin Oncol **14**(3): 219-224.

Kaplan, R. N., B. Psaila, et al. (2007). "Niche-to-niche migration of bone-marrow-derived cells." Trends Mol Med **13**(2): 72-81.

Kaplan, R. N., S. Rafii, et al. (2006). "Preparing the "soil": the premetastatic niche." Cancer Res **66**(23): 11089-11093.

Kaplan, R. N., R. D. Riba, et al. (2005). "VEGFR1-positive haematopoietic bone marrow progenitors initiate the pre-metastatic niche." Nature **438**(7069): 820-827.

Karagiannis, E. D. and A. S. Popel (2008). "A systematic methodology for proteome-wide identification of peptides inhibiting the proliferation and migration of endothelial cells." Proc Natl Acad Sci U S A **105**(37): 13775-13780.

Karaman, M. W., S. Herrgard, et al. (2008). "A quantitative analysis of kinase inhibitor selectivity." Nat Biotechnol **26**(1): 127-132.

Karl, E., Z. Zhang, et al. (2007). "Unidirectional crosstalk between Bcl-xL and Bcl-2 enhances the angiogenic phenotype of endothelial cells." Cell Death Differ **14**(9): 1657-1666.

Karnoub, A. E., A. B. Dash, et al. (2007). "Mesenchymal stem cells within tumour stroma promote breast cancer metastasis." Nature **449**(7162): 557-563.

Karpanen, T., M. Egeblad, et al. (2001). "Vascular endothelial growth factor C promotes tumor lymphangiogenesis and intralymphatic tumor growth." Cancer Res **61**(5): 1786-1790.

Kataru, R. P., H. Kim, et al. (2011). "T lymphocytes negatively regulate lymph node lymphatic vessel formation." Immunity **34**(1): 96-107.

Kataru, R. P., Y. G. Lee, et al. (2014). "Interactions of immune cells and lymphatic vessels." Adv Anat Embryol Cell Biol **214**: 107-118.

Kawamura, H., X. Li, et al. (2008). "Neuropilin-1 in regulation of VEGF-induced activation of p38MAPK and endothelial cell organization." Blood **112**(9): 3638-3649.

Kerbel, R. S. (2011). "Reappraising antiangiogenic therapy for breast cancer." Breast **20 Suppl 3**: S56-60.

Kim, I. S. and S. H. Baek (2010). "Mouse models for breast cancer metastasis." Biochem Biophys Res Commun **394**(3): 443-447.

Kim, U., H. C. Park, et al. (1988). "Differential permeability of lymphatic and blood vessels in determining the route of metastasis as demonstrated by indirect lymphography." Clin Exp Metastasis **6**(4): 291-299.

Kimura, C., M. Hayashi, et al. (2013). "Endothelium-dependent epithelial-mesenchymal transition of tumor cells: exclusive roles of transforming growth factor beta1 and beta2." Biochim Biophys Acta **1830**(10): 4470-4481.

Kobayashi, H., J. M. Butler, et al. (2010). "Angiocrine factors from Akt-activated endothelial cells balance self-renewal and differentiation of haematopoietic stem cells." Nat Cell Biol **12**(11): 1046-1056.

Kodera, Y., Y. Katanasaka, et al. (2011). "Sunitinib inhibits lymphatic endothelial cell functions and lymph node metastasis in a breast cancer model through inhibition of vascular endothelial growth factor receptor 3." Breast Cancer Res **13**(3): R66.

Koskimaki, J. E., E. Lee, et al. (2013). "Synergy between a collagen IV mimetic peptide and a somatotropin-domain derived peptide as angiogenesis and lymphangiogenesis inhibitors." Angiogenesis **16**(1): 159-170.

Kovacic, J. C., R. Gupta, et al. (2010). "Stat3-dependent acute Rantes production in vascular smooth muscle cells modulates inflammation following arterial injury in mice." J Clin Invest **120**(1): 303-314.

Krishnamurthy, S., Z. Dong, et al. (2010). "Endothelial cell-initiated signaling promotes the survival and self-renewal of cancer stem cells." Cancer Res **70**(23): 9969-9978.

Kuang, D. M., Q. Zhao, et al. (2008). "Tumor-educated tolerogenic dendritic cells induce CD3epsilon down-regulation and apoptosis of T cells through oxygen-dependent pathways." J Immunol **181**(5): 3089-3098.

Lee, A. H., S. E. Pinder, et al. (2006). "Prognostic value of lymphovascular invasion in women with lymph node negative invasive breast carcinoma." Eur J Cancer **42**(3): 357-362.

Lee, E., E. J. Fertig, et al. (2014). "Breast cancer cells educate lymphatic endothelial cells within pre-metastatic niches to promote metastasis." Nat Commun, in revision.

Lee, E., J. E. Koskimaki, et al. (2013). "Inhibition of Lymphangiogenesis and Angiogenesis in Breast Tumor Xenografts and Lymph Nodes by a Peptide Derived from Transmembrane Protein 45A." Neoplasia **15**(2): 112-124.

Lee, E., N. B. Pandey, et al. (2014). "Pre-treatment of mice with tumor-conditioned media accelerates metastasis to lymph nodes and lungs: a new spontaneous breast cancer metastasis model." Clin Exp Metastasis **31**(1): 67-79.

Lee, E., E. V. Rosca, et al. (2011). "Small peptides derived from somatotropin domain-containing proteins inhibit blood and lymphatic endothelial cell proliferation, migration, adhesion and tube formation." Int J Biochem Cell Biol **43**(12): 1812-1821.

Lee, H., J. Deng, et al. (2010). "STAT3-induced S1PR1 expression is crucial for persistent STAT3 activation in tumors." Nat Med **16**(12): 1421-1428.

Lee, S. J., H. J. Seol, et al. (2013). "Gene silencing of c-Met leads to brain metastasis inhibitory effects." Clin Exp Metastasis **30**(7): 845-854.

Lehmann, B. D., J. A. Bauer, et al. (2011). "Identification of human triple-negative breast cancer subtypes and preclinical models for selection of targeted therapies." J Clin Invest **121**(7): 2750-2767.

Lehtonen, A., S. Matikainen, et al. (2002). "Granulocyte-macrophage colony-stimulating factor (GM-CSF)-induced STAT5 activation and target-gene expression during human monocyte/macrophage differentiation." J Leukoc Biol **71**(3): 511-519.

Li, H., Y. Adachi, et al. (2011). "Insulin-like growth factor-I receptor blockade reduces tumor angiogenesis and enhances the effects of bevacizumab for a human gastric cancer cell line, MKN45." Cancer **117**(14): 3135-3147.

Liao, D., Y. Luo, et al. (2009). "Cancer associated fibroblasts promote tumor growth and metastasis by modulating the tumor immune microenvironment in a 4T1 murine breast cancer model." PLoS One **4**(11): e7965.

Lin, J., A. S. Lalani, et al. (2005). "Inhibition of lymphogenous metastasis using adeno-associated virus-mediated gene transfer of a soluble VEGFR-3 decoy receptor." Cancer Res **65**(15): 6901-6909.

Lin, J., C. Lemke, et al. (2011). "ADAM17 overexpression promotes angiogenesis by increasing blood vessel sprouting and pericyte number during brain microvessel development." Int J Dev Biol **55**(10-12): 961-968.

Liu, F., J. Cao, et al. (2013). "Stat3-targeted therapies overcome the acquired resistance to vemurafenib in melanomas." J Invest Dermatol **133**(8): 2041-2049.

Loeffler, M., J. A. Kruger, et al. (2006). "Targeting tumor-associated fibroblasts improves cancer chemotherapy by increasing intratumoral drug uptake." J Clin Invest **116**(7): 1955-1962.

Lorusso, G. and C. Ruegg (2012). "New insights into the mechanisms of organ-specific breast cancer metastasis." Semin Cancer Biol **22**(3): 226-233.

Lu, J., X. Ye, et al. (2013). "Endothelial Cells Promote the Colorectal Cancer Stem Cell Phenotype through a Soluble Form of Jagged-1." Cancer Cell **23**(2): 171-185.

Lu, X., C. H. Yan, et al. (2010). "In vivo dynamics and distinct functions of hypoxia in primary tumor growth and organotropic metastasis of breast cancer." Cancer Res **70**(10): 3905-3914.

Lund, A. W. and M. A. Swartz (2010). "Role of lymphatic vessels in tumor immunity: passive conduits or active participants?" J Mammary Gland Biol Neoplasia **15**(3): 341-352.

Maehara, Y., S. Tomisaki, et al. (1997). "Lymph node metastasis and relation to tumor growth potential and local immune response in advanced gastric cancer." Int J Cancer **74**(2): 224-228.

Mancardi, S., E. Vecile, et al. (2003). "Evidence of CXC, CC and C chemokine production by lymphatic endothelial cells." Immunology **108**(4): 523-530.

Mannello, F. and D. Ligi (2013). "Resolving breast cancer heterogeneity by searching reliable protein cancer biomarkers in the breast fluid secretome." BMC Cancer **13**: 344.

Mantovani, A., R. Bonecchi, et al. (2006). "Tuning inflammation and immunity by chemokine sequestration: decoys and more." Nat Rev Immunol **6**(12): 907-918.

Martin, M. (2011). "Understanding the value of antiangiogenic therapy in metastatic breast cancer." Curr Opin Oncol **23 Suppl**: S1.

Marusyk, A. and K. Polyak (2010). "Tumor heterogeneity: causes and consequences." Biochim Biophys Acta **1805**(1): 105-117.

Masur, K., F. Schwartz, et al. (2006). "DPPIV inhibitors extend GLP-2 mediated tumour promoting effects on intestinal cancer cells." Regul Pept **137**(3): 147-155.

Mayerson, H. S., R. M. Patterson, et al. (1962). "Permeability of lymphatic vessels." Am J Physiol **203**: 98-106.

Mayorca-Guiliani, A. E., H. Yano, et al. (2012). "Premetastatic vasculogenesis in oral squamous cell carcinoma xenograft-draining lymph nodes." Oral Oncol **48**(8): 663-670.

Meadows, K. L. and H. I. Hurwitz (2012). "Anti-VEGF therapies in the clinic." Cold Spring Harb Perspect Med **2**(10).

Michielsen, A. J., J. N. O'Sullivan, et al. (2012). "Tumor conditioned media from colorectal cancer patients inhibits dendritic cell maturation." Oncoimmunology **1**(5): 751-753.

Mirsky, H. P., M. J. Miller, et al. (2011). "Systems biology approaches for understanding cellular mechanisms of immunity in lymph nodes during infection." J Theor Biol **287**: 160-170.

Mori, A., S. Arii, et al. (1999). "Vascular endothelial growth factor-induced tumor angiogenesis and tumorigenicity in relation to metastasis in a HT1080 human fibrosarcoma cell model." Int J Cancer **80**(5): 738-743.

Moschetta, M., M. Cesca, et al. (2010). "Angiogenesis inhibitors: implications for combination with conventional therapies." Curr Pharm Des **16**(35): 3921-3931.

Mumprecht, V. and M. Detmar (2009). "Lymphangiogenesis and cancer metastasis." J Cell Mol Med **13**(8A): 1405-1416.

Murdoch, C., M. Muthana, et al. (2008). "The role of myeloid cells in the promotion of tumour angiogenesis." Nat Rev Cancer **8**(8): 618-631.

Nair, R. R., J. H. Tolentino, et al. (2012). "Role of STAT3 in Transformation and Drug Resistance in CML." Front Oncol **2**: 30.

Nakamura, M., H. Matsui, et al. (2010). "Suppression of lymphangiogenesis induced by Flt-4 antibody in gastric low-grade mucosa-associated lymphoid tissue lymphoma by Helicobacter heilmannii infection." J Gastroenterol Hepatol **25 Suppl 1**: S1-6.

Nguyen, A., P. Chen, et al. (2004). "Role of CaMKII in hydrogen peroxide activation of ERK1/2, p38 MAPK, HSP27 and actin reorganization in endothelial cells." FEBS Lett **572**(1-3): 307-313.

Nguyen, D. X., P. D. Bos, et al. (2009). "Metastasis: from dissemination to organ-specific colonization." Nat Rev Cancer **9**(4): 274-284.

Nguyen, N. Q., S. P. Tabruyn, et al. (2006). "Prolactin/growth hormone-derived antiangiogenic peptides highlight a potential role of tilted peptides in angiogenesis." Proc Natl Acad Sci U S A **103**(39): 14319-14324.

Nishida, Y., S. Tsukushi, et al. (2013). "High incidence of regional and in-transit lymph node metastasis in patients with alveolar rhabdomyosarcoma." Int J Clin Oncol.

Nissen, L. J., R. Cao, et al. (2007). "Angiogenic factors FGF2 and PDGF-BB synergistically promote murine tumor neovascularization and metastasis." J Clin Invest **117**(10): 2766-2777.

Niu, G., T. Bowman, et al. (2002). "Roles of activated Src and Stat3 signaling in melanoma tumor cell growth." Oncogene **21**(46): 7001-7010.

Olszewski, W. L. (2003). "The lymphatic system in body homeostasis: physiological conditions." Lymphat Res Biol **1**(1): 11-21; discussion 21-14.

Ozawa, S., M. Ueda, et al. (1987). "Stimulation by EGF of the growth of EGF receptor-hyperproducing tumor cells in athymic mice." Int J Cancer **40**(5): 706-710.

Padera, T. P., A. Kadambi, et al. (2002). "Lymphatic metastasis in the absence of functional intratumor lymphatics." Science **296**(5574): 1883-1886.

Padua, D., X. H. Zhang, et al. (2008). "TGFbeta primes breast tumors for lung metastasis seeding through angiopoietin-like 4." Cell **133**(1): 66-77.

Paez-Ribes, M., E. Allen, et al. (2009). "Antiangiogenic therapy elicits malignant progression of tumors to increased local invasion and distant metastasis." Cancer Cell **15**(3): 220-231.

Paget, S. (1989). "The distribution of secondary growths in cancer of the breast. 1889." Cancer Metastasis Rev **8**(2): 98-101.

Panni, R. Z., D. C. Linehan, et al. (2013). "Targeting tumor-infiltrating macrophages to combat cancer." Immunotherapy **5**(10): 1075-1087.

Pawelek, J. M. (2008). "Cancer-cell fusion with migratory bone-marrow-derived cells as an explanation for metastasis: new therapeutic paradigms." Future Oncol **4**(4): 449-452.

Pawelek, J. M. and A. K. Chakraborty (2008). "Fusion of tumour cells with bone marrow-derived cells: a unifying explanation for metastasis." Nat Rev Cancer **8**(5): 377-386.

Peinado, H., M. Aleckovic, et al. (2012). "Melanoma exosomes educate bone marrow progenitor cells toward a pro-metastatic phenotype through MET." Nat Med **18**(6): 883-891.

Pepper, M. S. and M. Skobe (2003). "Lymphatic endothelium: morphological, molecular and functional properties." J Cell Biol **163**(2): 209-213.

Petrella, B. L. (2009). "Assessment of local proteolytic milieu as a factor in tumor invasiveness and metastasis formation: in vitro collagen degradation and invasion assays." Methods Mol Biol **511**: 75-84.

Plate, K. H., G. Breier, et al. (1992). "Vascular endothelial growth factor is a potential tumour angiogenesis factor in human gliomas in vivo." Nature **359**(6398): 845-848.

Podgrabinska, S., P. Braun, et al. (2002). "Molecular characterization of lymphatic endothelial cells." Proc Natl Acad Sci U S A **99**(25): 16069-16074.

Pollard, J. W. (2004). "Tumour-educated macrophages promote tumour progression and metastasis." Nat Rev Cancer **4**(1): 71-78.

Potente, M., H. Gerhardt, et al. (2011). "Basic and therapeutic aspects of angiogenesis." Cell **146**(6): 873-887.

Psaila, B. and D. Lyden (2009). "The metastatic niche: adapting the foreign soil." Nat Rev Cancer **9**(4): 285-293.

Ran, S., L. Volk, et al. (2010). "Lymphangiogenesis and lymphatic metastasis in breast cancer." Pathophysiology **17**(4): 229-251.

Raza, A., M. J. Franklin, et al. (2010). "Pericytes and vessel maturation during tumor angiogenesis and metastasis." Am J Hematol **85**(8): 593-598.

Reyes-Gibby, C. C., M. Spitz, et al. (2007). "Cytokine genes and pain severity in lung cancer: exploring the influence of TNF-alpha-308 G/A IL6-174G/C and IL8-251T/A." Cancer Epidemiol Biomarkers Prev **16**(12): 2745-2751.

Ribatti, D. (2011). "Antiangiogenic therapy accelerates tumor metastasis." Leuk Res **35**(1): 24-26.

Ribeiro, R. J., C. P. Monteiro, et al. (2012). "Tumor cell-educated periprostatic adipose tissue acquires an aggressive cancer-promoting secretory profile." Cell Physiol Biochem **29**(1-2): 233-240.

Rigamonti, N. and M. De Palma (2013). "A role for angiopoietin-2 in organ-specific metastasis." Cell Rep **4**(4): 621-623.

Rivera, C. G., E. V. Rosca, et al. (2011). "Novel peptide-specific quantitative structure-activity relationship (QSAR) analysis applied to collagen IV peptides with antiangiogenic activity." J Med Chem **54**(19): 6492-6500.

Rofstad, E. K., S. H. Tunheim, et al. (2002). "Pulmonary and lymph node metastasis is associated with primary tumor interstitial fluid pressure in human melanoma xenografts." Cancer Res **62**(3): 661-664.

Rosca, E. V., J. E. Koskimaki, et al. (2012). "Structure-activity relationship study of collagen-derived anti-angiogenic biomimetic peptides." Chem Biol Drug Des **80**(1): 27-37.

Rosca, E. V., J. E. Koskimaki, et al. (2011). "Development of a biomimetic peptide derived from collagen IV with anti-angiogenic activity in breast cancer." Cancer Biol Ther **12**(9): 808-817.

Rosca, E. V., J. E. Koskimaki, et al. (2011). "Anti-angiogenic peptides for cancer therapeutics." Curr Pharm Biotechnol **12**(8): 1101-1116.

Rouhanimanesh, Y., Y. Vanderstighelen, et al. (2001). "Intra-abdominal metastases from primary carcinoma of the lung." Acta Chir Belg **101**(6): 300-303.

Ruddell, A., M. I. Harrell, et al. (2008). "Dynamic contrast-enhanced magnetic resonance imaging of tumor-induced lymph flow." Neoplasia **10**(7): 706-713, 701 p following 713.

Ruffell, B., N. I. Affara, et al. (2012). "Differential macrophage programming in the tumor microenvironment." Trends Immunol **33**(3): 119-126.

Ruggeri, Z. M. (2003). "Von Willebrand factor, platelets and endothelial cell interactions." J Thromb Haemost **1**(7): 1335-1342.

Sadej, R., H. Romanska, et al. (2009). "CD151 regulates tumorigenesis by modulating the communication between tumor cells and endothelium." Mol Cancer Res **7**(6): 787-798.

Sahai, E. (2007). "Illuminating the metastatic process." Nat Rev Cancer **7**(10): 737-749.

Saladin, P. M., B. D. Zhang, et al. (2009). "Current trends in the clinical development of peptide therapeutics." IDrugs **12**(12): 779-784.

Scepansky, E., R. Goldstein, et al. (2011). "Preclinical orthotopic and intracardiac injection models of human breast cancer metastasis to bone and their use in drug discovery." Curr Protoc Pharmacol **Chapter 14**: Unit 14 18.

Schaaij-Visser, T. B., M. de Wit, et al. (2013). "The cancer secretome, current status and opportunities in the lung, breast and colorectal cancer context." Biochim Biophys Acta **1834**(11): 2242-2258.

Schacht, V., M. I. Ramirez, et al. (2003). "T1alpha/podoplanin deficiency disrupts normal lymphatic vasculature formation and causes lymphedema." EMBO J **22**(14): 3546-3556.

Schoppmann, S. F., G. Bayer, et al. (2004). "Prognostic value of lymphangiogenesis and lymphovascular invasion in invasive breast cancer." Ann Surg **240**(2): 306-312.

Schust, J., B. Sperl, et al. (2006). "Stattic: a small-molecule inhibitor of STAT3 activation and dimerization." Chem Biol **13**(11): 1235-1242.

Sennino, B., T. Ishiguro-Oonuma, et al. (2013). "Inhibition of c-Met reduces lymphatic metastasis in RIP-Tag2 transgenic mice." Cancer Res **73**(12): 3692-3703.

Sennino, B., T. Ishiguro-Oonuma, et al. (2012). "Suppression of tumor invasion and metastasis by concurrent inhibition of c-Met and VEGF signaling in pancreatic neuroendocrine tumors." Cancer Discov **2**(3): 270-287.

Shamloo, B. K., P. Chhabra, et al. (2012). "Novel adverse events of bevacizumab in the US FDA adverse event reporting system database: a disproportionality analysis." Drug Saf **35**(6): 507-518.

Shattil, S. J. and M. H. Ginsberg (1997). "Integrin signaling in vascular biology." J Clin Invest **100**(11 Suppl): S91-95.

Shekhar, M. P., R. Pauley, et al. (2003). "Host microenvironment in breast cancer development: extracellular matrix-stromal cell contribution to neoplastic phenotype of epithelial cells in the breast." Breast Cancer Res **5**(3): 130-135.

Shibata, M. A., J. Morimoto, et al. (2008). "Combination therapy with short interfering RNA vectors against VEGF-C and VEGF-A suppresses lymph node and lung metastasis in a mouse immunocompetent mammary cancer model." Cancer Gene Ther **15**(12): 776-786.

Shields, J. D. (2011). "Lymphatics: at the interface of immunity, tolerance, and tumor metastasis." Microcirculation **18**(7): 517-531.

Shields, J. D., M. E. Fleury, et al. (2007). "Autologous chemotaxis as a mechanism of tumor cell homing to lymphatics via interstitial flow and autocrine CCR7 signaling." Cancer Cell **11**(6): 526-538.

Shih, Y. J., K. F. Hsu, et al. (2012). "Synchronous hepatocellular carcinoma and sigmoid colon metastasis presenting as liver and intra-abdominal abscesses." Acta Gastroenterol Belg **75**(2): 278-279.

Shima, I., Y. Sasaguri, et al. (1995). "Expression of epidermal growth-factor (EGF), matrix metalloproteinase-9 (mmp-9) and proliferating cell nuclear antigen (pcna) in esophageal cancer." Int J Oncol **6**(4): 833-839.

Shipitsin, M., L. L. Campbell, et al. (2007). "Molecular definition of breast tumor heterogeneity." Cancer Cell **11**(3): 259-273.

Siddiquee, K., S. Zhang, et al. (2007). "Selective chemical probe inhibitor of Stat3, identified through structure-based virtual screening, induces antitumor activity." Proc Natl Acad Sci U S A **104**(18): 7391-7396.

Skobe, M., T. Hawighorst, et al. (2001). "Induction of tumor lymphangiogenesis by VEGF-C promotes breast cancer metastasis." Nat Med **7**(2): 192-198.

Spratlin, J. (2011). "Ramucirumab (IMC-1121B): Monoclonal antibody inhibition of vascular endothelial growth factor receptor-2." Curr Oncol Rep **13**(2): 97-102.

Srebrow, A., A. F. Muro, et al. (1993). "The CRE-binding factor ATF-2 facilitates the occupation of the CCAAT box in the fibronectin gene promoter." FEBS Lett **327**(1): 25-28.

Stacker, S. A., M. G. Achen, et al. (2002). "Lymphangiogenesis and cancer metastasis." Nat Rev Cancer **2**(8): 573-583.

Stearman, R. S., L. Dwyer-Nield, et al. (2008). "A macrophage gene expression signature defines a field effect in the lung tumor microenvironment." Cancer Res **68**(1): 34-43.

Stern, D. M., E. Kaiser, et al. (1988). "Regulation of the coagulation system by vascular endothelial cells." Haemostasis **18**(4-6): 202-214.

Steven, P., F. Bock, et al. (2011). "Intravital two-photon microscopy of immune cell dynamics in corneal lymphatic vessels." PLoS One **6**(10): e26253.

Stracke, M. L. and L. A. Liotta (1992). "Multi-step cascade of tumor cell metastasis." In Vivo **6**(4): 309-316.

Sugimoto, H., T. M. Mundel, et al. (2006). "Identification of fibroblast heterogeneity in the tumor microenvironment." Cancer Biol Ther **5**(12): 1640-1646.

Sulochana, K. N. and R. Ge (2007). "Developing antiangiogenic peptide drugs for angiogenesis-related diseases." Curr Pharm Des **13**(20): 2074-2086.

Swartz, M. A., N. Iida, et al. (2012). "Tumor microenvironment complexity: emerging roles in cancer therapy." Cancer Res **72**(10): 2473-2480.

Takeda, K. and S. Akira (2000). "STAT family of transcription factors in cytokine-mediated biological responses." Cytokine Growth Factor Rev **11**(3): 199-207.

Tammela, T. and K. Alitalo (2010). "Lymphangiogenesis: Molecular mechanisms and future promise." Cell **140**(4): 460-476.

Tanne, J. H. (2011). "FDA cancels approval for bevacizumab in advanced breast cancer." BMJ **343**: d7684.

Tashiro, Y., C. Nishida, et al. (2012). "Inhibition of PAI-1 induces neutrophil-driven neoangiogenesis and promotes tissue regeneration via production of angiocrine factors in mice." Blood **119**(26): 6382-6393.

Thompson, A. D., 3rd and S. S. Kakar (2005). "Insulin and IGF-1 regulate the expression of the pituitary tumor transforming gene (PTTG) in breast tumor cells." FEBS Lett **579**(14): 3195-3200.

Timoshenko, A. V., C. Chakraborty, et al. (2006). "COX-2-mediated stimulation of the lymphangiogenic factor VEGF-C in human breast cancer." Br J Cancer **94**(8): 1154-1163.

Tobler, N. E. and M. Detmar (2006). "Tumor and lymph node lymphangiogenesis--impact on cancer metastasis." J Leukoc Biol **80**(4): 691-696.

Tomayko, M. M. and C. P. Reynolds (1989). "Determination of subcutaneous tumor size in athymic (nude) mice." Cancer Chemother Pharmacol **24**(3): 148-154.

Tremmel, M., A. Matzke, et al. (2009). "A CD44v6 peptide reveals a role of CD44 in VEGFR-2 signaling and angiogenesis." Blood **114**(25): 5236-5244.

Turner, S. G. and J. A. Barrowman (1977). "Intestinal lymph flow and lymphatic transport of protein during fat absorption." Q J Exp Physiol Cogn Med Sci **62**(2): 175-180.

Valastyan, S. and R. A. Weinberg (2011). "Tumor metastasis: molecular insights and evolving paradigms." Cell **147**(2): 275-292.

van Dam, H., M. Duyndam, et al. (1993). "Heterodimer formation of cJun and ATF-2 is responsible for induction of c-jun by the 243 amino acid adenovirus E1A protein." EMBO J **12**(2): 479-487.

Vaupel, P., F. Kallinowski, et al. (1988). "Evaluation of oxygen diffusion distances in human breast cancer using cell line specific in vivo data: role of various pathogenetic mechanisms in the development of tumor hypoxia." Adv Exp Med Biol **222**: 719-726.

Von Marschall, Z., A. Scholz, et al. (2005). "Vascular endothelial growth factor-D induces lymphangiogenesis and lymphatic metastasis in models of ductal pancreatic cancer." Int J Oncol **27**(3): 669-679.

Warner, K. A., M. Miyazawa, et al. (2008). "Endothelial cells enhance tumor cell invasion through a crosstalk mediated by CXC chemokine signaling." Neoplasia **10**(2): 131-139.

Wason, D. and K. E. Richkind (1992). "The use of giant cell tumor conditioned media in cytogenetic studies of hematologic malignancies." Cancer Genet Cytogenet **61**(2): 126-130.

Weech, A. A., E. Goettsch, et al. (1934). "The Flow and Composition of Lymph in Relation to the Formation of Edema." J Exp Med **60**(1): 63-84.

Wei, L. H., M. L. Kuo, et al. (2003). "Interleukin-6 promotes cervical tumor growth by VEGF-dependent angiogenesis via a STAT3 pathway." Oncogene **22**(10): 1517-1527.

Wesley, U. V., M. McGroarty, et al. (2005). "Dipeptidyl peptidase inhibits malignant phenotype of prostate cancer cells by blocking basic fibroblast growth factor signaling pathway." Cancer Res **65**(4): 1325-1334.

Wick, N., P. Saharinen, et al. (2007). "Transcriptomal comparison of human dermal lymphatic endothelial cells ex vivo and in vitro." Physiol Genomics **28**(2): 179-192.

Wigle, J. T. and G. Oliver (1999). "Prox1 function is required for the development of the murine lymphatic system." Cell **98**(6): 769-778.

Wilker, E., J. Lu, et al. (2005). "Role of PI3K/Akt signaling in insulin-like growth factor-1 (IGF-1) skin tumor promotion." Mol Carcinog **44**(2): 137-145.

Witz, I. P. (2006). "Tumor-microenvironment interactions: the selectin-selectin ligand axis in tumor-endothelium cross talk." Cancer Treat Res **130**: 125-140.

Wong, C. C., H. Zhang, et al. (2012). "Inhibitors of hypoxia-inducible factor 1 block breast cancer metastatic niche formation and lung metastasis." J Mol Med (Berl) **90**(7): 803-815.

Xian, X., J. Hakansson, et al. (2006). "Pericytes limit tumor cell metastasis." J Clin Invest **116**(3): 642-651.

Xin, X., M. Majumder, et al. (2012). "Targeting COX-2 and EP4 to control tumor growth, angiogenesis, lymphangiogenesis and metastasis to the lungs and lymph nodes in a breast cancer model." Lab Invest **92**: 1115-1128.

Xing, F., J. Saidou, et al. (2010). "Cancer associated fibroblasts (CAFs) in tumor microenvironment." Front Biosci (Landmark Ed) **15**: 166-179.

Xiong, H., J. Hong, et al. (2012). "Roles of STAT3 and ZEB1 proteins in E-cadherin down-regulation and human colorectal cancer epithelial-mesenchymal transition." J Biol Chem **287**(8): 5819-5832.

Xue, Y., S. Lim, et al. (2012). "PDGF-BB modulates hematopoiesis and tumor angiogenesis by inducing erythropoietin production in stromal cells." Nat Med **18**(1): 100-110.

Yamamoto, M., H. Kikuchi, et al. (2008). "TSU68 prevents liver metastasis of colon cancer xenografts by modulating the premetastatic niche." Cancer Res **68**(23): 9754-9762.

Yeligar, S. M., K. Machida, et al. (2009). "Ethanol augments RANTES/CCL5 expression in rat liver sinusoidal endothelial cells and human endothelial cells via activation of NF-kappa B, HIF-1 alpha, and AP-1." J Immunol **183**(9): 5964-5976.

Yi, E. H., C. S. Lee, et al. (2013). "STAT3-RANTES autocrine signaling is essential for tamoxifen resistance in human breast cancer cells." Mol Cancer Res **11**(1): 31-42.

Yong, C., E. A. Bridenbaugh, et al. (2005). "Microarray analysis of VEGF-C responsive genes in human lymphatic endothelial cells." Lymphat Res Biol **3**(4): 183-207.

Yu, B., X. Chen, et al. (2013). "Stromal fibroblasts in the microenvironment of gastric carcinomas promote tumor metastasis via upregulating TAGLN expression." BMC Cell Biol **14**: 17.

Yu, H., D. Pardoll, et al. (2009). "STATs in cancer inflammation and immunity: a leading role for STAT3." Nat Rev Cancer **9**(11): 798-809.

Yu, T., Z. Wang, et al. (2013). "High interstitial fluid pressure promotes tumor progression through inducing lymphatic metastasis-related protein expressions in oral squamous cell carcinoma." Clin Transl Oncol.

Yuan, L., D. Moyon, et al. (2002). "Abnormal lymphatic vessel development in neuropilin 2 mutant mice." Development **129**(20): 4797-4806.

Zhang, X., M. H. Wrzeszczynska, et al. (1999). "Interacting regions in Stat3 and c-Jun that participate in cooperative transcriptional activation." Mol Cell Biol **19**(10): 7138-7146.

Zhang, X. H., X. Jin, et al. (2013). "Selection of bone metastasis seeds by mesenchymal signals in the primary tumor stroma." Cell **154**(5): 1060-1073.

Zheng, S., L. R. Chen, et al. (2007). "[Expression of PDGFR-alpha in gastrointestinal stromal tumor and its clinical significance]." Zhejiang Da Xue Xue Bao Yi Xue Ban **36**(3): 280-284.

Zheng, S., L. R. Chen, et al. (2007). "Analysis of mutation and expression of c-kit and PDGFR-alpha gene in gastrointestinal stromal tumor." Hepatogastroenterology **54**(80): 2285-2290.

Zheng, X., F. Jiang, et al. (2009). "ADAM17 promotes breast cancer cell malignant phenotype through EGFR-PI3K-AKT activation." Cancer Biol Ther **8**(11): 1045-1054.

Curriculum Vitae

1. EDUCATION

2009 – 2014	**Ph.D. in Chemical and Biomolecular Engineering** Johns Hopkins University, MD, USA
2006 – 2008	**M.S. in Pharmacy** Seoul National University, South Korea
1999 – 2006	**B.S. in Chemical and Biological Engineering** Seoul National University, South Korea

2. PROFESSIONAL EXPERIENCES

2009 – 2014	**Research Assistant** (Ph.D. Candidate) Department of Biomedical Engineering Johns Hopkins University School of Medicine, MD, USA (Mentor: Aleksander S. Popel, Ph.D.)
2011 – 2012	**Teaching Assistant** (Course: Kinetic Processes) Department of Chemical and Biomolecular Engineering Johns Hopkins University, MD, USA (Lecturer: An Goffin, Ph.D.)
2006 – 2008	**Research Assistant** (M.S. Candidate) School of Pharmacy Seoul National University, South Korea (Mentor: Youngro Byun, Ph.D.)
2007	**Teaching Assistant** (Course: Advanced Physical Pharmacy) School of Pharmacy, Seoul National University, South Korea (Lecturer: Youngro Byun, Ph.D.)
2006	**Teaching Assistant** (Course: Physical Pharmacy Laboratory) School of Pharmacy, Seoul National University, South Korea (Lecturer: Chong-Kook Kim, Ph.D.)

2001 – 2003 **Military Service**, Korea Army, South Korea

3. HONORS & AWARDS

2013 Invited Seminar, Breast Cancer Program
Sidney Kimmel Comprehensive Cancer Center
Johns Hopkins University School of Medicine, MD, USA

2012 Runner-up Award, Safeway Breast Cancer Symposium
Sidney Kimmel Comprehensive Cancer Center
Johns Hopkins University School of Medicine, MD, USA

2012 – 2013 Mogam Science Scholarship Award ($10,000)
Mogam (Green cross) Foundation, South Korea

2006 – 2008 BK21 National Fellowship, Korea Research Foundation, South Korea

2006 Graduation Honor (summa cum laude), Chemical and Biological Engineering
Seoul National University, South Korea

1999 – 2005 Merit-based scholarship for undergraduate students
Chemical and Biological Engineering
Seoul National University, South Korea

4. PUBLICATIONS

Lee, E., Fertig, E.J., Pandey, N.B., Popel, A.S., Breast cancer cells educate lymphatic endothelial cells within pre-metastatic niches to promote metastasis, **Nature Communications,** in revision

Lee, E., Pandey, N.B., Popel, A.S., Pre-treatment of mice with tumor-conditioned media accelerates metastasis to lymph nodes and lungs: a new spontaneous breast cancer metastasis model, **Clinical and Experimental Metastasis,** 31(1):67-79, 2014

Lee, E., Koskimaki, J.E., Pandey, N.B., Popel, A.S., Inhibition of lymphangiogenesis and angiogenesis in breast tumor xenografts and lymph nodes by a peptide derived from transmembrane protein 45A. ***Neoplasia,** 15(2):112-24, 2013 **(*Cover article)**

Koskimaki, J.E.*, **Lee, E.*,** Chen, W., Rivera, C.G., Rosca, E.V., Pandey, N.B., Popel, A.S., Synergy between a collagen IV mimetic peptide and a somatotropin-domain containing peptide as angiogenesis and lymphangiogenesis inhibitors. **Angiogenesis,** 16(1):159-70, 2013 **(*Equal contribution)**

Lee, E., Rosca, E.V., Pandey, N.B., Popel, A.S., Small peptides derived from somatotropin domain-containing proteins inhibit blood and lymphatic endothelial cell proliferation, migration, adhesion and tube formation. **International Journal of Biochemistry and Cell Biology,** 43:1812-21, 2011

Lee, E., Kim, Y.S., Bae, S.M., Kim, S.K., Jin, S., Chung, S.W., Lee, M., Jeon, O.C., Park, R.W., Kim, I.S., Byun, Y., Kim, S.Y., Polyproline-type helical-structured low-molecular weight heparin (LMWH)-taurocholate conjugate as a new angiogenesis inhibitor. **International Journal of Cancer**, 124: 2755-65, 2009

Koskimaki, J.E., Rosca, E.V., Rivera, C., **Lee, E.**, Chen, W., Pandey, N.B., Popel, A.S., Serpin-derived peptides are anti-angiogenic and suppress breast tumor growth in vivo. **Translational Oncology,** 5(2):92-7, 2012

Byun Y., **Lee, E.**, Jeon, O.C., Kim, S.Y., Park, R.W., Heparin conjugates and methods.
US Patent 8,088,753, 2012

Chu, L.H., **Lee, E.**, Bader, J.S., Popel, A.S., Angiogenesis interactome and time course microarray data reveal the distinct activation patterns in endothelial cells, under review

Rosca, E.V., Penet, M.F., Mori, N., Koskimaki, J.E., **Lee, E.**, Pandey, N.B., Bhujwalla, Z.M., Popel, A.S., A biomimetic collagen derived peptide exhibits anti-angiogenic and anti-lymphangiogenic activity in triple negative breast cancer, in revision

Lee, E., Lee, S.J., Koskimaki, J.E., Pandey, N.B., Popel, A.S., Collagen IV mimetic peptide exhibits anti-lymphangiogenic and anti-angiogenic activity inhibiting breast tumor metastasis and growth, in preparation

Lee, E., Popel, A.S., Crosstalk between tumor cells and endothelium: emerging roles of blood and lymphatic endothelial cell mediated signals in cancer progression, in preparation. **Expert Reviews in Molecular Medicine (invited)**

Lee, E., Pandey, N.B., Popel, A.S., Stromal lymphatic vessels influence breast tumor growth and pericyte recruitment, in preparation

Fertig, E.J.*, **Lee, E.***, Pandey, N.B., Popel, A.S., A comprehensive analysis of the secretome in human breast cancers, in preparation **(*Equal contribution)**

5. PRESENTATIONS

Lee, E., Pandey, N.B., Popel, A.S., Lymphatic endothelium promotes angiogenesis, tumor growth and metastasis in breast cancer. **Tumor Invasion and Metastasis AACR Special Conference,** San Diego, CA, USA, 2013

Lee, E., Koskimaki, J.E., Pandey, N.B., Popel, A.S., An endogenous peptide derived from a transmembrane protein 45A human inhibits lymphangiogenesis and angiogenesis. **Johns Hopkins Nano-Bio Symposium,** Baltimore, MD, USA, 2012

Lee, E., Pandey, N.B., Popel, A.S., Lymphatic endothelial cells induce angiogenesis in axillary and brachial lymph nodes preparing metastatic lymph nodes in breast cancer. ***Annual Breast Cancer Research Symposium,** Sidney Kimmel Comprehensive Cancer Center at Johns Hopkins Medical Institutions, Baltimore, MD, USA, 2012 **(*Poster award)**

Lee, E., Pandey, N.B., Popel, A.S., Cross talk between lymphatic endothelial cells and cancer cells reveals the molecular mechanism of 'soil preparation' in tumor metastasis. Molecular Mechanisms in Lymphatic Function & Disease, **Gordon Research Conference (GRC)**, Ventura, CA, USA, 2012

Lee, E., and Byun, Y., cRGD-LMWH-Taurocholate inhibits angiogenesis and tumor growth with tumor endothelium targeting. **American Association of Pharmaceutical Scientists (AAPS)**, Atlanta, GA, USA, 2008

Lee, E., Kim, S.K., and Byun, Y., A novel heparin taurocholate derivative as a VEGF antagonist. **American Association of Pharmaceutical Scientists (AAPS)**, San Diego, CA, USA, 2007

Lee, E., Lee, G.Y., and Byun, Y., Anti-angiogenic activities of new heparin derivatives for anti-cancer therapy. **13th International Symposium on Recent Advances in Drug Delivery Systems**, Salt Lake City, UT, USA, 2007